frontiers | Research Topics

Non-invasive diagnostic tools in the management of skin disorders

Edited by
Elisa Zavattaro, Paola Savoia and Federica Veronese

Published in
Frontiers in Medicine

ISSN 1664-8714
ISBN 978-2-8325-3482-3
DOI 10.3389/978-2-8325-3482-3

About Frontiers

Frontiers is more than just an open access publisher of scholarly articles: it is a pioneering approach to the world of academia, radically improving the way scholarly research is managed. The grand vision of Frontiers is a world where all people have an equal opportunity to seek, share and generate knowledge. Frontiers provides immediate and permanent online open access to all its publications, but this alone is not enough to realize our grand goals.

Frontiers journal series

The Frontiers journal series is a multi-tier and interdisciplinary set of open-access, online journals, promising a paradigm shift from the current review, selection and dissemination processes in academic publishing. All Frontiers journals are driven by researchers for researchers; therefore, they constitute a service to the scholarly community. At the same time, the *Frontiers journal series* operates on a revolutionary invention, the tiered publishing system, initially addressing specific communities of scholars, and gradually climbing up to broader public understanding, thus serving the interests of the lay society, too.

Dedication to quality

Each Frontiers article is a landmark of the highest quality, thanks to genuinely collaborative interactions between authors and review editors, who include some of the world's best academicians. Research must be certified by peers before entering a stream of knowledge that may eventually reach the public - and shape society; therefore, Frontiers only applies the most rigorous and unbiased reviews. Frontiers revolutionizes research publishing by freely delivering the most outstanding research, evaluated with no bias from both the academic and social point of view. By applying the most advanced information technologies, Frontiers is catapulting scholarly publishing into a new generation.

What are Frontiers Research Topics?

Frontiers Research Topics are very popular trademarks of the *Frontiers journals series*: they are collections of at least ten articles, all centered on a particular subject. With their unique mix of varied contributions from Original Research to Review Articles, Frontiers Research Topics unify the most influential researchers, the latest key findings and historical advances in a hot research area.

Find out more on how to host your own Frontiers Research Topic or contribute to one as an author by contacting the Frontiers editorial office: frontiersin.org/about/contact

Non-invasive diagnostic tools in the management of skin disorders

Topic editors

Elisa Zavattaro — University of Eastern Piedmont, Italy

Paola Savoia — Università degli Studi del Piemonte Orientale, Italy

Federica Veronese — Azienda Ospedaliero Universitaria Maggiore della Carità, Italy

Citation

Zavattaro, E., Savoia, P., Veronese, F., eds. (2023). *Non-invasive diagnostic tools in the management of skin disorders*. Lausanne: Frontiers Media SA.

doi: 10.3389/978-2-8325-3482-3

Table of contents

04 Editorial: Non-invasive diagnostic tools in the management of skin disorders
Elisa Zavattaro, Federica Veronese and Paola Savoia

07 Diagnostic Values of Dermatoscopy and CD31 Expression in Cutaneous Lymphangioma Circumscriptum
Lixia Lu, Siyu Yan, Mingliang Chen, Xiaoyan Huang and Juan Su

13 AKASI and Near-Infrared Spectroscopy in the combined effectiveness evaluation of an actinic keratoses preventive product in immunocompetent and immunocompromised patients
Federica Veronese, Silvia Seoni, Vanessa Tarantino, Matteo Buttafava, Chiara Airoldi, Kristen M. Meiburger, Elisa Zavattaro and Paola Savoia

25 Point-of-care ultrasound of peripheral nerves in the diagnosis of Hansen's disease neuropathy
Glauber Voltan, Fred Bernards Filho, Marcel Nani Leite, Natália Aparecida De Paula, Jaci Maria Santana, Claudia Maria Lincoln Silva, Josafá Gonçalves Barreto, Moises Batista Da Silva, Guilherme Conde, Claudio Guedes Salgado and Marco Andrey Cipriani Frade

39 Diagnostic accuracy of dermoscopy for onychomycosis: A systematic review
Sophie Soyeon Lim, Laura Hui, Jungyoon Ohn, Youngjoo Cho, Choon Chiat Oh and Je-Ho Mun

50 Silent peripheral neuropathy determined by high-resolution ultrasound among contacts of patients with Hansen's disease
Glauber Voltan, Wilson Marques-Júnior, Jaci Maria Santana, Claudia Maria Lincoln Silva, Marcel Nani Leite, Natália Aparecida De Paula, Fred Bernardes Filho, Josafá Gonçalves Barreto, Moises Batista Da Silva, Guilherme Conde, Claudio Guedes Salgado and Marco Andrey Cipriani Frade

64 Conventional and three-dimensional photography as a tool to map distribution patterns of in-transit melanoma metastases on the lower extremity
Kilian Müller, Carola Berking, Caroline Voskens, Markus V. Heppt, Lucie Heinzerling, Elias A. T. Koch, Rafaela Kramer, Susanne Merkel, Beatrice Schuler-Thurner, Vera Schellerer, Theresa Steeb, Anja Wessely and Michael Erdmann

73 Dermoscopic features of children scabies
Ying-li Nie, Hong Yi, Xiao-yan Xie, Gui-li Fu and Yuan-quan Zheng

79 Assessment of soluble skin surface protein levels for monitoring *psoriasis vulgaris* in adult psoriasis patients using non-invasive transdermal analysis patch: A pilot study
Kadri Orro, Kristiina Salk, Kristi Abram, Jelena Arshavskaja, Anne Meikas, Maire Karelson, Toomas Neuman, Külli Kingo and Pieter Spee

87 Non-invasive skin measurement methods and diagnostics for vitiligo: a systematic review
Parsa Abdi, Michelle R. Anthony, Christopher Farkouh, Airiss R. Chan, Amritpal Kooner, Simal Qureshi and Howard Maibach

frontiers | Frontiers in Medicine

TYPE Editorial
PUBLISHED 31 August 2023
DOI 10.3389/fmed.2023.1271195

OPEN ACCESS

EDITED AND REVIEWED BY
Robert Gniadecki,
University of Alberta, Canada

*CORRESPONDENCE
Elisa Zavattaro
✉ elisa.zavattaro@med.uniupo.it

RECEIVED 01 August 2023
ACCEPTED 14 August 2023
PUBLISHED 31 August 2023

CITATION
Zavattaro E, Veronese F and Savoia P (2023) Editorial: Non-invasive diagnostic tools in the management of skin disorders.
Front. Med. 10:1271195.
doi: 10.3389/fmed.2023.1271195

Editorial: Non-invasive diagnostic tools in the management of skin disorders

Elisa Zavattaro[1]*, Federica Veronese[2] and Paola Savoia[1]

[1]Department of Health Sciences, University of Eastern Piedmont, Novara, Italy, [2]Section of Dermatology, AOU Maggiore della Carità, Novara, Italy

KEYWORDS

non-invasive diagnostics, dermoscopy, skin imaging, digital technologies, artificial intelligence

Editorial on the Research Topic
Non-invasive diagnostic tools in the management of skin disorders

Dermatology is a branch of medicine mainly based on the visual inspection of tangible body, although several non-invasive tools can facilitate the diagnostic process (1).

Among these, dermoscopy currently represents the most common and important instrument that every Dermatologist uses in the clinical daily practice not only for diagnosis of pigmented lesions, but also of inflammatory and infectious skin diseases (2).

This Research Topic collects three papers concerning possible diagnostic applications of dermoscopy. A couple of papers have showed the dermoscopy efficacy in two infectious skin diseases. In detail, Nie et al. have reported their experience with such technique in the diagnosis of scabies in children, highlighting the need to search for the parasite in areas where skin is thinner and, thus, more susceptible to host the *Sarcoptes*. Accordingly, they suggested to carefully evaluate by dermoscopy both the finger seams and external genitalia; moreover, they have also showed typical dermoscopic patterns (i.e., the jet with contrail, the curvilinear scaly burrow) of scabies infestation, whose report in the literature are quite scarce. Moreover, some other not typical dermoscopic images have also been depicted in the iconographic part of the article. Given the fact that dermoscopy is a non-invasive methodology, this has a great importance when evaluating patients in pediatric age.

The systematic review by Lim et al. has investigated the accuracy of dermoscopy in the diagnosis of both onychomycosis and fungal melanonychia. More in detail, they reviewed a total of 24 articles dealing with the considered topic, and reported the most common and useful features associated with the two previously cited fungal infections. Unfortunately, given the lack of a homogenous terminology definitions among the studies included in the meta-analysis, the paper obtained only a limited strength in the results.

Also, the paper published by Lu et al., suggests the possible application of dermoscopy as an additional tool for the diagnosis of Cutaneous Lymphangioma Circumscriptum (CLC), a congenital malformation of superficial lymphatics characterized by a cluster of vesicular lesions, with a variable color depending on the presence of lymphatic fluid or blood components. Based on a retrospective analysis of 37 patients, the authors describe 4 different CLC dermoscopic patterns, two of which were not previously reported in the literature, comparing them with the histopathological features and contributing to the differential diagnosis.

A further important tool in dermatology is represented by those devices employing different wavelengths of the electromagnetic spectrum. Among these, the ultrasound (US) evaluation, and more recently the high-resolution ultrasound (HRUS), have garnered great acclaim, with ever-increasing number of publications (3, 4).

The potential role of HRUS in estimating the neurological damage in patients with Hansen's disease (HD) is addressed in two publications from Voltan, Filho et al. and Voltan, Marques-Júnior et al.. In detail, they compared the cross-sectional area of peripheral nerves evaluated through HRUS in 234 leprosy patients and 66 healthy volunteers, identifying a statistically significant difference and a characteristic asymmetry and focality pattern, useful for the early diagnosis of HD neuropathy. In the other paper, they proposed this technique for the screening of the household contacts of the HD patients, given their significantly higher disease risk than the general population.

Moreover, a new potential application of Near-Infrared Spectroscopy (NIRS), a non-invasive technique that evaluates the hemoglobin relative concentration variations (5), in the monitoring of patients affected by actinic keratoses (AK) has been proposed in the paper published by Veronese et al.. This study enrolled both immunocompetent ($n = 42$) and immunosuppressed ($n = 32$) patients, affected by grade I/II AK, treated with a topical product containing a high-protection sunscreen and a DNA repair complex (antioxidant plus DNA repair enzymes). The response to treatment was objectively assessed through the AKASI clinical score (6), together with NIRS assessment. This might represent a novel application of NIRS, thus investigating not only the diagnostic process but also the efficacy of a topical treatment in different categories of subjects.

Similarly, the paper published by Orro et al. presents a pilot study concerning the use of a non-invasive transdermal patch (FibroTx Transdermal Analysis Patch) for the sampling of inflammation-related proteins (IL-1α, IL-1RA CXCL-1/2, and hBD-1) from psoriatic skin. A difference between lesional and non-lesional skin and a decrease in protein levels during phototherapy has been demonstrated. Despite the relatively small number of subjects enrolled in this study, which requires an expansion on a larger sample, there is substantial evidence of the validity of this tool in monitoring the clinical course in psoriasic patients.

Regarding the management of vitiligo, the systematic review by Abdi et al. looks over the different methods able to evaluate the diagnosis, severity, and progression of such disease, thus including many tools, such as photography, biophysical approaches, and the newly developed reflectance confocal microscopy and optical coherence tomography. Despite the authors examined 64 studies, thus allowing an in-deep analysis, they concluded that a single methodic cannot provide conclusive information, also given the complexity of vitiligo symptoms and signs.

Finally, when considering not only the diagnostic but also the prognostic process, in their paper Müller et al. suggested the use of three-dimensional photography as a tool to analyze the distribution patterns of melanoma *in-transit* metastases (ITM) on the lower extremity, in comparison with conventional photography. This study was conducted on 46 patients, in which the localization of melanoma lesions was systematically correlated to anatomically determined lymphatic drainage pathways, to identify skin areas at higher risk of metastatic dissemination, to be subjected to a more accurate clinical examination during the follow-up. Unfortunately, it was not feasible to map the possible ITM sites in cases of primary melanoma affecting the foot, possibly due to the altered lymphatic drainage pathway attributable to surgery, indeed, finger amputations as well as surgical grafts or flaps are more frequently required.

In conclusion, this Research Topic shows the "state of the art" of some of the non-invasive diagnostic tools that are currently available in dermatology, including newly developed methodologies that guide future research and its translation. Furthermore, following the recent COVID-19 pandemic and the consequent strong need to develop new methodologies to interconnect consultants and patients through digital technologies, and also to employ traditional techniques in an alternative scope, it is clear that the mentioned tools and devices, in the next future, could harvest even more great importance in the dermatologic field.

Author contributions

EZ: Writing—original draft, Writing—review and editing. FV: Writing—review and editing. PS: Writing—original draft, Writing—review and editing.

Acknowledgments

We would like to thank all the authors that generously contributed to this topic and the staff of Frontiers for the precious help and assistance.

Conflict of interest

The authors declare that the research was conducted in the absence of any commercial or financial relationships that could be construed as a potential conflict of interest.

The author(s) declared that they were an editorial board member of Frontiers, at the time of submission. This had no impact on the peer review process and the final decision.

Publisher's note

References

1. Srivastava R, Manfredini M, Rao BK. Noninvasive imaging tools in dermatology. *Cutis.* (2019) 104:108–13.

2. Bleicher B, Levine A, Schwartz M, Markowitz O. A review through the looking glass: new advances in dermoscopy. *Ital J Dermatol Venereol.* (2018) 153:43–55. doi: 10.23736/S0392-0488.17.05777-7

3. Mandava A, Ravuri PR, Konathan R. High-resolution ultrasound imaging of cutaneous lesions. *Indian J Radiol Imaging.* (2013) 23:269–77. doi: 10.4103/0971-3026.120272

4. Levy J, Barrett DL, Harris N, Jeong JJ, Yang X, Chen SC. High-frequency ultrasound in clinical dermatology a review. *Ultrasound J.* (2021) 13:24. doi: 10.1186/s13089-021-00222-w

5. Mcintosh LM, Summers R, Jackson M, Mantsch HH, Mansfield JR, Howlett M, et al. Towards non-invasive screening of skin lesions by near-infrared spectroscopy. *J Invest Dermatol.* (2001) 116:175–81. doi: 10.1046/j.1523-1747.2001.00212.x

6. Dirschka T, Pellacani G, Micali G, Malvehy J, Stratigos AJ, Casari A, et al. A proposed scoring system for assessing the severity of actinic keratosis on the head: actinic keratosis area and severity index. *J Eur Dermatol Venereol.* (2017) 31:1295–302. doi: 10.1111/jdv.14267

frontiers in Medicine

ORIGINAL RESEARCH
published: 08 October 2021
doi: 10.3389/fmed.2021.738815

Diagnostic Values of Dermatoscopy and CD31 Expression in Cutaneous Lymphangioma Circumscriptum

Lixia Lu[1,2,3], *Siyu Yan*[4], *Mingliang Chen*[1,2,3], *Xiaoyan Huang*[5]* and *Juan Su*[1,2,3]*

[1] Department of Dermatology, Xiangya Hospital, Central South University, Changsha, China, [2] Hunan Key Laboratory of Skin Cancer and Psoriasis, Central South University, Changsha, China, [3] Hunan Engineering Research Center of Skin Health and Disease, Central South University, Changsha, China, [4] Department of Dermatology, The Third Xiangya Hospital, Central South University, Changsha, China, [5] Department of Pathology, Xiangya Hospital, Central South University, Changsha, China

Background: Cutaneous lymphangioma circumscriptum is characterized by clusters of deep-seated, vesicle-like papules. Cutaneous lymphangioma circumscriptum (CLC) is not a tumor but rather a congenital malformation of superficial lymphatics.

Objectives: The study aimed to describe the dermoscopic features of CLC and investigate the reason why marked blood components in CLC. Moreover, this study sought to increase awareness of the clinical characteristics of CLC and provide insights into CLC diagnosis.

Methods: A representative sample of patients with CLC with demographic information and pathological and dermoscopical results was analyzed. The immunohistochemistry of lymphangioma specimens with CD31 and D2-40 was performed. The clinical manifestations of CLC, demographic information, and the results of immunohistochemistry were statistically analyzed to validate the correlation.

Results: Besides the pattern of frog spawn-like blisters, lymphangioma also presented as either transparent or pigmented with dark-red to whitish/yellowish shades. Moreover, lymphangioma manifested as a pattern of dermatofibroma. Furthermore, CD31 was detected in the flattened endothelium and only present in dilated spaces containing enough blood or lymph components.

Limitations: This study is limited by its retrospective nature and statistical power.

Conclusion: Dermoscopy is useful for the diagnosis of CLC. CD31 positive staining and cystic-dilated spaces showed flattened inner and outer endothelia are the diagnostic features in hypopyon-like shape and blisters resembling frog spawn patterns in CLC. These features can assist in the diagnosis of CLC.

Keywords: dermoscopy, immunohistochemistry, CD31, dermatoscope, cutaneous lymphangioma circumscriptum

OPEN ACCESS

Edited by:
Ximena Wortsman,
University of Chile, Chile

Reviewed by:
Jie Liu,
Peking Union Medical College Hospital (CAMS), China
Francesco Lacarrubba,
University of Catania, Italy

***Correspondence:**
Juan Su
sujuanderm@csu.edu.cn
Xiaoyan Huang
168102104@csu.edu.cn

Specialty section:
This article was submitted to Dermatology, a section of the journal Frontiers in Medicine

Received: *12 July 2021*
Accepted: *24 August 2021*
Published: *08 October 2021*

Citation:
Lu L, Yan S, Chen M, Huang X and Su J (2021) Diagnostic Values of Dermatoscopy and CD31 Expression in Cutaneous Lymphangioma Circumscriptum. Front. Med. 8:738815. doi: 10.3389/fmed.2021.738815

INTRODUCTION

Cutaneous lymphangioma circumscriptum is a benign disorder with asymptomatic lesions, including discrete translucent vesicles (1, 2). Some of the common characteristics of cutaneous lymphangioma circumscriptum (CLC) are the presence of a group of transparent vesicles that are 2–4 mm in size, patterns similar to frog spawn, and diversity in color as a result of hemoglobin

degradation (3, 4). These skin lesions are located in any part of the body, and their color varies from clear to dark red depending on the presence of lymphatic fluid and/or blood components (3). CLC manifests striking characteristic features, differentiating it from other lymphatic or vascular diseases such as hemangiomas (5).

Dermoscopy is a non-invasive clinical diagnostic technique wherein the skin is magnified to observe the structure and color from the epidermis to the papillary layer (6, 7). This technique is extensively used in the diagnosis of skin-related tumors and hair-related and inflammatory skin diseases (8–10). However, reports on the application of dermoscopy in CLC diagnosis are scarce. Yellowish lacunae surrounded by a pale septum and pale red to bluish lacunae in CLC can be observed *via* dermoscopy (11). Some atypical lesions might be diagnosed as CLC by using adjunctive measures, such as dermoscopy and histology (12). In hypopyon-like types of CLC patterns, CLC was found to contain blood components. CD31 is a highly glycosylated Ig-like membrane receptor. It is the most abundant membrane glycoprotein constitutively expressed on the vascular endothelium (13). Therefore, we used immunohistochemistry to detect CD31 expression. This study aimed to examine dermoscopic CLC manifestations retrospectively, create a complement to existing CLC dermoscopic features, and understand why some CLC subtypes are manifested with blood components.

METHODS

After institutional review board approval, we viewed the pathological databases, outpatient records, and dermoscopic systems in Xiangya Hospital, Central South University and Hunan Province Children's Hospital from July 2017 to July 2019. Any patients with detailed demographic information (age, gender, and location), biopsy specimens, and dermoscopic and clinical data were included in this study. As a result, 584 patients with CLC were chosen. Next, patients were carefully excluded if any of their demographic information, specimens, and dermoscopic and clinical data were not available. Finally, only 37 patients were included in this study.

Nevertheless, other patients with CLC who had detailed demographic information (age, gender, and location), biopsy specimens, and clinical data were included in the subsequent immunohistochemical staining study. A total of 62 specimens were immune-stained with CD31 (a blood vessels marker) and D2-40 (a lymphatic vessels marker). All the patients provided informed consent. The use of the slides of these patients was approved by the Medical Ethical Committee of the hospitals and was conducted in accordance with the Declaration of Helsinki guidelines.

The final diagnosis of CLC was made by two professional dermato-pathologists (Professor Mingliang Chen and Dr. Xiaoyan Huang). At the time of the histologic and immunohistochemistry analyses, the dermato-pathologists were blinded to the clinical data. Thereafter, the electronic medical records were reviewed by Professor Juan Su and Dr. Lixia Lu for available clinical data on age, gender, clinical morphology, anatomic distribution, symptoms, and duration of clinical findings. The clinical images and dermoscopic features were assessed by two professional dermatologists (Dr. Lixia Lu and Dr. Siyun Yan). Medicam 800/1,000 (FotoFinder, Bad Birnbach, Germany) was used as the dermatoscopic instrument.

SPSS statistics 23.0 was used for the statistical analysis. A chi-square test was used to compare the differences among various groups. $p < 0.05$ was considered statistically significant.

RESULTS

The 37 patients who were diagnosed with CLC revealed the four types of dermoscopy features. Type 1 presented with clusters of dark reddish/complexion vesicles. Several lacunae were observed to be clustered like rice (**Figure 1A**a, upper left). Dermoscopy revealed multiple reddish, white-yellowish lacunae of different sizes, some of which were filled with blood components with hypopyon-like or crescent shapes. Several lacunae contained variable amounts of blood and blood sediments, resulting in an appearance similar to that of "half-and-half" blisters (**Figure 1A**a). H&E staining revealed dilated lymphatic vessels that contain lymph and inflammatory cells (**Figure 1A**b).

Type 2 presented with complexion papules/masses. The lesions were translucent and manifested as multiple blisters that partially fused into a patch and were partially independent (**Figure 1B**a, upper left). Blisters resembling frog spawn or translucent vesicles were observed without blood inclusions; dermoscopic examination showed representative changes in CLC (**Figure 1B**a). Histological analysis also verified the dermoscopic diagnosis, whereas H&E staining revealed dilated lymphatic vessels with lymphatic fluids (**Figure 1B**b).

Type 3 showed white papules of varying sizes, with intermittent liquid efflux on the scrotum (**Figure 1C**, upper left). The independently distributed milky/whitish lacunae of different sizes and the punctate and dilated blood vessels around the papules were observed *via* dermoscopy (**Figure 1C**a). Histological analysis revealed the dilated lymphatic vessels that were positive for D2-40 (**Figure 1C**b).

The last type presented with a black/brown patch that had a clear boundary and a slightly hard texture on the right upper arm (**Figure 1D**a, upper left). This patch initially occurred as a black papule and gradually changed to a black and brown patch as it enlarged. Dermoscopic observations showed white-like circular unstructured areas distributed in the center and brown reticulate pigmentations in the periphery (**Figure 1D**a). Dermatofibroma was considered upon dermoscopic examination. However, dilated lymphatic vessels and fibroplasia were observed by H&E staining (**Figure 1D**b). Hence, the final diagnosis was CLC.

The detailed clinical manifestations are summarized in **Table 1**. The type of blister fills with a hypopyon-like/moon shape and red zone (46.0%, 17/37) and blisters resembling frog spawns (29.7%, 11/37) were the most common dermoscopic manifestations, accounting for 75.7% of the cases. The lesions were mainly distributed in the trunk (40.5%, 15/37) and limbs (29.7%, 11/37). Moreover, differential clinical diagnoses

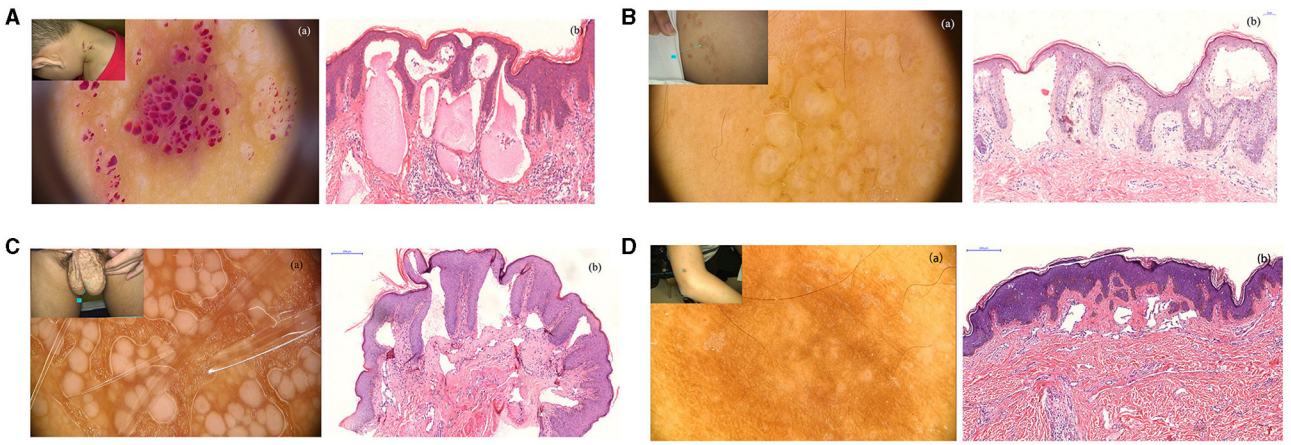

FIGURE 1 | (A) Clinical manifestations of patients with cutaneous lymphangioma circumscriptum (CLC), a cluster of vesicular dark reddish/complexion on the neck for 3 years; (a) reddish, white-yellowish lacuna of different sizes, some filled with blood as hypopyon-like or crescent shapes (non-polarized, 20×); (b) dilated lymphatic vessels with various sizes, containing lymph, erythrocytes, and inflammatory cells. (H&E stain; original magnification, 200×) (300 dpi × 300 dpi). **(B)** Clinical manifestations of patients with CLC, lacunae on the back of the left shoulder for 2 years. The patient had a history of CLC and treatment with surgery. (a) Dermatoscopic features of patients with CLC: blister resembling frog spawn or translucent vesicles (non-polarized, 20×). (b) A representative histological analysis of patients with CLC shows the lumen of different sizes and lymphangiectasis. (H&E stain; original magnification, 200×) (300 dpi × 300 dpi). **(C)** Clinical manifestations of patients with CLC, papules on the scrotum for several years, liquid intermittent efflux. (a) White unstructured areas of varying sizes, independent of each other (non-polarized, 40×). (b) A representative histological analysis of patients with CLC shown in dilated lymphatic vessels and immunohistochemical staining, showing positive D2-40 staining (H&E stain; original magnification, 100×) (300 dpi × 300 dpi). **(D)** Clinical manifestations of patients with CLC (A), brown patch enlarging gradually on the right arm. (a) White unstructured areas in the center, brown reticular pigmentation in the periphery (non-polarized, 70×). (b) A representative histological analysis of patients with CLC shown in lymphangiectasis, accompanied with fibroplasia (H&E stain; original magnification, 100×) (300 dpi × 300 dpi).

TABLE 1 | The clinical manifestations, dermatoscopic findings, and histological features of patients with cutaneous lymphangioma circumscriptum (CLC).

Dermatoscopic features	Age, y Mean ± SD(range)	Frequency *n* (%)	Gender (M:F)	Location	Clinical features	Primary diagnosis/ differential diagnosis	Histology
Hypopyon-like/crescent shape	20.4 ± 9.6 (5–36)	17 (46.0%)	1:2	Limbs (8) Trunk (5) Head and Neck (4)	Reddish and complexion papule/ plaque/mass/ Vesicular/lacunae	Angiokeratoma, Hemangioma, CLC, Verruca plana, Venous malformation, Melanoma	Dilated lymphatics, some containing lymph, erythrocytes and inflammatory cells
Blister resembling frog spawn or translucent vesicle	17.8 ± 8.6 (4–25)	11 (29.7%)	1:2.7	Limbs (3) Trunk (5) Head and Neck (3)	Complexion/yellowish/ Translucentpapule/ plaque/mass/ Vesicular/lacunae	Angiokeratoma, CLC, Hemangioma, Verruca plana, herpes zoster	Lymphangiectasia of different size
Milky/whitish lacunae	20 ± 4.9 (17–30)	5 (13.5%)	1:1.5	Scrotum (2) Trunk (3)	Papules, intermittent liquid efflux	Skin mucinosis	Dilated lymphatic vessels and D2-40 staining was positive
Brown reticulate pigmentation	24 ± 3.7 (20–36)	4 (10.8%)	1:1	Limbs (2) Trunk (2)	Brown patch, gradually enlarge	Dermatofibroma, Nevus	lymphangiectasia, accompanying with fibroplasia

included angiokeratoma, hemangioma, verruca vulgaris, venous malformation, melanoma, skin mucinosis, and nevus. The former three diagnoses were the most common differential diagnoses.

The reasons that lead to the clinical manifestations of lymphangioma as dermoscopic type 1, hypopyon-like or crescent shape, were investigated. The blood component as a contributor to lymphangioma subtypes was investigated *via* immunohistochemistry to detect CD31. Combining CD31 expression and clinical manifestations, CD31 was detected in the inner flattened endothelium of the CLC lesions and was only obvious in cystic-dilated spaces, containing sufficient blood components or lymph.

A female patient presented with transparent blister-like beads on a string in the vulva for 3 years (**Figure 2A**a), accompanied by pain and transparent secretion sometimes. H&E staining showed extended lymphatic vessels in the papillary and upper dermis and the lymph run-off (**Figure 2A**b). The immunohistochemistry for D2-40 revealed two endothelial layers (inner and outer endothelial), separated by a fluid phase, containing abundant

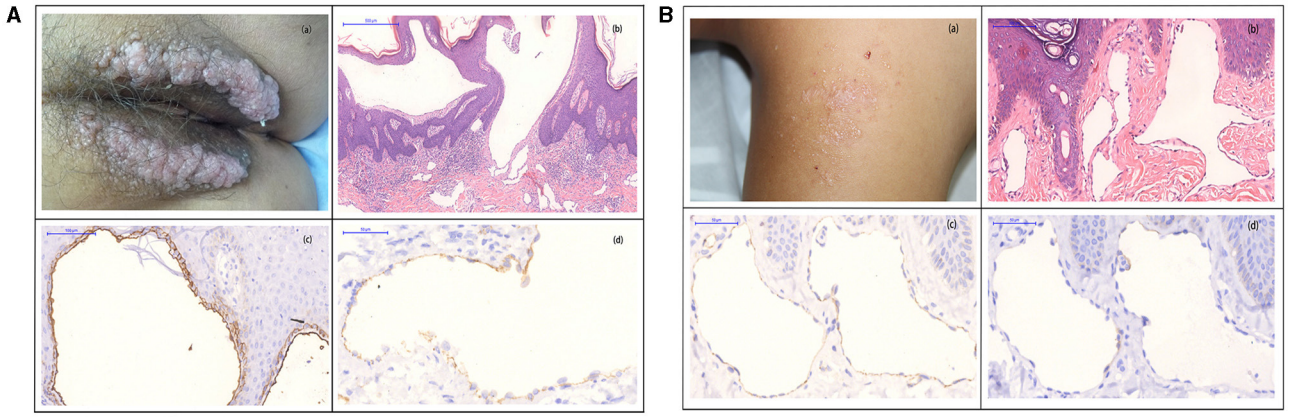

FIGURE 2 | (A) (a) Biopsy specimens were taken from transparent blister-like beads on a string from the vulva. (b) H&E staining showed cystic-dilated spaces, containing numerous erythrocytes and leukocytes in the papillary and upper reticular dermis (original magnification, 100×). (c) D2-40 staining showed two layers of the inner (red arrow) and outer (black arrow)-flattened endothelial (original magnification, 200×). (d) Immunohistochemistry showed CD31 expression in the inner-flattened endothelium (original magnification, 400×) (300 dpi × 300 dpi). **(B)** (a) Biopsy specimens were taken from the complexion papule in the dorsum, and the papule has a little lymph. (b) H&E staining showed evidently extended lymphatic vessels in the papillary and upper dermis (original magnification, 200 ×). (c) High magnification of D2-40 staining showed a single endothelial layer (red arrow), the absence of two endothelial layers of the inner- and outer-flattened endothelium (original magnification, 400×). (d) Immunohistochemical staining for CD31 showed negative expression in the flattened endothelium (original magnification, 400×) (300 dpi × 300 dpi).

TABLE 2 | Associations between the clinical manifestation and clinicopathologic characteristics of lymphangioma cases.

Variables	Clinical manifestation			*P*-value*
	With enough erythrocyte/ lymph (*N* = 34)	Without enough erythrocyte/ lymph (*N* = 28)	Total	
Age, years (*N*, %)				0.37
<31	22 (35.5%)	15 (24.2%)	37 (59.7%)	
≥31	12 (19.4%)	13 (21.0%)	25 (40.3%)	
Gender (*N*, %)				0.28
Male	25 (40.3%)	17 (27.4%)	42 (67.7%)	
Female	9 (14.5%)	11 (17.7%)	20 (32.3%)	
Location (*N*, %)				0.12
Head and neck	3 (4.8%)	6 (9.7%)	9 (14.5%)	
Trunk (including vulva)	19 (30.6%)	14 (22.6%)	33 (53.2%)	
Extremities	12 (16.1%)	8 (12.9%)	20 (32.3%)	
CD31 staining (N, %)				**1.120E-07**
Positive	29 (46.8%)	4 (6.5%)	33 (53.2%)	
Negative	5 (8.1%)	24 (38.7%)	29 (46.8%)	
Endothelia layer (*N*, %)				**3.6945E-09**
Monolayer	28 (45.2%)	2 (3.2%)	30 (87.1%)	
Multilayer	6 (9.7%)	26 (41.9%)	32 (12.9%)	

*Analysis by χ^2 test or Fisher's exact-test; For the 62 lymphangioma cases, the median age of the whole group of patients was 31 years (range, 4–78 years). *significant association, if present. The bold values means significant association, if present.*

erythrocytes and lymph. The inner endothelium is flattened, whereas the outer layer is rounded (**Figure 2A**c). The two endothelial layers were absent in the space, containing few or no blood and lymph. CD31 staining showed expression in the inner-flattened endothelium (**Figure 2A**d).

Another male patient presented to us with a small and flattened complexion papule in the dorsum for 5 years (**Figure 2B**a). A laser was used, but it was recurrent after 3 months of treatment. H&E staining showed evidently extended lymphatic vessels in the papillary and upper dermis (**Figure 2B**b). D2-40 staining presented a single endothelial layer, but no two distinctive layers (**Figure 2B**c). CD31 staining showed no expression in the flattened endothelium (**Figure 2B**d).

Associations among the clinical manifestation and clinicpathological characteristics of lymphangioma are summarized in **Table 2**. The median age was 31 years old, and males accounted for the majority of the patients (67.7%, 42/62). Lesions were mainly distributed in the trunk and extremities (85.4%, 53/62). The patients were then divided into two groups according to their clinical manifestations, namely, with and without abundant blood components or lymph. The variables (age, gender, and location) of the patients showed no statistical significance. However, CD31 staining was positive, and the two endothelial layers were obvious in the spaces containing erythrocytes and lymph. This phenomenon was not observed in lymphangioma characterized by the absence of blood and lymph.

DISCUSSION

This work systematically reviewed the available evidence of the dermoscopic structures among lymphangiomas and investigated why some lymphangiomas are marked by blood components. We speculated that these characteristics can be used to differentiate CLC from other diseases, including angiokeratomas, venous

malformations, melanomas, hemangiomas, verruca plana, and herpes zoster. A lymphangioma is a benign tumor that occurs in the lymphatic system. It is regarded as a congenital malformation of the lymphatic vessel or lymphatic vessel hyperplasia. Clinically and pathologically, a lymphangioma is divided into three categories: simple lymphangioma, cavernous lymphangioma, and cystic lymphangioma associated with lymphatic malformation (14). A lymphangioma is characterized by lesions involving lymphatic and blood vessels. The histopathological features of CLC are presented as highly dilated lymphatic vessels lined with squamous epithelial cells, which are rich with lymphatic liquid and lymphocytes and sometimes mixed with blood (15).

Dermoscopy is a non-invasive, *in vivo* imaging technique that allows for the visualization of subsurface skin structures. According to the literature, CLC displays two distinct dermoscopical patterns: the yellow-pale septa pattern in the absence of erythrocytes and the yellow to red/pink/bluish lacunae pattern due to the presence of blood (15, 16). Our study also verified that these two patterns had the highest proportion in the patients, accounting for 75.5% of the total cases. Aside from the common dermoscopic patterns, two previously undescribed types of CLC, namely, milky/whitish lacunae and brown reticulate pigmentations, were also observed. The milky/whitish lacunae pattern must be differentiated from skin mucinosis, whereas the brown reticulate pattern should be differentiated from dermatofibroma and pigmented nevus. The deepest skin structure observed by dermoscopy was the papilla layer; so, when the dilated lymphatic vessels are located under the dermal papilla, the dermoscopy cannot observe it well. Our study presents a summary and a supplement to existing dermoscopic manifestations of lymphangioma and provides assistance in the diagnosis of lymphoma and selection of the appropriate treatments. As we all know, the recurrence rate is high in CLC (17). A retrospective study showed that a recurrent rate of 29% was found in 196 lesions of 186 patients during 3 years. Approximately 60% of patients with relapse recurred within 1 year and 80% recurred within 3 years (18). Therefore, follow-up is necessary.

Among the 584 patients with lymphangioma, only 37 patients were examined *via* dermoscopy, suggesting that the use of dermoscopy needs to be improved. Dermoscopy can distinguish CLC from hemangiomas, melanomas, and other phenotypically similar skin lesions. There are no departments of pathology in primary hospitals and township health centers. Hence, dermoscopy can be a useful tool in the diagnosis of CLC that may, otherwise, be missed in hospitals without pathology departments. However, dermoscopy can only reflect the pathological mapping of superficial skin lesions. Thus, dermoscopy can sometimes easily lead to misdiagnosis. Clinical examination should be combined with various methods, and a biopsy should be performed as necessary to make a correct diagnosis.

The reason CLC contains blood components was explored *via* immunohistochemistry to detect CD31 expression in CLC. Bhawan et al. reported CD31 expression in endothelial cells in lymphangiomas (19). However, the relationship between CD31 expression and the clinical manifestations of CLC remains uncertain. Our results showed that the two endothelial layers were only obvious in cystic-dilated spaces, containing abundant erythrocytes or lymph. Oiso et al. reported that a lymphangioma with reddish vesicles contains two flattened endothelial layers, but the lumen of yellowish vesicles lacks such manifestations (12). Our results were consistent with that observation. The double layer of endothelial cells in the lumen with hypopyon-like or crescent-shaped CLC was also found in cystic-dilated spaces filled with lymph. Our results may shed light on the pathogenesis of frequent blood leakage inside dilated spaces in CLC.

DATA AVAILABILITY STATEMENT

The original contributions presented in the study are included in the article/supplementary material, further inquiries can be directed to the corresponding authors.

ETHICS STATEMENT

The patients in this manuscript have given written informed consent to publication of their case details and the use of patients' biopsy slides was approved by the Medical Ethical Committee of Xiangya hospital, Central South University and was conducted per the Declaration of Helsinki guidelines.

AUTHOR CONTRIBUTIONS

LL and SY: writing-review and editing, preparation, creation and/or presentation of the published work by those from the original research group, specifically critical review, commentary, or revision - including pre- or post-publication stages, investigation, conducting a research and investigation process, specifically performing the experiments, or data/evidence collection, and formal analysis, application of statistical, mathematical, computational, or other formal techniques to analyze or synthesize study data. LL, JS, SY, and XH: writing-original draft preparation, creation and/or presentation of the published work, and specifically writing the initial draft (including substantive translation). JS and XH: supervision, oversight and leadership responsibility for the research activity planning and execution, and including mentorship external to the core team. LL, SY, and MC: data curation, management activities to annotate (produce metadata), scrub data, and maintain research data (including software code, where it is necessary for interpreting the data itself) for initial use and later reuse. JS and XH: conceptualization, ideas and formulation or evolution of overarching research goals and aims. All authors contributed to the article and approved the submitted version.

FUNDING

This study was funded by grants from the National Natural Science Foundation of China (Grant No. 81974478 to JS) and the Hunan Provincial Natural Science Fund (Grant No. 2019JJ40498 to MC).

ACKNOWLEDGMENTS

We thank JS, Xiangya Hospital, Central South University (87# Xiangya Road, Changsha, 410008, Hunan, China. Tel:+86-15116408921; Fax: 0086-731-84327332; Mail: sujuanderm@csu.edu.cn) for supervising this study. Thanks Dr. Zhenwei Tang for the English revision in this paper.

REFERENCES

1. Indrani S, Agarwal S. Cutaneous lesions from lymphangioma circumscriptum. *ANZ J Surg*. (2017) 87:e20–1. doi: 10.1111/ans.12930
2. Fatima S, Uddin N, Idrees R, Khurram M, Ahmad Z, Ahmad R, et al. Lymphangioma circumscriptum: clinicopathological spectrum of 29 cases. *J Coll Physicians Surg Pak*. (2015) 25:658–61.
3. Patel GA, Schwartz RA. Cutaneous lymphangioma circumscriptum: frog spawn on the skin. *Int J Dermatol*. (2009) 48:1290–5. doi: 10.1111/j.1365-4632.2009.04226.x
4. Zaballos P, Del Pozo LJ, Argenziano G, Karaarslan IK, LandiC, Vera A, et al. Dermoscopy of lymphangioma circumscriptum: a morphological study of 45 cases. *Aust J Dermatol*. (2018) 59:e189–93. doi: 10.1111/ajd.12668
5. Gencoglan G, Inanir I, Ermertcan AT. Hypopyon-like features: new dermoscopic criteria in the differential diagnosis of cutaneous lymphangioma circumscriptum and haemangiomas? *J Eur Acad Dermatol Venereol*. (2012) 26:1023–5. doi: 10.1111/j.1468-3083.2011.04136.x
6. Braun RP, Kaya G, Masouye I. Krischer J, Aaurat JH. Histopathologic correlation in dermoscopy: a micropunch technique. *Arch Dermatol*. (2003) 139:349–51. doi: 10.1001/archderm.139.3.349
7. Richey PM, Norton SA. John Tyndall's Effect on Dermatology. *JAMA Dermatol*. (2017) 153:308. doi: 10.1001/jamadermatol.2016.0505
8. Ronger-Savle S, Julien V, Duru G, Raudrant D, Dalle S, Thomas L. Features of pigmented vulval lesions on dermoscopy. *Br J Dermatol*. (2011) 164:54–61. doi: 10.1111/j.1365-2133.2010.10043.x
9. Masushita S, Kageshita T, Ishihara T. Comparison of dermoscopic and histopathological finding in a mucous melanoma of the lip. *Br J Dermatol*. (2005) 152:1324–6. doi: 10.1111/j.1365-2133.2005.06463.x
10. Martin JM, Bella-Navarro R, Jorda E. Vascular patterns in dermoscopy. *Actas Dermo Sifiliogr*. (2012) 103:357–75. doi: 10.1016/j.adengl.2012.06.007
11. Massa AF, Menezes N, Baptista A, Moreira AI. Ferreira EO. Cutaneous Lymphangioma circumscriptum - dermoscopic features. *An Bras Dermatol*. (2015) 90:262–4. doi: 10.1590/abd1806-4841.20153652
12. Oiso N, Itoh T, Miyake M, Satou T, Kawada A. Cutaneous lymphangioma circumscriptum with marked blood presence: histopathologic evaluation of the endothelial cells. *Eur J Dermatol*. (2014) 24:127–8. doi: 10.1684/ejd.2013.2248
13. Novinska MS, Rathore V, Newman DK, et al. *Chapter 11 - Pecam-1. Platelets*. 2nd ed. Cambridge, MA: Academin Press (2007). p. 221–30.
14. Wang J-Y. Liu L-F, Mao X-H. Treatment of lymphangioma circumscriptum with topical imiquimod 5% cream. *Dermatol Surg*. (2012) 38:1566–9. doi: 10.1111/j.1524-4725.2012.02528.x
15. Amini S, Kim NH, Zell DS, Oliviero MC. Rabinovitz HS. Dermoscopic-histopathologic correlation of cutaneous lymphangioma circumscriptum. *Arch Dermatol*. (2008) 144:1671–2. doi: 10.1001/archderm.144.12.1671
16. Arpaia N, Cassano N, Vena GA. Dermoscopic features of cutaneous lymphangioma circumscriptum. *Dermatol Surg*. (2006) 32:852–4. doi: 10.1111/j.1524-4725.2006.32174.x
17. Browse NL, Whimster I, Stewart G, Helm CW, Wood JJ. Surgical management of 'lymphangioma circumscriptum'. *Br J Surg*. (1986) 73:585–8. doi: 10.1002/bjs.1800730724
18. Alqahtani A, Nguyen LT, Flageole H, Shaw K, Laberge JM. 25 years' experience with lymphangiomas in children. *J Pediatr Surg*. (1999) 34:1164–8. doi: 10.1016/s0022-3468(99)90590-0
19. Bhawan J, Silva C, Taungjaruwinai WM. Inconsistent immunohistochemical expression of lymphatic and blood endothelial cell markersin cutaneous lymphangiomas. *J Cutan Pathol*. (2013) 40:801–6. doi: 10.1111/cup.12184

Conflict of Interest: The authors declare that the research was conducted in the absence of any commercial or financial relationships that could be construed as a potential conflict of interest.

frontiers | Frontiers in Medicine

TYPE Original Research
PUBLISHED 07 September 2022
DOI 10.3389/fmed.2022.987696

OPEN ACCESS

EDITED BY
Salvador Gonzalez,
University of Alcalá, Spain

REVIEWED BY
Philippe Lefrançois,
McGill University, Canada
Natasa Krsto Rancic,
University of Niš, Serbia

*CORRESPONDENCE
Elisa Zavattaro
elisa.zavattaro@med.uniupo.it

SPECIALTY SECTION
This article was submitted to Dermatology, a section of the journal Frontiers in Medicine

RECEIVED 06 July 2022
ACCEPTED 01 August 2022
PUBLISHED 07 September 2022

CITATION
Veronese F, Seoni S, Tarantino V, Buttafava M, Airoldi C, Meiburger KM, Zavattaro E and Savoia P (2022) AKASI and Near-Infrared Spectroscopy in the combined effectiveness evaluation of an actinic keratoses preventive product in immunocompetent and immunocompromised patients. *Front. Med.* 9:987696. doi: 10.3389/fmed.2022.987696

AKASI and Near-Infrared Spectroscopy in the combined effectiveness evaluation of an actinic keratoses preventive product in immunocompetent and immunocompromised patients

Federica Veronese[1], Silvia Seoni[2], Vanessa Tarantino[1], Matteo Buttafava[3], Chiara Airoldi[4], Kristen M. Meiburger[2], Elisa Zavattaro[1,4]* and Paola Savoia[1,3,5]

[1]SCDU Dermatologia, AOU Maggiore della Carità, Novara, Italy, [2]Biolab, PolitoBIOMed Lab, Department of Electronics and Telecommunications, Politecnico di Torino, Turin, Italy, [3]School of Medicine, University of Eastern Piedmont, Novara, Italy, [4]Department of Translational Medicine, University of Eastern Piedmont, Novara, Italy, [5]Department of Health Sciences, University of Eastern Piedmont, Novara, Italy

Introduction: The high incidence of actinic keratoses among both the elderly population and immunocompromised subjects and the considerable risk of progression from *in situ* to invasive neoplasms makes it essential to identify new prevention, treatment, and monitoring strategies.

Objective: The aim of this study was to evaluate the efficacy on AKs of a topical product (®Rilastil AK Repair 100 +) containing high-protection sunscreens, a DNA Repair Complex with antioxidant and repairing action against UV-induced DNA damage, and nicotinamide, a water-soluble derivative of vitamin B3 that demonstrated several photoprotective effects both *in vitro* and *in vivo*.

Methods: The study enrolled 74 Caucasian patients, which included 42 immunocompetent and 32 immunosuppressed subjects. The efficacy of the treatment has been evaluated through the clinical index AKASI score and the non-invasive Near-Infrared Spectroscopy method.

Results: The AKASI score proved to be a valid tool to verify the efficacy of the product under study, highlighting an average percentage reduction at the end of treatment of 31.37% in immunocompetent patients and 22.76% in organ transplant recipients, in comparison to the initial values, with a statistically significant reduction also in the single time intervals (T0 vs. T1 and T1 vs. T2) in both groups. On the contrary, the Near-Infrared Spectroscopy (a non-invasive technique that evaluates hemoglobin relative concentration variations) did not find significant differences for O_2Hb and HHb signals before and after the

treatment, probably because the active ingredients of the product under study can repair the photo-induced cell damage, but do not significantly modify the vascularization of the treated areas.

Conclusion: The results deriving from this study demonstrate the efficacy of the product under study, confirming the usefulness of the AKASI score in monitoring treated patients. Near-Infrared Spectroscopy could represent an interesting strategy for AK patients monitoring, even if further large-scale studies will be needed.

KEYWORDS

prevention, immunosuppression, actinic keratoses, AKASI, NIRS

Introduction

In the last decades, the concept of "field cancerization" (FC), a biological process in which large skin surfaces are affected by carcinogenic alterations, and the consequent need for treatment of actinic keratoses (AKs), has become more and more important.

Figueras-Nart et al. has recently defined the skin FC as an area affected by multiple AKs, together with visible sun damage and at least two of the following characteristics: atrophy, telangiectasias, hypo/hyperpigmented skin and "glass paper skin" (1). In this area, histologically, it is possible to recognize sub-clinical lesions with atypical keratinocytes, nuclear pleomorphism, loss of cell polarity, dermal solar elastosis and vascular ectasia (2), together with obvious AKs, that are characterized by the presence of parakeratosis and lymphocytic infiltrate (3).

Patients with FC have a higher risk of developing Squamous Cell Carcinoma (SCC) than individuals with isolated AKs (4). For this reason, it's important to treat the whole FC since the treatment of the single lesion is associated to the risk of evolution of the visible and sub-clinical AKs of the surrounding area (5).

In literature, the annual risk of evolution in invasive SCC (iSCC) is estimated of 0.075% for a single AK in individuals without a personal history of Non-Melanoma Skin Cancer (NMSC) and 0.53% for individuals with previous lesions (6). Also, NMSCs are the most frequent cancers in immunosuppressed patients, with 27% of patients affected, and steady incidence increase over the years as the immunosuppression time progresses (7, 8).

In this context, not only the treatment but also the prevention of the development and evolution of AKs acquires a fundamental role. The use of photoprotection is recommended as an adjuvant for any type of treatment (9, 10). Daily use of sunscreen with SPF 50 + favors the spontaneous regression of AKs and reduces the incidence of iSCC in both immunocompetent and immunosuppressed patients (8, 10–12).

However, sunscreens protect against UV-induced DNA damage but are not effective once the damage has been established; for this reason, Krutmann et al. (13) report that, especially in high- and very high-risk subjects (**Table 1**), active ingredients capable of repairing DNA damage (e.g., endonuclease and photolyase) should be employed during the whole year.

Several studies have been recently conducted on devices containing sunscreens (SPF 50–100 +) and DNA repair enzymes (10, 14–16); in particular, in 2019 we carried out a study concerning the efficacy of the product ®Rilastil AK Repair 100 + (a photoprotector containing SPF UVB 131 and UVA 53, and a DNA Repair Complex (DRC) with antioxidant and repairing action against UV-induced DNA damage) compared to a simple photoprotector (17).

The product formulation is reported in **Table 2** and has been recently modified with the introduction of nicotinamide instead of vitamin E. In this paper, we used the clinical index for AKs AKASI score and a non-invasive Near-Infrared Spectroscopy (NIRS) method to evaluate the efficacy of the new product formulation.

Materials and methods

Study design

This was a prospective observational study conducted in our Dermatology Unit, in Novara (Italy). Continuous enrollment was carried out between patients visited both in general clinics and in those specifically dedicated to transplant carriers from March to September 2021, with a follow-up extended until February 2022. The study protocol was approved by the Local Ethical Committee (CE80/18) and was conducted in accordance with the Helsinki's Declaration.

TABLE 1 Patients requiring use of sunscreens and DNA repair ingredients.

High-risk	Very high-risk
Presence of Aks	Presence of > 10 Aks in the FC
Previous treatment for Aks	Immunosuppressed patients or organ transplant recipients (OTRs)
Previous NMSC in immunocompetent patients	Patients affected by Xeroderma Pigmentosus
Patients with clinical signs of skin photodamage	

TABLE 2 ®Rilastil AK Repair 100 + composition.

Active principles	Function
Physical and Chemical filters UVB-UVA	Photoprotection
DNA Repair Complex (amino acids, vegetable hydrolyzed proteins, ATP)	DNA repair and antioxidant
Epigallocatechin gallate	Antioxidant
Nicotinamide	Photoprotection and anti-inflammatory

The study population consisted of 74 Caucasian patients: 42 immunocompetent and 32 immunosuppressed, among which 31 organ transplant recipients (OTRs) and 1 under treatment with Teriflunomide. Inclusion criteria were: i) age > 40 years; ii) clinical evidence of AKs (grade I or II) on the face and scalp; iii) personal history of previous NMSC; and, only for OTRs, iv) immunosuppressive treatment for at least 5 years; exclusion criteria were represented by the incapacity to sign the informed consent and to properly apply the products or by the presence of genetic disorders conditioning the development of NMSCs (i.e., Gorlin-Goltz syndrome, Xeroderma Pigmentosums, Epidermodysplasia Verruciformis).

At the baseline visit (T0) we collected the information about patient personal data (gender, age), endogenous and exogenous risk factor (phototype, previous actinic burns, history of NMSC, occupational and/or recreational UV exposure, artificial UV exposure, use of sunscreens), and previous treatment for AKs. The participants were instructed to apply the product under study (®Rilastil AK Repair 100 +) to the photo-damaged areas twice daily (morning and early afternoon) for 6 months. The cream was provided by the manufacturer (Ganassini Corporate, Milano) to patients free of charge; patients were asked to return the finished tubes, to verify the application of the correct amount of the product.

The patients were re-evaluated after 3 (T1) and 6 (T2) months. At each visit, photographic documentation was collected, and the AKASI score was calculated, based on literature suggestions (18, 19). In detail, the head was divided into four regions (scalp, forehead, left/right cheek, ear, chin, and nose). In each region, the percentage of the area affected by AKs was estimated (score 0–6), and the severity of three clinical AK signs (distribution, erythema, and thickness) was assessed (score 0–4 for each parameter). The total score ranges from 0 to 18 (18).

Fifteen patients (8 immunocompetent and 7 immunosuppressed) were also evaluated through NIRS spectroscopy at T0 and T2. In collaboration with PoliToBIOMed Lab (Turin Polytechnic University) we acquired the change in the relative concentration of oxygenated (O_2Hb) and deoxygenated (HHb) hemoglobin (Hb), using the commercial device NIRO® 200-NX (Hamamatsu). The signals were acquired at a sampling frequency of 5 Hz. All signals were filtered using a band-pass Chebyshev filter, in order to remove the frequencies outside the range 10–250 mHz. The instrument has two probes: the emitter (LED light source with wavelengths of 735–810 nm) and the detector (a photodiode). The distance between the two probes influences the depth of the analyzed area and the assessed area of the body. For our application, we placed the probes at a distance of 2.5 cm from each other, in order to analyze the superficial area under the skin. For each patient, signals were acquired both on healthy skin (no UV-induced damage) and on the AK site (before and after treatment) (**Figure 1**).

For the evaluation of the vascular response of the tissue, the NIRS signals were acquired according to the following protocol (20, 21):

- acquisition of the baseline signal for 1.5 min.
- application of an ice pack near the probes (vasoconstrictor stimulus) for 1.5 min.
- removal of the ice pack and acquisition of vascular response for 1.5 min.

This acquisition protocol allows us to verify if there is a different vascular response to a vasoconstrictor stimulus (i.e., the ice pack application) between T0 and T2.

Statistical analysis

We performed a descriptive analysis of the whole study population and separately for immunocompetent and immunosuppressed. Absolute and relative frequencies were reported for categorical data while, for numerical one, we used mean and standard deviations (SD) or median and interquartile range, as appropriate. Demographic and clinical data between immunocompetent and immunosuppressed were compared and results of chi-square or Fisher test and *t*-test were reported. Moreover, the AKASI score at T0 was calculated for different levels of risk factor and *t*-tests were performed.

Then, we evaluated the differences of AKASI score between time (T1 vs. T0 and T2 vs. T0) separately for immunocompetent

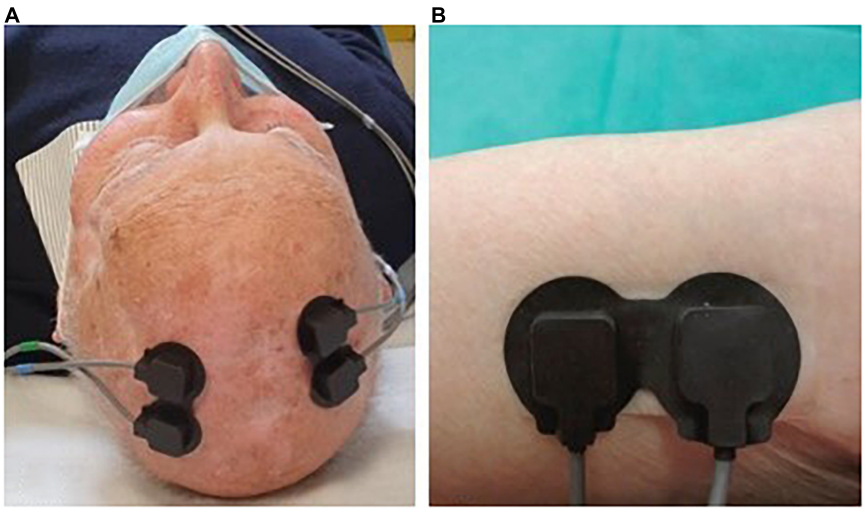

FIGURE 1
Example of positioning the probes on Aks **(A)** and on healthy skin **(B)**.

and immunosuppressed and statistical significativity was tested using Wilcoxon paired *t*-tests. We also compared the difference among the two groups of patients. Moreover, we calculated the percentage variation in time between time. Finally, the proportion of subjects who achieved a reduction of at least 50–75–100% in AKASI score at the end of the study was also evaluated.

For the NIRS signal analysis, the dataset consists of 18 signals acquired on the lesion before and after treatment with the cream. Three patients presented more than one lesion on which the NIRS analysis was done, hence increasing the NIRS dataset by 3 when compared to the number of analyzed subjects. The signals were divided into three moments of acquisition (baseline, ice application and after ice removal). The analyzed epochs are the following:

- O_2Hb before: variation in oxygenated Hb concentration before ice application;
- O_2Hb after: variation after ice pack application;
- HHb before: variation of the deoxygenated Hb concentration before ice application;
- HHb after: variation after ice application (see **Figure 2**).

During the ice pack application, the signals were often corrupted by artifacts, such as the motion artifacts, hence only the baseline and after ice removal epochs were analyzed. For all signals acquired on the lesion, pre- and post-treatment and on healthy skin, 18 parameters were estimated, 14 in the time domain and 4 in the frequency domain. The AK lesion parameters before and after-treatment were normalized with the parameters of the healthy skin, maintaining the correspondence of the patient.

A multivariate analysis of variance (MANOVA) was applied to the 18 time and frequency parameters to the verify if there were statistical differences between the vascular response before and after the treatment. The *p*-value and MANOVA dimension (d) were used to determine whether the two groups showed statistically significant differences and could be considered as belonging to two separate groups ($d = 1$). The statistical analysis was composed by 4 MANOVA tests (HHb before, HHb after ice application, O_2Hb before and O_2Hb after ice application), and for this we applied the Bonferroni correction to re-define the significance level α equal to 0.0125 (i.e., 0.05/4).

The clinical data collected were analyzed with SAS 9.4 software and the significance level was set at 0.05.

Results

Clinical characteristics of the study population

The statistical analysis was performed considering separately the immunocompetent and immunocompromised subjects. General analyses at T0 were conducted to verify any statistically significant differences between these two populations.

The clinical characteristics and risk factors of the study population, global and specific of the two subgroups, are reported in **Table 3**. Particularly, the mean ± SD value of AKASI score found in the total of subjects at T0 was equal to 3.92 ± 2.20; in the immunocompetent population, it was 4.47 ± 2.26, while among the immunosuppressed it was 3.21 ± 1.94.

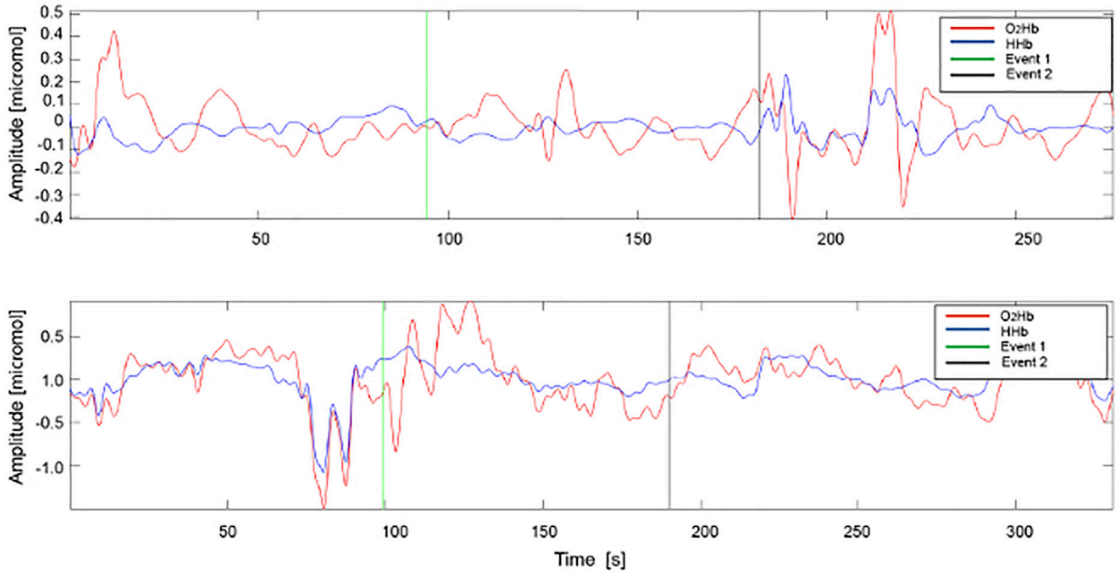

FIGURE 2
Example of acquisition of O_2Hb and HHb signals in AK before **(A)** and after **(B)** treatment. HHb signals are represented in blue and O_2Hb signals in red. Event 1: ice application, Event 2: ice removal.

Previous treatment for AKs had been overall carried out by 63 (85.14%) subjects (36 immunocompetent and 27 immunosuppressed). Moreover, 17 subjects (22.97%), reported previous use of a similar product.

From this preliminary analysis, it emerged that immunocompetent patients had a significantly higher average age than immunosuppressed subjects (respectively 77.67 ys and 68.16 ys); moreover, the percentage of subjects with phototype II was significantly higher among the immunocompetent than immunosuppressed (88.10% vs. 28.13%). It should be noted that all subjects included in the study, both in the immunocompetent subgroup and in the transplant subgroup, had phototype II or III.

There was also a statistically significant difference in the two groups regarding the previous use of photoprotectors, which was higher in immunosuppressed patients (50% vs. 21.43%), with a *p*-value of 0.010.

Therefore, we analyzed all the possible associations between known risk factors for AKs and the AKASI score at T0; in addition, the association between the AKASI score at T0 and the presence or absence of previous treatments for AKs, use of analogs of the medical device under study and other NMSCs was also evaluated.

The difference in the mean AKASI score at T0 between immunosuppressed and immunocompetent patients reaches a *p*-value of 0.013 (3.21 ± 1.94 and 4.47 ± 2.26, respectively).

The 46 subjects with phototype II have an average AKASI score of 4.37 ± 2.18 at the time of enrollment, while the 28 subjects with phototype III of 3.19 ± 2.08 (*p*-value 0.024).

Finally, the 54 subjects with a previous NMSC diagnosis have an average AKASI score at T0 of 4.29 ± 2.29, and the 20 subjects without previous NMSC of 2.95 ± 1.63 (*p*-value 0.019).

Subsequently, the partial AKASI scores were analyzed in the 74 subjects at T0 and an average AKASI score on the scalp was found to be greater than the other three partial areas.

All the results are reported in Table 4.

Response to treatment

Overall, from the 74 patients treated with® Rilastil AK Repair 100 +, 6 patients between T0 and T1 and 4 patients between T1 and T2 were lost to follow-up. So, the analysis of the AKASI score trend resulting from the treatment was carried out on 68 patients (39 immunocompetent and 29 immunosuppressed) between T0 and T1 and 64 patients (37 immunocompetent and 27 immunosuppressed) between T0 and T2.

The AKASI seemed to decrease among time: at T0 the mean score was 3.92 (SD 2.20), at T1 3.16 (SD 2.05) while in the last visit it was 2.73 (SD 1.64). When we analyzed immunocompetent and immunosuppressed separately, we observed that the score had a significant reduction in time (all *p*-values < 0.001). Moreover, we were not able to see a significant differences of AKASI in time (T1 vs. T0 and T2 vs. T0) between the two groups of patients (*p*-value 0.444 and 0.006, respectively). In Table 5 we reported also the percentage reduction of AKASI between time (part A) and we observed that among T0-T2 there was an average percentage reduction

TABLE 3 A descriptive comparison of risk factors and anamnestic data between the two groups of patients.

	Total patients (n = 74)		Immunocompetent (n = 42)		Immunosuppressed (n = 32)		p-value
	N	%	N	%	N	%	
Gender							
Female	12	16.22	9	21.43	3	9.38	0.163
Male	62	83.78	33	78.57	29	90.63	
Age							
Mean ± SD		73.55 ± 10,61		77.67 ± 9,30		68.16 ± 9.89	**<0.001**
Outdoor Profession							
Yes	27	36.49	14	33.33	13	40.63	0.518
No	47	63.51	28	66.67	19	59.37	
Phototype							
II	46	62.16	37	88.10	9	28.13	**<0.001**
III	28	37.84	5	11.90	23	71.88	
Previous sun exposure							
Intensive	41	55.41	24	57.14	17	53.13	0.735
Occasional	33	44.59	18	42.86	15	46.87	
Use of photoprotectors							
Yes	25	33.78	9	21.43	16	50	**0.010**
No	49	66.22	33	78.57	16	50	
Previous actinic burns							
Yes	35	47.30	21	50	14	43.75	0.593
No	39	52.7	21	50	18	56.25	
Artificial UV exposure							
Yes	5	6.76	3	7.14	2	6.25	0.879
No	69	93.24	39	92.86	30	93.75	
AKASI score T0							
Mean ± SD		3.92 ± 2.20		4.47 ± 2.26		3.21 ± 1.94	**0.0013**
Previous NMSC							
Yes	54	72.97	31	73.81	23	71.88	0.852
No	20	27.03	11	26.19	9	28.12	
Previous NMSC type (n = 54)							
SCC	14	25.93	9	29.03	5	21.74	0.7461
BCC	26	48.15	15	48.39	11	47.83	
SCC and BCC	14	25.93	7	22.58	7	30.43	
Previous Aks treatment							
Yes	63	85.14	36	85.71	27	84.38	0.872
No	11	14.86	6	14.29	5	15.62	
Treatments type							
Photodynamic therapy	3	4.05	2	4.76	1	3.13	0.723
Local therapy*	25	33.78	13	30.95	12	37,50	0.555
Surgery	37	50	18	42.86	19	59,38	0.159
Cryotherapy	54	72.97	32	76.19	22	68.75	0.475
Use of analogs of ® AK Repair							
Yes	17	22.97	8	19.05	9	28.13	0.357
No	57	77.03	34	80.95	23	71.87	

Statistically significant values are in bold. * The following therapies are included: imiquimod, 5% -FU, piroxicam, ingenol mebutate.

TABLE 4 Association between risk factors and anamnestic data with the mean AKASI score at T0.

Variable	N	AKASI score T0 mean ± SD	AKASI score T0 median (IQR)	*p*-value
Gender				
Female	12	3.13 ± 1,81	3.40 (2.7)	0.176
Male	62	4.08 ± 2.25	3.60 (3.4)	
Immunosuppression				
Yes	32	3.21 ± 1.94	2.50 (2.8)	**0.013**
No	42	4.47 ± 2,26	4.20 (2.4)	
Outdoor profession				
Yes	27	4.02 ± 2.01	3.60 (3.2)	0.774
No	47	3.87 ± 2.33	3.60 (3.4)	
Phototype				
II	46	4.37 ± 2.18	4.10 (2.4)	**0.024**
III	28	3.19 ± 0.08	2.40 (3.3)	
Previous sun exposure				
Intensive	41	4.35 ± 2.43	3.80 (3.6)	0.062
Occasional	33	3.39 ± 1.78	3.20 (2.6)	
Use of photoprotection				
Yes	25	3.33 ± 1.84	2.60 (2.8)	0.096
No	49	4.23 ± 2.33	4 (2.8)	
Previous actinic burns				
Yes	35	4.34 ± 2.14	4.20 (2.8)	0.127
No	39	3.55 ± 2.22	3.40 (2.8)	
Artificial UV exposure				
Yes	5	4.60 ± 4.03	4 (2,4)	0.481
No	69	3.88 ± 2.06	3.60 (3.2)	
Previous NMSC				
Yes	54	4.29 ± 2.29	3.90 (3.2)	**0.019**
No	20	2.95 ± 1.63	2.80 (2.2)	
Previous NMSC type (*n* = 54)				
SCC	14	4.03 ± 2.03	3.60 (3)	0.129
BCC	26	3.85 ± 2.41	3.40 (3)	
SCC and BCC	14	5.34 ± 2.12	5.40 (2)	
Use of analogs of Rilastil AK repair				
Yes	17	4.31 ± 1.91	3.80 (2.4)	0.419
No	57	3.81 ± 2.29	3.40 (3.2)	
Partial AKASI score at T0 (Mean ± SD)				
Scalp		1.55 ± 1.63		
Forehead		0.89 ± 0.72		
Right half face		0.79 ± 0.64		
Left half face		0.70 ± 0.63		

Statistically significant values are in bold. At the bottom of the table, AKASI score averages stratified based on the location.

in AKASI score of 31.37% for immunocompetent and 22.76% among immunosuppressed patients (part B).

Then, we calculated the number (and the relative percentages) of subjects who had an improvement in AKASI scores at the end of the study of 50%, 75%, and 100% (Figure 3).

TABLE 5 The AKASI reduction in time in both immunocompetent and immunosuppressed patients.

PART A	Period evaluated	Patients evaluated	Difference of mean ± SD
Immunocompetent	T0-T1	39	−0.76 ± 1.33
	T0-T2	37	−1.59 ± 1.58
Immunosuppressed	T0-T1	29	−0.90 ± 1.07
	T0-T2	27	−0.90 ± 1.30
PART B	**Period evaluated**	**Patients evaluated**	**Mean percentage changes ± SD**
Immunocompetent	T0-T1	39	−14.11% ± 31.68
	T0-T2	37	−31.37% ± 40.08
Immunosuppressed	T0-T1	29	−25.17% ± 37.12
	T0-T2	27	−22.76% ± 35.37

In the immunocompetent group, the AKASI 100 (complete clearance) was achieved by 2 patients (5.41%), the AKASI 75 by 3 (8.11%), and the AKASI 50 by 10 (27.03%).

In the immunosuppressed group, no patient achieved an AKASI 100, whereas AKASI 75 was reached by 1 patient (3.70%) and AKASI 50 in 5 (18.52%).

In Figure 4 the clinical images of two treated patients, from T0 to T2, are reported.

NIRS results

Analysis with NIRS spectroscopy was conducted at T0 and T2 on a smaller group of 15 patients (8 immunocompetent and 7 immunosuppressed).

The MANOVA did not show significant differences for the O_2Hb and HHb signals in the two analyzed epochs (before and after ice application) between pre- and post-treatment (Table 6).

The *p*-value and d (dimension of the space in which the variances of the groups fall) allow us to understand if the two groups show statistical differences and therefore can be considered as two distinct groups (d = 1). In our case, the calculated values do not allow a distinction.

Figure 5 shows the first two canonical variables estimated through the MANOVA, in the four conditions of the O_2Hb and HHb signals before and after ice application.

Discussion

The rising incidence of AKs, in particular in immunosuppressed subjects, and the high risk of evolution of these "*in situ*" neoplasms toward invasive tumors, make their treatment and the identification of appropriate tools for response monitoring essential.

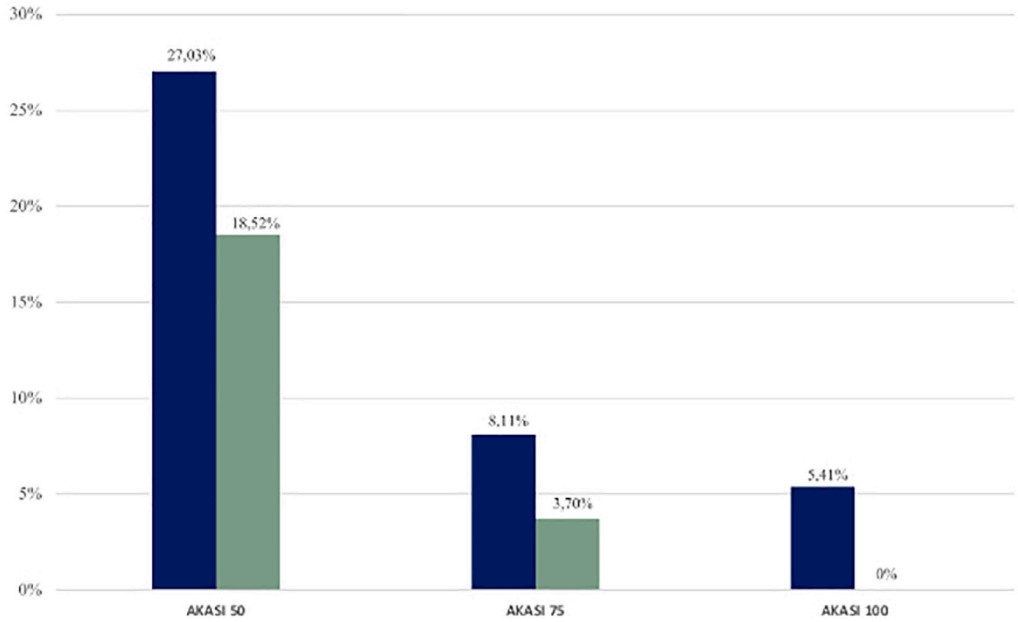

FIGURE 3
Percentages of immunocompetent (blue) and immunosuppressed (green) patients who achieved AKASI 50, 75, and 100.

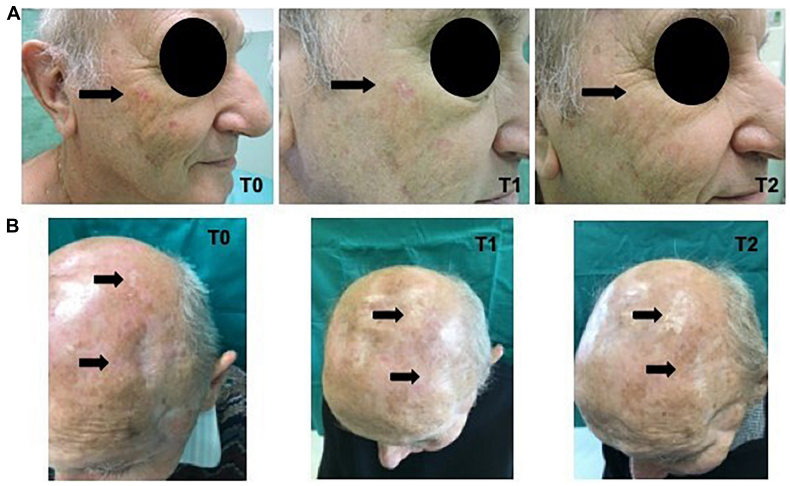

FIGURE 4
(A) Immunosuppressed patient. **(B)** Immunocompetent patient.

TABLE 6 *P*-value and d of the O_2Hb and HHb signals in the two epochs before and after.

	O_2Hb before	O_2Hb after	HHb before	HHb after
***p*-value**	0,122	0,169	0,218	0,116
d	0	0	0	0

The use of high-protection UV filters has proved to be useful against the skin chronic photoirradiation damage (8, 9). However, recent studies have shown that new medical devices are more effective in primary prevention, especially in higher-risk patients (12–16). In a previous randomized controlled study (17), we demonstrated the effectiveness of a new class I medical device containing active ingredients with antioxidant and repairing action for the prevention and treatment of AKs in a cohort of 90 patients, which also included 28 chronically immunosuppressed subjects. At the end of the treatment, the reduction of the mean number of AKs was 54.7% in the treatment group, vs. 9.43% among the patients who had only used sunscreen. The present study represents the continuation

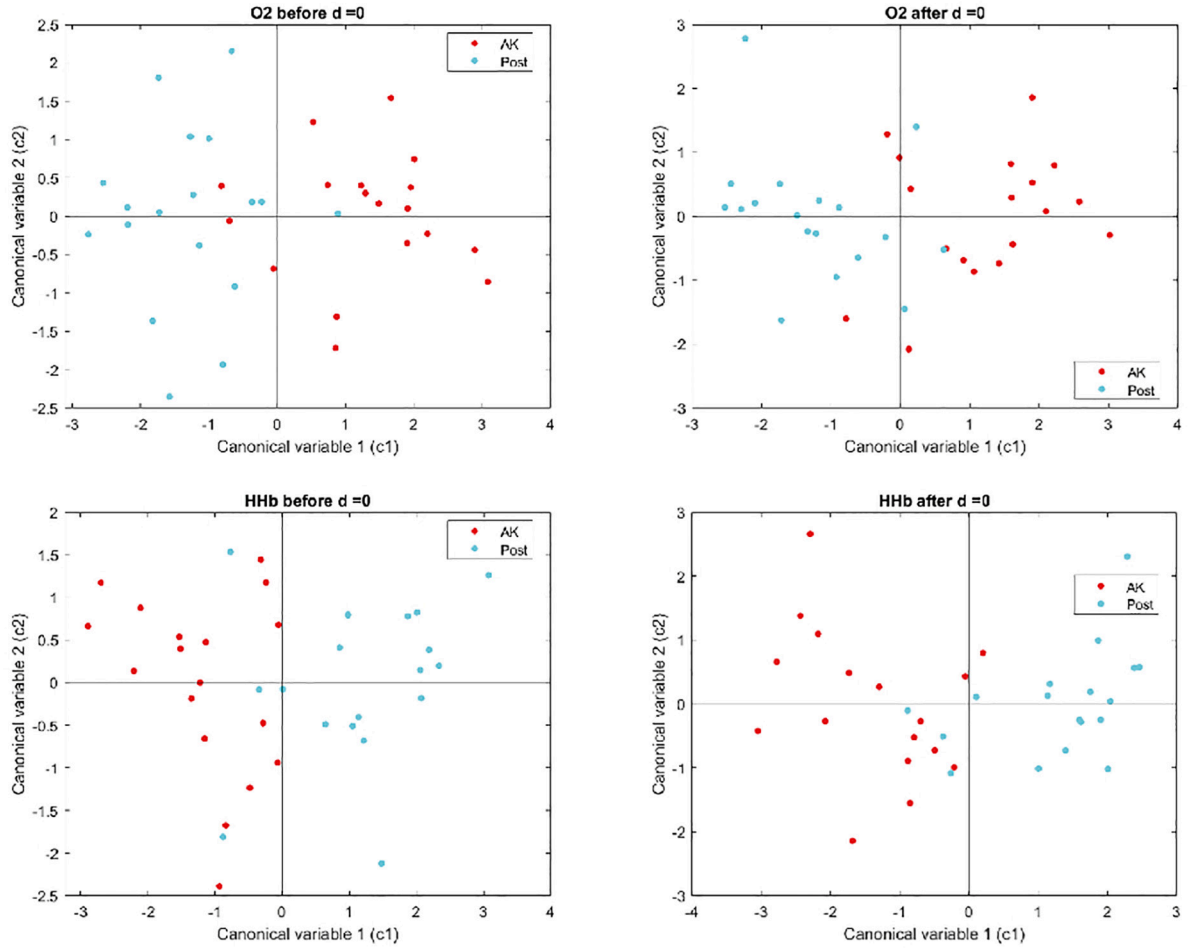

FIGURE 5
Graphical representation of the first two canonical variables estimated through the MANOVA for the O_2Hb and HHb signals, before and after ice application.

of the previous one, employing the new formulation of the product, characterized by the replacement of vitamin E with nicotinamide. This is a water-soluble derivative of vitamin B3, that demonstrated, both *in vitro* and *in vivo* several photoprotective effects, enhancing DNA repair, reducing the UV-induced suppression of skin immune responses, modulating inflammatory cytokine production, and restoring cellular energy levels after UV exposure (22, 23). In particular, in our experience, this molecule has proven able to protect human primary keratinocytes isolated from the FC from the UV-induced oxidative stress (24). Among the active ingredients of the product tested in this study there are also green tea polyphenols (epigallocatechin gallate) that demonstrated immune protective and antioxidant effects (25) and DNA repairs enzymes. Recent studies confirmed the effectiveness of the topical application of these molecules in the prevention and treatment of actinic keratoses. Notably, the T4 Endonuclease V (T4N5), derived from the UV-resistant bacterium *Micrococcus luteus*, significantly reduced actinic keratoses in treated patients (26, 27). Similar effects were obtained also by the treatment with topical products containing photolyase, derived from marine cyanobacteria and by the combination of high protection traditional sunscreens, endonuclease and photolyase (28, 29). Also, *in vitro* and *in vivo* experiments suggested a putative role in skin cancer prevention of OGG-1, another DNA repair enzyme derived from the mustard plant *Arabidopsis thaliana,* even its effective efficacy has yet to be confirmed in the clinical setting (30).

In this study, the assessment of the clearance of lesions in treated patients was performed using the AKASI score. This method allows to analyze both the extension of the actinic damage affected area, and the clinical characteristics of AK. Compared to the simple count of the lesions, the AKASI score has some advantages: i) it is a reproducible and reliable method; ii) takes greater account of the actinic damage within the FC area and iii) solves the difficulty of lesion counting in patients

with severe photodamage, where often the AKs are coalescing within an erythematous and inflamed area (18). Furthermore, the skills for the AKASI calculation are easily acquired and the calculation rapid, and therefore suitable for an assessment in the outpatient setting. In this study, the evaluations were carried out by 4 different dermatologists; nevertheless, the inter-operator reproducibility of the AKASI score has recently been confirmed (31).

In our study, the mean AKASI score calculated at T0 was significantly higher among the immunocompetent patients than in the OTRs (4.47 vs. 3.21; p-value 0.013). This discrepancy may be justified by the fact that the mean age, and consequently the risk of chronic actinic damage (32), was significantly higher in the immunocompetent group (77.67 vs. 68.16; p-value < 0.001). It should also be noted that the immunocompromised subjects enrolled in this study followed a periodic surveillance program and had been trained in the constant use of photoprotectors, which have been proven to be sufficiently effective in the prevention of actinic keratoses (9–11, 13). Moreover, a prevalence of subjects with phototype II was observed in the OTRs group (88.10% vs. 28.13) with a consequent predominancy of phototypes III in the immunocompetent group. It should be remembered that all the patients enrolled in our study presented phototype II and III. In fact, the phenotypic characteristics of the population hailing from the geographical area in which it was conducted make phototype I very rare; furthermore, a mandatory inclusion criterion was the presence of AKs, that are extremely unfrequent in subjects with brown/black skin (phototypes IV, V, and VI) (32, 33).

A significantly higher AKASI score (p-value 0.019) was found in subjects with a previous NMSC history. This data agrees with a retrospective study which analyzed the association between AKASI score and risk of evolution from Aks to iSCC, demonstrating that the patients with AKASI > 7 may have a higher risk of developing iSCC (19).

In our experience, the AKASI score proved to be a valid tool to verify the efficacy of the product under study, highlighting an average percentage reduction at the end of treatment of 31.37% in immunocompetent patients and 22.76% in organ transplant recipients, in comparison to the initial values. The reduction in AKASI values was statistically significant in the single time intervals (T0 vs. T1 and T1 vs. T2) in both groups of treated patients. The demonstration of the efficacy of the treatment also in the group of solid organ recipients represents a particularly important data, in consideration on the high propensity of these subjects to develop skin neoplasms (4), and of the scarcity of literature to support the efficacy and the safety of medical devices for the prevention and treatment of AK and FC in this specific subset of patients (17). In fact, the reduced efficiency in tumor surveillance, resulting from the long-term use of immunosuppressive drugs, could cause a lower capacity to respond to treatments.

In our study, the use of the AKASI score also allowed us to identify treatment response thresholds to evaluate the treatment outcomes, based on those prosed by Schmitz et al. (34), with a complete clearance of the lesions (AKASI 100) reached in 2 immunocompetent patients and the achievement of AKASi 75 in 8.11% of the immunocompetent and 3.7% of the immunosuppressed patients, and of AKASI 50 in 27.03% and 18.52%, respectively.

Another innovative aspect of our project was the use of NIRS, a non-invasive technique that evaluates hemoglobin relative concentration variations, for the assessment of the response to treatment. The feasibility of this method for the AK monitoring has already been demonstrated in previous studies conducted by our group (20, 21), in which we identified through a multivariate analysis of variance a different vascular response in AK compared to healthy skin and in the lesions themselves before and after treatment with Imiquimod 3.75%. In the present study, however, despite the evidence of clinical response to treatment, we did not find significant differences for O_2Hb and HHb signals in the two periods. At baseline condition (before epochs), the vascularization of the AK lesions before and after the topical cream did not show statistically significant differences. This result confirms those shown in our previous study, in which NIRS signals did not detect any significant differences between the vascularity in AK lesions before and after Imiquimod 3.75% (35). In the previous study, the HHb signals showed statistically significant differences only after ice application, demonstrating the importance of the vasoconstrictor stimulus for the vascular response assessment. Notably, the two groups of signals showed a statistical difference only after the application of the stimulus. In the present study, both HHb and O_2Hb signals showed no significant differences, even after the application of the vasoconstrictor stimulus. The dissimilarity between the intense pro-inflammatory and immunomodulating effect exerted by imiquimod (35), and the mechanism of action of the product used in the current study could justify this possible incongruity. Its ingredients, in fact, acts by repairing the UV-induced DNA damage and reducing the oxidative stress provoked by the photo exposure, but have only a moderate anti-inflammatory action and do not significantly modify the vascularization of the treated areas (22, 23, 36). The absence of statistical significance could also be due to the relative scarceness of the sample monitored by NIRS, compared to the study previously conducted (21), or to a different severity and extent of the lesions assessed. Unfortunately, the studies are not easily comparable on this point, since the evaluation of the extension was previously carried out in agreement with the grading proposed by Olsen (37) and not through the AKASI score.

Conclusion

Herein, we demonstrate the effectiveness in AK prevention and treatment of a topical product that combines high-protection sunscreens with anti-oxidant molecules and enzymes capable to repair photo-induced DNA damages, confirming the validity of this therapeutic strategy even in patients under long-term immunosuppressive treatment.

Based on our experience, AKASI has proven to be a valuable tool in monitoring these patients, while further large-scale studies will be needed to confirm the possible application of NIRS in this setting.

Due to the high incidence of chronic actinic damage and the related lesions (*i.e.,* FC, AK, and iSCC) both in the general and chronically immunosuppressed population, we believe that the results deriving from this study may represent strategies of interest for the treatment and monitoring of patients suffering from these pathological conditions.

Data availability statement

The raw data supporting the conclusions of this article will be made available by the authors, without undue reservation.

Ethics statement

The studies involving human participants were reviewed and approved by Comitato Etico Interaziendale AOU Maggiore della Carità di Novara. The patients/participants provided their written informed consent to participate in this study.

Author contributions

FV, SS, KM, EZ, and PS contributed to conception and design of the study. MB organized the database. CA performed the statistical analysis. PS wrote the first draft of the manuscript. FV, SS, KM, CA, and EZ wrote sections of the manuscript. All authors contributed to manuscript revision, read, and approved the submitted version.

Acknowledgments

We thank the Ganassini Corporate, Milano, Italy, for the support in the completion of this study. We also thank the Ganassini for providing the study product.

Conflict of interest

The authors declare that the research was conducted in the absence of any commercial or financial relationships that could be construed as a potential conflict of interest.

Publisher's note

References

1. Figueras Nart I, Cerio R, Dirschka T, Dréno B, Lear JT, Pellacani G, et al. Progressing evidence in AK (PEAK) working group. defining the actinic keratosis field: a literature review and discussion. *J Eur Acad Dermatol Venereol.* (2018) 32:544–63. doi: 10.1111/jdv.14652

2. Tan JM, Lambie D, Sinnya S, Sahebian A, Soyer HP, Prow TW, et al. Histopathology and reflectance confocal microscopy features of photodamaged skin and actinic keratosis. *J Eur Acad Dermatol Venereol.* (2016) 30:1901–11.

3. Fernández-Figueras MT, Carrato C, Sáenz X, Puig L, Musulen E, Ferrándiz C, et al. Actinic keratosis with atypical basal cells (AK I) is the most common lesion associated with invasive squamous cell carcinoma of the skin. *J Eur Acad Dermatol Venereol.* (2015) 29:991–7. doi: 10.1111/jdv.12848

4. Willenbrink TJ, Ruiz ES, Cornejo CM, Schmults CD, Arron ST, Jambusaria-Pahlajani A. Field cancerization: definition, epidemiology, risk factors, and outcomes. *J Am Acad Dermatol.* (2020) 83:709–17.

5. Ribeiro Torezan LA, Festa-Neto C. Cutaneous field cancerization: clinical, histopathological and therapeutic aspects. *An Bras Dermatol.* (2013) 88:775–86. doi: 10.1590/abd1806-4841.20132300

6. Werner RN, Sammain A, Erdmann R, Hartmann V, Stockfleth E, Nast A. The natural history of actinic keratosis: a systematic review. *Br J Dermatol.* (2013) 169:502–18.

7. Naldi L, Belloni Fortina A, Lovati S, Barba A, Gotti E, Tessari G, et al. Risk of nonmelanoma skin cancer in Italian organ transplant recipients. A registry-based study. *Transplantation.* (2000) 70:1479–84. doi: 10.1097/00007890-200011270-00015

8. Ulrich C, Jürgensen JS, Degen A, Hackethal M, Ulrich M, Patel MJ, et al. Prevention of non-melanoma skin cancer in organ transplant patients by regular use of a sunscreen: a 24-months, prospective, case-control study. *Br J Dermatol.* (2009) 161(Suppl. 3):78–84. doi: 10.1111/j.1365-2133.2009.09453.x

9. Arenberger P, Arenbergerova M. New and current preventive treatment options in actinic keratosis. *J Eur Acad Dermatol Venereol.* (2017) 31(Suppl. 5):13–7.

10. Moscarella E, Di Brizzi EV, Casari A, De Giorgi V, Di Meo N, Fargnoli MC, et al. Italian expert consensus paper on the management of patients with actinic keratoses. *Dermatol Ther.* (2020) 33:e13992. doi: 10.1111/dth.13992

11. Surber C, Ulrich C, Hinrichs B, Stockfleth E. Photoprotection in immunocompetent and immunocompromised people. *Br J Dermatol.* (2012) 167(Suppl. 2):85–93.

12. Puig S, Granger C, Garre A, Trullàs C, Sanmartin O, Argenziano G. Review of clinical evidence over 10 years on prevention and treatment of a film-forming medical device containing photolyase in the management of field cancerization in

actinic keratosis. *Dermatol Ther (Heidelb).* (2019) 9:259–70. doi: 10.1007/s13555-019-0294-1

13. Krutmann J, Berking C, Berneburg M, Diepgen TL, Dirschka T, Szeimies M. New strategies in the prevention of actinic keratosis: a critical review. *Skin Pharmacol Physiol.* (2015) 28:281–9. doi: 10.1159/000437272

14. Eibenschutz L, Silipo V, De Simone P, Buccini PL, Ferrari A, Carbone A, et al. A 9-month, randomized, assessor-blinded, parallel-group study to evaluate clinical effects of film-forming medical devices containing photolyase and sun filters in the treatment of field cancerization compared with sunscreen in patients after successful photodynamic therapy for actinic keratosis. *Br J Dermatol.* (2016) 175:1391–3. doi: 10.1111/bjd.14721

15. Carducci M, Pavone PS, De Marco G, Lovati S, Altabas V, Altabas K, et al. Comparative effects of sunscreens alone vs sunscreens plus DNA repair enzymes in patients with actinic keratosis: clinical and molecular findings from a 6-month, randomized, clinical study. *J Drugs Dermatol.* (2015) 14:986–90.

16. Moscarella E, Argenziano G, Longo C, Aladren S. Management of cancerization field with a medical device containing photolyase: a randomized, double-blind, parallel-group pilot study. *J Eur Acad Dermatol Venereol.* (2017) 31:e401–3. doi: 10.1111/jdv.14209

17. Veronese F, Zavattaro E, Orioni G, Landucci G, Tarantino V, Airoldi C, et al. Efficacy of new class I medical device for actinic keratoses: a randomized controlled prospective study. *J Dermatolog Treat.* (2021) 2:625–30. doi: 10.1080/09546634.2019.1687820

18. Dirschka T, Pellacani G, Micali G, Malvehy J, Stratigos AJ, Casari A, et al. A proposed scoring system for assessing the severity of actinic keratosis on the head: actinic keratosis area and severity index. *J Eur Acad Dermatol Venereol.* (2017) 1:1295–302. doi: 10.1111/jdv.14267

19. Schmitz L, Gambichler T, Gupta G, Stücker M, Dirschka T. Actinic keratosis area and severity index (AKASI) is associated with the incidence of squamous cell carcinoma. *J Eur Acad Dermatol Venereol.* (2018) 32:752–6. doi: 10.1111/jdv.14682

20. Seoni S, Meiburger KM, Veronese F, Tarantino V, Zavattaro E, Salvi M, et al. Non-invasive analysis of actinic keratosis using a cold stimulation and near-infrared spectroscopy. *Annu Int Conf IEEE Eng Med Biol Soc.* (2019) 2019:467–70.

21. Seoni S, Savoia P, Veronese F, Zavattaro E, Tarantino V, Meiburger KM. Non-invasive analysis of actinic keratosis before and after topical treatment using a cold stimulation and near-infrared spectroscopy. *Medicina (Kaunas).* (2020) 56:482. doi: 10.3390/medicina56090482

22. Damian DL. Nicotinamide for skin cancer chemoprevention. *Australas J Dermatol.* (2017) 58:174–80.

23. Snaidr VA, Damian DL, Halliday GM. Nicotinamide for photoprotection and skin cancer chemoprevention: a review of efficacy and safety. *Exp Dermatol.* (2019) 28(Suppl. 1):15–22. doi: 10.1111/exd.13819

24. Camillo L, Gironi LC, Zavattaro E, Esposto E, Savoia P. Nicotinamide attenuates UV-induced stress damage in human primary keratinocytes from cancerization fields. *J Invest Dermatol.* (2022) 142:1466–77.e1. doi: 10.1016/j.jid.2021.10.012

25. Rosenthal A, Stoddard M, Chipps L, Herrmann J. Skin cancer prevention: a review of current topical options complementary to sunscreens. *J Eur Acad Dermatol Venereol.* (2019) 33:1261–7. doi: 10.1111/jdv.15522

26. DeBoyes T, Kouba D, Ozog D, Fincher E, Moy L, Iwata K, et al. Reduced number of actinic keratoses with topical application of DNA repair enzyme creams. *J Drugs Dermatol.* (2010) 9:1519–21.

27. Stoddard M, Herrmann J, Moy L, Moy R. Improvement of actinic keratoses using topical DNA repair enzymes: a randomized placebo-controlled trial. *J Drugs Dermatol.* (2017) 16:1030–4.

28. Puviani M, Barcella A, Milani M. Eryfotona AK-NMSC in the treatment of cancerization field in patients with actinic keratosis or non-melanoma skin cancer: a report of six cases. *G Ital Dermatol Venereol.* (2013) 148:1–6.

29. Carducci M, Pavone PS, De Marco G, Lovati S. Comparative effects of sunscreens alone vs sunscreens plus DNA repair enzymes in patients with actinic keratosis: clinical and molecular findings from a 6-month, randomized, clinical study. *J Drugs Dermatol.* (2015) 14:986–90.

30. Emanuele E, Altabas V, Altabas K. Topical application of preparations containing DNA repair enzymes prevents ultraviolet-induced telomere shortening and c-FOS proto-oncogene hyperexpression in human skin: an experimental pilot study. *J Drugs Dermatol.* (2013) 12:1017–21.

31. Pellacani G, Gupta G, Micali G, Malvehy J, Stratigos AJ, Casari A, et al. Actinic keratosis area severity index (AKASI): reproducibility study and comparison with total lesion count. *Br J Dermatol.* (2018) 179:763–4. doi: 10.1111/bjd.16559

32. Fargnoli MC, Altomare G, Benati E, Borgia F, Broganelli P, Carbone A, et al. Prevalence and risk factors of actinic keratosis in patients attending Italian dermatology clinics. *Eur J Dermatol.* (2017) 27:599–608. doi: 10.1684/ejd.2017.3126

33. Flohil SC, van der Leest RJ, Dowlatshahi EA, Hofman A, de Vries E, Nijsten T. Prevalence of actinic keratosis and its risk factors in the general population: the Rotterdam study. *J Invest Dermatol.* (2013) 133:1971–8. doi: 10.1038/jid.2013.134

34. Schmitz L, von Dobbeler C, Gupta G, Gambichler T, Szeimies RM, Morton CA, et al. Photodynamic therapy leads to significant improvement of actinic keratosis area and severity index (AKASI). *Photodiagnosis Photodyn Ther.* (2018) 21:66–70. doi: 10.1016/j.pdpdt.2017.10.007

35. Sauder DN. Immunomodulatory and pharmacologic properties of imiquimod. *J Am Acad Dermatol.* (2000) 43:S6–11.

36. Yarosh DB, Rosenthal A, Moy R. Six critical questions for DNA repair enzymes in skincare products: a review in dialog. *Clin Cosmet Investig Dermatol.* (2019) 2:617–24. doi: 10.2147/CCID.S220741

37. Olsen EA, Abernethy ML, Kulp-Shorten C, Callen JP, Glazer SD, Huntley A, et al. A double-blind, vehicle-controlled study evaluating masoprocol cream in the treatment of actinic keratoses on the head and neck. *Am Acad Dermatol.* (1991) 24:738–43. doi: 10.1016/0190-9622(91)70113-g

frontiers | Frontiers in Medicine

TYPE Original Research
PUBLISHED 09 September 2022
DOI 10.3389/fmed.2022.985252

OPEN ACCESS

EDITED BY
Federica Veronese,
Azienda Ospedaliero Universitaria Maggiore della Carità, Italy

REVIEWED BY
Abdallah El-Sayed Allam,
Tanta University, Egypt
Plamen Todorov Todorov,
Plovdiv Medical University, Bulgaria

*CORRESPONDENCE
Glauber Voltan
gvoltan@gmail.com

SPECIALTY SECTION
This article was submitted to Dermatology, a section of the journal Frontiers in Medicine

RECEIVED 03 July 2022
ACCEPTED 05 August 2022
PUBLISHED 09 September 2022

CITATION
Voltan G, Filho FB, Leite MN, De Paula NA, Santana JM, Silva CML, Barreto JG, Da Silva MB, Conde G, Salgado CG and Frade MAC (2022) Point-of-care ultrasound of peripheral nerves in the diagnosis of Hansen's disease neuropathy.
Front. Med. 9:985252.
doi: 10.3389/fmed.2022.985252

Point-of-care ultrasound of peripheral nerves in the diagnosis of Hansen's disease neuropathy

Glauber Voltan[1]*, Fred Bernards Filho[1], Marcel Nani Leite[2], Natália Aparecida De Paula[2], Jaci Maria Santana[2], Claudia Maria Lincoln Silva[2], Josafá Gonçalves Barreto[3], Moises Batista Da Silva[3], Guilherme Conde[3], Claudio Guedes Salgado[3] and Marco Andrey Cipriani Frade[1]

[1]Department of Interne Medicine - Dermatology, Faculty of Medicine of Ribeirão Preto, University of São Paulo, São Paulo, Brazil, [2]Faculty of Medicine of Ribeirão Preto, University of São Paulo, São Paulo, Brazil, [3]Federal University of Pará, Belém, Pará, Brazil

Introduction: Hansen's disease (HD) is the most common cause of treatable peripheral neuropathy in the world that may or may not involve skin manifestations, and physical examination based on simplified neurologic evaluation is a subjective and inaccurate procedure. High-resolution ultrasound (HRUS) can be used to evaluate peripheral nerves and is a validated technique of good reproducibility, permitting a detailed and precise examination.

Objectives: We proposed to establish objective criteria for absolute values of the measurement of the CSA of peripheral nerves and their indices of the ΔCSA and ΔTpT in the diagnosis of Hansen's disease neuropathy as compared with healthy voluntaries.

Materials and methods: In municipalities from different regions of Brazil, we randomly selected 234 volunteer Brazilian patients diagnosed with leprosy to be submitted to peripheral nerve echography and compared with 49 healthy Brazilian volunteers.

Results: Hansen Disease assessed by high resolution ultrasound is a primarily neural disease that leads to multiple hypertrophic mononeuropathy characterized by CSA values exceeding normal limits (Med CT = 10.2 mm^2; UT = 9.8 mm^2; UPT = 9.3 mm^2; CFFH = 18.3 mm^2; T = 9.6 mm^2), and the pattern of asymmetry (ΔCSA>2.5 mm^2 with RR 13) and focality (ΔTPT > 2.5 mm^2 with RR 6.4) of this thickening has higher sensitivity (76,1%) and specificity (87,8 %) for its early diagnosis that laboratory tests. Analyzing each subject, the percentage of thickened nerves detected among the total number of nerves assessed was higher among patients with HD than among healthy individuals ($p < 0.0001$). Individuals with two or more thickened nerves were at 24.1 times higher relative risk (95% CI: 6.74–88.98) of HD.

KEYWORDS

leprosy, Hansen's disease, neuropathy, high-resolution ultrasound, cross-sectional area

Introduction

Hansen's disease (HD) is the most common cause of treatable peripheral neuropathy in the world. *Mycobacterium leprae* mainly resides in macrophages and Schwann cells, affecting myelination. It causes a primary neural disease involving the immunologic system (being induced or maintained by an immune response to the bacillus), and the neural damage results in disability and maintenance of stigmas. As proposed by the World Health Organization, nerve thickening is one of the cardinal signs for the diagnosis of a case of leprosy (1). When the first signals of nerve damage can be noted, at least 30% of the nerve fibers may be affected (2, 3). HD is a neural disease that may or may not involve skin manifestations (4–11). Cases of peripheral neuropathy accompanied by nerve thickening should lead clinicians to suspect a diagnosis of HD (12). Physical examination based on simplified neurologic evaluation including the palpation of peripheral nerves helps the diagnosis of nerve thickening and neuritis; however, this is a subjective procedure that may not detect the condition in very early cases, even by well-trained professionals (13).

High-resolution ultrasound (HRUS) can be used to evaluate most peripheral nerves and is a validated technique of good reproducibility, permitting a detailed and precise examination (14, 15). With HRUS, the peripheral nerves appear on a longitudinal view (cord-like pattern) as multiple tubular hypoechoic structures (dark gray bundles) intermingled with hyperechoic lines (perineurium—white), with their ensemble being covered with a hyperechoic line (epineurium). On a transversal view (honeycomb pattern), these structures are hypoechoic and round (fascicles) surrounded by hyperechoic bands (perineurium), and all of these fascicles are surrounded by a denser outer line (epineurium) (14, 15). HD has been characterized by greater peripheral nerve thickening defined by the increase in their cross-sectional area (CSA) (9, 10), usually asymmetrical (9), followed by other morphological changes, such as echogenicity and/or fascicular pattern; perineurium thickening; and peripheral nerve vascularization that can be detected by intraneural and/or perineural Doppler signals (16, 17). In addition to parameters regarding the absolute values of CSA measurements, Frade et al. (10), among others, have suggested the measurement of the asymmetry index [ΔCSA = (>right or left CSA) – (<right or left CSA)] in the evaluation of leprosy and have demonstrated that this index is highly sensitive and specific for the differentiation between the nerves of healthy individuals and the nerves of patients with leprosy. Regardless of the classification as multibacillary or paucibacillary, the fusiform thickening of the ulnar nerve starts in the ulnar sulcus and reaches a maximum of 4 cm above the medial epicondyle (9, 10, 18–20). However, Frade et al. (10) have pointed out that the difference between the measurement of the thickened ulnar nerve in the distal region of the arm and that in the elbow region, or vice versa, had more than 90% specificity for leprosy. This characteristic finding may be of help, especially in the diagnosis of primary or pure neural leprosy (PNL), in which the skin lesions are absent and in the differentiation between leprosy and other neuropathies, in which a diffuse nerve increase may occur.

So, we proposed to establish the objective criteria of the measurements of absolute values of the CSAs of the peripheral nerves and their indices of the asymmetry and focality in the diagnosis of Hansen's disease neuropathy as compared with healthy voluntaries.

Ethical considerations

The present study was approved by the Research Ethics Committee of the University Hospital, Faculty of Medicine of Ribeirão Preto, University of São Paulo (protocol no. 2.165.032, MH-Brasil and 92228318.1.0000.5440). Written informed consent was obtained from all participants, including the parents/guardians of subjects younger than 18 years. All procedures involving human beings followed the ethical standards of the Declaration of Helsinki (1975/2008).

Casuistry

Municipalities of different regions of Brazil (north, northeast, and southwest) whose health professionals had been habilitated by the National Reference Center for Sanitary Dermatology with emphasis on leprosy of HCFMRP-USP were selected between 2016 and 2020. In these regions, we randomly selected 234 volunteer Brazilian patients diagnosed with leprosy by these teams to be submitted to peripheral nerve echography. As a comparative (control) sample of healthy Brazilian volunteers, we used cases of our service, as reported by Voltan et al. (2022) (Annex 1); to carry out this work, we obtained a sample number of 97 for the Brazilian population of 211 million inhabitants, with a confidence level of 95% and a margin of error of 10%. Our sample consisted of 66 individuals; however, since the distribution of the CSA of the right and left nerves was homogeneous, 132 neural points were considered for statistical analysis, being the largest sample among the evaluated studies and fulfilling the sample calculation criteria for our population. Calculation performed with https://calculareconverter.com.br/calculo-amostral/ and verified at https://solvis.com.br/calculos-de-amostragem/ for 211 million and 132 neural points of 66 individuals with 95% CI have a margin of error of up to 8.53%. In addition, we included in the same data bank unpublished data on the 18 tibial nerves of nine individuals aged 15–60 years (mean: 7.6 $\pm$ 0.94 mm^2; median: 8.0 mm^2).

Clinical evaluation

Clinical evaluation was performed by dermatologists and HD specialists habilitated by the program of the Health Ministry.

The teams were not involved in the capture and HRUS analysis of the images.

Peripheral nerve echography

The general portable ultrasound devices used were Mindray M5, Samsung HM70-A, and Vinno6, equipped with high-frequency transducers, with frequencies ranging from 4 to 17 MHz. Each nerve was scanned on crosswise and lengthwise sections, and the cross-sectional area (CSA) of the transversal sections was obtained with adjustment of the angle perpendicular to the insonated nerve surface, without pressure on the structures. The neural points assessed were defined according to their proximity to anatomical bone references, facilitating the reproducibility of the method by being well-established sites for neural compression or more common sites of electrophysiological assessment. The CSA was determined at these sites with a continuous trace, internally to the hyperechoic borders of the epineurium (Figures 1A,B). For comparison with the literature, all patients were submitted to already established echographic assessment of 10 neural sites, that is, median nerves in the carpal tunnel (between the scaphoid and pisiform bones); ulnar nerves in the cubital tunnel (between the medial epicondyle and olecranon) and in the distal third of the arm (cubital pretunnel—3–5 cm above the medial epicondyle); the common fibular nerves in the fibular head topography; and the tibial nerves in the tarsal tunnel, all of them bilaterally. As an exception, four new additional sites were established for the assessment of routine focality, that is, common fibular nerves in the thigh (pre-fibula head or distal third of the thigh between 3 and 8 cm proximal to the fibula head) and median nerves in the distal third of the forearm (3–5 cm proximal to the carpal tunnel). The nerves of the upper limbs were assessed with the patient sitting and with elbows flexed 60–90°, while the nerves of the lower limbs were assessed with the patient sitting or in the dorsal decubitus with legs slightly flexed 90–130°.

All data collection procedures were carried out during active search campaigns in different regions of Brazil. After 2 or 3 months of collection, the same researcher opened the images

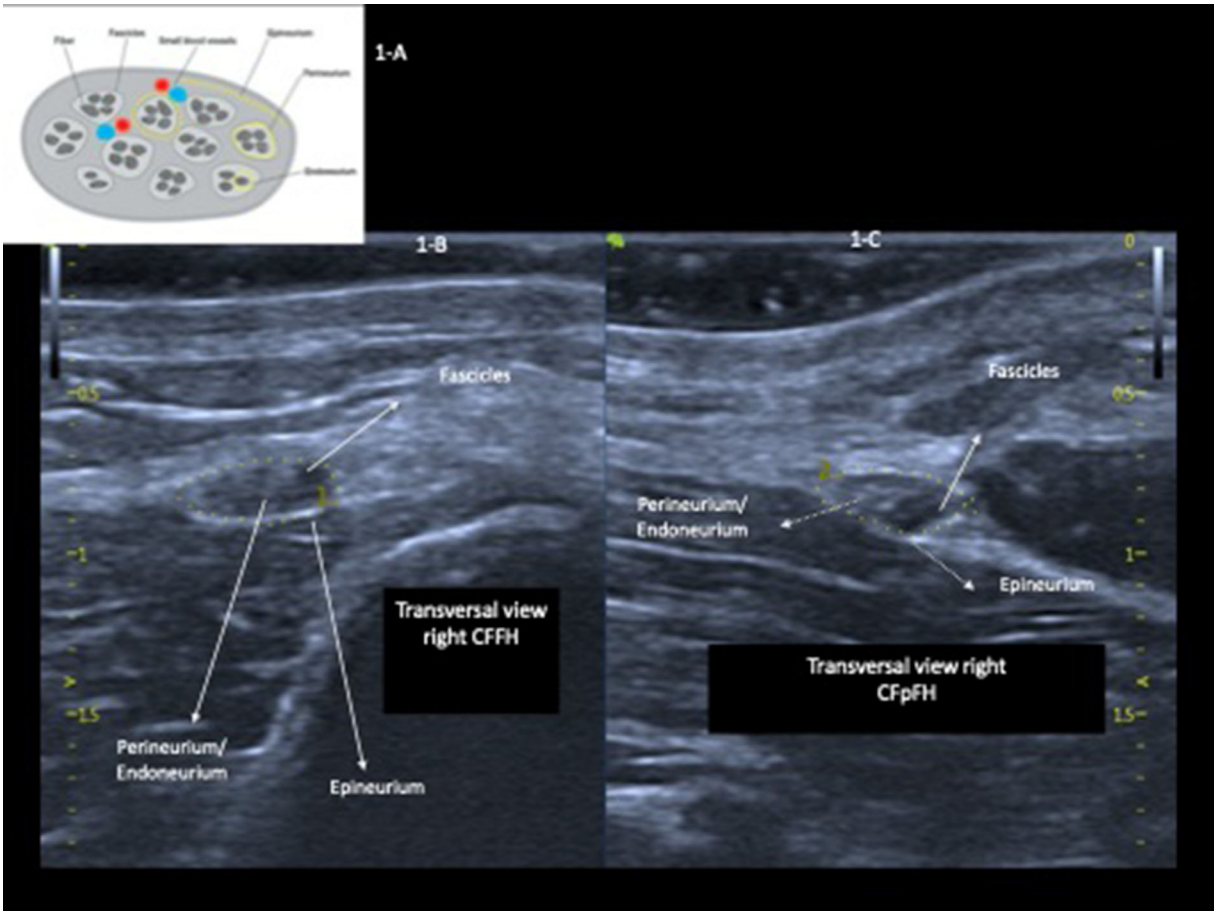

FIGURE 1
Drawing of a cross-section of a peripheral nerve **(A)**; high-resolution echography of the ulnar nerve in the right (RPT) and the left (LPT) cubital pretunnel with preserved cross-sectional area, echogenicity, and fascicular pattern **(B,C)**.

on his personal computer and analyzed each image, extracting only objective data from the CSA for statistical analysis. All other results were obtained using mathematical formulas performed in Excel to arrive at ΔCSA and ΔTpT. In short, the researcher's experience helped in carrying out the measurements, but as they are objective data, if any other researcher performs them following the same standards, they should have the same results.

Statistical analysis

Excel® software was used to transpose the CSA values (mm^2) obtained from photographs of the ultrasound examination, and Prism 8 software for macOS was used for later data analysis. The means, standard deviations, and median absolute CSA values were calculated for each of the 14 nerve sites assessed (seven on the right side and seven on the left side). The paired *t*-test was used to analyze asymmetries. We calculated the indices (Δ) of the differences of absolute CSA values between the right and the left side (ΔCSAs) and of the differences between the absolute CSA values in the same nerve. The neural sites were considered to be thickened when their CSA values, extracted from the database from Voltan et al. (2022), were higher than the reference values for normal individuals summed to two times the values of the standard deviations (SDs). Similarly, each neural site was considered to be asymmetrical when the ΔCSA was higher than the reference values plus two times the SD for normal individuals. The same reasoning was used for the ΔTPT to consider the focality. The total number of thickened/altered neural sites was counted using the "cont.se" function of Excel software, and the total number of altered sites in terms of asymmetry (ΔCSA) and focality (ΔTPT) was calculated for in each one.

The total number of thickened neural sites was calculated for each individual using the "cont.se" function of Excel. Similarly, each neural site was considered to be asymmetrical or with focality when the ΔCSA and ΔTPT, respectively, were higher than RV + 2 SD. The total number of altered sites in terms of asymmetry (ΔCSA) and focality (ΔTPT) was calculated using the "cont.se" function of Excel. In order to assess the discriminatory power for the diagnosis of Hansen's neuropathy by ultrasound, the ROC curve was applied to the number of altered sites according to CSA, ΔCSA, and ΔTPT as compared with the values obtained for healthy individuals.

Results

The clinical–demographic characteristics and the anti-PGL1 results of the population sample studied are given in Table 1.

TABLE 1 Distribution of the population sample by sex, age range, state of origin, operational classification, and anti-PGL 1 data.

Variables		*N*	%
Sex	Male	113	48.29
	Female	121	51.71
Age (years)	4–14	38	16.24
	15–60	176	75.21
	60–81	20	8.55
Region of origin.	North	72	30.77
	Northeast	67	28.63
	Southeast	95	40.60
Classification of Hansen's disease	DD	159	67.95
	DT	36	15.38
	DV	18	7.69
	I	5	2.14
	PN	5	2.14
	T	4	1.71
	V	7	2.99
Anti-PGL 1	Negative (0.47 ± 0.32)	86	36.75
	Positive (2.85 ± 3.96)	64	27.35
	Not determined	84	35.90
Mean Anti-PGL 1 index	1.49 ± 2.85	150	64.10

DD, dimorphic–dimorphic; HDT, dimorphic–tuberculoid; DV, dimorphic–Virchowian; I, indeterminate; PN, pure neural; T, tuberculoid; VL, virchowian.

The values detected for the patients with HD were compared with the normal CSA patterns of healthy Brazilian individuals based on the values established by Voltan et al. (2022).

Absolute CSA values (mm^2) of the peripheral nerves and their indices

The 234 patients were assessed by bilateral HRUS of the peripheral nerves: median in the carpal tunnel (Med CT), ulnar in the cubital tunnel (UT) and cubital pretunnel (UPT), common fibular in the fibula head (CFFH), and tibial in the medial malleolus (T). Based on initial observations during fieldwork, new sites were routinely established as follows: median nerve in the forearm (Med FA) and the common fibular nerve in the thigh proximal to the fibula head (CFTH), and for this reason, there was a variation of the sample (n), with measurements of Med TC being obtained for 100 (43 %) patients and measurements of CFTH being obtained for 151 (64.5 %) patients.

The mean, standard deviation, and median values of the absolute CSA values in mm^2 and of the differences between the right and left sides (ΔCSA) and between sites of the same nerve (ΔTPT) are presented in Table 2 according to age range.

TABLE 2 Distribution of ultrasound measurements (CSA, ΔCSA, and ΔTPT) according to age range, total sample, and upper limit.

Variables	Age range (years)	4–14	15–30	31–45	46–60	62–81	Sample (15–60 years)	Upper limit (HVs) (mean + 2SD)
	(*n*) Men	14	24	36	25	14	85	–
	(*n*) Women	24	38	29	24	6	91	–
	(*n*) Total (Right + Left)	76	124	130	98	40	352	–
	Mean ± SD [median]	10.3 ± 2.8 [11]	22,3 ±4,9 [22]	37.0 ± 4.0 [37]	52.2 ± 4.2 [52]	69.9 ± 5.2 [69]	36.1 ± 12.6 [36]	–
	Site	Mean ± SD [median]						
Peripheral nerves	Med CT	7.8 ± 2.2 [7]	10.1 ± 2.8 [10]	11.0 ± 2.8 [10.9]	12.1 ± 3.2 [12]	11.3 ± 3.3 [11]	11.0 ± 3.0 [10.7]	10.2
	UT	5.7 ± 1.8 [5]	7.8 ± 3.1 [7]	8.3 ± 3.0 [8]	9.1 ± 3.2 [9]	10.8 ± 4.1 [10]	8.3 ± 3.2 [7.9]	9.8
	UPT	5.3 ± 1.8 [5]	7.9 ± 4.9 [7]	9.3 ± 6.9 [7]	9.7 ± 4.5 [8.5]	11.4 ± 7.3 [9.4]	8.9 ± 5.7 [7]	9.3
	CFFH	10.4 ± 3.9 [10]	15.9 ± 5.2 [15]	18.9 ± 6.4 [18]	21.2 ± 7.0 [20.7]	19.5 ± 6.5 [17.8]	18.4 ± 6.5 [17]	18.3
	T	6.8 ± 2.1 [7]	9.2 ± 4.2 [9]	11.5 ± 4.9 [10.6]	12.8 ± 5.0 [11.9]	14.0 ± 7.0 [11.8]	11.0 ± 4.9 [10]	9.6
ΔCSA (mm^2)	Med CT	1.3 ±1.3 [1.0]	1.7 ± 1.6 [1.0]	1.5 ± 1.3 [1]	2.6 ± 2.1 [2]	2.8 ± 2.0 [2.6]	1.9 ± 1.8 [1.3]	2.2
	UT	1.1 ± 1.2 [1]	1.8 ± 1.7 [1]	1.9 ± 1.8 [1.2]	1.8 ± 1.5 [1.9]	1.7 ± 2.3 [1]	1.9 ± 1.7 [1.2]	3.1
	UPT	1.0 ± 0.8 [1]	1.6 ± 1.8 [1]	2.5 ± 5.0 [1.1]	2.5 ± 4.3 [1]	2.8 ± 2.6 [2]	2.2 ± 3.9 [1.0]	1.4
	CFFH	1.5 ± 1.5 [1]	2.3 ± 2.5 [1.3]	3.6 ± 5.9 [2]	3.8 ± 3.7 [3]	4.2 ± 3.6 [4.3]	3.2 ± 4.4 [2]	2.3
	T	1.1 ± 1.2 [1]	1.4 ± 1.6 [1]	2.3 ± 3.0 [2.0]	2.9 ± 3.1 [2.0]	3.8 ± 3.0 [2.4]	2.1 ± 2.7 [1.1]	–
ΔTPT (mm^2)	Ulnar (UT and UPT)	0.9 ± 1.1 [1]	1.8 ± 2.9 [1]	2.7± 5.1 [1]	2.2 ± 3.2 [1.3]	3.3 ± 4.5 [1.8]	2.2 ± 3.9 [1]	2.6
Analysis of new neural sites	Total $n = 100$	16	34	62	62	26	158	–
Peripheral nerves	Med FA	6.4 ± 2.0 [6.7]	9.5 ± 3.7 [8.3]	9.9 ± 3.4 [9.0]	9.8 ± 2.4 [9.9]	13.0 ± 12.3 [10.4]	9.8 ± 3.1 [9.3]	–
ΔCSA (mm^2)	Med FA	1.6 ± 1.1 [1.5]	1.9 ± 1.9 [1.6]	2.2 ± 2.0 [1.4]	1.5 ± 1.5 [1.2]	5.8 ± 13 [3.1]	1.9 ± 1.8 [1.3]	–
ΔTPT (mm^2)	Median (CT and FA)	1.5 ± 1.0 [1.4]	2.4 ± 2.0 [1.7]	2.5 ± 2.0 [1.8]	2.9 ± 2.4 [2.0]	5.4 ± 9.6 [3.2]	2.6 ± 2.2 [1.9]	–
	Total n = 151	22	68	102	80	30	250	–
Pripheral nerve	CFTH	9.3 ± 3.2 [8.9]	14.5 ± 4.7 [13.9]	17.8 ± 6.8 [16]	18.8 ± 5.2 [18.5]	18.3 ± 6.8 [17.3]	17.2 ± 6.0 [16]	–
ΔCSA (mm2)	CFTH	1.2 ± 1.4 [0.6]	1.8 ± 1.6 [1.6]	4.3 ± 4.7 [3.5]	3.8 ± 3.8 [3.0]	5.8 ±4.3 [4.7]	3.4 ± 3.9 [2.2]	–
ΔTPT (mm^2)	Fibular (CF and TH)	1.2 ± 0.9 [1]	2.6 ± 2.6 [2]	3.6 ± 3.4 [2.4]	3.5 ± 2.6 [2.8]	3.5 ± 2.9 [2.8]	3.3 ± 2.9 [2.4]	–

(n), number; Med, median; CT, carpal tunnel; UT, ulnar tunnel; UPT, ulnar pretunnel; CFFH, common fibular in the fibula head; T, tibial; FA, forearm; CFTH, common fibular thigh; ΔCSA, difference between the right and left nerves at the same site of assessment; ΔTPT, difference between the same nerve at different sites.
Data are reported as mean ± standard deviation, and mean (mm^2).

Assessment of CSA values according to gender

The absolute peripheral nerve CSA values (age range: 15–60 years) divided into male and female gender tended to be higher for men, with a difference at the sites of the Med FA, UT, UPT, and CFFH nerves (Figure 2).

Assessment of CSA values according to age range

We observed a gradual increase in mean and median peripheral nerve CSAs with increasing age range in patients diagnosed with Hansen's disease. There was a significant difference between the age-group of 0–14 years and the

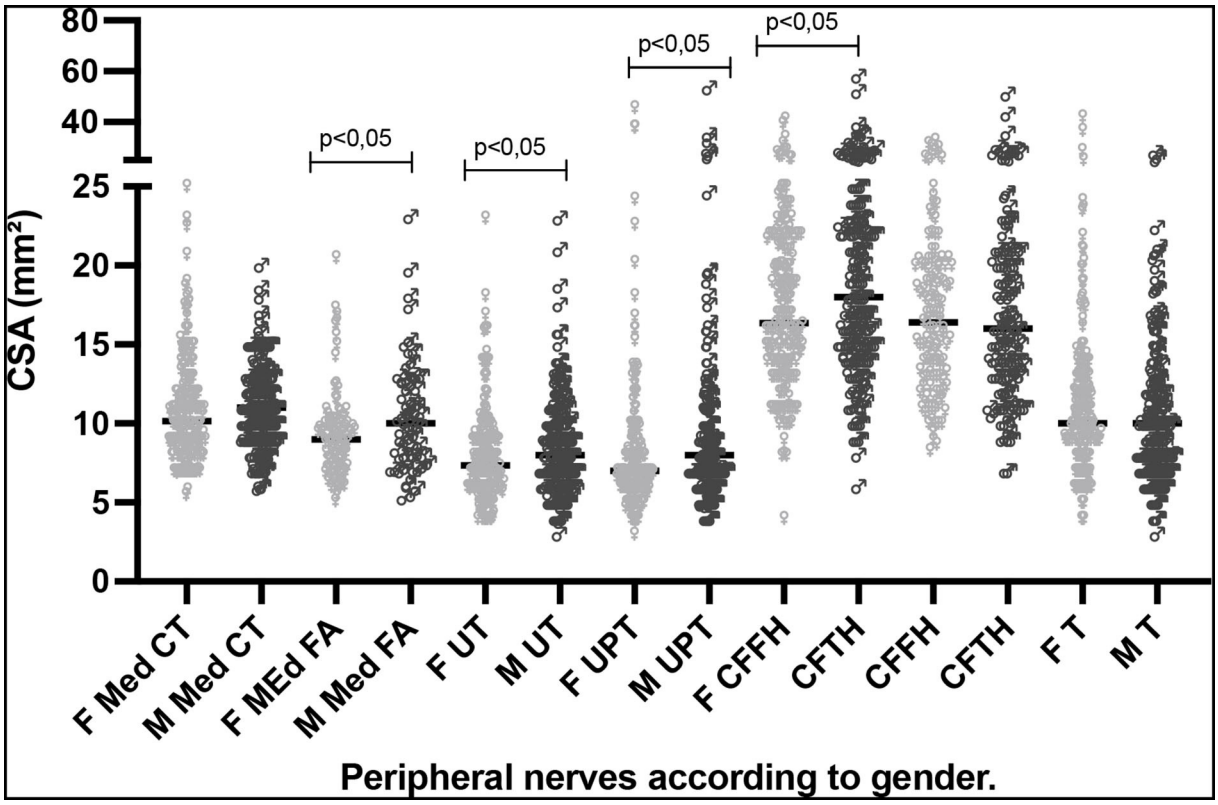

FIGURE 2
Distribution of CSA (mm^2) values at neural sites according to male and female gender for the age range of 15–60 years. F, female; M, male; CSA, cross-sectional area; Med CT, median carpal tunnel; Med FA, median forearm; UT, cubital ulnar tunnel; UPT, cubital ulnar pretunnel; CFFH, common fibular head of the fibula; CFTH, common fibular thigh; T, tibial.

remaining groups ($p < 0.05$). Among the age-groups of 15–60 and > 60 years, this increase occurred only for the UT, UPT, and tibial sites, as shown in Table 2 and Figure 3.

As observed for the absolute values, the ΔCSA and ΔTPT values differed between the age-group of 0–14 years and the remaining groups ($p < 0.05$), except for the Med FA site. Comparison of the age-groups of 15–60 and > 60 years revealed that the differences (Δ) were greater in the age-group of >60 years at the Med CT, Med FA, CFTH, and T sites, as shown in Table 2 and Figure 4.

Comparative analysis of healthy individuals and patients with leprosy

We compared 49 healthy individuals (98 neural sites) with 176 individuals diagnosed with leprosy (352 neural sites) in the age range of 15–60 years.

Since these were not paired samples and did not have parametric distribution, we compared both the absolute CSA values of peripheral nerves and the differences between them using the Mann–Whitney test.

The results revealed higher median and mean absolute CSA values of peripheral nerves among the patients with leprosy compared with healthy individuals at all possible comparison sites, as illustrated in detail in Figure 5.

The mean absolute CSA value of the tibial nerves of patients was 11.0 ± 4.9 and was higher than the value detected in healthy individuals, as also observed by Voltan et al. (unpublished data) who obtained a mean value of 7.6 ± 0.94 mm^2 and a median of 8.0 mm^2, and as reported by Kerasnoudis et al. (21) (6.36 ± 1.4), Tagliafico et al. (22) (9.6 ± 4), Boehm et al. (23) (9.1 ± 2.2), and Grimm et al. (24) (10.2 ± 2.0).

Regarding the asymmetry of CSA values at each neural site assessed as calculated by the respective differences between sides (ΔCSA), we observed higher mean and median differences in the group of patients with leprosy than in the group of healthy individuals at all neural sites, except for the tibial nerve, which showed no difference. The mean and median values of focality, measured by the difference between two sites in the same nerve (ΔTPT) for the ulnar tunnel/ pretunnel nerve, were also higher in the group of patients with leprosy than in healthy individuals (Figures 5, 6).

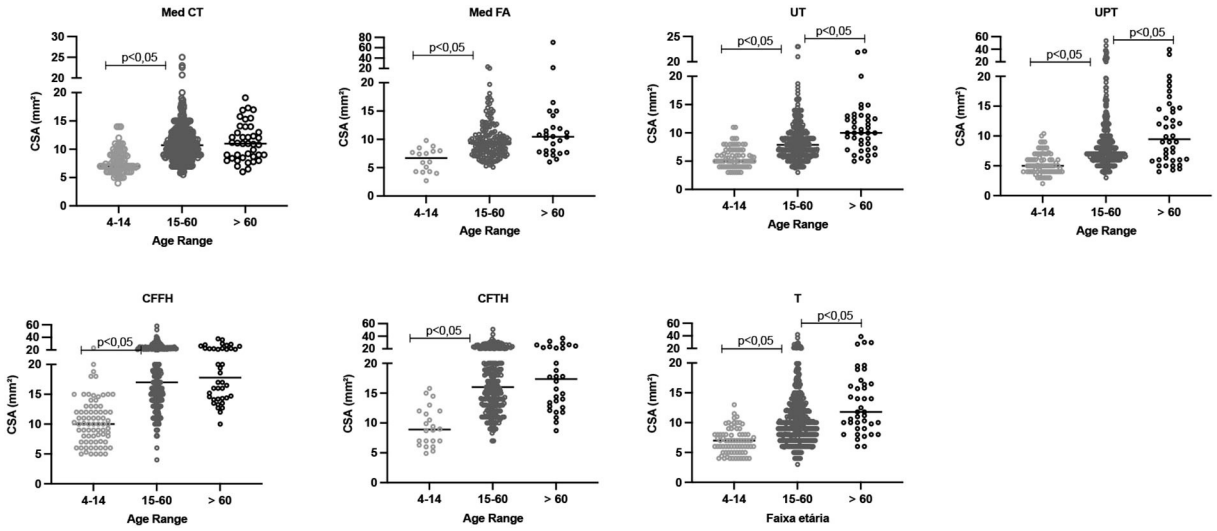

FIGURE 3
Distribution of absolute CSA (mm^2) values for the neural sites assessed in patients with leprosy according to age range, with differences highlighted ($p < 0.05$). CSA, cross-sectional area; Med CT, median carpal tunnel; Med FA, median forearm; UT, cubital ulnar tunnel; UPT, cubital ulnar pretunnel; CFFH, common fibular in the fibula head; CFTH, common fibular thigh; T, tibial.

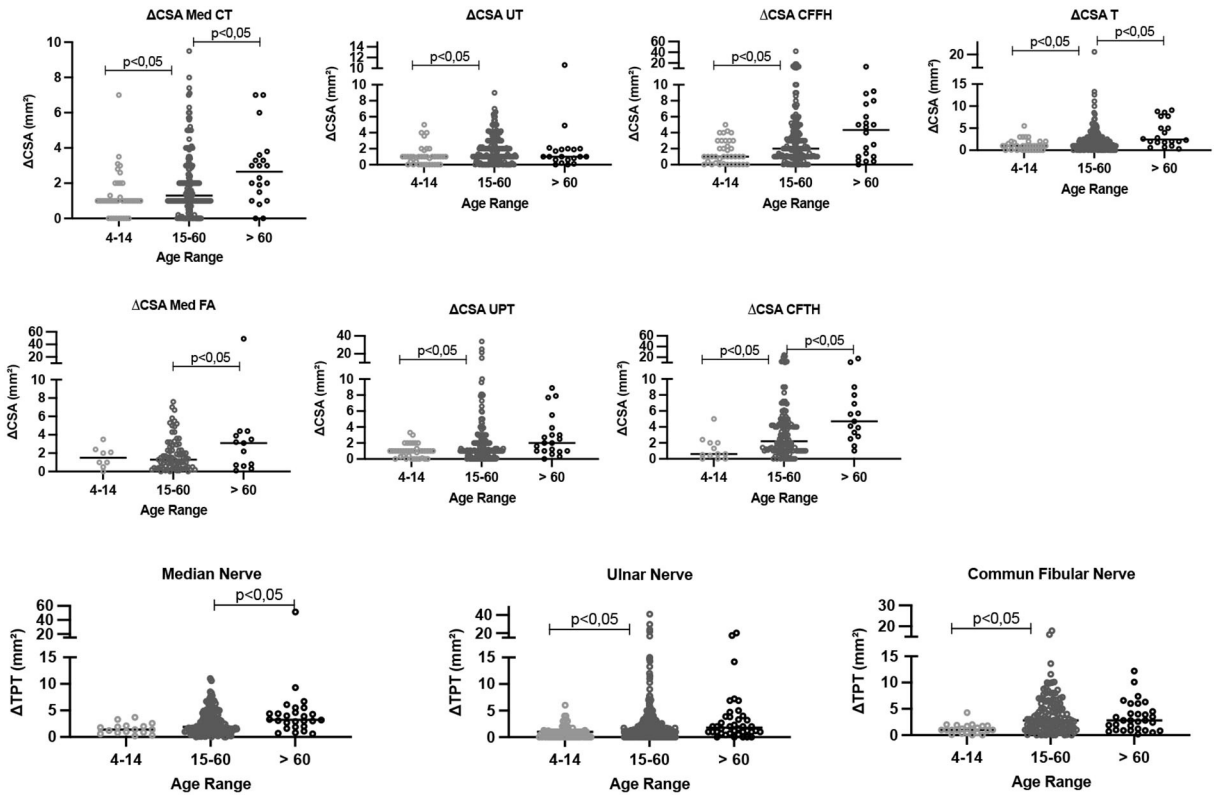

FIGURE 4
Comparative analysis of the difference between the right and left CSA values (ΔCSA) and the values in the same nerve (ΔTPT) according to age range. CSA, cross-sectional area; Med CT, median carpal tunnel; Med FA, median forearm; UT, cubital ulnar tunnel; UPT, cubital ulnar pretunnel; CFFH, common fibular in the fibula head; CFTH, common fibular thigh; T, tibial. ΔCSA, difference between the right and the left nerve at the same site of assessment, ΔTPT, difference between different sites of the same nerve.

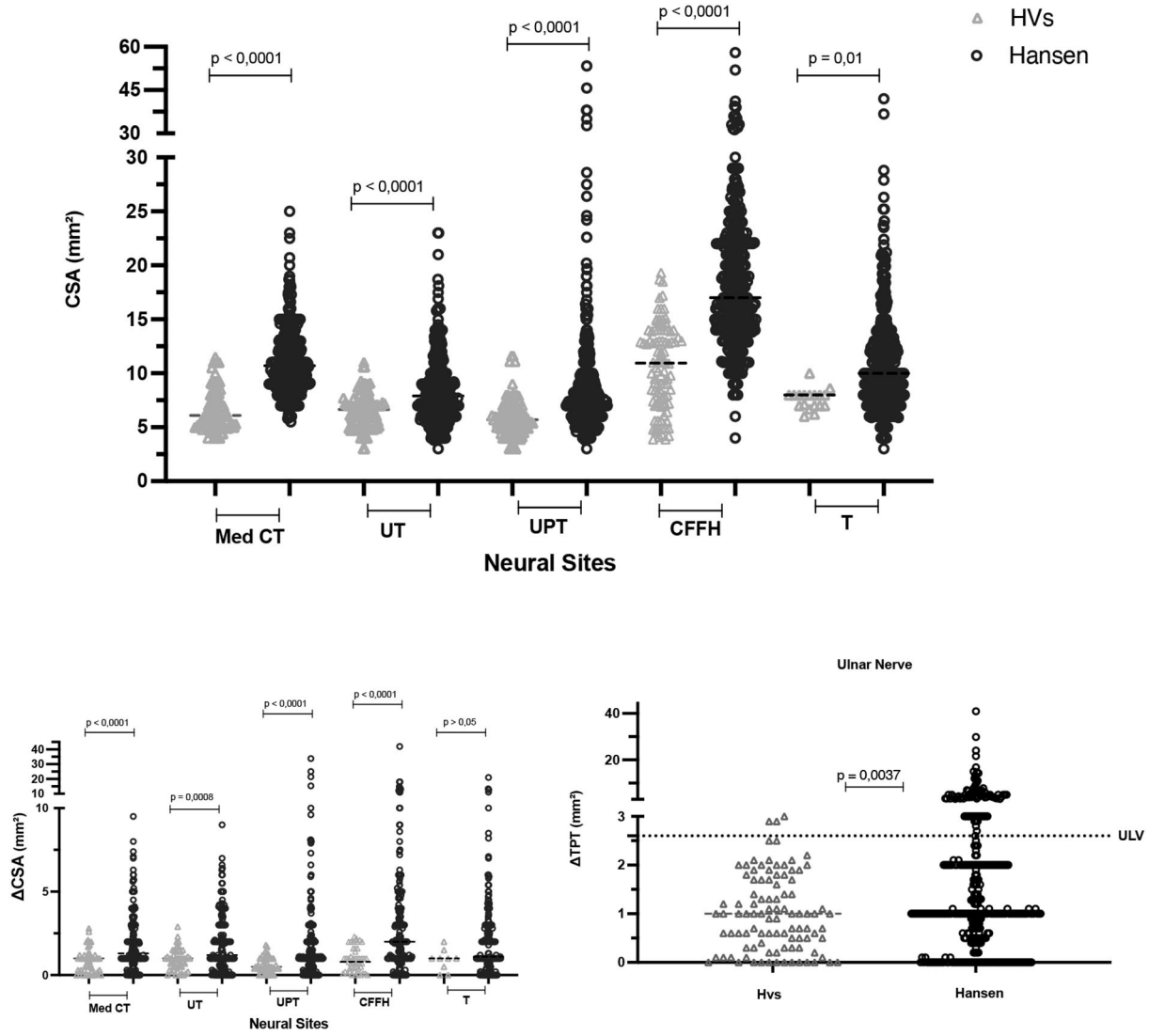

FIGURE 5
Comparative analysis of peripheral nerve CSA, ΔCSA (mm^2), and ΔTPT (mm^2) values between healthy individuals and patients with Hansen's disease aged 15–60 years. CSA, cross-sectional area; Med CT, median carpal tunnel; Med FA, median forearm; UT, cubital ulnar tunnel; UPT, cubital ulnar pretunnel; CFFH, common fibular in the fibula head; CFpFH, common fibular proximal fibular head; T, tibial; ΔCSA, difference between the right and the left nerve at the same site of assessment; ΔTPT, difference between the same nerve at different sites of assessment; HVs, healthy volunteers; Hansen, patients with Hansen's disease.

Analysis of the absolute number and percentage of thickened nerves per individual

Analyzing each subject, the percentage of thickened nerves detected among the total number of nerves assessed was higher among patients with HD than among healthy individuals ($p < 0.0001$). The ROC curve revealed an AUC of 89.1 (95% CI: 84.6–93.5%, $p < 0.0001$) (Figure 7). These findings indicate that when the percentage of thickened nerves was higher than 16.5% (more than two altered nerve sites), the sensitivity reached 76.1% (CI: 69.3–81.8) and specificity reached 87.8% (75.8–94.3), with a relative risk for HD of 6.2.

Considering the 16.5% sensitivity detected, for a binomial analysis, we divided our sample into subjects with up to two nerves altered (≤ 2) and individuals with more than two nerves altered (>2). The chi-square value with Yates correction was

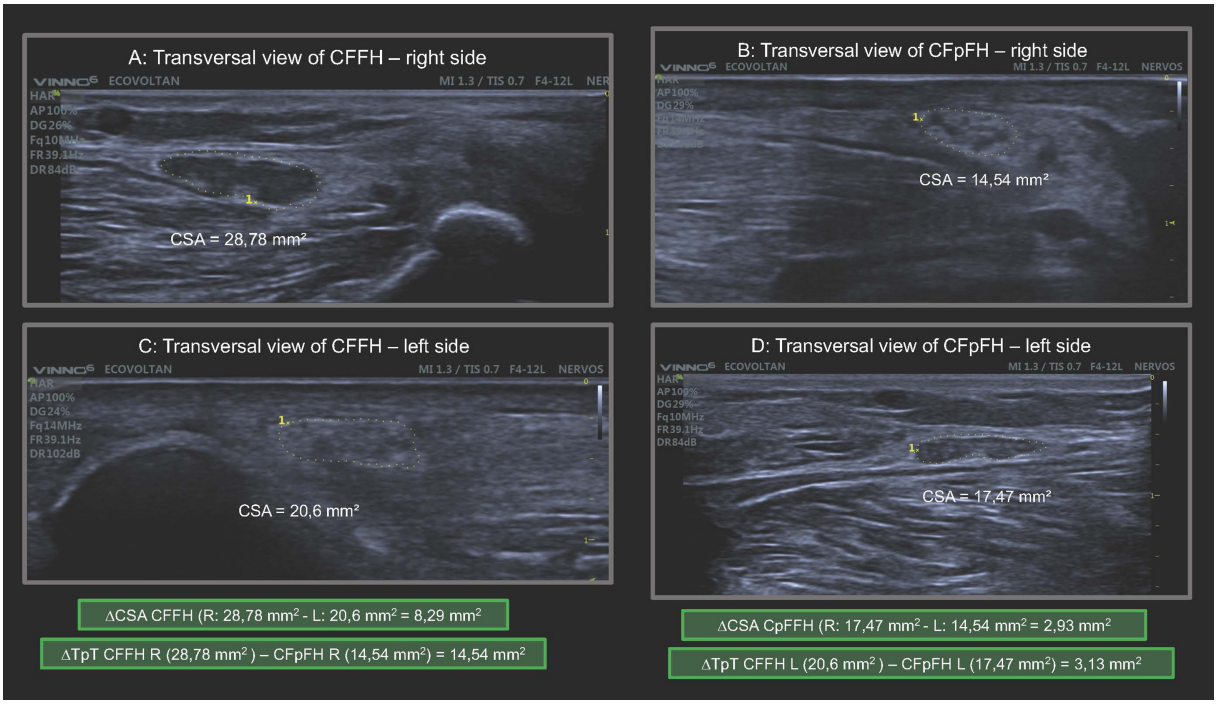

FIGURE 6
Transversal view of common fibular nerve on the right and left sides in the same HD patient demonstrating enlargement of peripheral nerve, asymmetry (ΔCSA) and focality (ΔTpT) major than normal references values. CSA, cross-sectional área; CFFH, common fibular nerve at fibular head; CFpFH, common fibular nerve proximal at fibular head; R, right; L, left; ΔCSA, asymmetry; ΔTpT, focality. In the green frame we highlight the calculation of ΔCSA and ΔTpT.

52.03 ($p < 0.00001$), with individuals having two or more thickened nerves at 24.1 times higher relative risk (95% CI: 6.74–88.98) of Hansen's disease.

Analysis by number of asymmetrical sites per subject

Analysis of asymmetries among the neural sites (ΔCSA) defined as altered (more than RV ± 2 SD) per individual by the ROC curve when comparing healthy individuals and patients with HD revealed that the area under the curve was 85.09 (95% CI: 0.79–0.90, $p < 0.0001$), as demonstrated in Figure 8. Our data showed 79% sensitivity (72.37–84.35) and 87.8% specificity (75, 76–94, 27) when more than 10% of the neural sites evaluated presented altered ΔCSA (>2.5 mm^2), with a relative risk of 6.45 for HD.

Considering the 10% sensitivity index detected, for a binomial analysis, and dividing our sample into individuals who had zero nerves altered in terms of asymmetry and individuals with one or more altered asymmetries (≥1), the chi-square value with Yates correction was 71.6 ($p < 0.0001$), and individuals with one or more asymmetrical nerves were found to be at 13 times higher relative risk (95% CI: 5.98–28.79) of HD.

Analysis by the difference between two sites of the same nerve per individual (Focality)

When comparing healthy individuals with patients with HD, we checked the cutoff point for the number of altered ΔTpT per individual, and we found no difference between groups ($p > 0.05$) (Table 3, Figure 9).

For a binomial analysis, we divided our sample into individuals who had no altered ΔTPT and individuals with one or more altered ΔTPT (≥1). The chi-square value with Yates correction was 18.3 ($p < 0.0001$), and individuals with one or more altered ΔTPT were found to have a 6.4 higher relative risk (95% CI: 2.5–21.9) of HD.

Discussion

Over the last decade, HRUS has become an invaluable diagnostic method for the assessment of peripheral nerves, being used for the assessment of focal and diffuse thickening and of echotextural changes and fascicular patterns in various neuropathies. These features can be quantified objectively by measuring the CSA of the nerve. An increased CSA of the

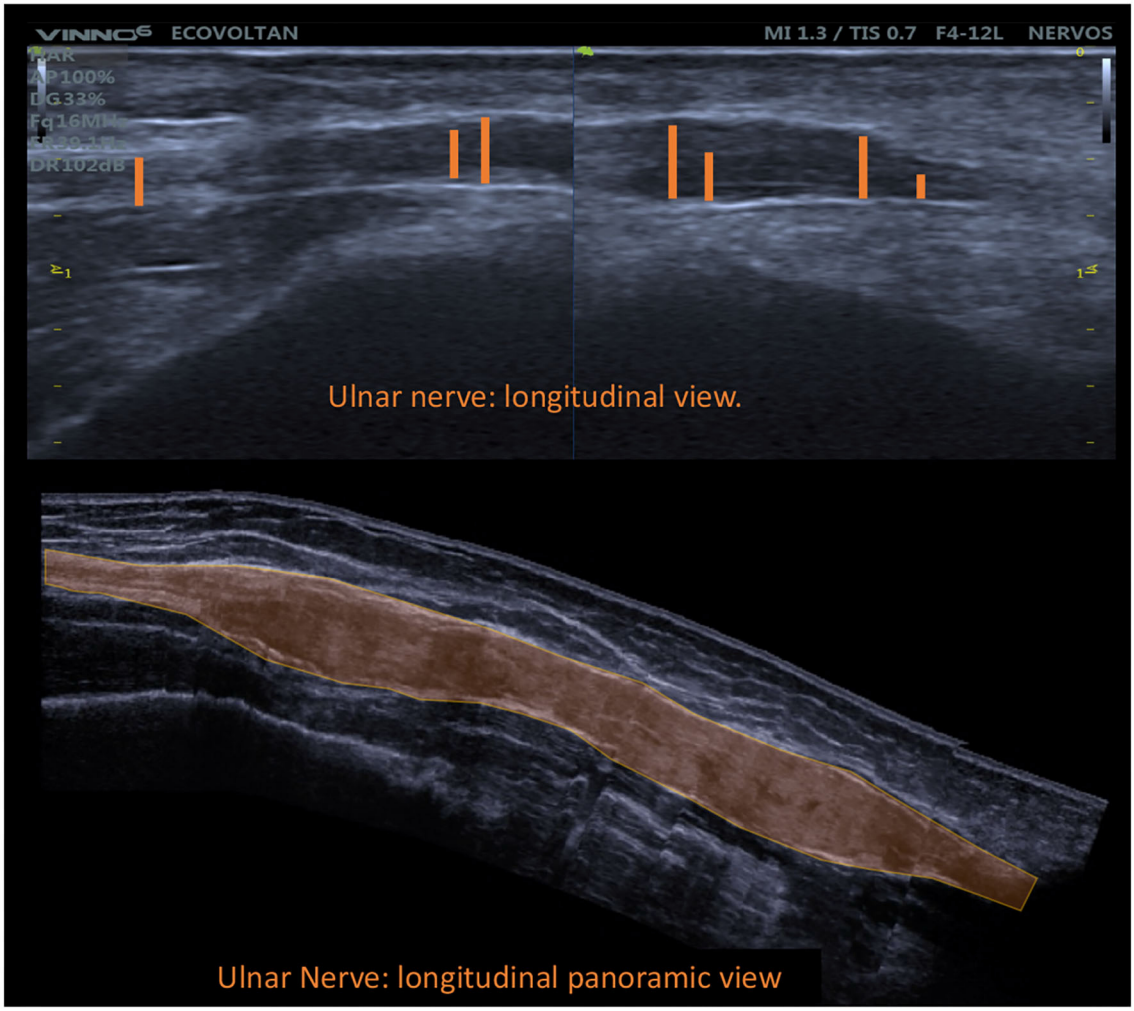

FIGURE 7
Longitudinal view of the common fibular nerve with fusiform enlargement demonstrating focality (ΔTpT).

nerve involved permits a precise localization in compressive neuropathies and in neural tumors (25, 26).

The more severe consequences of leprosy such as deformities and disability are due to neurologic involvement (11). For this reason, the WHO suggests more studies with peripheral nerve ultrasound in neuropathy of leprosy since palpation of peripheral nerves is subjective and requires training (13), with agreement between pairs of professionals trained in the technique of nerve palpation being unsatisfactory (27), while HRUS has better cost-effectiveness than other methods, such as magnetic resonance (15, 28).

In the present study, the age range of 15–60 years was selected because it shows lower variation of absolute CSA values (mm^2) of peripheral nerves (29), with lower values among children and adolescents and higher values among older individuals. Another important factor for this choice was the epidemiological distribution based on the time of disease incubation and risk of transmission, proposed for HD by dividing the age ranges into lower and higher than 15 years.

Our study stands out by involving the largest series in the world for the assessment of the peripheral nerves of patients with leprosy, with all examinations being performed by the same physician specialized in imaging diagnosis during an active search within the community and not solely within hospitals and reference centers.

The assessment of the differences in the CSA of the neural sites (ΔCSA and ΔTPT) distributed according to age range (Figure 4) demonstrated that the youngest has shorter time of disease and, consequently, lower differences between sides (ΔCSA) and between sites of the same nerve (ΔTPT). Only the ulnar nerve did not show change in the ΔCSA and ΔTPT with

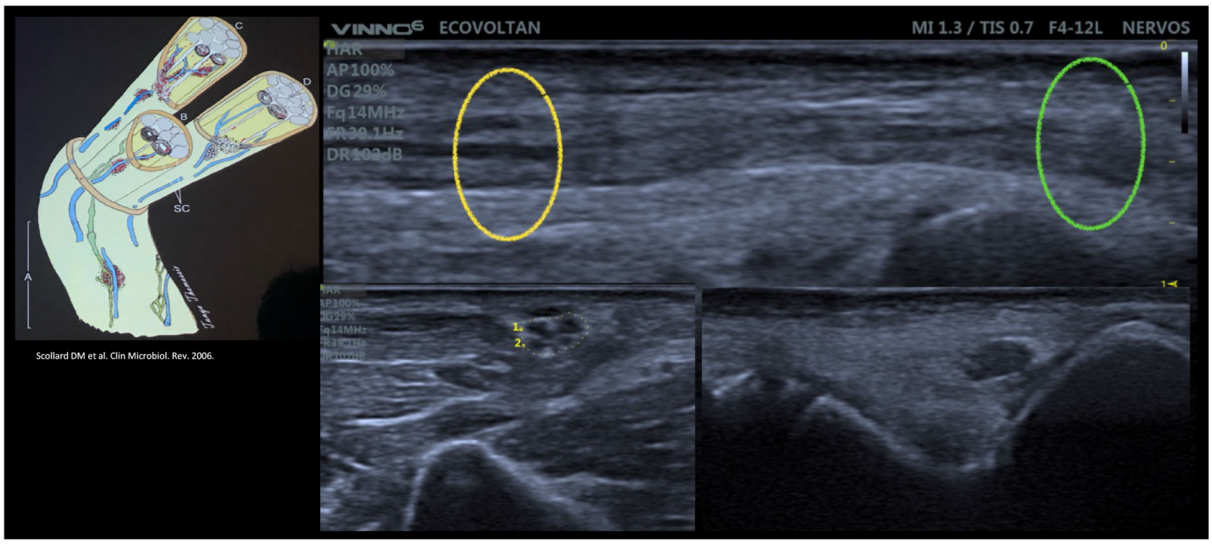

FIGURE 8
Intraneural focality pattern [Scollard pattern (4) demonstrated by Voltan, G and Frade, MAC with the high-resolution ultrasound] of the ulnar nerve on the longitudinal view (up) and transversal view (down right and down left) showing the different fascicle patterns in the same nerve.

age, highlighting as an important nerve for the assessment of HD neuropathy.

For all neural sites, patients with HD presented higher absolute CSA values than healthy individuals ($p < 0.0001$), confirming the data reported by Frade et al. (10) in a study conducted at a reference center for HD.

Regarding asymmetry between the right and left sides, patients with HD also had higher ΔCSA values than healthy individuals (Figure 10), which is also in agreement with the data reported by Frade et al. (10).

Regarding focality, that is, the difference between two sites on the same nerve (the ulnar nerve), the highest mean, standard deviation, and median ΔTPT values were obtained for the HD group (HD: 2.3 ± 3.9 mm^2/HV: 1.0 ± 0.8 mm^2; median 1.0 mm^2) (Figure 11). These changes characterize the neuropathy of HD as hypertrophic, asymmetrical, and focal, findings which confirm the data reported by Frade et al. (10) and Pottecher et al. (30).

Klauser et al. (31), Klauser et al. (32), and Miyamoto et al. (33) have reported that thickening of the median nerve in cases confirmed as having carpal tunnel syndrome occurs inside the tunnel. Nagappa et al. (34) recently showed that the thickening 2 cm proximal of the carpal tunnel for the median nerve discriminates leprosy from the carpal tunnel syndrome (34). The localization of neural thickening, such as in the ulnar nerve in the cubital pretunnel, helps in the diagnosis of leprosy neuropathy (10, 15, 19, 20, 35).

Jain et al. (20) detected at least one thickened nerve in 18/20 (90%) patients with leprosy and concluded that neural involvement affects a larger number of nerves and various neural

TABLE 3 ROC curve table comparing the percentage of nerves with at least one altered ΔTpT (>2.5 mm^2 - focality) between healthy individuals and patients with leprosy.

	Sensitivity%	95% CI	Specificity%	95% CI	Likelihood ratio
>0.5000	39.77	32.83–47.15%	93.88	83.48–97.90%	6.496
>1.500	8.523	5.233–13.58%	100.0	92.73–100.0%	

sites in leprosy. Considering nerves greater than the upper normal limits to be altered (mean ± 2 SD), our data identified altered CSAs in 157/176 (89%) cases, in agreement with Jain et al. (20). In addition, 113 patients (64%) had altered absolute CSA values in at least three sites of peripheral nerves, a fact that defines leprosy neuropathy as hypertrophic.

Several laboratory tests have been studied for the diagnosis of leprosy, such as the use of anti-PGL1, which showed lower sensitivity than other antigens but did not affect specificity, and a meta-analysis showed mean sensitivity of 59.1% (95% CI 50.6–671) and specificity of 91.7% (95% CI 83.9–94.9). In 78 studies, ELISA was the test predominantly investigated among all available serological tests, with sensitivity ranging widely from 0 to 100% and specificity ranging from 13 to 100% (36).

Peripheral nerve thickening viewed by HRUS showed superior sensitivity and specificity for the diagnosis of HD neuropathy. Thus, if an individual has at least two neural sites (16.5%) defined as thickened, this finding has 76.1% sensitivity and 87.8% specificity, with an RR of 24. When at least one neural site (10%) of the nerves assessed shows asymmetrical

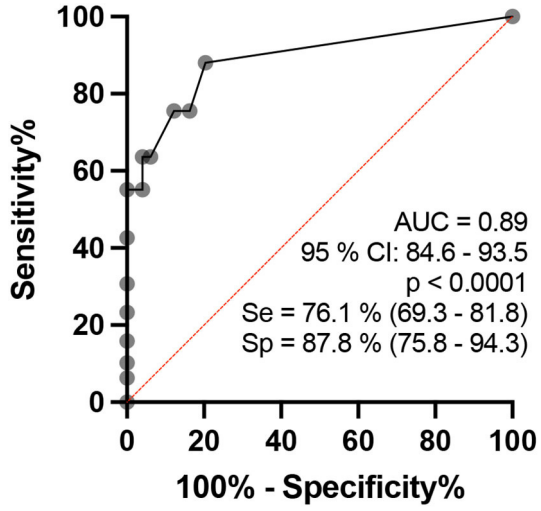

FIGURE 9
ROC curve analysis of the percentage of altered nerves among the nerves assessed per individual in healthy and HD groups.

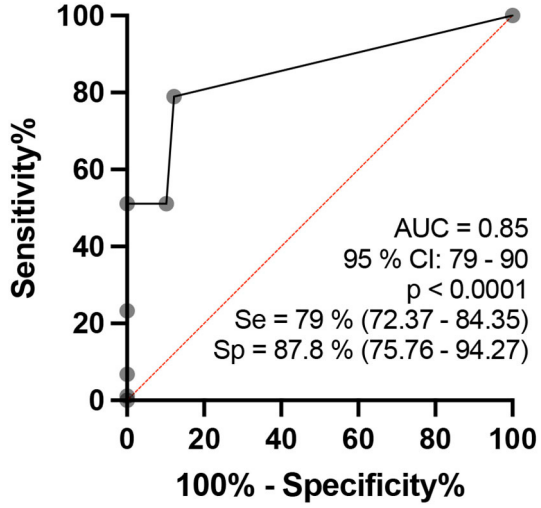

FIGURE 10
ROC curve analysis of the percentages of the number of asymmetries of the neural sites assessed per individual, which is considered to be altered (ΔCSA>2.5 mm^2) when comparing the healthy and HD groups in the age range of 15 to 60 years.

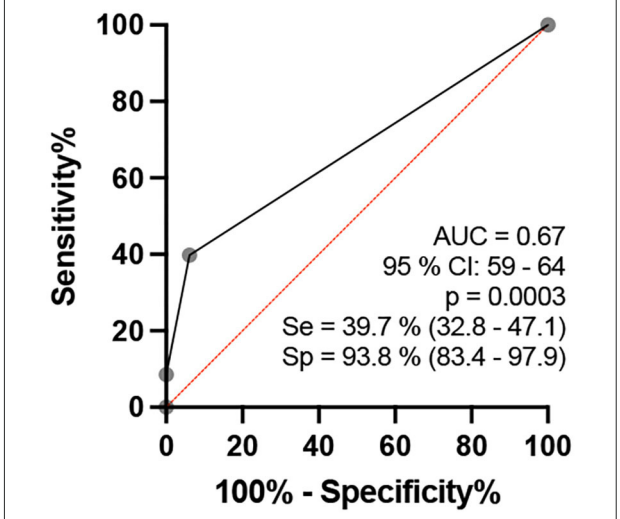

FIGURE 11
ROC curve analysis of the percentage of the number of altered ΔTpT (>2.5 mm^2 - focality) of the neural sites assessed per individual when comparing the healthy and leprosy groups in the age range of 15–60 years.

thickening, sensitivity is 72.4% and specificity is 87.8%, with an RR of 13. Regarding the ΔTPT of the ulnar nerve lesion, 40% of the patients had at least one nerve, with a difference of more than 2.6 mm^2, 39.7% sensitivity, 100% specificity, and an RR of 6.4 times.

Also, the authors bring some tips about when screening the patients:

- El Gency et al. (12) concluded that "a peripheral neuropathy accompanied by neural thickening with or without cutaneous manifestations should lead the clinician to think about HD," so we indicate that for patients without sensory loss classified as glove or boot who present islands of sensitivity alteration, the clinician could perform ultrasound of peripheral nerves following the protocol for leprosy.
- Every individual with clinical suspicion of leprosy plus the clinical suspicion of neuritis (pain or shock in the nerve path) should be evaluated by high-resolution ultrasound following the protocol for leprosy.
- Every individual who is in contact with a patient with leprosy should be scanned by HRUS in order to carry out future follow-ups so that we can make an early diagnosis when there is nerve thickening associated with some functional loss.

There are some limitations to the study: All patients with HD were not assessed for the Med FA (median forearm) and CFTH (common fibular thigh), we did not compare these two neural points between HD and HV groups, and our data did not compare patients with HD with other neuropathies. Other limitations may be the use of three different machines, which may have some difference in relation to the CSA obtained on different machines, but we tried to strictly follow the protocols for measuring the CSA, which makes the study quite robust. All our data collection was carried out during active patient search campaigns in four Brazilian states; therefore, it was not carried out in referral hospitals. Therefore, we assume that these patients had a shorter time of disease or infection, perhaps even early; however, it is very difficult to answer this question exactly since

the pathophysiology and natural history of the disease in patients with leprosy 2–5 years, according to some authors.

Conclusion

HD assessed by HRUS is established as a primary neural disease that leads to multiple hypertrophic mononeuropathy characterized by CSA values exceeding normal limits: Med CT = 10.2 mm^2; UT = 9.8 mm^2; UPT = 9.3 mm^2; CFFH = 18.3 mm^2; T = 9.6 mm^2.

An individual with at least two thickened nerves assessed in the active search campaign has a 23.1 greater chance of having leprosy than a healthy individual.

HD neuropathy is characterized not only by an increased CSA but also by the pattern of asymmetry (ΔCSA>2.5 mm^2 with an RR of 13) and focality (ΔTPT>2.5 mm^2 with an RR of 6.4) of this thickening, with high sensitivity and specificity for its early diagnosis.

Peripheral nerve ultrasound based on the protocol for the assessment of leprosy neuropathy (Med CT, UT, UPT, CFFH, and T nerves) can be used as a point-of-care method for the early diagnosis of HD neuropathy.

Data availability statement

The raw data supporting the conclusions of this article will be made available by the authors, without undue reservation.

Ethics statement

The studies involving human participants were reviewed and the present study was approved by the Research Ethics Committee of the University Hospital, Faculty of Medicine of Ribeirão Preto, University of São Paulo (protocol no. 2.165.032, MH-Brasil and 92228318.1.0000.5440). Written informed consent to participate in this study was provided by the participants' legal guardian/next of kin.

Author contributions

GV and MF: contributed on all stage of this study, to conception and design of the study, performed the statistical analysis, to manuscript revision, read, and approved the submitted version. FF, ND, CSi, ML, JS, JB, CSa, GC, and MD: contributed to conception and design of the study, to data collection, obtaining, analyzing and interpreting data, and approved the submitted version. All authors contributed to the article and approved the submitted version.

Funding

Coordenação de Aperfeiçoamento de Pessoal de Nível Superior - Brazil (CAPES) - Finance Code 001. National Council for Scientific and Technological Development (CNPq). Center of National Reference in Sanitary Dermatology and HD - Hospital of the Medical School of Ribeirão Preto, Ribeirão Preto, São Paulo, Brazil; the Brazilian Health Ministry (MS/FAEPAFMRP-USP: 749145/ 2010 and 767202/2011); Oswaldo Cruz Foundation (Fiocruz) Ribeirão Preto - TED 163/2019 - Process: No 25380.102201/2019-62/ Project Fiotec: PRES-009-FIO-20; VALE S.A. 27756/2019.

Conflict of interest

The authors declare that the research was conducted in the absence of any commercial or financial relationships that could be construed as a potential conflict of interest.

Publisher's note

All claims expressed in this article are solely those of the authors and do not necessarily represent those of their affiliated organizations, or those of the publisher, the editors and the reviewers. Any product that may be evaluated in this article, or claim that may be made by its manufacturer, is not guaranteed or endorsed by the publisher.

Supplementary material

The Supplementary Material for this article can be found online at: https://www.frontiersin.org/articles/10.3389/fmed.2022.985252/full#supplementary-material

References

1. World Health Organization. *Guidelines for the Diagnosis, Treatment and Prevention of Leprosy*. New Delhi: World Health Organization, Regional Office for South-East Asia (2017). Licence: CC BY-NC-SA 3.0 IGO.

2. Chacha JJ, Peters L, Rivitti EA, Sotto MN, Lourenço S, Melnikov P. Sistema nervoso periférico e pressupostos da agressão neural na hanseníase. *An Bras Dermatol.* (2009) 84:495–500. doi: 10.1590/S0365-059620090005 00008

3. Alemu Belachew W, Naafs B. Position statement: LEPROSY: diagnosis, treatment and follow-up. *J Eur Acad Dermatology Venereol.* (2019) 33:1205–13. doi: 10.1111/jdv.15569

4. Scollard DM, Adams LB, Gillis TP, Krahenbuhl JL, Truman RW, Williams DL. The continuing challenges of leprosy. *Clin Microbiol Rev.* (2006) 19:338–81. doi: 10.1128/CMR.19.2.338-381.2006

5. Ebenezer GJ, Polydefkis M, Scollard DM. Mechanisms of nerve injury in leprosy. In Scollard DM, Gillis TP, editors. *International Textbook of Leprosy.* (2016). Available online at: https://m3u9w4p9.stackpathcdn.com/sites/default/files/ITL_9_2%20FINAL.pdf

6. Garbino JA, Marques W Jr, Barreto JA, Heise CO, Rodrigues MM, Antunes SL, et al. Primary neural leprosy: Systematic review | Hanseníase neural primária: Revisão sistemática. *Arq Neuropsiquiatr.* (2013) 71:397–404. doi: 10.1590/0004-282X20130046

7. Bernardes F Filho, Paula NA, Leite MN, Abi-Rached TLC, Vernal S, Silva MBD, et al. Evidence of hidden leprosy in a supposedly low endemic area of Brazil. *Mem Inst Oswaldo Cruz.* (2017) 112:822–8. doi: 10.1590/0074-02760170173

8. Lugão HB, Frade MAC, Marques-Jr W, Foss NT, Nogueira-Barbosa MH. Ultrasonography of leprosy neuropathy: a longitudinal prospective study. *PLoS Negl Trop Dis.* (2016) 10:1–14. doi: 10.1371/journal.pntd.0005111

9. Lugão HB, Nogueira-Barbosa MH, Marques W, Foss NT, Frade MAC. Asymmetric nerve enlargement: a characteristic of leprosy neuropathy demonstrated by ultrasonography. *PLoS Negl Trop Dis.* (2015) 9:1–11. doi: 10.1371/journal.pntd.0004276

10. Frade MA, Nogueira-Barbosa MH, Lugão HB, Furini RB, Marques Júnior W, Foss NT. New sonographic measures of peripheral nerves: a tool for diagnosis of peripheric nerve involvment in leprosy. *Hansenol Int.* (2013) 36:71. doi: 10.1590/S0074-02762013000300001

11. The Lancet Neurology. Leprosy as a neurological disease. *Lancet Neurol.* (2009) 8:217. doi: 10.1016/S1474-4422(09)70026-2

12. El Gency HI, Ghanema M, Hussein SA, Almaghraby OS, Rashad W. Peripheral neuropathy is not the end but the beginning. *Lepr Rev.* (2017) 88:574–82. doi: 10.47276/lr.88.4.574

13. Van Brakel WH, Saunderson P, Shetty V, Brandsma JW, Post E, Jellema R, et al. International workshop on neuropathology in leprosy - consensus report. *Lepr Rev.* (2007) 78:416–33. doi: 10.47276/lr.78.4.416

14. Wortsman X, Jemec GBE. *Dermatologic Ultrasound with Clinical and Histologic Correlations.* (2013). doi: 10.1007/978-1-4614-7184-4

15. Martinoli C, Bianchi S, Derchi LE. Ultrasonography of peripheral nerves. *Semin Ultrasound CT MRI.* (2000) 21:205–13. doi: 10.1016/S0887-2171(00)90043-X

16. Suk, Jung Im, Walker, Francis O, Cartwright MS. Ultrasound of Peripheral Nerves. *Curr Neurol Neurosci Rep.* (2013) 13:1–7. doi: 10.1007/s11910-012-0328-x

17. Martinoli C, Bianchi S, Derchi LE. Ultrasonography of peripheral nerves. *Neurol Sci.* (2000) 21(4 SUPPL.):205–13.

18. Lugão HB, Frade MAC, Mazzer N, Foss NT, Nogueira-Barbosa MH. Leprosy with ulnar nerve abscess: ultrasound findings in a child. *Skeletal Radiol.* (2017) 46:137–40. doi: 10.1007/s00256-016-2517-1

19. Bathala L, N Krishnam V, Kumar HK, Neladimmanahally V, Nagaraju U, Kumar HM, et al. Extensive sonographic ulnar nerve enlargement above the medial epicondyle is a characteristic sign in Hansen's neuropathy. *PLoS Negl Trop Dis.* (2017) 11:1–10. doi: 10.1371/journal.pntd.0005766

20. Jain S, Visser LH, Praveen TL, Rao PN, Surekha T, Ellanti R, et al. High-resolution sonography : a new technique to detect nerve damage in leprosy. *PLoS Negl Trop Dis.* (2009) 3:1–7. doi: 10.1371/journal.pntd.0000498

21. Kerasnoudis A, Pitarokoili K, Behrendt V, Gold R, Yoon MS. Cross sectional area reference values for sonography of peripheral nerves and brachial plexus. *Clin Neurophysiol.* (2013) 124:1881–8. doi: 10.1016/j.clinph.2013.03.007

22. Tagliafico A, Cadoni A, Fisci E, Bignotti B, Padua L, Martinoli C. Reliability of side-to-side ultrasound cross-sectional area measurements of lower extremity nerves in healthy subjects. *Muscle Nerve.* (2012) 46:717–22. doi: 10.1002/mus.23417

23. Boehm J, Scheidl E, Bereczki D, Schelle T, Arányi Z. High-resolution ultrasonography of peripheral nerves: measurements on 14 nerve segments in 56 healthy subjects and reliability assessments. *Ultraschall der Medizin.* (2014) 35:459–67. doi: 10.1055/s-0033-1356385

24. Grimm A, Axer H, Heiling B, Winter N. Nerve ultrasound normal values – Readjustment of the ultrasound pattern sum score UPSS. *Clin Neurophysiol.* (2018) 129:1403–9. doi: 10.1016/j.clinph.2018.03.036

25. Peer S, Gruber H. *Atlas of Peripheral Nerve Ultrasound 2013 With Anatomic and MRI Correlation.* Berlin; Heidelberg: Springer (2013). doi: 10.1007/978-3-642-25594-6

26. Bignotti B, Tagliafico A, Martinoli C. Ultrasonography of peripheral nerves: anatomy and pathology. *Ultrasound Clin.* (2014) 9:525–36. doi: 10.1016/j.cult.2014.03.006

27. Chen S, Wang Q, Chu T, Zheng M. Inter-observer reliability in assessment of sensation of skin lesion and enlargement of peripheral nerves in leprosy patients. *Lepr Rev.* (2006) 77:371–6. doi: 10.47276/lr.77.4.371

28. Martinoli C, Derchi LE, Bertolotto M, Gandolfo N, Bianchi S, Fiallo P, et al. US and MR imaging of peripheral nerves in leprosy. *Skeletal Radiol.* (2000) 29:142–50. doi: 10.1007/s002560050584

29. Lothet EH, Bishop TJ, Walker FO, Cartwright MS. Ultrasound-derived nerve cross-sectional area in extremes of height and weight. *J Neuroimaging.* (2019) 29:406–9. doi: 10.1111/jon.12590

30. Pottecher P, Flageul B, Sibileau E, Laredo JD, Bousson V. Peripheral hypertrophic neuropathy due to leprosy: ultrasound and MR imaging findings. *Diagn Interv Imaging.* (2016) 97:471–3. doi: 10.1016/j.diii.2015.09.014

31. Klauser AS, Halpern EJ, Faschingbauer R, Guerra F, Martinoli C, Gabl MF, et al. Bifid median nerve in carpal tunnel syndrome: assessment with US cross-sectional area measurement. *Radiology.* (2011) 259:808–15. doi: 10.1148/radiol.11101644

32. Klauser AS, Halpern EJ, De Zordo T, Feuchtner GM, Arora R, Gruber J et al. Carpal tunnel syndrome assessment with US: value of additional cross-sectional area measurements of the median nerve in patients versus healthy volunteers. *Radiology.* (2009) 250:171–7. doi: 10.1148/radiol.2501080397

33. Miyamoto H, Halpern EJ, Kastlunger M, Gabl M, Arora R, Bellmann-Weiler R, et al. Carpal tunnel syndrome: diagnosis by means of median nerve elasticity-improved diagnostic accuracy of US with sonoelastography. *Radiology.* (2014) 270:481–6. doi: 10.1148/radiol.13122901

34. Nagappa M, Pujar GS, Keshavan AH, Bathala L, Jain RD, Das A, et al. Sonographic pattern of median nerve enlargement in Hansen's neuropathy. *Acta Neurol Scand.* (2021) 144:155–60. doi: 10.1111/ane.13432

35. Visser LH, Jain S, Lokesh B, Suneetha S, Subbanna J. Morphological changes of the epineurium in leprosy: a new finding detected by high-resolution sonography. *Muscle Nerve.* (2012) 46:38–41. doi: 10.1002/mus.23269

36. Gurung P, Gomes CM, Vernal S, Leeflang MMG. Diagnostic accuracy of tests for leprosy: a systematic review and meta-analysis. *Clin Microbiol Infect.* (2019) 25:1315–27. doi: 10.1016/j.cmi.2019.05.020

frontiers | Frontiers in Medicine

TYPE Systematic Review
PUBLISHED 31 October 2022
DOI 10.3389/fmed.2022.1048913

OPEN ACCESS

EDITED BY
Devinder Mohan Thappa,
Jawaharlal Institute of Postgraduate Medical Education and Research (JIPMER), India

REVIEWED BY
Ahu Yorulmaz,
Ankara City Hospital, Turkey
Barbara Ruaro,
University of Trieste, Italy
Inda Astri Aryani,
Sriwijaya University, Indonesia

*CORRESPONDENCE
Je-Ho Mun
jehomun@snu.ac.kr

SPECIALTY SECTION
This article was submitted to Dermatology, a section of the journal Frontiers in Medicine

RECEIVED 20 September 2022
ACCEPTED 10 October 2022
PUBLISHED 31 October 2022

CITATION
Lim SS, Hui L, Ohn J, Cho Y, Oh CC and Mun J-H (2022) Diagnostic accuracy of dermoscopy for onychomycosis: A systematic review. *Front. Med.* 9:1048913. doi: 10.3389/fmed.2022.1048913

Diagnostic accuracy of dermoscopy for onychomycosis: A systematic review

Sophie Soyeon Lim[1], Laura Hui[2], Jungyoon Ohn[3,4], Youngjoo Cho[5], Choon Chiat Oh[2] and Je-Ho Mun[3,4]*

[1]Alfred Health, Melbourne, VIC, Australia, [2]Department of Dermatology, Singapore General Hospital, Singapore, Singapore, [3]Department of Dermatology, Seoul National University College of Medicine, Seoul, South Korea, [4]Institute of Human-Environment Interface Biology, Seoul National University, Seoul, South Korea, [5]Department of Applied Statistics, Konkuk University, Seoul, South Korea

Background: Dermoscopy is a non-invasive adjuvant diagnostic tool that allows clinicians to visualize microscopic features of cutaneous disorders. Recent studies have demonstrated that dermoscopy can be used to diagnose onychomycosis. We performed this systematic review to identify the characteristic dermoscopic features of onychomycosis and understand their diagnostic utility.

Methods: We searched the Medline, Embase, Scopus, and Cochrane databases from conception until May 2021. Studies on the dermoscopic features of onychomycosis were screened. The exclusion criteria were as follows: fewer than 5 cases of onychomycosis, review articles, and studies including onychomycosis cases that were not mycologically verified. Studies on fungal melanonychia were analyzed separately. We adhered to the MOOSE guidelines. Independent data extraction was performed. Data were pooled using a random effects model to account for study heterogeneity. The primary outcome was the diagnostic accuracy of the dermoscopic features of onychomycosis. This was determined by pooling the sensitivity and specificity values of the dermoscopic features identified during the systematic review using the DerSimonian-Laird method. Meta-DiSc version 1.4 and Review Manager 5.4.1 were used to calculate these values.

Results: We analyzed 19 articles on 1693 cases of onychomycosis and 5 articles on 148 cases of fungal melanonychia. Commonly reported dermoscopic features of onychomycosis were spikes or spiked pattern (509, 30.1%), jagged or spiked edges or jagged edge with spikes (188, 11.1%), jagged proximal edge (175, 10.3%), subungual hyperkeratosis (131, 7.7%), ruins appearance, aspect or pattern (573, 33.8%), and longitudinal striae (929, 54.9%). Commonly reported features of fungal melanonychia included multicolor

(101, 68.2%), non-longitudinal homogenous pigmentation (75, 50.7%) and longitudinal white or yellow streaks (52, 31.5%).

Conclusion: This study highlights the commonly identified dermoscopic features of onychomycosis. Recognizing such characteristic dermoscopic features of onychomycosis can assist clinicians diagnose onychomycosis by the bedside.

KEYWORDS

fungal nail infection, onychomycosis, dermoscopy, fungal melanonychia, onychoscopy

Introduction

Dermoscopy is a non-invasive diagnostic tool that helps clinicians to visualize microscopic features of cutaneous disorders, including skin cancers, connective tissue disorders and inflammatory dermatologic conditions, that are not discernible on naked eye examination (1–3). Consequently, it optimizes diagnostic accuracy and minimizes the need for unnecessary biopsies (4).

Onychomycosis is a communicable fungal nail infection caused by dermatophytes, non-dermatophyte molds, and yeasts. It is the most common nail disorder worldwide and severe disease can cause significant nail dystrophy and pain (5). Fungal melanonychia is a rare manifestation of a fungal nail infection, which presents with brown-black pigmentation of the nail unit. Accurate diagnosis of fungal nail disorders is important as systemic treatments are required for at least 2–3 months and topical treatments for more than 12 months. Misdiagnosis should be avoided, as systemic treatments risk hepatic damage (6) and unnecessary economic burden on the healthcare system. Clinically, onychomycosis may resemble traumatic onycholysis, nail psoriasis, or trachyonychia, and differentiating fungal melanonychia from nail melanoma is crucial. Dermoscopy can help to identify onychomycosis and fungal melanonychia at the bedside. Therefore, we conducted a systematic review to identify the characteristic dermoscopic features of onychomycosis and melanonychia, as well as a meta-analysis to determine the diagnostic performance and accuracy of dermoscopy in diagnosing onychomycosis.

Methods

This study adhered to the Meta-analyses of Observational Studies in Epidemiology (MOOSE) statement, with appropriate adjustments made as per the recommendations for systematic reviews and meta-analyses of diagnostic test accuracy (7, 8). The study protocol is registered in PROSPERO (Reg. No.: CRD42021268430).

Literature search

Ovid MEDLINE (including Epub Ahead of Print, In-Process, and Other Non-Indexed Citations), Embase, Scopus, and the Cochrane Central Register of Controlled Trials were searched from inception to May 2021 by three reviewers (SSL, JO, LHLY). The research question was in patients with onychomycosis (P), what are the common dermoscopic features (I) that add to clinical examination (C) in diagnosing onychomycosis (O). Therefore, search terms included "dermoscopy" or synonyms (including dermatoscopy, videodermoscopy, onychoscopy and epiluminescence microscopy) and "onychomycosis" or synonyms (including tinea unguium). Medical subject headings (MeSH) terms were also included.

Eligibility criteria

All published studies involving at least five cases of mycologically proven onychomycosis with dermoscopic findings were included. Studies reporting fewer than five cases were excluded due to risk of selection bias. Studies of fungal melanonychia were analyzed separately.

Study selection and data extraction

Three reviewers (SSL, JO, and LHLY) independently screened the titles and abstracts of all identified articles, and then screened the full text of potentially eligible articles. Non-English articles were screened by reviewing their titles and abstracts translated in English. Duplicate studies and review articles were excluded. None of the cases required a fourth author (JHM) to resolve any disagreement. The parameters extracted from each article included the first author's surname, date of publication, journal name, number of onychomycosis or fungal melanonychia cases, number of control cases, type of control cases (e.g., healthy or psoriasis),

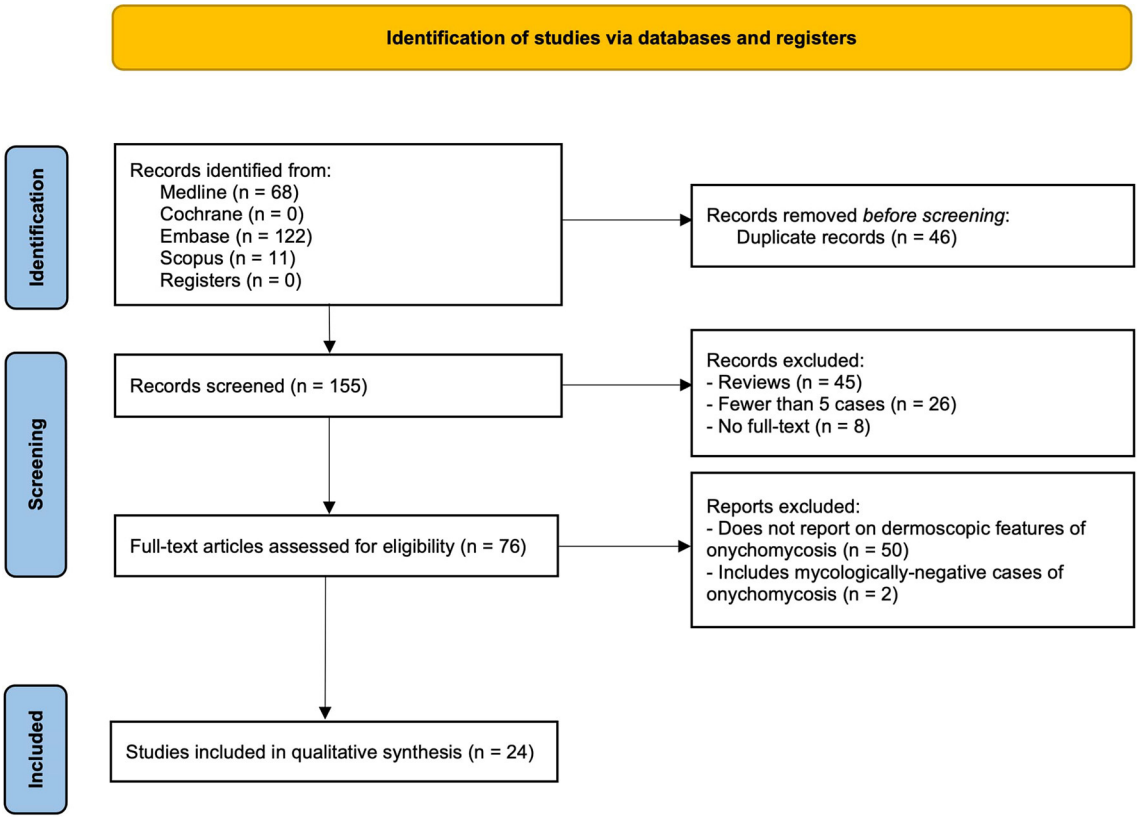

FIGURE 1
Flow diagram illustrating search strategy.

definition and prevalence of dermoscopic features, as well as their sensitivity and specificity if reported. Study authors were not contacted.

Risk of bias assessment

Two reviewers (SSL and JO) appraised the articles according to the Quality Assessment of Diagnostic Accuracy Studies (QUADAS2) guidelines (9).

Statistical analysis of the primary study outcome

The primary study outcome was diagnostic accuracy of the common dermoscopic features of onychomycosis. This was measured by pooling the sensitivity and specificity values using the DerSimonian-Laird method. We used a random-effects model to account for study heterogeneity. Pooled sensitivity and specificity values and their 95% confidence intervals (CI), forest plots, and summary receiver operating characteristics (SROC) curves were generated using Meta-DiSc version 1.4 (Hospital Ramon y Cajal and Universidad Complutense de Madrid) and Review Manager 5.4.1 (Cochrane, Oxford, UK).

Results

Literature search and included studies

A total of 201 articles were identified, of which 46 were duplicates (Figure 1). Of the 155 screened articles, 24 were full-text articles discussing common dermoscopic features in five or more cases of mycologically proven fungal nail disease. The characteristics of the 24 eligible studies are summarized in Table 1. Nineteen articles were on onychomycosis and five were on fungal melanonychia. Of the 19 onychomycosis articles, 11 had a control group consisting of nail psoriasis, traumatic onycholysis, and healthy or mycologically negative nails. A meta-analysis was performed on the data with controls. However, it was not conducted for fungal melanonychia, as

TABLE 1 Characteristics of the eligible studies.

First author and journal	Publication date	Study population	Number of patients	Number of controls (Y/N)*	Control characteristics
Abdallah, *J Cosmet Dermatol*	2020	Onychomycosis	40	N	-
Ankad, *Indian Dermatol Online J*	2020	Onychomycosis	20	Y, 40	Nail psoriasis ($n = 35$), traumatic onycholysis ($n = 5$)
Bhat, *Dermatol Pract Concept*	2018	Onychomycosis	81	N	-
Bodman, *J Am Podiatr Med Assoc*	2017	Onychomycosis	35	Y, 17	Mycologically negative nails
Chetana, *Int J Dermatol*	2018	Onychomycosis	234	N	-
De Crignis, *Int J Dermatol*	2014	Onychomycosis	336	N	-
El-Hoshy, *Eur J Dermatol*	2015	Onychomycosis	40	Y, 40	Healthy nails
Elfar, *J Egypt Women Dermatol*	2015	Onychomycosis	17	Y, 15	Traumatic onycholysis ($n = 9$), dermatophyte-negative psoriasis ($n = 6$)
Elmas, *Postepy Dermatol Alergol*	2020	Fungal melanonychia	42	N	-
Islamoglu, *Erciyes Med J*	2019	Onychomycosis	100	N	-
Jesus-Silva, *Dermatol Pract Concept*	2015	Onychomycosis	155	N	-
Jo, *Br J Dermatol*	2018	Onychomycosis	30	Y, 30	Trachyonychia
Kayarkatte, *Indian J Dermatol Venereol Leprol*	2020	Onychomycosis	88	Y, 12	Mycologically negative nails
Kaynak, *Arch Dermatol*	2018	Onychomycosis	149	Y, 56	Mycologically negative nails
Kilinc Karaarslan, *Clin Exp Dermatol*	2015	Fungal melanonychia	20	N	-
Kim, *Ann Dermatol*	2020	Fungal melanonychia	20	14	Subungual melanoma
Maatouk, *Curr Med Mycol*	2019	Onychomycosis	45	N	-
Nada, *Arch Dermatol*	2020	Onychomycosis	80	Y, 40	Healthy nails
Nargis, *Indian Dermatol Online J*	2018	Onychomycosis	60	N	-
Ohn, *J Am Acad Dermatol*	2016	Fungal melanonychia	18	Y, 62	Nail matrix naevus ($n = 27$), melanoma ($n = 11$), melanocytic activation ($n = 24$)
Piraccini, *J Eur Acad Dermatol Venereol*	2013	Onychomycosis	37	Y, 13	Traumatic onycholysis
Ramos Pinheiro, *J Eur Acad Dermatol*	2020	Onychomycosis	110	Y, 82	Traumatic onycholysis
Starace, *Mycoses*	2021	Fungal melanonychia	48	N	-
Yadav, *Indian J Dermatol*	2016	Onychomycosis	36	Y, 10	Nail psoriasis

*Y: Yes, N: No.

only two of the five fungal melanonychia articles had a control group.

Dermoscopic features of onychomycosis

Nineteen studies reported dermoscopic features of 1,693 cases of onychomycosis. Commonly identified dermoscopic features of onychomycosis were spikes or spiked pattern (481, 28.4%) (10–18), jagged or spiked edges or jagged edge with spikes (188, 11.1%) (19–25), jagged proximal edge (175, 10.3%) (10, 12, 16, 18), subungual hyperkeratosis (131, 7.7%) (15, 19, 20, 25, 26), ruins appearance, aspect or pattern (573, 33.8%) (15, 19, 22, 24, 27, 28), and longitudinal striae (929, 54.9%) (10–18, 20–23, 27) (Table 2). Other dermoscopic findings included distal irregular termination (331, 19.6%) (10–12, 14–16, 18, 20, 22) and aurora borealis pattern (293, 17.3%) (11, 12, 15, 17, 20, 23). Frequently described color changes were homogenous leukonychia (304, 18.0%) (12, 15, 16, 20, 22, 23, 28), yellow (216, 12.8%) (13, 15, 16, 23, 26) and brown (212, 12.5%) (12, 15, 16, 22, 23, 26).

Terms with similar definitions or those used interchangeably were grouped for meta-analysis upon careful examination of the authors' definitions. When we grouped spikes or spiked pattern, jagged or spiked edges, distal streaks, jagged edge with spikes and jagged proximal edge as "spike pattern", the pooled sensitivity was 77.3% (95% CI, 73.2–81.1%) and specificity was 96.2% (95% CI, 93.1–98.2%) (Figure 2). Pooled sensitivity of subungual hyperkeratosis and ruins appearance, aspect or pattern was 67.1% (95% CI, 62.5–71.5%) and specificity was 64.7% (95% CI, 58.1–70.8%). For longitudinal striae, pooled sensitivity was 67.3% (95% CI, 61.7–72.6%) and specificity 95.6% (95% CI, 90.7–98.4%).

TABLE 2 Dermoscopic features of onychomycosis reported in one or more articles.

First author and publication date	Sample size	Jagged edge with spikes	Spiked pattern	Jagged proximal edge	Distal streaks	Longitudinal striae	Subungual hyperkeratosis	Ruin appearance/ aspect/pattern	Black dots and globules	Distal irregular termination	Dryness & scaling of adjacent skin	Linear edge	Onycholysis	Pits	Splinter hemorrhages	White/ homogenous leukonychia	Punctate leukonychia	Black	Brown	Orange	Yellow	Chromonychia	Aurora borealis
Abdallah et al. (10)	40		24 (60%)	20 (50%)		33 (82.5%)				19 (47.5%)		0 (0%)										36 (90%)	
Ankad et al. (19)	20	18 (90%)					5 (25%)	13 (65%)						0 (0%)	1 (5%)								
Bhat et al. (11)	81		69 (85.19%)			63 (77.78%)				33 (40.74%)													63 (77.78%)
Bodman (20)	35	34 (97.1%)				31 (88.6%)	22 (62.9%)		23 (65.7%)	27 (77.1%)	13 (37.1%)	2 (5.7%)	24 (68.6%)			28 (80.0%)						32 (86.4%)	27 (71.1%)
Chetana et al. (12)	234		101 (43.16%)	70 (29.91%)		115 (49.15%)			Black dots: 44 (18.80%) Black globules 35 (15.38%)	81 (34.62%)		8 (3.42%)		13 (5.56%)	6 (2.56%)	98 (41.88%)		79 (33.76%)	127 (54.27%)	46 (19.66%)	104 (44.44%)		61 (26.07%)
De Crignis et al. (27)	336					267 (79.46%)		296 (88.09%)															
El-Hoshy et al. (13)	40		40 (100%)			33 (82.5%)																	
Elfar et al. (21)	17	13 (76.47%)				16 (94.12%)						0 (0%)			2 (11.76%)								
Islamoglu et al. (22)	100	6 (6%)				66 (66%)		54 (54%)		20 (20%)					8 (8%)	28 (28%)	16 (16%)	10 (10%)	20 (20%)				
Jesus-Silva et al. (14)	155		39 (25.16%)			94 (60.65%)				67 (43.22%)		34 (21.94%)											
Jo et al. (26)	30				28 (93.3%)		22 (73.3%)						20 (66.7%)	2 (6.7%)					7 (23.3%)		28 (93.3%)		

(Continued)

10.3389/fmed.2022.1048913

TABLE 2 (Continued)

First author and publication date	Sample size	Jagged edge with spikes	Spiked pattern	Jagged proximal edge	Distal streaks	Longitudinal striae	Subungual hyperkeratosis	Ruin appearance/ aspect/pattern	Black dots and globules	Distal irregular termination	Dryness & scaling of adjacent skin	Linear edge	Onycholysis	Pits	Splinter hemorrhages	White/ homogenous leukonychia	Punctate leukonychia	Black	Brown	Orange	Yellow	Chromonychia	Aurora borealis
Kayarkatte et al. (15)	88		76 (86.4%)			22 (25%)	75 (85.2%)	52 (59.1%)		72 (81.8%)	73 (83%)		85 (96.6%)			30 (34.1%)		8 (9.1%)	24 (27.3%)		44 (50%)	75 (85.2%)	17 (85%)
Kaynak et al. (28)	149							143 (95.97%)								88 (59.06%)	113 (75.84%)	33 (22.15%)					
Maatouk et al. (16)	45		25 (55.5%)	25 (55.5%)		31 (68.75%)				5 (11.1%)		2 (4.4%)		4 (8.8%)	2 (4.4%)	10 (22.2%)		0 (0%)	15 (33.3%)	6 (13.3%)	14 (31.1%)		
Nada et al. (17)	80		60 (75%)			66 (82.5%)																	76 (95%)
Nargis et al. (18)	60		47 (78.3%)	60 (100%)		60 (100%)				7 (11.7%)												23 (38.3%)	
Piraccini et al. (23)	37	37 (100%)				32 (86.49%)			23 (62.16%)			0 (0%)				22 (59.46%)		9 (24.32%)	19 (51.35%)	9 (24.32%)	26 (70.27%)		32 (86.49%)
Ramos Pinheiro et al. (24)	110	59 (53.6%)						15 (13.6%)					5 (4.55%)										
Yadav et al. (25)	36	21 (58.33%)					7 (19.44%)															13 (36.11%)	

10.3389/fmed.2022.1048913

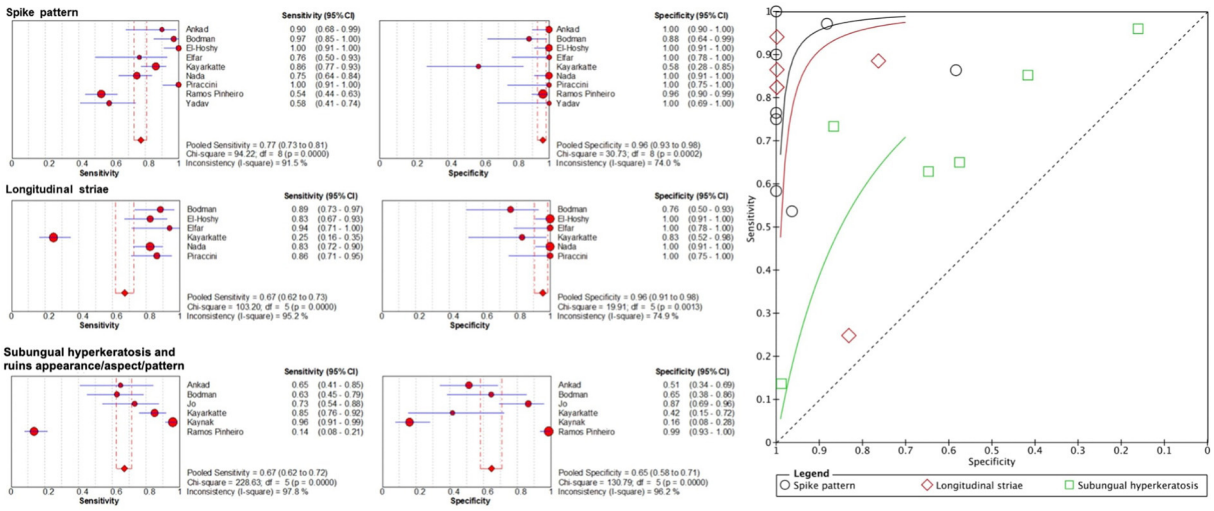

FIGURE 2
Sensitivity and specificity of important dermoscopic features of onychomycosis and their summary receiver operating characteristics (SROC) curves.

Dermoscopic features of fungal melanonychia

Five studies reported dermoscopic features of 148 cases of fungal melanonychia (Table 3) (29–31, 33). These cases demonstrated longitudinal white or yellow streaks (52, 35.1%) (31–33), nail surface scales (39, 33.1%) (31–33) and subungual hyperkeratosis (41, 27.7%) (31–33) (Table 3), which are also common dermoscopic features of onychomycosis. Homogenous pigmentation (75, 50.7%) (29, 30, 33) or longitudinal pigmentation (54, 36.5%) (29, 31–33) was frequently observed, and the most common colors were multicolor (101, 68.2%) (29–33), brown (84, 56.8%) (29, 31–33) and black (46, 31.1%) (29, 31–33). The pigmentation in melanonychia arising from a fungal infection tends to appear brown due to the production of fungal melanin *via* the pentaketide pathway (31). This is in contrast to melanomas, where melanin is made from tyrosine, and commonly appears as darkly pigmented and black. Findings that appear specific to fungal melanonychia, such as "reverse triangle" (30, 20.3%) (30–33), due to fungal invasion from the distal nail plate and "superficial transverse striation" (41, 27.7%) (29, 30, 33), were also reported. All cases had negative findings for melanoma, such as the lack of the Hutchinson sign (0%) (30–33) and triangular sign (0%) (31, 32).

Quality assessment

The risk of bias in the eligible articles was evaluated according to the QUADAS2 guidelines (Table 4). Studies with "unclear" patient selection bias did not specify their method of patient selection, such as whether patients were recruited prospectively or retrospectively or whether patients were enrolled consecutively or randomly. Studies had a low risk of bias in terms of the index test (dermoscopy), reference standard (clear diagnosis of non-onychomycosis nails), flow, and timing. However, the risk of bias in the reference standard for one article was deemed high, as two cases with a positive potassium hydroxide result were not classified as onychomycosis as they primarily displayed features of other nail disorders (19). Studies had low applicability concerns with patient selection and reference standards, but two studies had high applicability concerns with the index test because they did not provide clear definitions or representative images for dermoscopic features (25, 27).

Discussion

The role of dermoscopy is well established in diagnosing cutaneous malignancies such as malignant melanoma and non-melanoma skin cancers (34, 35). Its use expands to various inflammatory and infectious disorders, including onychomycosis. By conducting a systematic review of 19 articles on 1,693 cases of onychomycosis and 5 articles on 148 cases of fungal melanonychia, we could enlarge the sample size and thus the statistical power to identify the dermoscopic features with diagnostic utility. Recognizing common dermoscopic features of onychomycosis can help clinicians to expedite accurate diagnosis and management. The most frequently reported patterns in onychomycosis

TABLE 3 Dermoscopic features of fungal melanonychia.

First author and publication date	Sample size	Pattern					Pigmentation		Color						Melanonychia				Nail melanoma-associated patterns		
		Subungual hyperkeratosis	White or yellow streaks	Nail surface scales	Reverse triangular pattern	Superficial transverse striation	Longitudinal	Homogenous	Multicolor (> 2)	Yellow	Black	Brown	Gray	Striata or Longitudinal	Distal partial diffuse	Prox partial diffuse	Distal linear	Total diffuse	Hutchinson's sign	Pseudo- Hutchinson's sign	Triangular sign
Elmas et al. (29)	42					11 (26.1%)	4 (9.5%)	33 (78.5%)	38 (90.4%)		19 (45.2%)	21 (50%)	11 (26.1%)							4 (9.5%)	
Kilinc Karaaslan et al. (30)	20				2 (10%)	7 (35%)		20 (100%)	19 (95%)		1 (5%)			7 (35%)	5 (25%)	4 (20%)	2 (10%)	2 (10%)	0 (0%)	2 (10%)	
Kim et al. (31)	20	7 (35%)	18 (90%)	14 (70%)	10 (50%)		6 (30%)		13 (65%)	8 (40%)	10 (50%)	18 (90%)	0		7 (35%)	1 (5%)	4 (20%)	2 (10%)	0 (0%)	0 (0%)	0 (0%)
Ohn et al. (32)	18	10 (55.6%)	16 (88.9%)	13 (72.2%)	7 (38.9%)		8 (44.4%)	10 (55.6%)	16 (88.9%)	14 (77.8%)	10 (55.6%)	11 (61.1%)	3 (16.7%)						0 (0%)	1 (5.6%)	0 (0%)
Starace et al. (33)	48	24 (50%)	18 (37.5%)	22 (45.8%)	11 (22.9%)	23 (47.9%)	36 (75%)	12 (25%)	15 (31.3%)	5 (10.4%)	6 (12.5%)	34 (70.8%)	11 (22.9%)	20 (41.67%)	8 (16.7%)	2 (4.17%)	1 (2.08%)	17 (35.4%)	0 (0%)	0 (0%)	

10.3389/fmed.2022.1048913

TABLE 4 Quality assessment of the included studies.

First author and publication date	Risk of bias				Applicability		
	Patient selection	Index test	Reference standard	Flow and timing	Patient selection	Index test	Reference standard
Abdallah et al. (10)	Unclear	Low	Low	Low	Low	Low	Low
Ankad et al. (19)	Low	Low	High	Low	Low	Low	Low
Bhat et al. (11)	Low	Low	N/A (no control group)	Low	Low	Low	Low
Bodman (20)	Unclear	Low	Low	Low	Low	Low	Low
Chetana et al. (12)	Low	Low	N/A (no control group)	Low	Low	Low	Low
De Crignis et al. (27)	Low	Low	N/A (no control group)	Low	Low	High	Low
El-Hoshy et al. (13)	Unclear	Low	Low	Low	Low	Low	Low
Elfar et al. (21)	Low	Low	Low	Low	Low	Low	Low
Elmas et al. (29)	Low	Low	N/A (no control group)	Low	Low	Low	Low
Islamoglu et al. (22)	Low	Low	N/A (no control group)	Low	Low	Low	Low
Jesus-Silva et al. (14)	Unclear	Low	Low	Low	Low	Low	Low
Jo et al. (26)	Low	Low	Low	Low	Low	Low	Low
Kayarkatte et al. (15)	Unclear	Low	Low	Low	Low	Low	Low
Kaynak et al. (28)	Unclear	Low	Low	Low	Low	Low	Low
Kilinc Karaaslan et al. (30)	Unclear	Low	N/A (no control group)	Low	Low	Low	Low
Kim et al. (31)	Unclear	Low	Low	Low	Low	Low	Low
Maatouk et al. (16)	Low	Low	N/A (no control group)	Low	Low	Low	Low
Nada et al. (17)	Low	Low	Low	Low	Low	Low	Low
Nargis et al. (18)	Low	Low	N/A (no control group)	Low	Low	Low	Low
Ohn et al. (32)	Unclear	Low	Low	Low	Low	Low	Low
Piraccini et al. (23)	Low	Low	Low	Low	Low	Low	Low
Ramos Pinheiro et al. (24)	Low	Low	Low	Low	Low	Low	Low
Starace et al. (33)	Low	Low	N/A (no control group)	Low	Low	Low	Low
Yadav et al. (25)	Unclear	Low	Low	Low	Low	High	Low

included spikes or spiked patterns, ruins appearance, aspect or pattern and longitudinal striae. After pooling the dermoscopic terminology that were closely related or used interchangeably, "spike pattern" and longitudinal striae had high specificity (96.2 and 95.6%, respectively) and moderate sensitivity (77.3 and 67.3%, respectively) for onychomycosis. Detecting these features can raise clinicians' suspicion of onychomycosis and expedite further investigations. Ruins appearance, aspect or pattern and subungual hyperkeratosis had moderate sensitivity (71.6%) and specificity (64.7%) for onychomycosis as these features can also be observed in other nail disorders including nail psoriasis and allergic contact dermatitis. Other dermoscopic features characterizing onychomycosis were distal irregular termination, aurora borealis, homogenous leukonychia, and brown discoloration.

We also found that the most frequently described dermoscopic features of fungal melanonychia were longitudinal white or yellow streaks and nail surface scales. Unlike melanocytic melanonychia, fungal melanonychia is characterized by non-longitudinal homogenous pigmentation and reverse triangular patterns (32). Moreover, our data demonstrate that subungual hyperkeratosis frequently occurs in fungal melanonychia.

This study has some limitations. There was considerable heterogeneity in the study design and terminology definitions of the enrolled studies, which may have limited the strength of our study. We sought to clarify dermoscopic terminology by identifying commonly used terms and narrowing their definitions to accurately pool and compare the findings. Future studies with standardized terminology are necessary, ideally through an expert panel, to facilitate clear communication among clinicians.

To our knowledge, this is the first systematic review of dermoscopic features of onychomycosis. Given the limited sample sizes of existing studies on this topic, pooling their results provides us an overview of the most common features of onychomycosis and the frequency at which they present in patients. Understanding these characteristic dermoscopic features of onychomycosis can assist clinicians diagnose onychomycosis by the bedside.

Data availability statement

The original contributions presented in the study are included in the article/supplementary material, further inquiries can be directed to the corresponding author.

Author contributions

J-HM and CO: conceptualization, resources, and supervision. J-HM: methodology and project administration. YC, J-HM, and CO: validation. SL, JO, and LH: formal analysis. SL and LH: investigation, data curation, writing—original draft, and visualization. JO, YC, CO, and J-HM: writing—review and editing. All authors: software. All authors contributed to the article and approved the submitted version.

Conflict of interest

The authors declare that the research was conducted in the absence of any commercial or financial relationships that could be construed as a potential conflict of interest.

Publisher's note

All claims expressed in this article are solely those of the authors and do not necessarily represent those of their affiliated organizations, or those of the publisher, the editors and the reviewers. Any product that may be evaluated in this article, or claim that may be made by its manufacturer, is not guaranteed or endorsed by the publisher.

References

1. Marghoob NG, Liopyris K, Jaimes N. Dermoscopy: A Review of the Structures That Facilitate Melanoma Detection. *J Am Osteopath Assoc.* (2019) 119:380–90. doi: 10.7556/jaoa.2019.067

2. Pizzorni C, Giampetruzzi AR, Mondino C, Facchiano A, Abeni D, Paolino S et al. Nailfold capillaroscopic parameters and skin telangiectasia patterns in patients with systemic sclerosis. *Microvasc Res.* (2017) 111:20–4. doi: 10.1016/j.mvr.2016.12.003

3. Golińska J, Sar-Pomian M, Rudnicka L. Dermoscopic features of psoriasis of the skin, scalp and nails - a systematic review. *J Eur Acad Dermatol Venereol.* (2019) 33:648–60. doi: 10.1111/jdv.15344

4. Carli P, De Giorgi V, Crocetti E, Mannone F, Massi D, Chiarugi A et al. Improvement of malignant/benign ratio in excised melanocytic lesions in the 'dermoscopy era': a retrospective study 1997-2001. *Br J Dermatol.* (2004) 150:687–92. doi: 10.1111/j.0007-0963.2004.05860.x

5. Lipner SR, Scher RK. Onychomycosis: Clinical overview and diagnosis. *J Am Acad Dermatol.* (2019) 80:835–51. doi: 10.1016/j.jaad.2018.03.062

6. Fávero MLD, Bonetti AF, Domingos EL, Tonin FS, Pontarolo R. Oral antifungal therapies for toenail onychomycosis: a systematic review with network meta-analysis toenail mycosis: network meta-analysis. *J Dermatolog Treat.* (2020) 33:121–30. doi: 10.1080/09546634.2020.1729336

7. Moher D, Liberati A, Tetzlaff J, Altman DG. Preferred reporting items for systematic reviews and meta-analyses: the PRISMA statement. *J Clin Epidemiol.* (2009) 62:1006–12. doi: 10.1016/j.jclinepi.2009.06.005

8. McGrath TA, Alabousi M, Skidmore B, Korevaar DA, Bossuyt PMM, Moher D et al. Recommendations for reporting of systematic reviews and meta-analyses of diagnostic test accuracy: a systematic review. *Syst Rev.* (2017) 6:194. doi: 10.1186/s13643-017-0590-8

9. Whiting P, Rutjes AW, Reitsma JB, Bossuyt PM, Kleijnen J. The development of QUADAS: a tool for the quality assessment of studies of diagnostic accuracy included in systematic reviews. *BMC Med Res Methodol.* (2003) 3:25. doi: 10.1186/1471-2288-3-25

10. Abdallah NA, Said M, Mahmoud MT, Omar MA. Onychomycosis: Correlation between the dermoscopic patterns and fungal culture. *J Cosmet Dermatol.* (2020) 19:1196–204. doi: 10.1111/jocd.13144

11. Bhat YJ, Mir MA, Keen A, Hassan I. Onychoscopy: an observational study in 237 patients from the Kashmir Valley of North India. *Dermatol Pract Concept.* (2018) 8:283–91. doi: 10.5826/dpc.0804a06

12. Chetana K, Menon R, David BG. Onychoscopic evaluation of onychomycosis in a tertiary care teaching hospital: a cross-sectional study from South India. *Int J Dermatol.* (2018) 57:837–42. doi: 10.1111/ijd.14008

13. El-Hoshy KH, Abdel Hay RM, El-Sherif RH, Salah Eldin M, Moussa MF. Nail dermoscopy is a helpful tool in the diagnosis of onychomycosis: A case control study. *Eur J Dermatol.* (2015) 25:494–5. doi: 10.1684/ejd.2015.2637

14. Jesus-Silva MA, Fernandez-Martinez R, Roldan-Marin R, Arenas R. Dermoscopic patterns in patients with a clinical diagnosis of onychomycosis-results of a prospective study including data of potassium hydroxide (KOH) and culture examination. *Dermatol Pract Concept.* (2015) 5:39–44. doi: 10.5826/dpc.0502a05

15. Kayarkatte MN, Singal A, Pandhi D, Das S, Sharma S. Nail dermoscopy (onychoscopy) findings in the diagnosis of primary onychomycosis: A cross-sectional study. *Indian J Dermatol Venereol Leprol.* (2020) 86:341–9. doi: 10.4103/ijdvl.IJDVL_100_19

16. Maatouk I, Haber R, Benmehidi N. Onychoscopic evaluation of distal and lateral subungual onychomycosis: A cross-sectional study in Lebanon. *Curr.* (2019) 5:41–4. doi: 10.18502/cmm.5.2.1161

17. Nada EEA, El Taieb MA, El-Feky MA, Ibrahim HM, Hegazy EM, Mohamed AE et al. Diagnosis of onychomycosis clinically by nail dermoscopy versus microbiological diagnosis. *Arch Dermatol.* (2020) 312:207–12. doi: 10.1007/s00403-019-02008-6

18. Nargis T, Pinto M, Shenoy MM, Hegde S. Dermoscopic Features of Distal Lateral Subungual Onychomycosis. *Indian Dermatol Online J.* (2018) 9:16–9. doi: 10.4103/idoj.IDOJ_40_17

19. Ankad BS, Gupta A, Alekhya R, Saipriya M. Dermoscopy of onycholysis due to nail psoriasis, onychomycosis and trauma: a cross sectional study in skin of color. *Indian Dermatol Online J.* (2020) 11:777–83. doi: 10.4103/idoj.IDOJ_475_19

20. Bodman MA. Point-of-care diagnosis of onychomycosis by dermoscopy. *J Am Podiatr Med Assoc.* (2017) 107:413–8. doi: 10.7547/16-183

21. Elfar NN, Abdel-Latif AM, Labeh EA. Role of onychoscopy in differentiation between distal subungual onychomycosis, psoriasis, and traumatic oncholysis. *J Egypt Women Dermatol Soc.* (2015) 12:145–9. doi: 10.1097/01.EWX.0000469303.65552.a1

22. Islamoglu ZGK, Demirbas A, Unal M, Findik D. Nail digital dermoscopy in onychomycosis: a correlation with clinical type, gender, and culture examination. *Erciyes Med J.* (2019) 41:288–94. doi: 10.14744/etd.2019.94210

23. Piraccini BM, Balestri R, Starace M, Rech G. Nail digital dermoscopy (onychoscopy) in the diagnosis of onychomycosis. *J Eur Acad Dermatol Venereol.* (2013) 27:509–13. doi: 10.1111/j.1468-3083.2011.04323.x

24. Ramos Pinheiro R, Dias Domingues T, Sousa V, Galhardas C, Apetato M, Lencastre A, et al. comparative study of onychomycosis and traumatic toenail onychodystrophy dermoscopic patterns. *J Eur Acad Dermatol Venereol.* (2019) 33:786–92. doi: 10.1111/jdv.15358

25. Yadav TA, Khopkar US. White streaks: dermoscopic sign of distal lateral subungual onychomycosis. *Indian J Dermatol.* (2016) 61:174151. doi: 10.4103/0019-5154.174151

26. Jo G, Park JS Yu DA, Ohn J, Sheu SL, Mun JH. Onychoscopy of trachyonychia: an analysis of 30 patients and comparison with onychomycosis. *Br J Dermatol.* (2018) 179:491–3. doi: 10.1111/bjd.16431

27. De Crignis G, Valgas N, Rezende P, Leverone A, Nakamura R. Dermatoscopy of onychomycosis. *Int J Dermatol.* (2014) 53:e80–e157. doi: 10.1111/ijd.12104

28. Kaynak E, Goktay F, Gunes P, Sayman E, Turan D, Baygul A et al. The role of dermoscopy in the diagnosis of distal lateral subungual onychomycosis. *Arch Dermatol.* (2018) 310:57–69. doi: 10.1007/s00403-017-1796-2

29. Elmas OF, Metin MS. Dermoscopic findings of fungal melanonychia. *Postepy Dermatol.* (2020) 37:180–3. doi: 10.5114/ada.2020.94836

30. Kilinc Karaarslan I, Acar A, Aytimur D, Akalin T, Ozdemir F. Dermoscopic features in fungal melanonychia. *Clin Exp Dermatol.* (2015) 40:271–8. doi: 10.1111/ced.12552

31. Kim H-J, Kim T-W, Park S-M, Lee H-J, Kim G-W, Kim H-S et al. Clinical and Dermoscopic Features of Fungal Melanonychia: Differentiating from Subungual Melanoma. *Ann Dermatol.* (2020) 32:460–5. doi: 10.5021/ad.2020.32.6.460

32. Ohn J, Choe YS, Park J, Mun JH. Dermoscopic patterns of fungal melanonychia: A comparative study with other causes of melanonychia. *J Am Acad Dermatol.* (2017) 76:488–93.e2. doi: 10.1016/j.jaad.2016.08.013

33. Starace M, Ambrogio F, Bruni F, Piraccini BM, Alessandrini A. Dermatophytic melanonychia: A Case Series of an increasing disease. *Mycoses.* (2021) 64:511–9. doi: 10.1111/myc.13237

34. Lan J, Wen J, Cao S, Yin T, Jiang B, Lou Y et al. The diagnostic accuracy of dermoscopy and reflectance confocal microscopy for amelanotic/hypomelanotic melanoma: a systematic review and meta-analysis. *Br J Dermatol.* (2020) 183:210–9. doi: 10.1111/bjd.18722

35. Reiter O, Mimouni I, Gdalevich M, Marghoob AA, Levi A, Hodak E et al. The diagnostic accuracy of dermoscopy for basal cell carcinoma: A systematic review and meta-analysis. *J Am Acad Dermatol.* (2019) 80:1380–8. doi: 10.1016/j.jaad.2018.12.026

frontiers | Frontiers in Medicine

TYPE Original Research
PUBLISHED 17 January 2023
DOI 10.3389/fmed.2022.1059448

OPEN ACCESS

EDITED BY
Federica Veronese,
Azienda Ospedaliero Universitaria Maggiore della Carità, Italy

REVIEWED BY
Bernard Naafs,
Stichting Global Dermatology, Netherlands
Marcia Rodrigues Jardim,
Oswaldo Cruz Foundation (FIOCRUZ), Brazil
Kalliopi Pitarokoili,
St. Josef Hospital, Germany

*CORRESPONDENCE
Glauber Voltan
✉ gvoltan@gmail.com;
✉ drglauber@humanizarejuina.com
Marco Andrey Cipriani Frade
✉ mandrey@fmrp.usp.br

SPECIALTY SECTION
This article was submitted to Dermatology, a section of the journal Frontiers in Medicine

RECEIVED 01 October 2022
ACCEPTED 21 December 2022
PUBLISHED 17 January 2023

CITATION
Voltan G, Marques-Júnior W, Santana JM, Lincoln Silva CM, Leite MN, De Paula NA, Bernardes Filho F, Barreto JG, Da Silva MB, Conde G, Salgado CG and Frade MAC (2023) Silent peripheral neuropathy determined by high-resolution ultrasound among contacts of patients with Hansen's disease. *Front. Med.* 9:1059448. doi: 10.3389/fmed.2022.1059448

Silent peripheral neuropathy determined by high-resolution ultrasound among contacts of patients with Hansen's disease

Glauber Voltan[1,2]*, Wilson Marques-Júnior[3], Jaci Maria Santana[2], Claudia Maria Lincoln Silva[1,2], Marcel Nani Leite[1,2], Natália Aparecida De Paula[1,2], Fred Bernardes Filho[2], Josafá Gonçalves Barreto[4], Moises Batista Da Silva[4], Guilherme Conde[5], Claudio Guedes Salgado[4] and Marco Andrey Cipriani Frade[1,2]*

[1]Healing and Hansen's Disease Laboratory, Ribeirão Preto Medical School, University of São Paulo, Ribeirão Preto, São Paulo, Brazil, [2]National Referral Center for Sanitary Dermatology and Hansen's Disease, Dermatology Division, Internal Medicine Department, Ribeirão Preto Medical School, University of São Paulo, Ribeirão Preto, São Paulo, Brazil, [3]Division of Neuromuscular Disorders, Department of Neurosciences and Behavioral Sciences, Ribeirão Preto Medical School, University of São Paulo, Ribeirão Preto, São Paulo, Brazil, [4]Dermato-Immunology Laboratory, Institute of Biological Sciences, Federal University of Pará, Marituba, Brazil, [5]Decision Support Laboratory, Federal University of Pará West, Santarem, Brazil

Introduction: Hansen's disease (HD) primarily infects peripheral nerves, with patients without HD being free of peripheral nerve damage. Household contacts (HHCs) of patients with HD are at a 5–10 times higher risk of HD than the general population. Neural thickening is one of the three cardinal signs that define a case of HD according to WHO guidelines, exclusively considering palpation examination that is subjective and may not detect the condition in the earliest cases even when performed by well-trained professionals. High-resolution ultrasound (HRUS) can evaluate most peripheral nerves, a validated technique with good reproducibility allowing detailed and accurate examination.

Objective: This study aimed to use the peripheral nerve HRUS test according to the HD protocol as a diagnostic method for neuropathy comparing HHCs with healthy volunteers (HVs) and patients with HD.

Methods: In municipalities from 14 different areas of Brazil we selected at random 83 HHC of MB-patients to be submitted to peripheral nerve ultrasound and compared to 49 HVs and 176 HD-patients.

Results: Household contacts assessed by HRUS showed higher median and mean absolute peripheral nerve cross-sectional area (CSA) values and greater asymmetries (ΔCSA) compared to HVs at the same points. Median and mean absolute peripheral nerve CSA values were higher in patients with HD compared to HCCs at almost all points, while ΔCSA values were equal at all points. Mean ± SD focality (ΔTpT) values for HHCs and patients with HD, respectively, were 2.7 ± 2.2/2.6 ± 2.2 for the median nerve, 2.9 ± 2.7/3.3 ± 2.9 for the common fibular nerve ($p > 0.05$), and 1.3 ± 1.3/2.2 ± 3.9 for the ulnar nerve ($p < 0.0001$).

Discussion: Considering HRUS findings for HHCs, asymmetric multiple mononeuropathy signs (thickening or asymmetry) in at least 20% of the nerves evaluated could already indicates evidence of HD neuropathy. Thus, if more nerve points are assessed in HHCs (14 instead of 10), the contacts become more like patients with HD according to nerve thickening determined by HRUS, which should be a cutting-edge tool for an early diagnosis of leprosy cases.

KEYWORDS

leprosy, Hansen's disease, household contacts, neuropathy, high-resolution ultrasound, cross-sectional area (CSA), multiple mononeuropathy

Introduction

Hansen's disease (HD), one of the oldest chronic infectious diseases affecting humans, whose etiologic agent is *Mycobacterium leprae* (*M. leprae*) and *Mycobacterium lepromatosis*, an obligate intracellular pathogen with tropism for macrophages and Schwann cells, primarily infects peripheral nerves and involves the skin and other tissues (1–3). HD is a current and challenging disease still representing a public health problem in developing countries such as Brazil, which ranks second in the world in the number of new cases per year, with more than twenty thousand new cases per year (4, 5). HD has no primary prevention, which means that there is no specific vaccine against *M. leprae*, and diagnostic and prognostic tests are not feasible or well-established in clinical routine (3). The incubation period of HD is variable, ranging from 6 months to more than 20 years, with an average period of 2–4 years, due to its very slow growth (6).

The predominance of multibacillary (MB) cases with nerve impairment indicate a late diagnosis and underscores the ineffectiveness of epidemiological control in many countries (7). Moreover, new cases not only involving high functional impairment but also affecting children reflect the failure of early HD detection and indicate continued transmission (8). People with untreated HD are generally considered to be the main source of transmission; however, because of the complex relationships between genetic, immunological, and environmental factors, most infected contacts will not develop HD, although recent studies have reported that they may be healthy carriers and transmit *M. leprae* to susceptible individuals (9–13). Some authors have demonstrated the presence of viable *M. leprae* strains in skin smear samples from patients as well as in environmental samples obtained from around their homes, revealing that the occurrence of new cases among people without previous contact with those with untreated HD may be due to other undisclosed sources of infection such as water, soil, and animals (14–17).

Contacts of MB patients diagnosed with HD are at 5 to 10 times higher risk of HD than the general population (1, 18, 19). Contact with patients with HD is the main determinant of the incidence of HD (10, 13, 19–29), and the type of contact is not limited to family relationships (18).

There are no patients with HD without peripheral nerve damage, but the exact mechanism underlying the condition is still unknown (30). Scollard (30) suggested that neuropathy may occur partly by the invasion of Schwann cells from the outside to inside, and Graham Weddell observed that HD-related damage occurs at places where there is movement, such as the wrist, elbow, knee, and ankle. Such movements lead to micro-trauma to which the body responds by sending repair cells, including macrophages. For these cells to get into the endoneurium, where the micro-trauma is located, the endothelial cells of the blood vessels in the endoneurium will express adhesion molecules (30).

In a study assessing the neuropathy occurring in HD, Defaria (31) concluded that the condition is a mixed primary peripheral polyneuropathy involving motor and sensory fibers whose earliest neural lesion appears by asymmetric axonal neuropathy and as diffuse demyelination in the later stage. In addition, neuropathy is present in all clinical forms, including those of some contacts.

The diagnosis is essentially clinical, based on a thorough dermatoneurological examination, and in the presence of hypochromic macules, the use of Semmes-Weinstein monofilaments improves its accuracy (32). Current diagnostic tools such as ELISA, PCR, and electroneuromyography (ENMG) have proved to be effective for an early diagnosis of HD and are useful for the evaluation of the efficacy of therapy, but their use is limited in HD, which has been considered a marginalized disease. In addition, these diagnostic methods are only available at referral centers and in teaching and research services (6, 31). Furthermore, pure neural HD, accounting for 5–10% of index cases that present with asymmetric neuropathy in the absence of bacilli in skin smears, remains a diagnostic challenge, often requiring a nerve biopsy, rarely available in the "clusters" and in the areas of higher endemicity (33, 34). Santos et al. (22) demonstrated that, among contacts of patients with HD eligible for a biopsy due to a change in ENMG, 27.8% showed anatomopathological changes suggestive of HD.

In 1977, some authors detected a clearly greater gradual reduction in nerve conduction velocity in the contacts of

patients with HD than in HVs, suggesting that a careful (probably improved) method of recording sensory nerve action potentials in the radial cutaneous nerve branch to the index finger could be of help by confirming a diagnosis of leprosy and by detecting the disease in contacts of patients with leprosy before any clinical or bacteriological evidence of leprosy (35).

Neural thickening is one of the three cardinal signs defining a case of HD proposed by the World Health Organization guidelines (36), although only exclusively considering the clinical findings obtained by the palpation technique. When the first signs of neural damage can be noticed, at least 30% of the nerve fibers may show damage (37, 38). HD is a neural disease that may or may not have cutaneous manifestations (2, 3, 39–44). On the contrary, cases of peripheral neuropathy accompanied by neural thickening, with or without cutaneous manifestations, should lead the clinician to suspect the diagnosis of HD (45). Physical examination based on simplified neurological assessment, including palpation of the peripheral nerves, aids in the diagnosis of neural thickening and neuritis; however, this method is subjective, and the earliest cases may not be detected even by well-trained professionals (46, 47).

High-resolution ultrasound (HRUS) can evaluate most peripheral, superficial, and deep nerves and is a validated technique with good reproducibility allowing detailed and accurate examination (48–51). A hand-held ultrasound device can readily identify nerve enlargement in individuals with leprosy, notable in areas with limited healthcare resources because of the portability and low-cost nature of such devices (51, 52).

In the case of pure or primary neural leprosy (PNL), serial scans could be valuable in monitoring treatment and reactions, particularly when it is impossible to determine whether the patient is in remission. In addition, the authors suggest the US as a likely useful tool in the diagnosis of PNH (42, 49, 51).

This study proposes to assess the HRUS of peripheral nerves with an HD protocol as a diagnostic method for asymmetric and fusiform (focal) multiple mononeuropathy by comparing the household contacts of patients with untreated HD with healthy individuals and with those diagnosed with untreated HD.

Materials and methods

Ethical statement

This study was approved by the Research Ethics Committee of Hospital das Clínicas, Faculdade de Medicina de Ribeirão Preto, Universidade de São Paulo (protocol number 2.165.032, MH-Brazil and 92228318.1.0000.5440). Written informed consent was obtained from all participants, including the parents and guardians of each participant under 18 years of age. All procedures involving human subjects are in accordance with the ethical standards of the Declaration of Helsinki (1975/2008).

Sample

Between 2016 and 2020, municipalities from different regions of Brazil (north, northeast, and southeast) whose health professionals were trained by the National Reference Center in Health Dermatology with an emphasis on HD of HCFMRP-USP were selected. In these regions, we randomly selected 176 patients (HD) and 83 household contacts (HHC) from the MB (multibacillary) patients HD by the teams. All of them were Brazilian volunteers to be submitted to peripheral nerve ultrasound. As a comparative sample of healthy Brazilian volunteers, we used 49 healthy individuals (HVs) among the cases of our service, and as a comparative sample of patients diagnosed with HD (HD), we used cases of our service as published by Voltan et al. (53, 54).

Before being submitted to the HD protocol through the HRUS, all HHCs were clinically evaluated by specialist physicians, dermatologists, or leprologists. Exclusion criteria were all individuals with neurological symptoms such as loss of strength, paresthesia, electric shock-like pain, pain or cramps, with a body mass index $\geq$35.0 kg/m^2, a diagnosis of metaboli [c]c disease (diabetes mellitus, hypothyroidism or hyperthyroidism) or other peripheral neuropathies, and an amputated limb.

Clinical evaluation

The clinical evaluation was performed by dermatologists and HD specialists trained by the Ministry of Health program. The teams were not involved in the execution and analysis of the HRUS images.

Echography of the peripheral nerves

Between 2016 and 2020, a physician from our group with a specialization in US and imaging diagnosis and with extensive experience in the neuromuscular US used portable general US devices with high-frequency linear transducers ranging from 4 to 17 MHz. Each peripheral nerve was scanned in transverse and longitudinal sections, and the cross-sectional area (CSA) of transverse sections was obtained with adjustment of the angle perpendicular to the insonated nerve surface and without pressing the structures. The neural points evaluated were selected due to their proximity to bone anatomical references, facilitating the reproducibility of the method, and because they are known sites for neural compression or more common electrophysiological evaluation, besides being already well-established in the literature. The CSA was measured at these points with a continuous trace, within the hyperechoic borders of the epineurium (Figures 1A, B). For comparison with the literature, all patients underwent echographic evaluation of

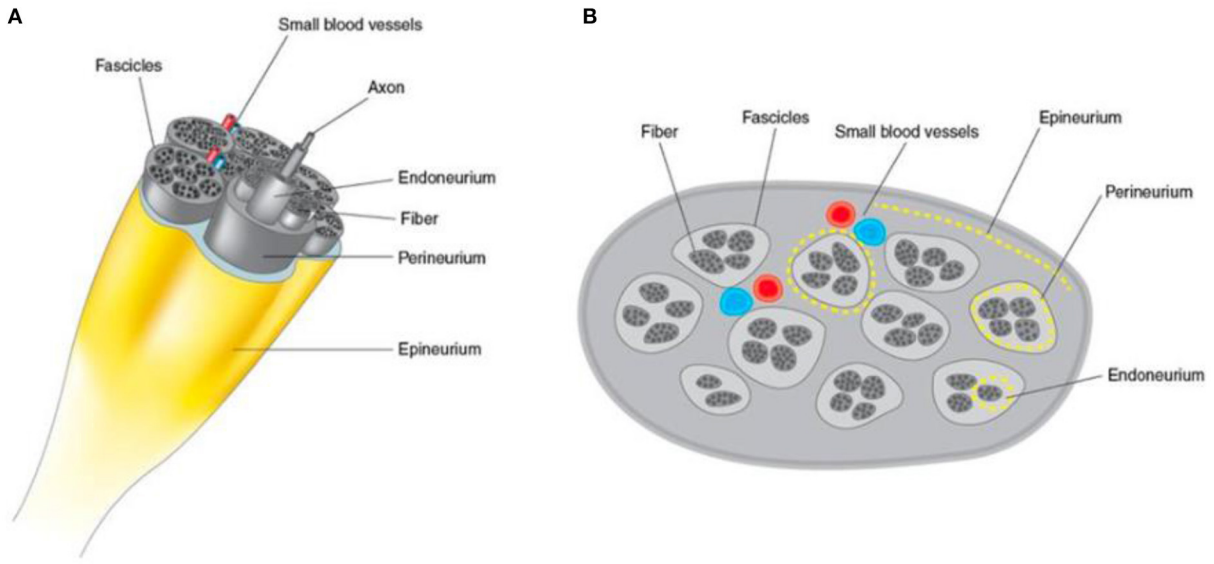

FIGURE 1
Schematic representation of the cross-sectional view of a normal peripheral nerve and its morphological structures obtained by HRUS. **(A)** 3D view and **(B)** with a honeycomb pattern.

10 established neural points, namely, the median nerves in the carpal tunnel (Med CT); the ulnar nerves in the cubital tunnel (UT) and the distal third of the arm (cubital pre-tunnel: 3–5 cm above the medial epicondyle)-(UpT); the common fibular nerves in the topography of the fibular head (CFFH); and the tibial nerves in the tarsal tunnel (T), all bilaterally. Exceptionally, in addition to these, four new points were established for routine focality assessment, i.e., the common fibular nerves proximal to the fibular head (3–8 cm proximal to the head of the fibula)-(CFpFH) and median nerves in the distal third of the forearm (Med pCT) (2–5 cm proximal to the carpal tunnel). The upper limb nerves were evaluated with the patient sitting and with elbows flexed between 60 and 90°. The nerves of the lower limbs were evaluated with the patient sitting or in lateral decubitus with legs slightly flexed between 90 and 130°.

Statistical analysis

Cross-sectional area values obtained from photographs of the US exams were plotted using the Excel® software and further analyzed using Prism 8 for macOS software. We calculated the means, standard deviations, and medians of absolute CSA values for each of the 14 points of the nerves evaluated (7 on the right side and 7 on the left side). The paired *t*-test was applied to analyze asymmetries. We calculated the indices (Δ) of the differences in absolute CSA values between the right and left sides (ΔCSAs - asymmetry) and of the differences in absolute CSA values between segments of the same nerve (ΔTpT - focality). Neural points were considered to be altered (thickened) when their absolute CSA values were greater than the reference values for normal individuals added to 2 times the standard deviation values (RV + 2 SD). Each neural point was considered to be asymmetric when ΔCSA was greater than its RV + 2 SD, and each neural point was considered to have fusiform or focal thickening when ΔTpT was greater than RV + 2 SD. We also calculated the total number of neural points with increased CSA per individual using the "cont.se" function of the Excel program, as well as the total number of points altered with respect to asymmetry (ΔCSA) and focality (ΔTpT) for each individual. The HV, HHC, and HD groups were compared by the unpaired *T*-test and the non-parametric Mann-Whitney test using the Prism program. To evaluate the discriminatory capacity of the US for the diagnosis of HD neuropathy, the ROC curve was applied to the numbers of altered points according to CSA, ΔCSA, and ΔTpT, which were then compared to the respective numbers obtained for healthy individuals.

Results

The demographic characteristics, place of birth, and respective anti-PGL1 serology results of the population sample evaluated are described in Table 1.

For comparison of the values obtained for the patients, we considered the values established by Voltan et al. (54) as normality standards (healthy individuals—none of whom

TABLE 1 Distribution of the population sample of HHDs (contacts of patients with HD) by sex, age group, region of origin, and anti-PGL-I data.

Variables		N	%
Sex	Male	34	41.46
	Female	49	58.54
Age (years)	04 a 15	14	17.07
	15 a 60	69	82.93
Region of origin	North	48	58.54
	Northeast	11	13.41
	Southeast	23	28.05
Anti-PGL 1	Negative (0.47 ± 0.32)	20	24.39
	Positive (2.85 ± 3.96)	8	9.76
	Not rated	54	65.85

had any known contact with leprosy) for CSAs in the Brazilian population.

We have been following 11 HHCs from the southwest—Jardinópolis/SP for 3 years, 5 of whom have developed HD with neuropathy.

Absolute CSA values (mm^2) of the peripheral nerves and their indices

The 83 HHCs were evaluated by bilateral HRUS of the following peripheral nerves: Med CT, UT UpT, CFFH, and T. Based on initial observations during fieldwork, additional evaluation of new analysis points of the Med Ab and CFpFH was established as routine in the examinations. Thus, the sample number (n) varied, with measurements of 24 (29.2 %) HHCs being obtained for Med pCT and 38 (46.3 %) HHCs for CFpFH. In 21 HHCs, 14 neural points (MCT, Med pCT, UT, UpT, CFFH, CFpFH, T) were evaluated.

The means, standard deviations, and median absolute CSA values in mm^2 and the values of the differences between the right and left sides (ΔCSAs/ΔAsymmetry) and between two points of the same nerve (Δ TpT/Δfocality) are listed in Table 2 according to age group.

Comparative analysis of healthy individuals, household contacts of patients diagnosed with HD, and patients with HD

We compared 49 healthy individuals (98 neural points) with 69 household contacts (HHCs) of patients diagnosed with HD (138 neural points) and with 176 patients diagnosed with HD (352 neural points) in the age range of 15–60 years.

Since the samples were unpaired and did not have parametric distribution, both the absolute values of the peripheral nerve CSAs and the values of the differences between the CSAs were compared by the non-parametric Mann-Whitney test.

Our results showed higher medians and means of the absolute values of the CSAs of peripheral nerves and greater asymmetries (ΔCSA) in the HHCs compared to the healthy volunteers at all points amenable to comparison, except for the ΔCSA of the tibial nerve, which was equal for the two groups. There was no difference in focus (ΔTpT) of the ulnar nerve between these groups although the mean ± standard deviation showed higher values for the household contacts (HHC = 1.3 ± 1.3 x HVs = 1.0 ± 0.8). The median and mean absolute values of peripheral nerve CSAs were higher in HDs than in HCCs at almost all points except for the Med Ct and UT neural points, which were equal. Asymmetry (ΔCSA) did not differ between groups at any point. The mean ± SD focality (ΔTpT) values of HCC and patients with HD were 2.7 ± 2.2/2.6 ± 2.2 for the median nerve, 2.9 ± 2.7/3.3 ± 2.9 for the common fibular nerve ($p > 0.05$), and 1.3 ± 1.3/2.2 ± 3.9 for the ulnar nerve ($p < 0.0001$), respectively, as demonstrated in Figure 2.

In 29 HHCs and 91 patients with HD, we were able to discriminate the ΔTpT (focality) of the median nerve between thickening in the carpal tunnel or proximal to the carpal tunnel, and we obtained greater nerve thickening proximal to the carpal pre-tunnel in 2 HHCs (7%) x 20 HD (22%) (Figure 3) and greater nerve enlargement on the carpal tunnel in 19 HHCs (65%) x 49 HD (53%). The chi-square value was 8.9, with $p < 0.05$.

Absolute number and percentage of thickened nerves per individual

The nerves were considered to be enlarged when their CSA was greater than the mean ± 2 SD of the normal values established in the study by Voltan et al. (54).

To determine a possible relationship between the categorical variables, thickened nerves, neural points with asymmetry between right and left sides (ΔCSA), and nerves with the difference between segments of the same nerve (focality/ ΔTpT), we compared by the chi-square test and ROC curve household contacts of untreated patients diagnosed with HD, healthy individuals, and patients diagnosed with HD.

When we compared the mean, standard deviation, and median [Md ± SD (M)] values of the index of the number of nerves with increased CSA per individual, we detected a significant difference ($p < 0.05$) between all groups: healthy subjects [0.04 ± 0.09 (0)], HHC [0.27 ± 0.26 (0.2)], and HD

TABLE 2 Distribution of ultrasound measurements (CSA, ΔCSA, ΔTpT) according to age range in HHCs and upper normal limit in HVs.

Variables	Age range (years)	04–15	15–30	31–45	46–60		Upper normal Limit (HVs)
						(15–60 y)	(mean + 2 SD)
	(*n*) Men	7	14	10	3	27	–
	(*n*) Women	7	15	19	8	42	–
	(*n*) Total (right + left)	28	58	58	22	138	–
	Mean ± SP [median]	10.3 ± 2.9 [11]	23.2 ± 4.7 [22]	36.3 ± 4.0 [37]	52.3 ± 4.4 [52]	29.2 ± 13.5 [29]	–
	Site	Mean ± SD [median]					
Peripheral nerve CSA (mm^2)	Med CT	7.2 ± 2.0 [7.1]	10.3 ± 10.3 [9.0]	10.7 ± 3.0 [10.0]	12.9 ± 4.0 [11.7]	10.9 ± 3.3 [10.0]	10.2
	UT	5.2 ± 1.4 [5]	7.0 ± 1.8 [7]	8.0 ± 1.9 [7.9]	9.1 ± 4.5 [8]	7.7 ± 2.3 [7.5]	9.8
	UPT	5.3 ± 1.5 [5.2]	6.5 ± 1.5 [6.6]	7.2 ± 1.7 [7]	8.2 ± 3.2 [7.0]	7.0 ± 2.0 [7]	9.3
	CFFH	9.4 ± 2.7 [10]	15.3 ± 4.2 [14.6]	17.5 ± 5.1 [16.5]	15.4 ± 4.1 [14.4]	16.2 ± 4.6 [15.3]	18.3
	T	6.4 ± 1.8 [6.9]	8.1 ± 2.4 [8]	9.8 ± 2.8 [9.8]	9.3 ± 3.4 [8.0]	9.0 ± 2.8 [8.7]	–
ΔCSA (mm^2)	Med CT	1.3 ±1.3 [1.0]	2.0 ± 1.2 [2.0]	1.4 ± 1.1 [1]	2.8 ± 3.5 [1.5]	1.8 ± 1.8 [1.2]	2.2
	UT	0.7 ± 0.6 [0.9]	1.3 ± 1.5 [1]	1.3 ± 1.1 [1.0]	1.8 ± 1.2 [2.0]	1.4 ± 1.2 [1.0]	3.1
	UPT	0.7 ± 0.9 [0.5]	1.3 ± 1.2 [1]	1.5 ± 1.3 [1.0]	1.9 ± 1.8 [1]	1.5 ± 1.4 [1.0]	1.4
	CFFH	1.7 ± 1.7 [1]	2.9± 3.2 [1.7]	3.2 ± 3.1 [2]	1.9 ± 1.4 [2]	2.8 ± 2.9 [2]	2.3
	T	1.0 ± 1.0 [1]	1.7 ± 1.8 [1.4]	1.8 ± 2.0 [1.0]	1.4 ± 1.5 [1.0]	1.7 ± 1.8 [1.0]	–
ΔTpT (mm^2)	Ulnar (UT and UPT)	0.7 ± 0.6 [0.9]	1.1 ± 0.9 [1]	1.3 ± 1.4 [1]	2.1 ± 1.9 [1.5]	1.3 ± 1.3 [1]	2.6
Analysis of new neural sites							
	Total $n = 48$	6	10	26	6	42	–
Peripheral nerve CSA (mm^2)	Med pCT	4.9 ± 0.87 [4.6]	7.9 ± 2.3 [7.2]	8.4 ± 2.0 [8.2]	11.6 ± 3.6 [10.3]	8.7 ± 2.6 [8.3]	–
ΔCSA (mm2)	Med pCT	0.7 ± 0.7 [0.4]	1.5 ± 1.1 [0.9]	1.3 ± 1.7 [0.7]	2.8 ± 3.3 [1.7]	1.5 ± 1.8 [0.9]	–
ΔTpT (mm^2) -	Median (CT and pCT)	0.9 ± 0.9 [0.8]	1.6 ± 1.0 [1.4]	2.8 ± 2.2 [2.8]	4.0 ± 2.9 [3.8]	2.7 ± 2.2 [2.3]	–
	Total $n = 76$	10	28	32	6	66	–
Peripheral nerve CSA (mm^2)	CFpFH	7.4 ± 2.2 [7.0]	13.9 ± 3.4 [14.8]	17.0 ± 4.4 [15.8]	19.7 ± 5.7 [18.3]	15.9 ± 4.4 [15.5]	–
ΔCSA (mm2)	CFpFH	1.1 ± 0.9 [1.0]	2.4 ± 2.2 [1.3]	2.8 ± 2.3 [2.5]	6.3 ± 3.6 [6.3]	2.9 ± 2.6 [2.0]	–
ΔTpT (mm^2)	Fibular common (FH e pFH)	0.6 ± 0.7 [0.3]	2.9 ± 2.8 [2]	2.8 ± 2.8 [2.0]	3.9 ± 2.6 [4.3]	2.9 ± 2.8 [2.0]	–

Data are reported as mean ± standard deviation and median (mm^2). (*n*), number; Med, median; CT, carpal tunnel; pCT, proximal to the carpal tunnel; UT, ulnar tunnel; UPT, ulnar pre-tunnel; CFFH, common fibular in the fibula head; T, tibial; CFpFH, common fibular proximal to the fibular head; ΔCSA, difference between the right and left nerves at the same site of assessment; ΔTpT, difference between the same nerve at different sites; HVs, healthy volunteers; HHCs, household contacts of patients with HD.

10.3389/fmed.2022.1059448

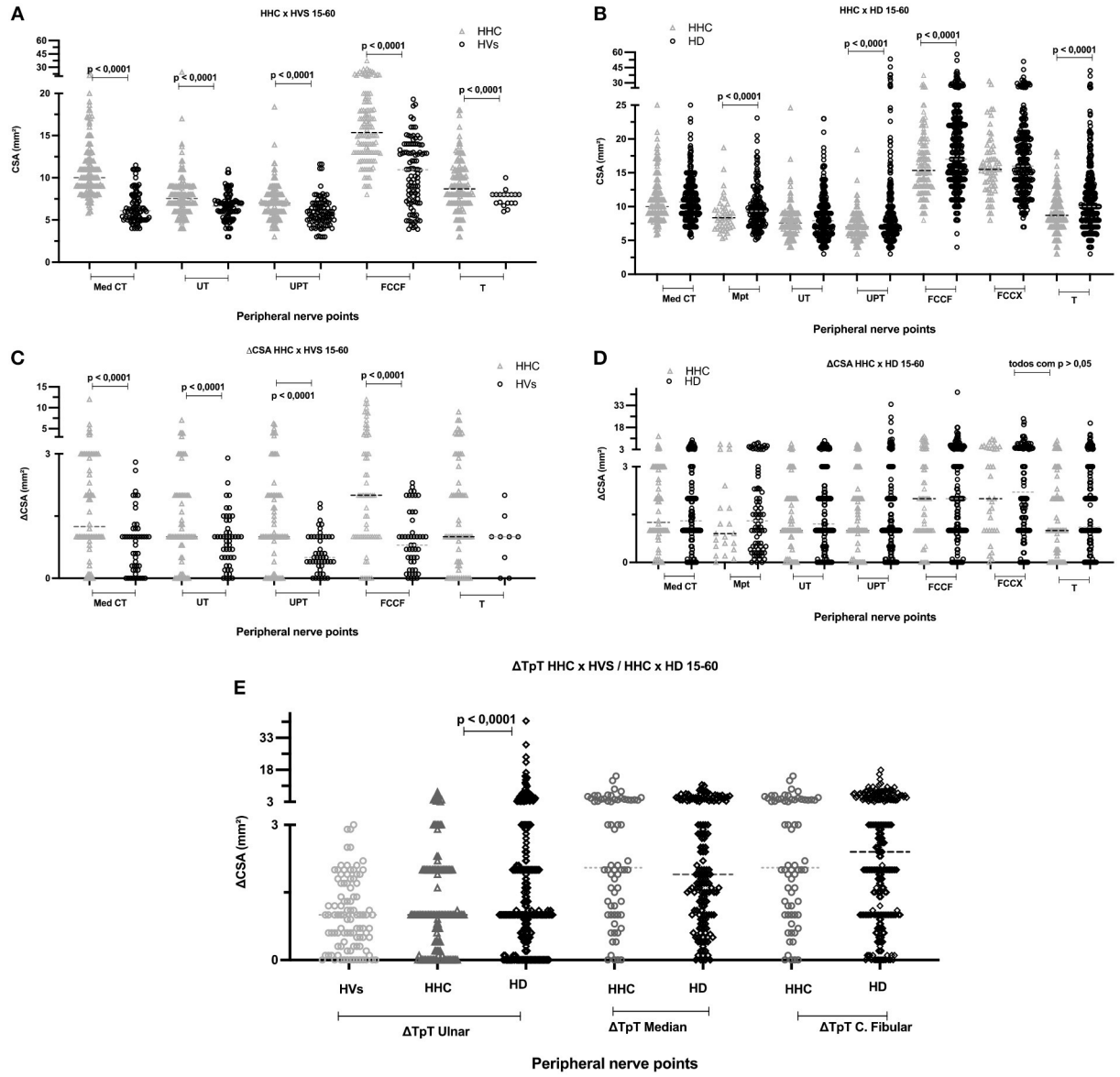

FIGURE 2
Absolute CSA values (mm^2) of peripheral nerve sites for HVs and HHC [**(A)** up on the left]; absolute CSA values of peripheral nerves sites for HHC and HD [**(B)** up on the right]. ΔCSA (mm^2) of right and left sides at the same assessment site for HVs and HHC [**(C)** middle on the left]; ΔCSA (mm^2) of right and left sides at the same assessment site for HHC and HD [**(D)** middle on the right]. ΔTpT (mm^2) of the different sites of the same nerve for HVs, HHC, and HD [**(E)** below]. (n), number; Med, median; CT, carpal tunnel; UT, ulnar tunnel; UPT, ulnar pre-tunnel; CFFH, common fibular nerve in the fibula head; T, tibial; MpT, median nerve in the proximal carpal tunnel; CFpFH, common fibular nerve proximal to the fibular head; CSA, cross-sectional area; ΔCSA, difference between the right and left nerves at the same site of assessment; ΔTpT, difference between the same nerve at different sites; HVs, healthy volunteers; HHC, household contacts of patients with HD; HD, Hansen's disease.

[0.41 ± 0.29 (0.4)]. Regarding ΔCSA altered beyond normality, we detected the following differences: HVs [0.02 ± 0.08 (0)] x HHCs [0.3 ± 0.23 (0.2)] and HVs x HD [0.32 ± 0.24 (0.4)]. Also, we detected higher than normal neural focality (ΔTpT) in the HD group [0.24 ± 0.32 (0)] compared to HHCs [0.13 ± 0.27 (0)] and in the HHC group compared to HVs [0.03 ± 0.12 (0)].

HHCs vs. HVs

When comparing healthy individuals to contacts of patients diagnosed with HD aged 15–60 years, we observed that the percentage of thickened nerves per nerve evaluated per individual was higher in contacts of patients with HD than in healthy subjects ($p < 0.0001$). Analysis by the ROC curve

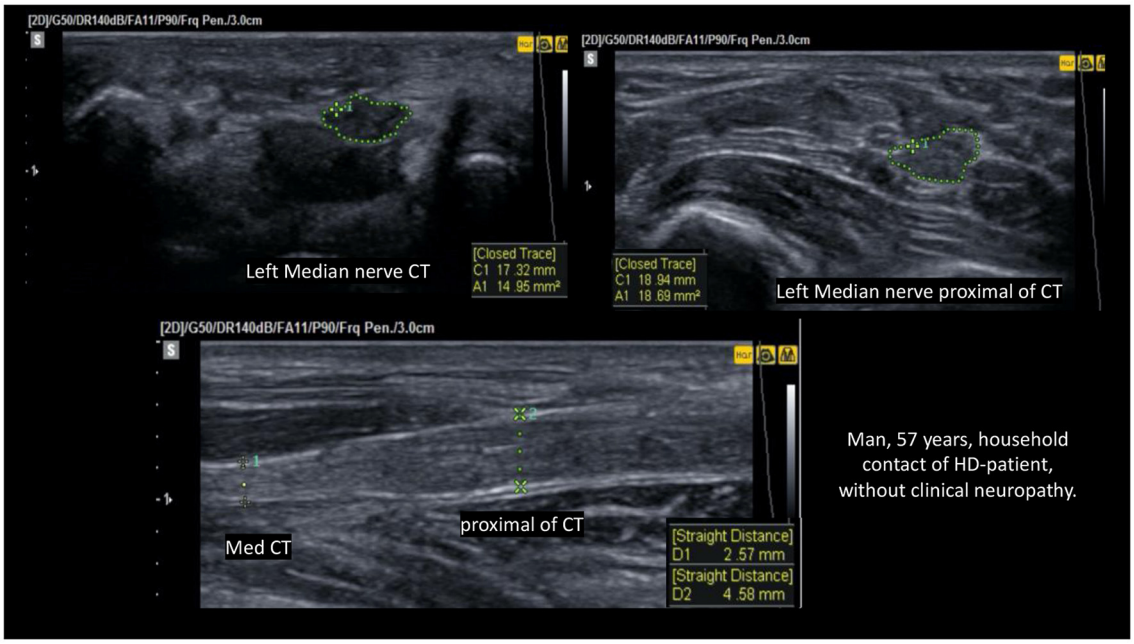

FIGURE 3
Fusiform thickening of the left median nerve regarding focality (ΔTpT) CSA pCT > CSA CT; ΔTpT = 18.69 −14.95 = 3.7 mm^2 > ULV (upper limit value).

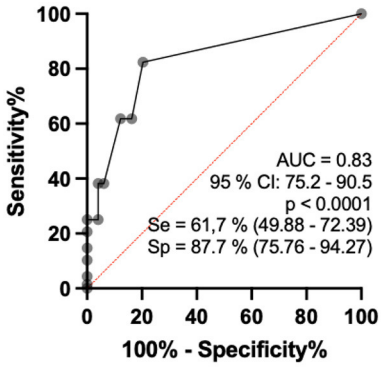

FIGURE 4
Analysis by the ROC curve of the percentage indices of altered nerves among the nerves evaluated per individual comparing the groups of healthy individuals and contacts of patients with HD aged 15–60 years.

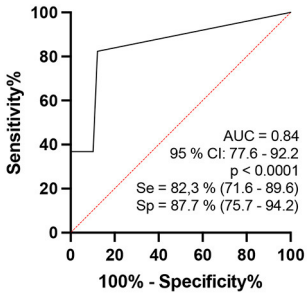

FIGURE 5
ROC curve analysis of the percentage indices of the number of asymmetries (ΔCSA) of the evaluated neural points considered to be altered per individual when comparing the groups of healthy persons and contacts of patients with HD (b – on the right).

revealed that the AUC was 83.0 (95% CI: 75.4–90.5%, $p < 0.0001$), and when the percentage of altered nerves among those evaluated was higher than 16.5%, sensitivity reached 61.7% (CI: 49.9 to 72.4) and specificity reached 87.8% (75.8 to 94.3), with a relative risk of 5.0 (Figure 4).

Regarding the number of asymmetries between neural points (ΔCSA) per individual defined as altered (greater than the reference mean + 2DP) by the ROC curve, comparison between healthy individuals and contacts of patients diagnosed with leprosy aged 15–60 years revealed a ROC curve of 84.9 (95% CI: 0.77–0.92, $p < 0.0001$) and when the percentage index of neural points defined as asymmetric was >10% of the points evaluated, sensitivity was 82.3% (71.6–89.6) and specificity was 87.8% (75.76–94.27), with a relative risk of 6.72, as shown in Figure 5.

In the analysis regarding the number of focalities among the points of the same nerve (ΔTpT) defined as altered (greater than

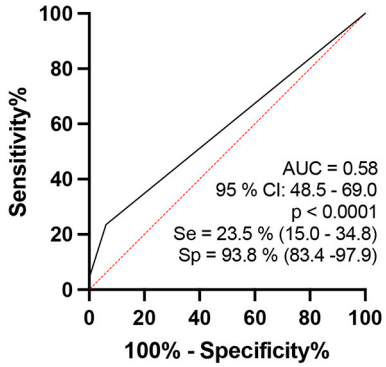

FIGURE 6
ROC curve analysis of the percentage indices of the number of focalities (ΔTpT) of the evaluated neural points considered to be altered per individual when comparing the groups of healthy persons and contacts of HD patients aged 15–60 years.

the reference mean ± 2DP) per individual by the ROC curve, when comparing healthy individuals to contacts of patients diagnosed with HD aged 15–60 years, the area under the curve was 58.2 (95% CI: 0.50–0.65, $p < 0.05$), and when the percentage index of neural points defined as having focality was >25% of the points evaluated, sensitivity was 39.7% (32.8–47.1) and specificity was 76.4% (65.1–84.9), with a relative risk of 1.69, as shown in Figure 6.

HHCs x HDs

When we compared contacts of patients diagnosed with HD to patients aged 15–60 years, we observed that the percentage of thickened nerves per nerve evaluated per individual was higher among patients with HD than among their contacts ($p = 0.0003$). Considering analysis by the ROC curve, we observed that the AUC was 64.8 (95% CI: 0.57–0.72, $p = 0.0003$) and when the values of the percentage of altered nerves among those evaluated were higher than 55%, sensitivity reached 30.6% (CI: 24.3–37.8) and specificity reached 85.3% (75–91.8), with a relative risk of 2.0 (Figure 6). Considering the percentage index of specificity found (82.3%), for a binomial analysis, we divided our samples into individuals with up to 6 nerves altered (<6) and individuals with more than 6 nerves altered (≥6). The chi-square value with Yates' correction was 6.5 ($p < 0.05$), and we found that individuals with six or more thickened nerves had a relative risk of 0.48 and an odds ratio of 0.39 (Figure 7).

Discussion

We found only one article (55) in the literature that evaluated by the US a peripheral nerve of contacts of the patient diagnosed with HD (PubMed; keywords: leprosy + contacts + ultrasound + nerves), and three other authors suggested that the US can be used for the evaluation of HD contacts (55–57). To the best of our knowledge, our sample of the number of nerves evaluated with HRUS of peripheral nerves in HHC and patients must be the largest in the world.

When we analyze healthy individuals, contacts of patients diagnosed with HD, and patients with HD, we note neural involvement even before the individuals develop the disease. There is thickening with increased CSA in all nerves of HD contacts compared to healthy individuals although this thickening is lower compared to patients with HD. Our results support the findings of other studies by objectively demonstrating that the contact factor increases the risk of developing HD (6, 11, 13, 19, 22–24); furthermore, peripheral nerve US with an HD protocol demonstrated that the neuropathy secondary to HD is a multiple peripheral mononeuropathy, confirming the results of other authors (22, 40, 43, 44, 58–64).

Moreover, given the natural history of the disease, these data show the primary neural involvement of HD detected with objective diagnostic imaging criteria. We question whether this early peripheral nerve involvement might be a subclinical phase of the disease or a host immune response. In any case, if there is nerve involvement, it is to be expected that there was an interaction between the pathogen and host, although not all individuals do develop the disease (9–13, 16).

Regarding the morphological aspects of the behavior of the disease with respect to the involvement of peripheral nerves, when we analyze the asymmetry criteria, we can observe that the contacts of MB-patients with HD already have more asymmetrical nerves (median, ulnar and fibular), with above normal differences between the right and left sides when compared to healthy individuals, as observed by Frade et al. (40) and Lugão et al. (43) and also when healthy individuals are compared to patients. However, since asymmetry (ΔCSA) was already installed in household contacts, this criterion showed no difference between HHC and patients (Figure 8).

Regarding focality within the same nerve, there was no difference between healthy subjects and contacts in the ulnar nerve; however, there was a difference between contacts and patients, demonstrating the late occurrence of this event in the natural history of the disease, as observed by Bathala et al. (59, 65) and Frade et al. (40) when comparing healthy individuals to those diagnosed with HD. The ΔTpT focality of the median nerve and the common fibular nerve was similar in HHCs and patients with HD.

Nagappa et al. (66) concluded that a median nerve enlargement of 2.0 cm proximal to the distal wrist crease distinguishes leprosy from carpal tunnel syndrome (CTS). In our study, we showed that patients with HD and their contacts had equal ΔTpT values in the median nerve, and the proportion of HHC with median nerve thickening in the carpal pre-tunnel

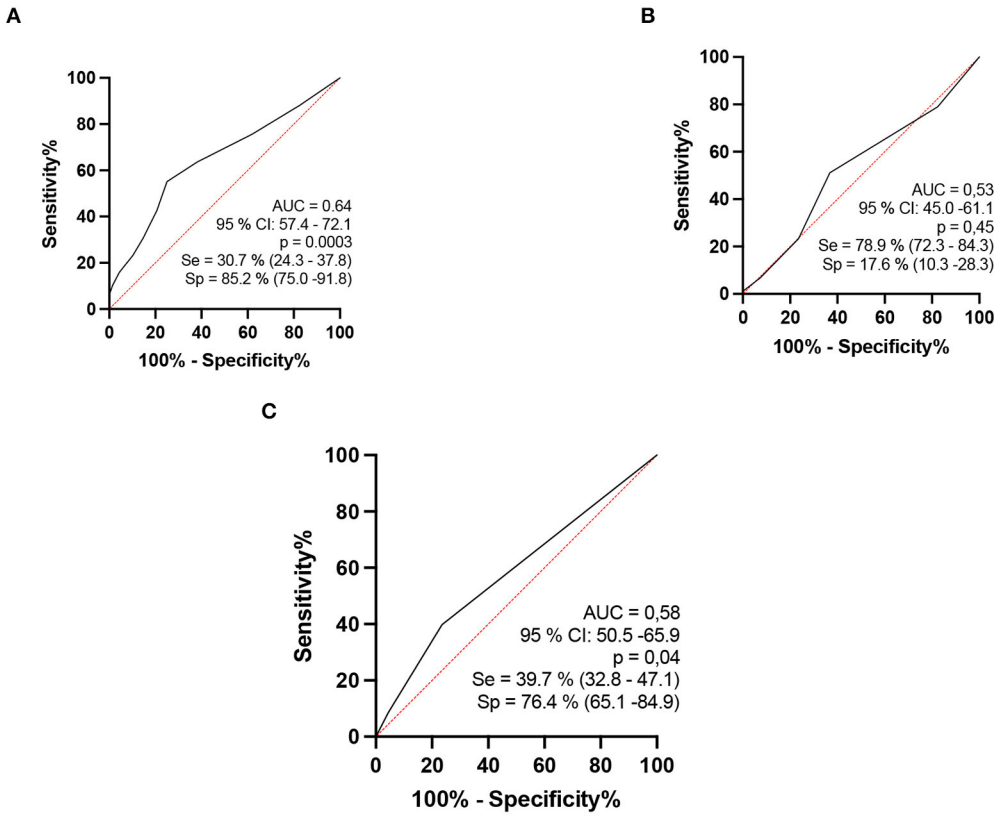

FIGURE 7
Analysis by the ROC curve comparing HHC and patients with HD aged 15–60 years: percentage indices of altered nerves among the nerves evaluated per individual [**(A)** up on the right]. The percentage indices of the number of asymmetries (ΔCSA) [**(B)** up on the left]. The percentage indices of the number of focalities (ΔTpT) [**(C)** as mentioned later].

had 4.1 OR with 90% specificity and positive predictive value compared to patients with HD. Thus, given the difference between healthy and sick subjects, we could characterize focality as a more specific marker of the disease (Figure 9). We would consider the asymmetry criteria to be more sensitive and probably of earlier detection for the characterization of peripheral nerve involvement in the evolutive phases of HD. This finding also shows that serial evaluation of leprosy contacts is a unique tool for assistance programs in public administration, being of help for an early diagnosis and thus contributing to the elimination of the disease (67).

A meta-analysis of the accuracy of diagnostic tests for HD (68) that included 78 studies concluded that, although test accuracy appears reasonable, the studies suffered from heterogeneity and poor methodological quality, most of them evaluating the detection of IgM antibodies against phenolic glycolipid-I by ELISA with 63.8% sensitivity (95% CI: 55.0–71.8) and 91.0% specificity (95% CI: 86.9–93.9) in 39 of the studies while the sensitivity of qPCR (five studies) was 78.5% (95% CI: 61.9–89.2) and specificity was 89.3% (95% CI 61.4–97.8). The sensitivity of conventional PCR (17 studies) was 75.3% (95% CI 67.9–81.5) and specificity was 94.5% (95% CI: 91.4–96.5). Regarding peripheral nerve ultrasonography in the evaluation of HD neuropathy, several studies have considered it as a method with good efficacy, reproducibility, and diagnostic accuracy, besides its accessible cost and availability, even for point of care (40, 43, 47, 49, 59, 69–76).

Healthy individuals had nerves without thickening compared to contacts who had up to 20% of nerves with thickening and to patients who had up to 40% of nerves with increased CSA, results similar to those reported by Wilder-Smith et al. regarding neural dysfunction of peripheral nerves documented by ENMG, which was greater in patients with HD, followed by HHC and HVs (77). The same applies to the number of asymmetries per individual which was higher in HD compared to contacts and healthy individuals.

We also evaluated 4 new neural points in 21 contacts and 78 patients, for a total of 14 rather than 10 points. The AUC of the sum of the thickened nerves increased, thus also increasing the sensitivity and specificity of peripheral nerve US with a protocol for HD evaluation. However, increasing the number of neural points in the evaluation

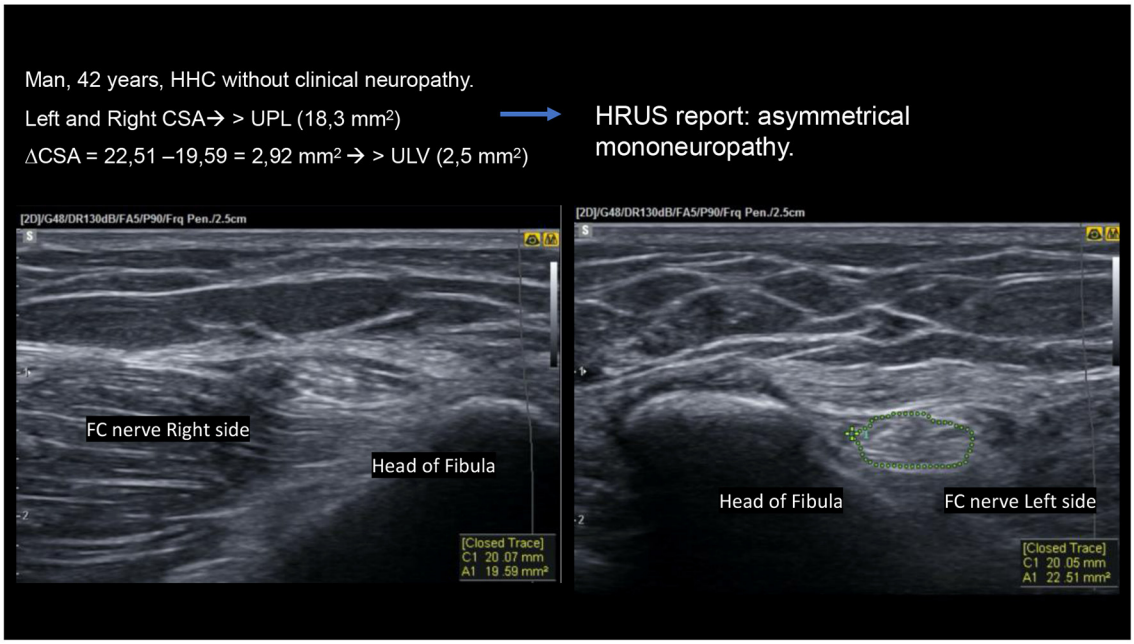

FIGURE 8
High-resolution ultrasound (HRUS) images of the same HHC of a patient with HD with asymmetrical mononeuropathy of the common fibular nerve on the head of the fibula.

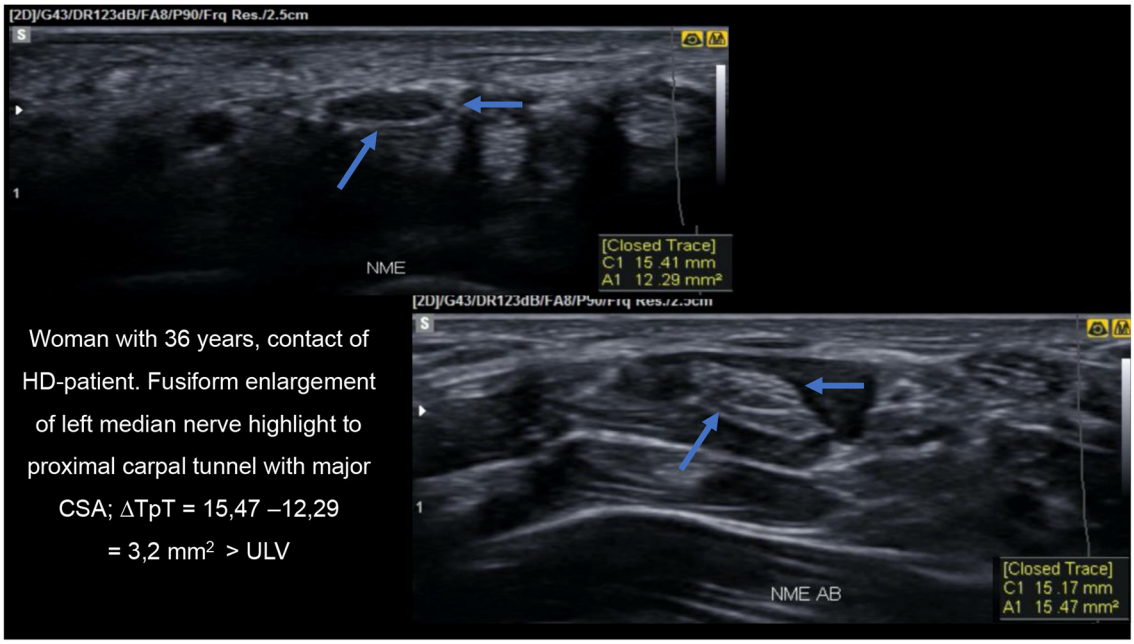

FIGURE 9
HRUS image demonstrating thickening of the median nerve proximal to the carpal tunnel on transverse view.

no longer revealed differences in asymmetry and focality between HHC and patients with HD, with the two groups being equal.

About the limitations of our study, perhaps a prospective study with an evaluation of the peripheral nerves of the contacts that show the neural thickening documented by the peripheral

nerve US examination may bring more information regarding the development of the pathology. Another limitation of our study was that we did not have data on the ΔTpT (Δfocality) of the median and common fibular nerves of HVs. The data presented could also reflect on the individual's immunity acting against the nerve and promoting thickening and asymmetry, or the subclinical infection itself.

Conclusion

Peripheral nerve US with a protocol for HD (median, ulnar, common fibular, and tibial nerves) revealed HD as an asymmetric and/or focal peripheral multiple mononeuropathy.

Considering HRUS findings, if asymmetric multiple mononeuropathy signs (thickening or asymmetry) are detected in at least 20% of the nerves evaluated in the HHCs, these findings could already indicate evidence of HD neuropathy. Thus, if more nerve points are assessed in HHCs (14 instead of 10), these individuals become more like patients with HD according to the nerve thickening determined by HRUS, which should be a cutting-edge tool for an early diagnosis of leprosy cases.

Neural hypertrophy detected by HRUS in all peripheral nerve points seems to differentiate contacts from healthy volunteers, but the enlargement of three of seven neural points (median CT, ulnar-tunnel, and commun fibular nerve in pre-head fibula) was similar to that of patients with HD. Asymmetry of peripheral nerves was greater in the HHC group at all neural points compared to healthy volunteers, except in the tibial point, and was similar when compared to patients with HD at all points evaluated. Both findings could constitute important alerts for early and/or subclinical HD, mainly asymmetry, with 82.3% sensitivity and 87.7% specificity, respectively.

Finally, the peripheral nerve focalities of the median and common fibular nerves were similar for HHC and patients with HD, except for the ulnar nerve whose values were higher in patients with HD than in HHC. These data could also suggest important findings for the median and common fibular nerves of individuals with early and/or subclinical HD, which can be properly assessed only by HRUS, while ulnar nerve focality seems to be a late event in the natural course of the HD.

Data availability statement

The raw data supporting the conclusions of this article will be made available by the authors, without undue reservation.

Ethics statement

The studies involving human participants were reviewed and approved by Ethics Committee of Hospital das Clínicas da Faculdade de Medicina de Ribeirão Preto da Universidade de São Paulo. Written informed consent to participate in this study was provided by the participants' legal guardian/next of kin.

Author contributions

GV and MF contributed on all stage of this study, conception and design of the study, performed the statistical analysis, manuscript revision, read, and approved the submitted version. FB, ND, CMLS, ML, JS, JB, CGS, GC, and MD contributed to conception and design of the study, to data collection, obtaining, analyzing and interpreting data, and approved the submitted version. All authors contributed to the article and approved the submitted version.

Funding

This work was funded by Coordenação de Aperfeiçoamento de Pessoal de Nível Superior - Brazil (CAPES) - Finance Code 001, National Council for Scientific and Technological Development (CNPq), Center of National Reference in Sanitary Dermatology and HD - Hospital of the Medical School of Ribeirão Preto, Ribeirão Preto, São Paulo, Brazil, the Brazilian Health Ministry (MS/FAEPAFMRP-USP: 749145/ 2010 and 767202/2011), Oswaldo Cruz Foundation (Fiocruz) Ribeirão Preto - TED163/2019 - Process: No. 25380.102201/2019-62/Project Fiotec: PRES-009-FIO-20, and VALE S.A. 27756/2019.

Conflict of interest

The authors declare that the research was conducted in the absence of any commercial or financial relationships that could be construed as a potential conflict of interest.

Publisher's note

Supplementary material

The Supplementary Material for this article can be found online at: https://www.frontiersin.org/articles/10.3389/fmed.2022.1059448/full#supplementary-material

References

1. Goulart IMB, Bernardes Souza DO, Marques CR, Pimenta VL, Gonçalves MA, Goulart LR. Risk and protective factors for leprosy development determined by epidemiological surveillance of household contacts. *Clin Vaccine Immunol.* (2008) 15:101–5. doi: 10.1128/CVI.00372-07

2. The Lancet Neurology. Leprosy as a neurological disease. *Lancet Neurol.* (2009) 8:217. doi: 10.1016/S1474-4422(09)70026-2

3. Scollard DM, Adams LB, Gillis TP, Krahenbuhl JL, Truman RW, Williams DL. The continuing challenges of leprosy. *Clin Microbiol Rev.* (2006) 19:338–81. doi: 10.1128/CMR.19.2.338-381.2006

4. World Health Organization (WHO). Global leprosy (Hansen disease) update, 2020: impact of COVID-19 on global leprosy control. *Wkly Epidemiol Rec.* (2020) 96:421–44. Available online at: https://www.who.int/publications/i/item/who-wer9636-421-444

5. Salgado CG, Barreto JG, da Silva MB, Frade MAC, Spencer JS. What do we actually know about leprosy worldwide? *Lancet Infect Dis.* (2016) 16:778. doi: 10.1016/S1473-3099(16)30090-1

6. Goulart IMB, Goulart LR. Leprosy: diagnostic and control challenges for a worldwide disease. *Arch Dermatol Res.* (2008) 300:269–90. doi: 10.1007/s00403-008-0857-y

7. Carneiro M, Possuelo LG, Valim ARM. Neuropatia por hanseníase: atraso no diagnóstico ou um diagnóstico difícil? *Cad Saude Publica.* (2011) 27:2069. doi: 10.1590/S0102-311X2011001000020

8. de Oliveira MBB, Diniz LM. Leprosy among children under 15 years of age: literature review. *An Bras Dermatol.* (2016) 91:196–203. doi: 10.1590/abd1806-4841.20163661

9. Goulart LR, Goulart IMB. Leprosy pathogenetic background: a review and lessons from other mycobacterial diseases. *Arch Dermatol Res.* (2009) 301:123–37. doi: 10.1007/s00403-008-0917-3

10. Moet FJ, Meima A, Oskam L, Richardus JH. Risk factors for the development of clinical leprosy among contacts, and their relevance for targeted interventions. *Lepr Rev.* (2004) 75:310–26. doi: 10.47276/lr.75.4.310

11. Araujo S, Freitas LO, Goulart LR, Goulart IMB. Molecular evidence for the aerial route of infection of Mycobacterium leprae and the role of asymptomatic carriers in the persistence of leprosy. *Clin Infect Dis.* (2016) 63:1412–20. doi: 10.1093/cid/ciw570

12. Alter A, Grant A, Abel L, Alcaïs A, Schurr E. Leprosy as a genetic disease. *Mamm Genome.* (2011) 22:19–31. doi: 10.1007/s00335-010-9287-1

13. Patrocínio LG, Goulart IMB, Goulart LR, Patrocínio JA, Ferreira FR, Fleury RN. Detection of Mycobacterium leprae in nasal mucosa biopsies by the polymerase chain reaction. *FEMS Immunol Med Microbiol.* (2005) 44:311–6. doi: 10.1016/j.femsim.2005.01.002

14. Sharma R, Singh P, Loughry WJ, et al. Zoonotic leprosy in the southeastern United States. *Emerg Infect Dis.* (2015) 21:2127–34. doi: 10.3201/eid2112.150501

15. Deps PD. Como o mycobacterium leprae é transmitido. *Hansen int.* (2001) 26:31–6.

16. Mohanty PS, Naaz F, Katara D, et al. Viability of Mycobacterium leprae in the environment and its role in leprosy dissemination. *Indian J Dermatol Venereol Leprol.* (2016) 82:23–7. doi: 10.4103/0378-6323.168935

17. da Silva MB, Portela JM, Li W, et al. Evidence of zoonotic leprosy in Pará, Brazilian Amazon, and risks associated with human contact or consumption of armadillos. *PLoS Negl Trop Dis.* (2018) 12:6532. doi: 10.1371/journal.pntd.0006532

18. Douglas JT, Cellona R V, Fajardo TT, Abalos RM, Balagon MVF, Klatser PR. Prospective study of serological conversion as a risk factor for development of leprosy among household contacts. *Clin Diagn Lab Immunol.* (2004) 11:897–900. doi: 10.1128/CDLI.11.5.897-900.2004

19. Fine PEM, Sterne JAC, Pönnighaus JM, et al. Household and dwelling contact as risk factors for leprosy in northern Malawi. *Am J Epidemiol.* (1997) 146:91–102. doi: 10.1093/oxfordjournals.aje.a009195

20. Frade MAC, de Paula NA, Gomes CM, et al. Unexpectedly high leprosy seroprevalence detected using a random surveillance strategy in Midwestern Brazil: a comparison of ELISA and a rapid diagnostic test. *PLoS Negl Trop Dis.* (2017) 11:1–12. doi: 10.1371/journal.pntd.0005375

21. Lobato J, Costa MP, Reis Ede M, Gonçalves MA, Spencer JS, Brennan PJ, et al. Comparison of three immunological tests for leprosy diagnosis and detection of subclinical infection. *Lepr Rev.* (2011) 82:389–401.

22. Santos DF, Mendonça MR, Antunes DE, Sabino EF, Pereira RC, Goulart LR, et al. Molecular, immunological, and neurophysiological evaluations for early diagnosis of neural impairment in seropositive leprosy household contacts. *PLoS Negl Trop Dis.* (2018) 12:1–12. doi: 10.1371/journal.pntd.0006494

23. Gama RS, Gomides TA, Gama CF, Moreira SJ, de Neves Manta FS, de Oliveira LB, et al. High frequency of *M. leprae* DNA detection in asymptomatic household contacts. *BMC Infect Dis.* (2018) 18:1–6. doi: 10.1186/s12879-018-3056-2

24. Bazan-Furini R, Motta AC, Simão JC, Tarquínio DC, Marques W Jr, Barbosa MH, et al. Early detection of leprosy by examination of household contacts, determination of serum anti-PGL-1 antibodies and consanguinity. *Mem Inst Oswaldo Cruz.* (2011) 106:536–40. doi: 10.1590/S0074-02762011000500003

25. Wilder-Smith E, Wilder-Smith A, Van Brakel WH, Egger M. Vasomotor reflex testing in leprosy patients, healthy contacts and controls: a cross-sectional study in Western Nepal. *Lepr Rev.* (1996) 67:306–17. doi: 10.5935/0305-7518.19960031

26. Araújo S, Lobato J, Reis ÉD, Souza DO, Gonçalves MA, Costa AV, et al. Unveiling healthy carriers and subclinical infections among household contacts of leprosy patients who play potential roles in the disease chain of transmission. *Mem Inst Oswaldo Cruz.* (2012) 107(SUPPL.1):55–9. doi: 10.1590/S0074-02762012000900010

27. Feenstra SG, Nahar Q, Pahan D, Oskam L, Richardus JH. Social contact patterns and leprosy disease: a case-control study in Bangladesh. *Epidemiol Infect.* (2013) 141:573–81. doi: 10.1017/S0950268812000969

28. Vijayakumaran P, Jesudasan K, Mozhi NM, Samuel JDR. Does MDT Arrest transmission of leprosy to household contacts? *Int J Lepr Other Mycobact Dis.* (1998) 66:125–30.

29. Wilder-Smith E, Wilder-Smith A, Egger M. Peripheral autonomic nerve dysfunction in asymptomatic leprosy contacts. *J Neurol Sci.* (1997) 150:33–8. doi: 10.1016/S0022-510X(97)05363-X

30. Scollard DM. Endothelial cells and the pathogenesis of lepromatous neuritis: insights from the armadillo model. *Microbes Infect.* (2000) 2:1835–43. doi: 10.1016/S1286-4579(00)01335-6

31. Defaria RC, Silva MI. Electromyographic diagnosis of leprosy. *Arq Neuropsiquiatia.* (1990) 48:403–13.

32. Frade MAC, Rosa DJ de F, Bernardes Filho F, Spencer JS, Foss NT. Semmes-Weinstein monofilament: A tool to quantify skin sensation in macular lesions for leprosy diagnosis. *Indian J Dermatol Venereol Leprol.* (2021) 87:807–15. doi: 10.25259/ijdvl_622_19

33. Kulshreshtha D, Malhotra KP, Malhotra HS, et al. Mandating nerve biopsy: a step towards personalizing therapy in pure neuritic leprosy. *J Peripher Nerv Syst.* (2018) 23:190–6. doi: 10.1111/jns.12283

34. Ashok Kumar SK, Reddy BSN, Ratnakar C. Correlation of skin and nerve histopathology in leprosy. *Lepr Rev.* (1996) 67:119–25. doi: 10.5935/0305-7518.19960012

35. V. P. SHETTY, L. N. MEHTA, N. H. ANTIA APFI. Teased fiber study of early nerve lesions in leprosy and in contacts, with electrophysiological correlates V. *J of Neurol Neurosurg Psych.* (1977) 40:708–11.

36. World Health Organization. *Regional Office for South-East Asia. Guidelines for the diagnosis, treatment and prevention of leprosy*. World Health Organization. (2018). Available online at: https://apps.who.int/iris/handle/10665/274127

37. Alemu Belachew W, Naafs B. Position statement: leprosy: diagnosis, treatment, and follow-up. *J Eur Acad Dermatology Venereol.* (2019) 33:1205–13. doi: 10.1111/jdv.15569

38. Chacha JJ, Peters L, Rivitti EA, Sotto MN, Lourenço S, Melnikov P. Sistema nervoso periférico e pressupostos da agressão neural na hanseníase. *An Bras Dermatol.* (2009) 84:495–500. doi: 10.1590/S0365-05962009000500008

39. Filho FB, De Paula NA, Leite MN, et al. Evidence of hidden leprosy in a supposedly low endemic area of Brazil. *Mem Inst Oswaldo Cruz.* (2017) 112:822–8. doi: 10.1590/0074-02760170173

40. Frade MA, Nogueira-Barbosa MH, Lugão HB, Furini RB, Marques Junior W, Foss NT, et al. New sonographic measures of peripheral nerves: a tool for diagnosis of peripheric nerve involvment in leprosy. *Hansenol Int.* (2013) 36:71. doi: 10.1590/s0074-02762013000300001

41. Garbino JA, Marques W Jr, Barreto JA, Heise CO, Rodrigues MM, Antunes SL, et al. Hanseníase neural primária: revisão sistemática. *Arq Neuropsiquiatr.* (2013) 71:397–404. doi: 10.1590/0004-282X20130046

42. Lugão HB, Frade MAC, Marques W Jr, Foss NT, Nogueira-Barbosa MH. Ultrasonography of leprosy neuropathy: a longitudinal prospective study. *Small PLC, ed PLoS Negl Trop Dis.* (2016) 10:e0005111. doi: 10.1371/journal.pntd.0005111

43. Lugão HB, Nogueira-Barbosa MH, Marques W, Foss NT, Frade MAC. Asymmetric nerve enlargement: a characteristic of leprosy neuropathy demonstrated by ultrasonography. *PLoS Negl Trop Dis.* (2015) 9:1–11. doi: 10.1371/journal.pntd.0004276

44. Scollard DM, Truman RW, Ebeneze GJ. Mechanisms of nerve injury in leprosy. *Clin Dermatol*. (2015) 33:46–54. doi: 10.1016/j.clindermatol.2014.07.008

45. El Gency HI, Ghanema M, Hussein SA, Almaghraby OS, Rashad W. Peripheral neuropathy is not the end but the beginning. *Lepr Rev.* (2017) 88:574–82. doi: 10.47276/lr.88.4.574

46. Van Brakel WH, Saunderson P, Shetty V, Brandsma JW, Post E, Jellema R, et al. International workshop on neuropathology in leprosy–consensus report. *Lepr Rev*. (2007) 78:416–33.

47. Lugão HB. Avaliação da reprodutibilidade da ultrassonografia de nervos periféricos em pacientes com hanseníase e voluntários saudáveis. (2015) 40(Suppl 1):19825161.

48. Wortsman X, Jemec GBE. *Dermatologic Ultrasound with Clinical and Ultrasound Correlations*. 1st ed. New York, NY: Springer (2013). doi: 10.1007/978-1-4614-7184-4

49. Martinoli C, Derchi LE, Bertolotto M. US and MR imaging of peripheral nerves in leprosy. *Skeletal Radiol.* (2000) 29:142–50. doi: 10.1007/s002560050584

50. Kara M, Özçakar L, De Muynck M, Tok F, Vanderstraeten G. Musculoskeletal ultrasound for peripheral nerve lesions. *Eur J Phys Rehabil Med.* (2012) 48:665–74.

51. Martinoli C, Bianchi S, Derchi LE. Ultrasonography of peripheral nerves. *Semin Ultrasound CT MRI.* (2000) 21:205–13. doi: 10.1016/S0887-2171(00)90043-X

52. Schenone A, Martinoli C. Ultrasonography of peripheral nerves. *Neurol Sci*. (2000) 21(4 SUPPL.):205–213.

53. Voltan G, Bernards Filho F, Leite MN, De Paula NA, Santana JM, Silva CM, et al. Point-of-care ultrasound of peripheral nerves in the diagnosis of Hansen's disease neuropathy. *Front Med.* (2022) 9:5252. doi: 10.3389/fmed.2022.985252

54. Voltan G, Bernardes-filho F, Nogueira-barbosa MH, Andrey M, Frade C. Ultrasound reference values for peripheral nerve cross-sectional areas and indices in a sample of healthy individuals in Brazil. *Radiol Brasil*. (2022) 55:337–45. doi: 10.1590/0100-3984.2022.0020

55. Neto FB de A, Neto RA, Cardoso LMC. The first report of pure neuritic leprosy with involvement of the anterior femoral cutaneous nerve. *Neurol Int.* (2019) 11:15–7. doi: 10.4081/ni.2019.8001

56. Nagappa M, Visser LH, Bathala L. Peripheral nerve sonography, a novel technique for improving the diagnosis of Hansen's neuropathy. *Lepr Rev*. (2021) 92:202–6. doi: 10.47276/LR.92.3.202

57. Elias J Jr, Nogueira-Barbosa MH, Feltrin LT, Furini RB, Foss NT, Marques W Jr, et al. Role of ulnar nerve sonography in leprosy neuropathy with electrophysiologic correlation. *J Ultrasound Med.* (2009) 28:1201–9. doi: 10.7863/jum.2009.28.9.1201

58. Bernardes-Filho F, Lima FR, Voltan G, de Paula NA, Frade MAC. Leprosy case series in the emergency room: a warning sign for a challenging diagnosis. *Brazilian J Infect Dis.* (2021) 25:1634. doi: 10.1016/j.bjid.2021.101634

59. WHO WHO. Weekly epidemiological record. Global leprosy update, 2018: moving towards a leprosyfree world. *Wkly Epidemiol Rec*. (2019) 94:389–412. Available online at: https://www.who.int/publications/i/item/who-wer9435-36

60. Bathala LN, Krishnam V, Kumar HK, Neladimmanahally V, Nagaraju U, Kumar HM, et al. Extensive sonographic ulnar nerve enlargement above the medial epicondyle is a characteristic sign in Hansen's neuropathy. *PLoS Negl Trop Dis.* (2017) 11:1–10. doi: 10.1371/journal.pntd.0005766

61. Kumar N, Malhotra HS, Garg RK, et al. Comprehensive electrophysiology in leprous neuropathy - Is there a clinico-electrophysiological dissociation? *Clin Neurophysiol.* (2016) 127:2747–55. doi: 10.1016/j.clinph.2016.05.002

62. Nascimento OJM. Neuropatia da lepra: apresentações clínicas. *Arq Neuropsiquiatr*. (2013) 71:661–6. doi: 10.1590/0004-282X20130146

63. Jardim MR, Antunes SL, Santos AR, Nascimento OJ, Nery JA, Sales AM, et al. Criteria for diagnosis of pure neural leprosy. *J Neurol.* (2003) 250:806–9. doi: 10.1007/s00415-003-1081-5

64. Garbino JA, Ura S, Belone A de FF, Marciano LHSC, Fleury RN. Aspectos clínicos e diagnósticos da hanseníase primariamente neural. *Hansen Int. [Internet]. 30° de novembro de 1994 [citado 30° de dezembro de 2022]*. (2022) 19:124–9. Available online at: https://periodicos.saude.sp.gov.br/hansenologia/article/view/36507

65. Santos DF dos. Aspectos clínicos, moleculares, sorológicos e neurofisiológicos no diagnóstico precoce da neuropatia hansênica. *Tese apresentando ao Programa Pó-graduação em Ciências da Saúde da Fac Med da Univ Fed Uberlância, como requisito para obtenção do título Doutor em Ciências da Saúde*. (2017) 178.

66. Bathala L, Kumar K, Pathapati R, Jain S, Visser LH. Ulnar neuropathy in Hansen disease: clinical, high-resolution ultrasound and electrophysiologic correlations. *J Clin Neurophysiol.* (2012) 29:190–3. doi: 10.1097/WNP.0b013e31824d969c

67. Nagappa M, Pujar GS, Keshavan AH, Bathala L, Jain RD, Das A, et al. Sonographic pattern of median nerve enlargement in Hansen's neuropathy. *Acta Neurol Scand.* (2021) 144:155–60. doi: 10.1111/ane.13432

68. Bechelli LM. Prospects of global elimination of leprosy as a public health problem by the year 2000. *Int J Lepr Other Mycobact Dis*. (1994) 62:284–92.

69. Gurung P, Gomes CM, Vernal S, Leeflang MMG. Diagnostic accuracy of tests for leprosy: a systematic review and meta-analysis. *Clin Microbiol Infect.* (2019) 25:1315–27. doi: 10.1016/j.cmi.2019.05.020

70. Visser LH, Jain S, Lokesh B, Suneetha S, Subbanna J. Morphological changes of the epineurium in leprosy: a new finding detected by high-resolution sonography. *Muscle and Nerve.* (2012) 46:38–41. doi: 10.1002/mus.23269

71. Jain S, Visser LH, Suneetha S. Imaging techniques in leprosy clinics. *Clin Dermatol.* (2016) 34:70–8. doi: 10.1016/j.clindermatol.2015.10.014

72. Bignotti B, Tagliafico A, Martinoli C. Ultrasonography of peripheral nerves: anatomy and pathology. *Ultrasound Clin.* (2014) 9:525–36. doi: 10.1016/j.cult.2014.03.006

73. Jain S, Raju R, Visser LH. The diagnostic value of assessing nerve damage by high-resolution sonography and color Doppler in leprosy patients. In: *18th International Leprosy Congress*. (2013).

74. Frijlink DW, Brekelmans GJF, Visser LH. Increased nerve vascularization detected by color Doppler sonography in patients with ulnar neuropathy at the elbow indicates axonal damage. *Muscle and Nerve.* (2013) 47:188–93. doi: 10.1002/mus.23505

75. Becker DM, Tafoya CA, Becker SL, Kruger GH, Tafoya MJ, Becker TK. The use of portable ultrasound devices in low- and middle-income countries: a systematic review of the literature. *Trop Med Int Heal.* (2016) 21:294–311. doi: 10.1111/tmi.12657

76. Wheat SW, Stryjewska B, Cartwright MS, A. Hand-held ultrasound device for the assessment of peripheral nerves in leprosy. *J Neuroimaging.* (2021) 31:76–8. doi: 10.1111/jon.12797

77. Wilder-Smith A, Wilder-Smith E. Electrophysiological evaluation of peripheral autonomic function in leprosy patients, leprosy contacts, and controls. *Int J Lepr Other Mycobact Dis*. (1996)64:433–40.

frontiers | Frontiers in Medicine

TYPE Original Research
PUBLISHED 19 January 2023
DOI 10.3389/fmed.2023.1089013

OPEN ACCESS

EDITED BY
Paola Savoia,
Università degli Studi del Piemonte Orientale, Italy

REVIEWED BY
Kristen M. Meiburger,
Polytechnic University of Turin, Italy
Philippe Lefrançois,
McGill University, Canada

*CORRESPONDENCE
Michael Erdmann
✉ michael.erdmann@uk-erlangen.de

SPECIALTY SECTION
This article was submitted to Dermatology, a section of the journal Frontiers in Medicine

RECEIVED 03 November 2022
ACCEPTED 05 January 2023
PUBLISHED 19 January 2023

CITATION
Müller K, Berking C, Voskens C, Heppt MV, Heinzerling L, Koch EAT, Kramer R, Merkel S, Schuler-Thurner B, Schellerer V, Steeb T, Wessely A and Erdmann M (2023) Conventional and three-dimensional photography as a tool to map distribution patterns of in-transit melanoma metastases on the lower extremity. *Front. Med.* 10:1089013. doi: 10.3389/fmed.2023.1089013

Conventional and three-dimensional photography as a tool to map distribution patterns of in-transit melanoma metastases on the lower extremity

Kilian Müller[1], Carola Berking[2,3], Caroline Voskens[2,3], Markus V. Heppt[2,3], Lucie Heinzerling[4], Elias A. T. Koch[2,3], Rafaela Kramer[2,3], Susanne Merkel[3,5], Beatrice Schuler-Thurner[2,3], Vera Schellerer[6], Theresa Steeb[2,3], Anja Wessely[2,3] and Michael Erdmann[2,3]*

[1]Institute of Hygiene and Environmental Medicine, University Medicine Greifswald, Greifswald, Germany, [2]Department of Dermatology, Uniklinikum Erlangen, Deutsches Zentrum Immuntherapie (DZI), Friedrich-Alexander University Erlangen-Nürnberg (FAU), Erlangen, Germany, [3]Comprehensive Cancer Center Erlangen–European Metropolitan Area of Nuremberg (CCC ER-EMN), Erlangen, Germany, [4]Department of Dermatology and Allergy, University Hospital Munich, Ludwig Maximilian University of Munich, Munich, Germany, [5]Department of Surgery, Uniklinikum Erlangen, Friedrich-Alexander University Erlangen-Nürnberg, Erlangen, Germany, [6]Department of Pediatric Surgery, University Medicine Greifswald, Greifswald, Germany

Background: In melanoma, in-transit metastases characteristically occur at the lower extremity along lymphatic vessels.

Objectives: The objective of this study was to evaluate conventional or three-dimensional photography as a tool to analyze in-transit metastasis pattern of melanoma of the lower extremity. In addition, we assessed risk factors for the development of in-transit metastases in cutaneous melanoma.

Methods: In this retrospective, monocentric study first we compared the clinical data of all evaluable patients with in-transit metastases of melanoma on the lower extremity (n = 94) with melanoma patients without recurrence of disease (n = 288). In addition, based on conventional (n = 24) and three-dimensional photography (n = 22), we defined the specific distribution patterns of the in-transit metastases on the lower extremity.

Results: Using a multivariate analysis we identified nodular melanoma, tumor thickness, and ulceration as independent risk factors to develop in-transit metastases ITM (n = 94). In patients with melanoma on the lower leg (n = 31), in-transit metastases preferentially developed along anatomically predefined lymphatic pathways. In contrast when analyzing in-transit metastases of melanoma on the foot (n = 15) no clear pattern could be visualized. In addition, no difference in distance

between in-transit metastases and primary melanoma on the foot compared to the lower leg was observed using three-dimensional photography (n = 22).

Conclusion: A risk-adapted follow-up of melanoma patients to detect in-transit metastases can be applied by knowledge of the specific lymphatic drainage of the lower extremity. Our current analysis suggests a more complex lymphatic drainage of the foot.

KEYWORDS

melanoma, in-transit metastasis, lower extremity, lymphatic pathways, 3D photography

Introduction

Cutaneous melanoma is characterized by a high risk of metastases occurring in close proximity to the primary melanoma, along the route to and in regional lymph nodes, and as distant metastases (1). Despite approved adjuvant treatment options for primary high-risk melanoma (2) and life-prolonging therapies in the stage of distant metastasis (3), melanoma remains a fatal disease.

In-transit metastases (ITM) are a special kind of recurrence in the skin, observed predominantly in melanoma and approximately develop in 7% of the melanoma patients (4). They occur in the anatomical region between primary melanoma and the corresponding regional lymph node basin. The clinical course of patients developing ITM varies considerably, ranging from solitary lesions with prolonged relapse-free intervals up to subsequent, rapidly progressing systemic disease (1). ITM can be palpable and visible and therefore represent a significant psychological burden for patients (5). Apart from the proposed spreading along the draining lymphatic vessels, the biology of ITM formation is not fully understood and there is currently no way to identify patients at risk of developing ITM. Commonly known risk factors of melanoma including tumor thickness and ulceration of the primary melanoma also apply to patients who develop ITM. Patients with ITM at the leg have a better prognosis than those with ITM at other body sites (6). This may be related to the long lymphatic pathways of the lower extremity defined by a Japanese research group (7) in cadavers. Therefore, the area along defined lymphatic pathways where ITM occur would be predetermined based on the location of the primary melanoma.

In dermatology, different imaging modalities such as digital photography, dermoscopy, sonography, optical coherence tomography, and confocal microscopy are applied to document solitary skin lesions (8). Most of these modalities, currently predominantly applied in dermato-oncology (9) require specialized training, expensive equipment and are time consuming for the patients and medical staff (10). However, in order to image the total body, complex and standardized realignments of the camera or the patient are required. Since skin areas are distorted if they are not photographed at a vertical angle, they can only be assessed to a limited extent in conventional photography. Semiautomatic and image-processing 3D photography systems offer a patient- and user-friendly handling of total body photography (11), on which changes such as cutaneous melanoma metastases can be traced precisely using assisting image processing tools (12). These applications enable objective automated nevi count in patients with numerous pigmented lesions (13). Standardized total body 3D photography images provide a solid prerequisite for machine-based learning algorithms in dermatology (14) as demonstrated in detection and analysis of cherry angioma (15). 3D photography and customized image processing tools are applied for various dermatologic conditions: Area of vitiligo lesions was calculated accurately by manual multipoint polygon region annotation utilizing an area measurement application (16). Decrease in volume of infantile hemangioma during propranolol treatment was calculated using a portable 3D photography unit and software provided by the manufacturer (17). Wound characteristics such as area, perimeter, and volume were reliably determined by a prototype 3D-wound assessment monitor camera and for this purpose applied software (18). Facial asymmetry caused by morphea could be more properly rated by 3D stereophotogrammetry compared to 2D photography (19). Assessment of successful labial augmentation by filler injection was demonstrated using a 3D imaging system and a facial measurement and analysis tool (20). Thus, 3D images have so far been analyzed mainly by means of the software provided by the manufacturer of the camera systems. In the future, these high-resolution, standardized images, together with rapidly advancing machine learning in dermatology (21, 22), may offer great possibilities in diagnostics and management of skin diseases.

In the current work, we identified patients with ITM and melanoma of the lower extremities. To demonstrate the *in vivo* spread of tumor cells resulting in ITM along defined lymphatic pathways, standardized templates were created with annotated primary melanomas, ITM, and associated lymphatic pathways in a subset of 46 patients with available conventional and 3D photographic images.

Materials and methods

Patients

This monocentric, retrospective study analyzed 382 patients (female 263, male 119) with cutaneous melanoma of the lower extremity. The study was conducted in compliance with Good Clinical Practice (GCP) rules and the Declaration of Helsinki. Ethical review and approval were waived for this study due to its retrospective character and the analysis of standard patient data

Abbreviations: 3D, three-dimensional; ITM, in-transit metastasis.

raised in the context of regular treatment visits. Patients signed an informed consent form for treatment at our center and for the photo documentation in the context of regular treatment. All patients underwent standard treatment and follow-up at the Department of Dermatology of the Uniklinikum Erlangen, Germany, between October 2000 and July 2020. We identified patients in our institutional database followed by individual file review from the electronic patient records in the clinical documentation system Soarian® (Cerner, Health Services, Berlin, Germany). A dermatologist diagnosed ITM during clinical skin examination either at the time of primary melanoma diagnosis or during regular oncologic follow-up. Data were obtained for each patient, including gender, age at diagnosis of primary melanoma, histologic subtype (superficial spreading melanoma, nodular melanoma, acral lentiginous melanoma, melanoma not otherwise specified, or melanoma with unknown primary), mean Breslow tumor thickness (mm), ulceration (present, absent, or unknown), and localization of primary melanoma (foot, lower leg, or thigh). Additionally, we analyzed the number of detectable ITM (1–5, 6–10, 11–20, more than 20 or unknown), mean time between primary diagnosis of melanoma and first ITM (in months), and availability of clinical images (no images, conventional photography, or 3D photography).

Image acquisition

Conventional photography

Images of patients were generated during follow-up at the Department of Dermatology, Uniklinikum Erlangen, Germany, by digital 2D single-lens reflex cameras (Canon EOS-ID Mark III or Canon EOS-ID Mark IV, Canon Germany GmbH, Krefeld). In the majority of the patients, primary melanoma as well as ITM had already been resected. Therefore, the location of prior melanoma lesions on clinical images by residual scars were identified and cross-referenced with the patients' clinical file.

3D total body photography

Patients were imaged by a VECTRA 360WB medical photography platform system (VECTRA 360WB, Canfield Scientific, Parsippany, NJ, USA) available at our center since 2019 consisting of two concentrically orientated frameworks with a total of 92 high-resolution digital cameras that captured 92 standardized polarized images of the patient simultaneously. During image acquisition, undressed patients stood in a defined pose at a standardized position inside the imaging unit. The integrated Dermagraphix software (VECTRA-Software VAM Version 2.7.6, Canfield Scientific, Parsippany, NJ, USA) subsequently processed single images into a 3D body avatar, which covered up to 90% of the patient's body surface (11). Thus, a millimeter precise anatomical mapping of present lesions and scars was generated for each patient. The distance between primary melanoma and ITM was calculated *via* the skin surface distance-measuring tool of the Dermagraphix program.

Generation of a reference template of the leg

As a first step, a reference template of the leg was created in order to compare ITM spreading pathways of the lower extremity in our patients. Contours from defined angles (lateral, medial, ventral, and dorsal) of the reference leg were delineated from an original 3D image using GIMP (GNU image manipulation program, version 2.10.20). Additionally, we integrated bone benchmarks and segmented colored lymphatic drainage areas as described previously (7): posterolateral (red), posteromedial (yellow), anterolateral (green), and anteromedial (blue—including the toes).

Identification of melanoma lesions and transfer onto the leg template

Evaluable melanoma lesions or scars of primary melanoma and ITM were identified in 46 patients with melanoma on the lower leg or foot and cross-referenced with clinical data, previous photographic images, histologic results, and operation reports. In addition, we contacted patients in order to pinpoint the localization on conventional or 3D images. In annotated and standardized 3D images, these lesions were extracted by an affine transformation scheme consisting of 6 degrees of freedom (x, y, z, 3x rotation) and transformed back into our two-dimensional reference templates. In order to compensate individual anatomical difference between patients, images were standardized with fixed points of interest using bone benchmarks such as the patella, medial as well as lateral ankle, and toes *via* Paint-3D (Microsoft Corporation, Version 6.2004.20027.0). Conventional photographic images of melanoma lesions and scars on the leg of patients with ITM were retrieved from our photographic archive. We annotated melanoma lesions accordingly and transferred these onto the four reference templates using the software program Paint-3D (Paint-3D, Microsoft Cooperation, 6.2004.20027.0). For patients with melanoma of the right leg, annotated images were mirrored, so that a left leg was always depicted in the following analysis.

Statistical analysis

Our objective was to evaluate conventional or three-dimensional photography as a tool to analyze in-transit metastasis pattern of melanoma of the lower extremity. In addition, we assessed risk factors for the development of in-transit metastases in cutaneous melanoma. Specifically, data were analyzed using SPSS (SPSS, Version 24.0, IBM Deutschland GmbH, Ehingen). Clinical characteristics of patients with melanoma of the lower extremity with (n = 94) or without ITM (n = 288) were compared in order to determine specific risk factors to develop ITM. The chi-square test was applied for mutually exclusive categorical variables (i.e., gender of the patient, histological subtype, ulceration, and localization of the primary melanoma). Continuous variables (i.e., age of patient, Breslow tumor thickness, and the interval between primary melanoma and the occurrence of the first ITM) were analyzed using the Mann–Whitney U test between two independent patient groups (patients with melanoma on the leg without ITM versus patients with melanoma of the lower leg with ITM). Multivariate logistic regression analysis of categorical as well as continuous variables was applied to factors with a significance in the univariate analysis to assess the interaction of potentially predictive factors for the development of ITM of the lower extremity. In order to analyze differences between fully (n = 25), partially (n = 8), or non-matched (n = 15) metastatic patterns of ITM between the lower leg (n = 31) and the foot (n = 15) we applied the Mann–Whitney U test

of ordinally scaled variables in the two independent sample groups (melanoma on the leg versus melanoma on the foot). In all tests, a p-value < 0.05 was considered significant.

Results

Clinical risk factors of all patients with in-transit metastases on the lower extremity

Demographic and clinical characteristics were compared between 288 patients with melanoma on the lower extremity without ITM and 94 patients with melanoma on the lower extremity with ITM. Patients with ITM were significantly older and the primary melanoma was significantly more often a nodular or acral lentiginous subtype, had a greater tumor thickness, showed more commonly ulceration, and was located more distally compared to patients without ITM ($p < 0.001$) (Table 1). In a multivariate logistic regression analysis (Table 2) tumor thickness, ulceration, and nodular melanoma remained risk factors for development of ITM. Independent of the presence of ITM, in our cohort melanoma on the lower extremity was more common in women. In the 94 patients, the number of ITM ranged from a single lesion to more than 20 lesions. The time between diagnosis of primary melanoma and of ITM ranged from simultaneous detection to more than 20 years (Table 1).

TABLE 1 General patient characteristics.

		N	Patients without ITM *n* = 288	Patients with ITM *n* = 94	*P*-value
Gender	Male	119	86 (30%)	33 (35%)	0.340
	Female	263	202 (70%)	61 (65%)	
	Male-to-female ratio		1:2.4	1:1.9	
Age (years)	Mean		53	62	<0.001
	Median		53	65	
	Range		16–97	28–96	
Histologic subtype	SSM	226	198 (69%)	28 (30%)	<0.001
	NM	62	38 (13%)	24 (26%)	
	ALM	43	25 (9%)	18 (18%)	
	NOS	35	27 (22%)	21 (22%)	
	MUP	3	–	3 (3%)	
Tumor thickness (mm)	Mean		1.4	3.5	<0.001
	Median		0.9	1.9	
	Range		0.1–35.0	0.2–15.0	
	Unknown		–	8 (8%)	
Ulceration*	Present	81	44 (15%)	37 (46%)	<0.001
	Absent	288	244 (85%)	44 (54%)	
Location of melanoma**	Foot	75	49 (17%)	26 (28%)	<0.001
	Lower leg	159	112 (39%)	47 (52%)	
	Thigh	145	127 (44%)	18 (20%)	
Number of ITM	1–5			34 (36%)	
	6–10			18 (19%)	
	11–20			14 (15%)	
	>20			15 (16%)	
	Unknown			13 (14%)	
ITM localization**	Only proximal of melanoma			46 (80%)	
	Distal and proximal of melanoma			9 (20%)	
Time between melanoma and first ITM [months]	Mean			34	
	Median			19	
	Range			0–244	
Images (including MUP)	3D photography			29 (31%)	
	Conventional photography			32 (34%)	
	No evaluable images available			33 (35%)	

ITM, in-transit metastasis; SSM, superficial spreading melanoma; NM, nodular melanoma; ALM, acral lentiginous melanoma; NOS, not otherwise specified; MUP, melanoma of unknown primary; 3D, three-dimensional.

*Ulceration status was unknown ($n = 10$) or a MUP was present ($n = 3$).

**MUP ($n = 3$). Characteristics of patients with melanoma of the lower extremity with in-transit metastases ($n = 94$) compared to patients without recurrence of melanoma ($n = 288$) with regard to primary melanoma and in-transit metastases.

TABLE 2 Multivariate logistic regression analysis of risk factors for in-transit metastases of melanoma of the lower extremity.

		Univariate analysis			Multivariate analysis		
		Hazard ratio	95% CI	*P*-value	Hazard ratio	95% CI	*P*-value
Age (years)	<55	1.0			1.0		
	≥55	2.5	1.4–4.3	<**0.001**	1.5	0.8–2.8	0.214
Histologic subtype*	SSM	1.0			1.0		
	NM	4.7	2.4–9.0	<**0.001**	2.6	1.2–5.5	**0.011**
	ALM	4.6	2.1–9.8	<**0.001**	2.7	0.8–9.2	0.121
	NOS	2.1	0.8–5.4	0.111	1.7	0.6–4.9	0.296
Tumor thickness (mm)*	<1.0	1.0			1.0		
	≥1.0	10.5	4.6–23.6	<0.001	5.7	2.3–13.9	<**0.001**
Ulceration*	Present	1.00			1.0		
	Absent	5.1	2.9–8.9	<**0.001**	2.1	1.1–4.0	**0.032**
Location of melanoma	Foot	1.0			1.0		
	Lower leg	0.8	0.4–1.4	0.374	1.8	0.6–5.0	0.272
	Thigh	0.3	0.1–0.6	<**0.001**	0.6	0.2–1.8	0.349

CI, confidence interval; SSM, superficial spreading melanoma; NM, nodular melanoma; ALM, acral lentiginous melanoma; NOS, not otherwise specified; MUP, melanoma of unknown primary.
*Missing values: histologic subtype $n = 17$, tumor thickness $n = 8$, ulceration $n = 13$. Multivariate logistic regression analysis of significant variables in the univariate analysis was performed in a full dataset of 359 patients with melanoma of the lower extremity.
Bold values represent the $p < 0.05$.

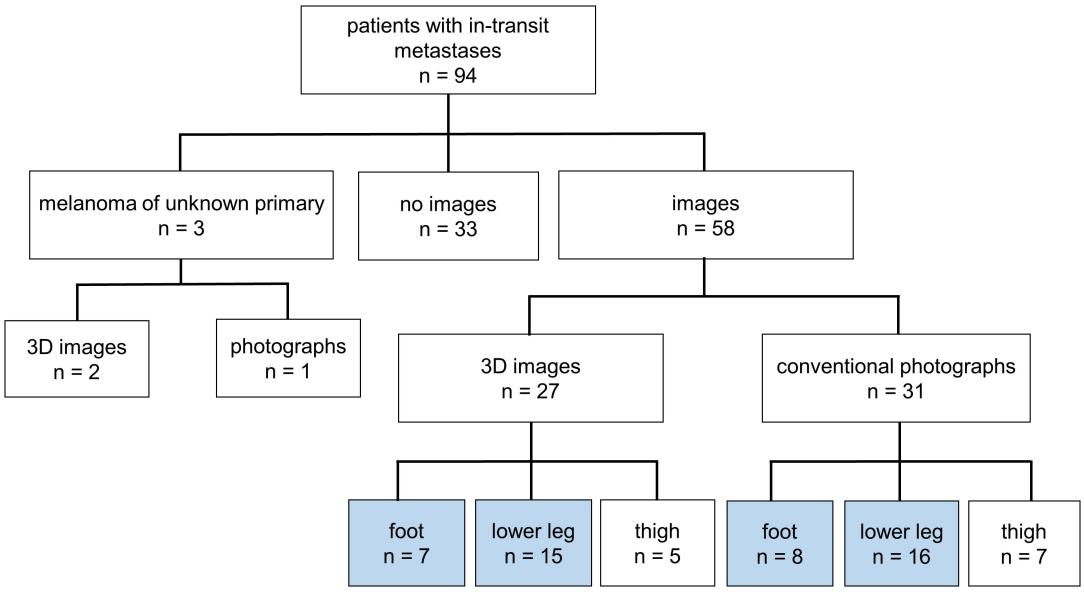

FIGURE 1
Overview of melanoma patients with in-transit metastases ($n = 94$) of the lower extremity. Definition of patients with available images taken by conventional or three-dimensional (3D) photography of the upper leg, lower leg, and foot.

Analysis of metastatic distribution pattern of in-transit metastases along lymphatic drainage pathways in 46 patients with evaluable conventional and three-dimensional photography

A total of 46 patients with melanoma of the lower leg ($n = 31$) or the foot ($n = 15$) and evaluable conventional ($n = 24$) or 3D-photography ($n = 22$) could be identified in our photo database (Figure 1, blue boxes) to correlate individual localization of ITM with previously reported anatomic lymphatic drainage pathways of the lower leg (7). Clinical data of these patients are summarized in Table 3. The anatomical distribution of all primary melanomas on the lower extremity and foot is shown in Figure 2A. We detected a strong correlation to known lymphatic vessels (full match) between primary melanoma of the lower leg ($n = 31$) and corresponding ITM (representative examples in Figure 2B) along the anteromedial (blue) or the anterolateral (green) lymphatic draining pathway in 22 of 31 patients (71%) (Table 4). A partial match was demonstrated in two patients (6%). In seven patients (23%), no association between the localization of primary melanoma and ITM could be

TABLE 3 Patients with melanoma of the lower leg and foot with analyzed in-transit metastases patterns.

		n	Conventional photography *n* = 24	3D-photography *n* = 22
Gender	Male	10	5 (21%)	5 (23%)
	Female	36	19 (79%)	17 (77%)
	Male-to-female ratio		1:3.8	1:3.4
Age (years)	Median		66	60
	Mean		70	66
	Range		28–87	29–87
Histologic subtype	SSM	12	7 (29%)	5 (23%)
	NM	9	6 (25%)	3 (14%)
	ALM	11	5 (21%)	6 (27%)
	NOS	14	6 (25%)	8 (36%)
Tumor thickness (mm)*	Median		3.5	3.3
	Mean		3.6	3.0
	Range		0.2–7.3	0.3–7.3
	Unknown		1 (4%)	2 (9%)
Ulceration*	Present	21	15 (79%)	6 (30%)
	Absent	18	4 (21%)	14 (70%)
Location of melanoma	Foot	15	8 (33%)	7 (32%)
	Lower leg	31	16 (67%)	15 (68%)
Number of ITM	1–5	13	4 (17%)	8 (36%)
	6–10	12	6 (25%)	7 (32%)
	11–20	11	7 (29%)	4 (18%)
	>20	10	7 (29%)	3 (14%)
Time between melanoma and first ITM (months)	Median		8	31
	Mean		22	53
	Range		0–120	0–244

ITM, in-transit metastasis; SSM, superficial spreading melanoma; NM, nodular melanoma; ALM, acral lentiginous melanoma; LMM, lentigo maligna melanoma; NOS, not otherwise specified; 3D, three-dimensional.
*Ulceration status was unknown ($n = 7$). Patient characteristics of 46 patients with primary melanoma of the lower extremity and the foot with in-transit metastases were analyzed by conventional or 3D photography.

detected. In melanoma of the foot ($n = 15$), a full and partial match between primary melanoma and ITM along the lymphatic pathways was present in only three patients (20%) and six patients (40%), respectively (representative examples in **Figure 2C** and **Table 4**). No congruence was detected in six patients (40%).

Absolute distance between primary melanoma and ITM measured *via* three-dimensional photography

Using 3D photography, the distance between primary melanoma and ITM along the skin surface could be measured in 27 patients (**Figure 3A**). Anatomically, the distance between primary melanoma and draining lymph nodes in the groin increases from the foot compared to the lower leg. Nevertheless, the mean, median, and range of distance between primary melanoma on the foot (27.8, 28.8, 1.8–67.4 cm) or lower leg (32.5, 30.9, and 1.6–71.2 cm) and corresponding ITM showed no significant difference in our cohort (**Figure 3B**).

Discussion

In-transit metastases develop along the way between the primary melanoma and the draining nodal basin and are a poor prognostic sign (6). Currently, the etiology of ITM is not fully understood. In the present study, conventional and 3D photography were used to chart and analyze the metastatic distribution of ITM of primary cutaneous melanoma of the lower extremity for the first time with regard to anatomically determined lymphatic drainage pathways (7) in a subset of 46 patients.

In general, about 4 to 10% of melanoma patients develop ITM (6, 23). The high rate of ITM (33%) in our clinical patient collective of 382 patients might be explained by the fact that it was limited to melanoma of the lower extremity, where ITM more often occur compared to other body sites (6). Additionally, patients with advanced or metastatic melanoma are more likely referred to a university skin cancer center, resulting in a high number of patients with ITM in our analysis.

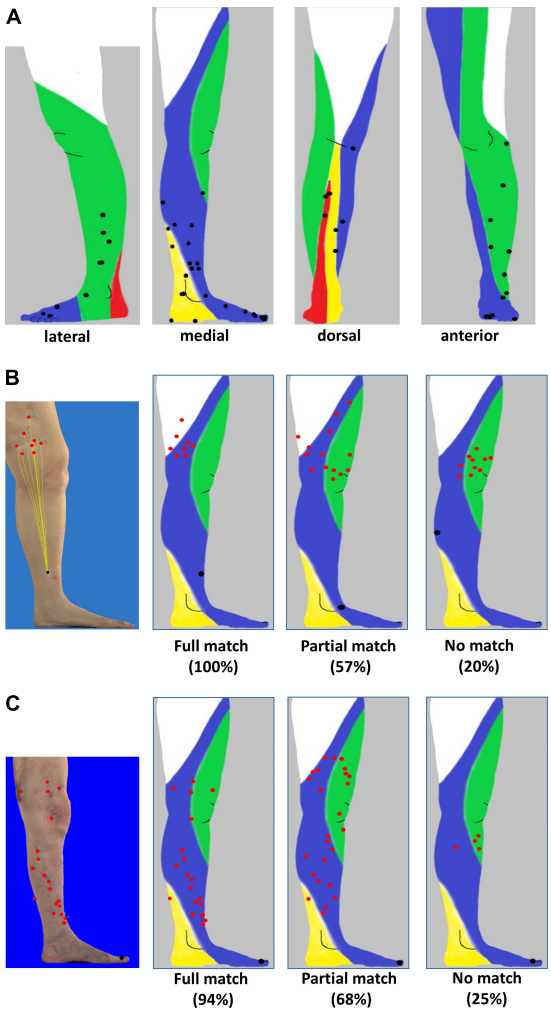

FIGURE 2
Distribution of primary melanoma and in-transit metastases localized to the lower leg and foot. **(A)** Lateral, medial, anterior, and dorsal projection of primary melanoma (black) of 58 patients based on photographic images and mapping to distinct anatomic lymphatic drainages regions of leg: posteromedial (yellow), anteromedial (blue), anterolateral (green), and posterolateral (red). **(B)** Melanoma of the lower leg: three-dimensional (3D) image of a primary melanoma and corresponding in-transit metastases as well as the supposed lymphatic drainage (left image). Representative examples of individual patients with primary melanoma (black) on the lower leg with a full match of 8/8 (100%) of in-transit metastases (red) developing in the corresponding anteromedial lymphatic region (second image from the left) and metastases developing partially (8/14, 57%, second image from the right) or not predominantly within (2/10, 20%) the expected localization (right image). **(C)** Melanoma on the foot. Annotation of in-transit metastases (red) on a 3D photographic image (left image). Examples of representative individual patients with primary melanoma (black) and corresponding in-transit metastases (red) occurring fully, partially, or not (images second from the left, second from the right, and right) in the expected lymphatic drainage area.

TABLE 4 Classification of in-transit metastatic patterns defined by localization of primary melanoma.

	Foot (n = 15)	Lower leg (n = 31)	P-value
Full match	3 (20%)	22 (71%)	
Partial match	6 (40%)	2 (6%)	0.007
No match	6 (40%)	7 (23%)	

Depending on the occurrence of in-transit metastases in the corresponding anatomical area of the primary melanoma, metastatic patterns are classified as full match (≥90%), partial match (<90% and ≥50%), or no match (<50%). While in melanoma of the lower leg the majority of in-transit metastases develop in the corresponding lymphatic drainage areas, melanoma of the foot shows a different metastatic pattern.

Our clinical cohort of 94 patients with ITM complements reports that comprised 54 (24), 380 (25), and 505 patients (6) with satellite metastases and ITM. While in our study only patients with melanoma of the lower extremity were included, this subgroup makes 40–60% of the comparable collectives in the literature. In particular, the different biology and prognosis of acral lentiginous melanoma (26) represent a possible confounder. The median tumor thickness of 2.9 mm and ulceration status of 46% in our patient cohort were comparable with other studies reporting a median tumor thickness of 3 mm and the presence of ulceration in 28–39% of the patients (6, 24). Tumor subtypes and further localization on the thigh, lower leg, or foot could not be compared because they were not stated separately for the lower extremity (6) or were not reported at all (24, 25). With regard to patient characteristics, the male-to-female ratio ranged from 1:2 in our study to 2:1 in the literature (6). This different distribution may be influenced by differences in the country-specific risk of sun exposure and behavior between Europe and Australia (27). The median age of patients was 65–75 years and confirms that ITM occur at an older age, but could not be exactly compared due to different timing at data collection (primary melanoma diagnosis or start of systemic therapy). In our study, the median interval until occurrence of ITM was 19 months, which is in line with 17.9 months stated in the literature (6). The number of ITM per patient has not been reported in the literature. The gender distribution in our patients with melanoma on the lower extremity was independent of the occurrence of ITM. Our data confirm negative prognostic factors in melanoma (1, 28) in patients with ITM compared to patients without recurrence such as tumor thickness, ulceration status, and nodular melanoma.

In a subset of 46 patients with evaluable conventional and 3D photography, the localization of melanoma lesions was systematically correlated to anatomically determined lymphatic drainage pathways (7). Our results show that the localization of primary melanoma on the lower leg indicates areas at risk which should be examined more closely during follow-up. In contrast, a full match between ITM and lymphatic drainage was present in only 20% of the patients with melanoma of the foot. This discrepancy may be caused by altered lymphatic drainage pathways due to surgery of the toes and sole of the foot. The fact that 9 of our 46 analyzed patients developed ITM distally of the primary melanoma indicates a significant surgical alteration of the lymphatic vessels including the draining nodal basin by prior sentinel node biopsy or lymphadenectomy.

Interestingly, one patient with amputation of the three toes due to melanoma developed ITM along both the anteromedial and the anterolateral lymphatic bundles. This may further support postoperative lymphatic alteration but could also indicate a yet unstudied differential lymphatic drainage of the toes and the plantar region. It is of interest that in order to identify anatomic lymphatic pathways, contrast injections were exclusively applied to the outer and inner edges of the foot as well as the interdigital spaces in a previous study (7).

As discussed by Shinaoka et al. (7), the results of the anatomic/radiologic study may not be fully applicable to the *in vivo* situation (such as the development of ITM analyzed in this work) as the study was performed on cadavers with

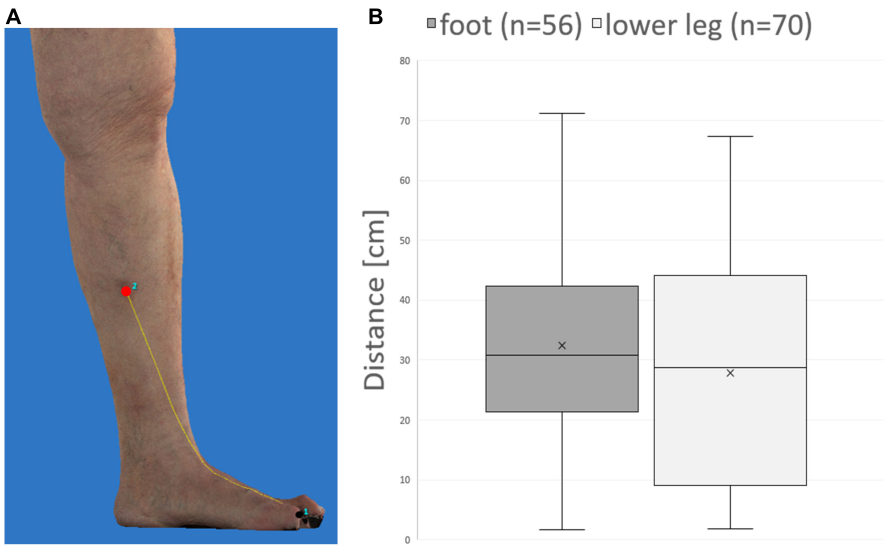

FIGURE 3
Distance measurement of primary melanoma and in-transit metastases on three-dimensional (3D) photography. **(A)** Example demonstrating measurement of the distance (yellow line) along the skin surface between primary melanoma (black) and an in-transit metastasis (red). **(B)** No significant difference between melanoma of the foot compared to the lower leg is detectable concerning mean, median, and range of distances between melanoma and corresponding in-transit metastases.

contrast injection into the foot followed by manual lymphatic drainage. In contrast, *in vivo* lymphatic fluid is transported by means of metabolically active muscle contraction in conduit and transport vessels.

To our knowledge, this is the first report to apply 3D photography to determine precise distances along the lymphatic pathways that melanoma cells must have traveled between primary melanoma and corresponding ITM. Since the distances between two lesions were calculated on a 3D leg model on the skin surface and the angles of the joints were taken into account, this almost exactly corresponds to the lymphatic pathways running in the upper corium. Although lymphatic pathways from the foot to the draining inguinal lymph node are anatomically longer than those from the lower leg, the distances between primary melanoma and associated ITM did not differ significantly in our cohort. Whether this is a biological, mechanical, or lymphogenic characteristic of melanoma of the foot, in which ITM develops with preferentially on the lower leg and thigh, cannot be answered by this study due to the insufficient number of patients examined by 3D photography (n = 22). In order to assess the significance for diagnostics and therapy, further investigations of ITM should also be performed including the trunk, the heck, and head.

Our study demonstrates for the first time the biological relevance of anatomically described lymphatic drainage pathways using ITM in melanoma of the lower extremity as a model. However, the limitations of our work must be considered before this knowledge can be applied for example to assess risk areas for ITM: (i) In our clinical collective we could only identify 94 patients with ITM of the leg in our center within a 20-year time frame, (ii) the analysis of ITM along lymphatic vessels was limited to melanoma of the lower leg and foot as only in the distal lower extremity lymphatic drainage patterns have been systematically investigated, (iii) evaluable photo documentation to analyze the lymphatic drainage patterns of melanoma of the lower leg and foot was only available in 46 patients, (iv) analysis of conventional, non-standardized photographs proved to be particularly difficult and possibly error-prone compared to 3D total body photography (in use in our department since 2019), (v) the localization of melanoma lesions was determined almost exclusively based on the presence of scars and comparison of the patients' medical records. Especially for primary melanomas excised with a safety margin (sometimes toe amputation), the localization of melanoma lesions had to be extrapolated in the middle of the scar, (vi) changes in the physiologic lymphatic drainage pathways due to surgery around primary melanomas, ITM, and lymphadenectomy may have occurred in all patients, and (vii) due to methodological reasons, the anatomical study did not examine toe and plantar drainage, which remain not well defined. Therefore, the poor correlation observed between ITM and primary melanoma at the foot in our cohort suggests a critical re-evaluation with regard to lymphatic drainage pathways of the toes and the plantar region.

In summary, our results demonstrate the *in vivo* relevance of anatomic lymphatic pathways in ITM formation in 46 evaluable patients with melanoma of the leg. Together with clinical risk factors that we have confirmed, this knowledge may be used for a better risk assessment in the follow-up of melanoma patients and to develop a model for ITM in melanoma of the leg in the future.

Data availability statement

The raw data supporting the conclusions of this article will be made available by the authors, without undue reservation.

Author contributions

ME and KM designed the study, performed data acquisition and analysis, and wrote the manuscript. ME, KM,

and SM interpreted the data. CB, CV, MH, LH, EK, RK, and BS-T collected patient data and clinical information. CB, CV, MH, LH, EK, RK, SM, BS-T, VS, TS, and AW critically revised the manuscript. All authors contributed to the article and approved the submitted version.

Acknowledgments

This study was performed as part of a medical doctoral thesis by KM, and results were presented virtually at the annual German Skin Cancer Conference of the Dermatologic Cooperative Oncology Group (DeCOG) in September 2021. We thank Christine Luff, Dominik Pappa, and Stefan Schnetz for their technical assistance.

Conflict of interest

The authors declare that the research was conducted in the absence of any commercial or financial relationships that could be construed as a potential conflict of interest.

Publisher's note

References

1. Gershenwald J, Scolyer R, Hess K, Sondak V, Long G, Ross M, et al. Melanoma staging: evidence-based changes in the American joint committee on cancer eighth edition cancer staging manual. *CA Cancer J Clin.* (2017) 67:472–92. doi: 10.3322/caac.21409

2. Luke J, Rutkowski P, Queirolo P, Del Vecchio M, Mackiewicz J, Chiarion-Sileni V, et al. Pembrolizumab versus placebo as adjuvant therapy in completely resected stage IIB or IIC melanoma (KEYNOTE-716): a randomised, double-blind, phase 3 trial. *Lancet.* (2022) 399:1718–29.

3. Wolchok J, Chiarion-Sileni V, Gonzalez R, Grob J, Rutkowski P, Lao C, et al. Long-term outcomes with nivolumab plus ipilimumab or nivolumab alone versus ipilimumab in patients with advanced melanoma. *J Clin Oncol.* (2022) 40:127–37.

4. Morton D, Thompson J, Cochran A, Mozzillo N, Nieweg O, Roses D, et al. Final trial report of sentinel-node biopsy versus nodal observation in melanoma. *N Engl J Med.* (2014) 370:599–609. doi: 10.1056/NEJMoa1310460

5. Kahler K, Egberts F, Gutzmer R. Palliative treatment of skin metastases in dermato-oncology. *J Dtsch Dermatol Ges.* (2013) 11:1041–5;quiz6.

6. Read R, Haydu L, Saw R, Quinn M, Shannon K, Spillane A, et al. In-transit melanoma metastases: incidence, prognosis, and the role of lymphadenectomy. *Ann Surg Oncol.* (2015) 22:475–81.

7. Shinaoka A, Koshimune S, Suami H, Yamada K, Kumagishi K, Boyages J, et al. Lower-limb lymphatic drainage pathways and lymph nodes: a CT lymphangiography cadaver study. *Radiology.* (2020) 294:223–9. doi: 10.1148/radiol.2019191169

8. Schneider S, Kohli I, Hamzavi I, Council M, Rossi A, Ozog D. Emerging imaging technologies in dermatology: part II: applications and limitations. *J Am Acad Dermatol.* (2019) 80:1121–31. doi: 10.1016/j.jaad.2018.11.043

9. Soglia S, Perez-Anker J, Lobos Guede N, Giavedoni P, Puig S, Malvehy J. Diagnostics using non-invasive technologies in dermatological oncology. *Cancers (Basel).* (2022) 14:5886.

10. Hibler B, Qi Q, Rossi A. Current state of imaging in dermatology. *Semin Cutan Med Surg.* (2016) 35:2–8.

11. Rayner J, Laino A, Nufer K, Adams L, Raphael A, Menzies S, et al. Clinical perspective of 3D total body photography for early detection and screening of melanoma. *Front Med (Lausanne).* (2018) 5:152. doi: 10.3389/fmed.2018.00152

12. Erdmann M, Heinzerling L, Schuler G, Berking C, Schliep S. Monitoring skin metastases during immuno- and targeted therapy using total-body 3D photography. *J Eur Acad Dermatol Venereol.* (2021) 35:e61–3. doi: 10.1111/jdv.16806

13. Betz-Stablein B, D'Alessandro B, Koh U, Plasmeijer E, Janda M, Menzies S, et al. Reproducible naevus counts using 3D total body photography and convolutional neural networks. *Dermatology.* (2022) 238:4–11. doi: 10.1159/000517218

14. Hogarty D, Su J, Phan K, Attia M, Hossny M, Nahavandi S, et al. Artificial intelligence in dermatology-where we are and the way to the future: a review. *Am J Clin Dermatol.* (2020) 21:41–7. doi: 10.1007/s40257-019-00462-6

15. Betz-Stablein B, Koh U, Edwards H, McInerney-Leo A, Janda M, Soyer H. Anatomic distribution of cherry angiomas in the general population. *Dermatology.* (2022) 238:18–26. doi: 10.1159/000517172

16. Kohli I, Isedeh P, Al-Jamal M, DaSilva D, Batson A, Canfield D, et al. Three-dimensional imaging of vitiligo. *Exp Dermatol.* (2015) 24:879–80. doi: 10.1111/exd.12791

17. Robertson S, Kimble R, Storey K, Gee Kee E, Stockton K. 3D photography is a reliable method of measuring infantile haemangioma volume over time. *J Pediatr Surg.* (2016) 51:1552–6. doi: 10.1016/j.jpedsurg.2016.04.013

18. Jorgensen L, Skov-Jeppesen S, Halekoh U, Rasmussen B, Sorensen J, Jemec G, et al. Validation of three-dimensional wound measurements using a novel 3D-WAM camera. *Wound Repair Regen.* (2018) 26:456–62. doi: 10.1111/wrr.12664

19. Abbas L, Joseph A, Day J, Cole N, Hallac R, Derderian C, et al. Measuring asymmetry in facial morphea via 3-dimensional stereophotogrammetry. *J Am Acad Dermatol.* (2023) 88:101–8. doi: 10.1016/j.jaad.2022.05.029

20. Nikolis A, Bertucci V, Solish N, Lane V, Nogueira A. An objective, quantitative assessment of flexible hyaluronic acid fillers in lip and perioral enhancement. *Dermatol Surg.* (2021) 47:e168–73.

21. Young A, Xiong M, Pfau J, Keiser M, Wei M. Artificial intelligence in dermatology: a primer. *J Invest Dermatol.* (2020) 140:1504–12. doi: 10.1016/j.jid.2020.02.026

22. Lee E, Maloney N, Cheng K, Bach D. Machine learning for precision dermatology: advances, opportunities, and outlook. *J Am Acad Dermatol.* (2021) 84:1458–9. doi: 10.1016/j.jaad.2020.06.1019

23. Testori A, Ribero S, Bataille V. Diagnosis and treatment of in-transit melanoma metastases. *Eur J Surg Oncol.* (2017) 43:544–60.

24. Nan Tie E, Lai-Kwon J, Rtshiladze M, Na L, Bozzi J, Read T, et al. Efficacy of immune checkpoint inhibitors for in-transit melanoma. *J Immunother Cancer.* (2020) 8:e000440. doi: 10.1136/jitc-2019-000440

25. Weide B, Faller C, Buttner P, Pflugfelder A, Leiter U, Eigentler T, et al. Prognostic factors of melanoma patients with satellite or in-transit metastasis at the time of stage III diagnosis. *PLoS One.* (2013) 8:e63137. doi: 10.1371/journal.pone.0063137

26. Bradford P, Goldstein A, McMaster M, Tucker M. Acral lentiginous melanoma: incidence and survival patterns in the United States, 1986-2005. *Arch Dermatol.* (2009) 145:427–34. doi: 10.1001/archdermatol.2008.609

27. Whiteman D, Bray C, Siskind V, Hole D, MacKie R, Green A. A comparison of the anatomic distribution of cutaneous melanoma in two populations with different levels of sunlight: the west of Scotland and Queensland, Australia 1982-2001. *Cancer Causes Control.* (2007) 18:485–91. doi: 10.1007/s10552-007-0123-1

28. Erdmann M, Sigler D, Uslu U, Gohl J, Grutzmann R, Schuler G, et al. Risk factors for regional and systemic metastases in patients with sentinel lymph node-negative melanoma. *Anticancer Res.* (2018) 38:6571–7.

frontiers | Frontiers in Medicine

TYPE Original Research
PUBLISHED 21 February 2023
DOI 10.3389/fmed.2023.1097999

OPEN ACCESS

EDITED BY
Elisa Zavattaro,
University of Eastern Piedmont, Italy

REVIEWED BY
Maryam Nasimi,
Tehran University of Medical Sciences, Iran
Yuping Ran,
Sichuan University, China

*CORRESPONDENCE
Gui-li Fu
✉ fuguili@zgwhfe.com
Yuan-quan Zheng
✉ zhengyuanquan@zgwhfe.com

†These authors have contributed equally to this work

SPECIALTY SECTION
This article was submitted to Dermatology, a section of the journal Frontiers in Medicine

RECEIVED 14 November 2022
ACCEPTED 07 February 2023
PUBLISHED 21 February 2023

CITATION
Nie Y-l, Yi H, Xie X-y, Fu G-l and Zheng Y-q (2023) Dermoscopic features of children scabies.
Front. Med. 10:1097999.
doi: 10.3389/fmed.2023.1097999

Dermoscopic features of children scabies

Ying-li Nie†, Hong Yi†, Xiao-yan Xie, Gui-li Fu* and Yuan-quan Zheng*

Department of Dermatology, Wuhan Children's Hospital (Wuhan Maternal and Child Healthcare Hospital), Tongji Medical College, Huazhong University of Science and Technology, Wuhan, China

Scabies is a common skin disorder, caused by the ectoparasite *Sarcoptes scabiei*. The scabies mites burrow is highly diagnostic but illegible by the naked eye, because it is tiny and may completely be obscured by scratch and crust. The classic technique is opening the end of an intact mite burrow with a sharp instrument and inspecting its contents in the light microscope under loupe vision. Dermatoscope is a new method to diagnose scabies, with the advantages of non-invasive and more sensitive. This study verified the characteristic manifestations of scabies under dermoscopy. Under the closer examination of the curvilinear scaly burrow, the scabies mite itself may be seen as a dark equilateral triangular structure, which is often referred to as a "jet with contrail." Besides, this study found that the positive detection rate of microscopic characteristic manifestations under the dermoscopy ordered by the external genitals, the finger seams and the trunk, which were statistically different (P-value < 0.05). Of note, this is the first study to explore the regional distribution of the characteristic dermoscopic manifestations of scabies. We are the first to propose to focus on examining the external genitalia and finger seams with dermoscopy.

KEYWORDS

scabies, mite, dermatoscope, children, manifestations

Introduction

Scabies is a parasitic infestation of the skin caused by the mite *Sarcoptes scabiei*. Clinically, it is characterized by erythematous papules or vesicles. The typical distribution of skin lesions includes finger seams, the wrists, armpits, groins, buttocks, genitals and the breasts in women. In infants and young children, the palms, soles, and head are also commonly involved, which is rare in adults (1). Pruritus is the predominant hallmark of scabies regardless of age (2). Patients mainly complain the itchy rash worsening at night, which seriously disturbs sleep and affects the quality of life (3). Besides, the disease also causes high psychosocial and economic burden (4).

Burrows are formed as the adult female scabies mites excavate their way through the epidermis (5). The burrow is highly diagnostic. However, they are often unidentifiable by the naked eye, because scratch, crust and eczematization may completely obscure primary lesions (6). The only proof of the diagnosis of scabies is demonstration of scabies mite, its

eggs or feces pellets (7). There are a variety of methods to diagnose scabies, but no one is both convenient and reliable. Therefore, the diagnosis of scabies is currently challenging and often delayed.

Dermatoscope is one of the new methods to diagnose scabies (8). As we know, dermatoscope allows better visualization on skin lesions, with the advantages of non-invasive, real-time observation and more sensitive mode of evaluation. There are few studies on dermoscopy in scabies, let alone children scabies. The current literatures mainly consist of case reports (9). In this article, we aim to analyze the dermoscopic features of children scabies.

Materials and methods

Patients selection and data collection

We performed a retrospective analysis of children patients with clinical scabies or suspected scabies in department of dermatology, Wuhan Children's Hospital (Wuhan Maternal and Child Healthcare Hospital), from August 2020 to October 2022. All the included patients met the 2018 The International Alliance for the Control of Scabies (IACS) criteria for the diagnosis of scabies (10). The definition of the clinical scabies and suspected scabies was shown in **Table 1**. Those who had papular urticaria, atopic dermatitis, lichen planus, dermatitis herpetiformis, and infantile acropustulosis were excluded. The data of enrolled patients were collected by electronic medical records system, including demographic information, medical history, clinical symptoms and signs.

Dermoscopy

The CBS dermoscopy detection system was used to scan the clinically suspicious skin lesions of the patients, including the finger seams, armpits, trunk, buttocks and genitalia, etc. The 50× lens was used to move back and forth on all clinical prone sites one by one. All dermoscopic pictures were saved from the computer after examination.

The most arresting feature of scabies under dermoscopy was the burrow. Dermoscopy began with looking for the scabies burrow, which was the movement path of the scabies mite in the stratum corneum of the patients. The burrow entrance was usually where the scales was visible (the start of the sarcoptic curve), and the end of the burrow was usually where the blister was located (the end of the curve).

Under the closer examination of the curvilinear scaly burrow, the scabies mite itself was usually located at the end of the burrow a few millimeters in front of the small blister. The end of the burrow was wiped with an alcohol cotton swab. Through the cuticles, the mite itself was seen at the end of the burrow as a dark equilateral triangular structure, corresponding to the pigmented head and anterior legs of the scabies mite. The burrow and the dark triangular structure were often referred to as a "jet with contrail" (11). Because the scabies mite was white and difficult to find, the target of dermoscopic observation was mainly the burrow and dark triangular structure.

Statistical analysis

Continuous variables were displayed as means and standard deviation (SD). Categorical variables were expressed as frequency counts and percentages, and chi-square was used to evaluate the differences between groups. All statistics were analysed by using the SPSS 22.0 software, and P-value < 0.05 was selected as the threshold of statistical significance.

Results

Demographic features

We collected a total of 56 cases with clinical scabies and suspected scabies. All of them received dermoscopy examination. Among them, 34 patients were male, accounting for 60.7%, and 22 patients were female, accounting for 39.3%. The eldest patient was 16 years old and the youngest patient was an 8-month-old infant. Their mean (SD) age was 6.14 ± 4.07 years old.

The characteristic dermoscopic manifestations of scabies

In total, 50 patients presented the typical "jet with contrail" under dermoscopy. Those 50 cases were confirmed scabies. The burrow and dark triangular structure were shown on **Figure 1**. Even more, multiple burrows and dark triangular structure were seen in one dermoscopic image (**Figure 2**).

The regional distribution of the characteristic dermoscopic manifestations of scabies

Due to the small amounts, in this study, the neck, chest wall, abdomen, back, armpits and buttocks were all divided into the trunk. Only 6 patients could be found that the burrow and the dark triangular structure were on the trunk, versus 41 on the finger seams and 45 on the external genitals, relatively. The detection rates of characteristic dermoscopic manifestations of the finger seams and the external genitals were statistically significant compared with those of the trunk (all P-value < 0.05). The regional distribution of the characteristic dermoscopic manifestations of confirmed scabies was shown in **Table 2**.

The non-characteristic dermoscopic manifestations of scabies

The non-specific dermoscopic manifestations of scabies were mainly secondary skin lesions caused by pruritus and local eczema changes, such as erythema overlying scales, pustules, erosion, exudation, scratches, blood callus, pigmentation, and vascular changes. They were shown in **Figure 3**.

TABLE 1 Summary of the 2018 IACS criteria for the diagnosis of scabies.

A: Confirmed scabies	
At least one of:	A1: Mites, eggs or feces on light microscopy of skin samples A2: Mites, eggs or feces visualized on individual using high-powered imaging device A3: Mite visualized on individual using dermoscopy
B: Clinical scabies	
At least one of:	B1: Scabies burrows B2: Typical lesions affecting male genitalia B3: Typical lesions in a typical distribution and two history features
C: Suspected scabies	
One of:	C1: Typical lesions in a typical distribution and one history feature C2: Atypical lesions or atypical distribution and two history features
History features	
	H1: Itch H2: Close contact with an individual who has itch or typical lesions in a typical distribution

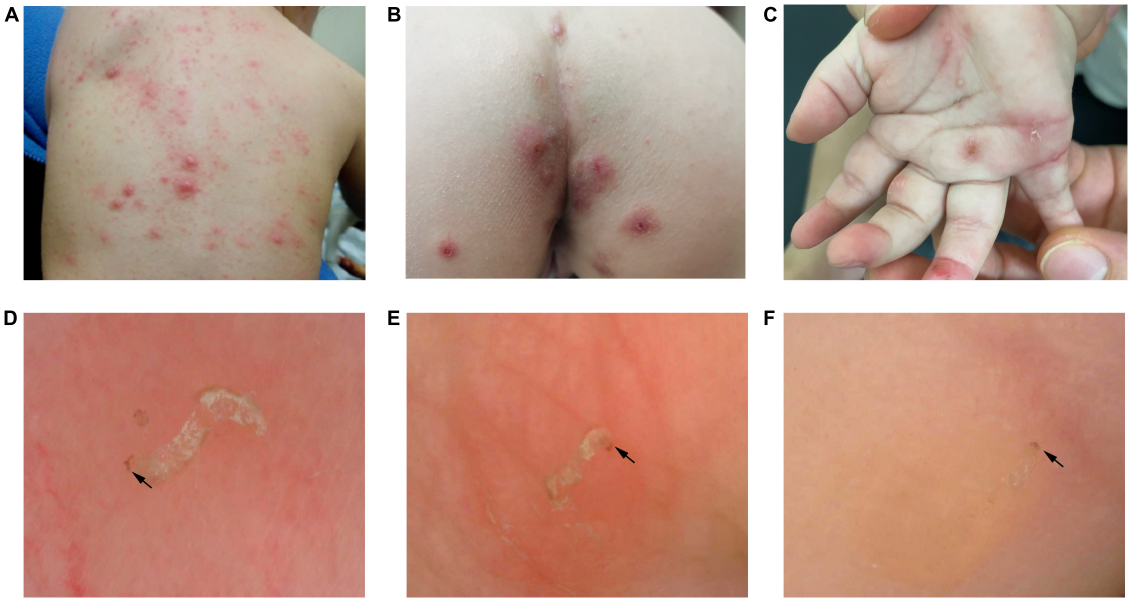

FIGURE 1
Panels **(A–C)** were clinical images. At the end of the curvilinear scaly burrow, the mite itself was seen as a dark triangular structure (black arrow) under dermoscope. Panel **(D)** was the dermoscopic image of trunk. Panel **(E)** was the dermoscopic image of external genital. Panel **(F)** was the dermoscopic image of finger seam.

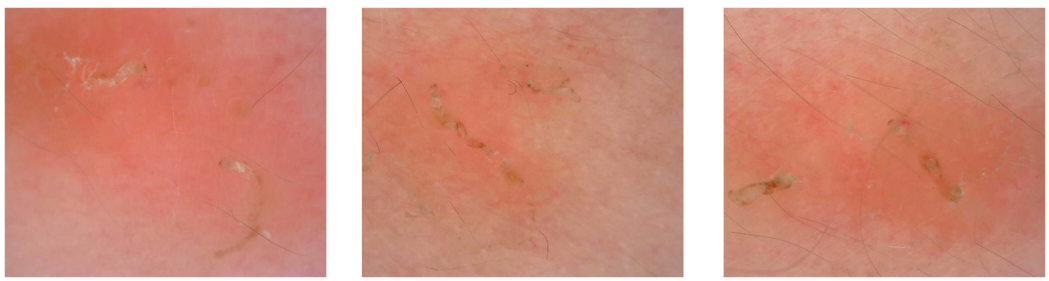

FIGURE 2
Multiple burrows were seen in one dermoscopic image.

TABLE 2 The regional distribution of the characteristic dermoscopic manifestations of 50 confirmed scabies patients.

Area	Burrow under dermatoscope		χ^2	*P*
	Positive (%)	Negative (%)		
Trunk	6 (12.0)	44 (88.0)		
Finger seams	41 (82.0)	9 (18.0)	49.177	<0.001*
External genitals	45 (90.0)	5 (10.0)	60.864	<0.001**

*Finger seams compared with trunk.
**External genitals compared with trunk.

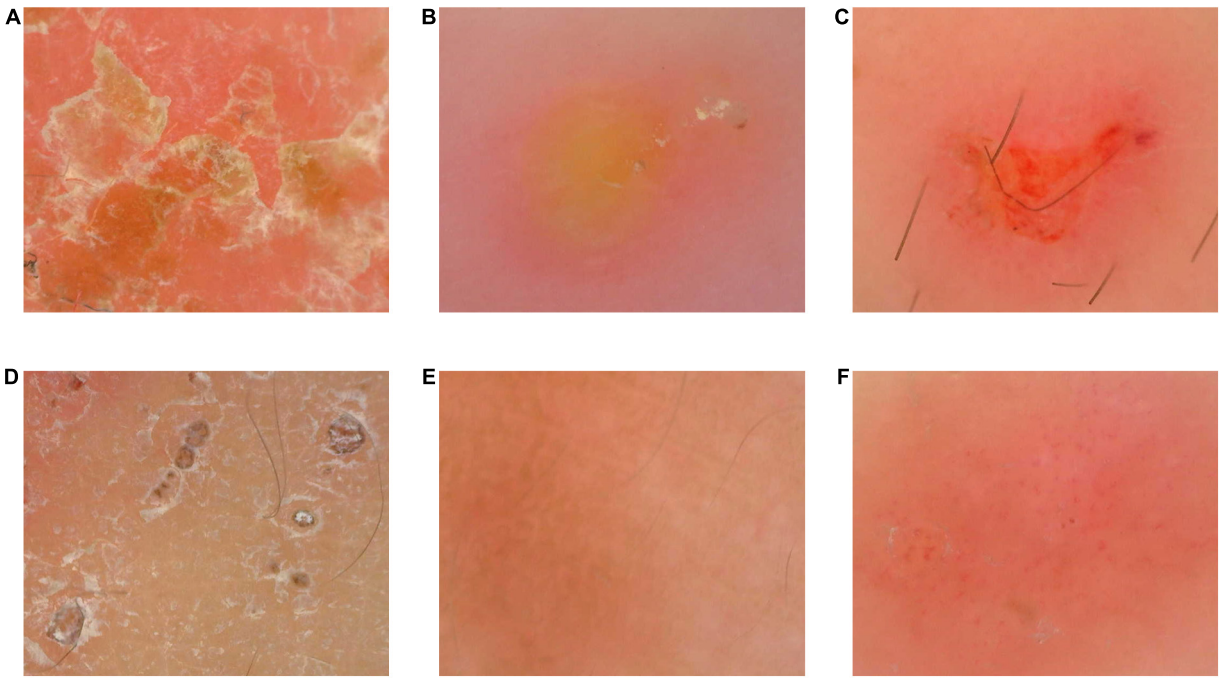

FIGURE 3
The non-specific dermoscopic manifestations of scabies. Panel **(A)** was erythema overlying scales. Panel **(B)** was pustule. The burrow and dark triangular structure were seen around the edge of pustule. Panel **(C)** was erosion and exudation. Panel **(D)** was scratches and blood callus. Panel **(E)** was pigmentation. Panel **(F)** was vascular changes. Punctate and globular vessels were focally distributed.

Discussion

Scabies can be both one of the easiest and one of the most difficult conditions to diagnose (6). The parasitological confirmation of the scabies mite forms the gold standard for diagnosis, including of the mite, its eggs or feces. The classic skin scrapings is by opening the end of an intact mite burrow with a sharp instrument and inspecting its contents in the light microscope under loupe vision. This test is poorly tolerated in children because of the pain and repeated tests from different sites may be needed (12). Adhesive tape test and burrow ink test (BIT) are painless and simple, but its sensitivity is low (13, 14). Reflectance confocal microscopy (RCM) and optical coherence tomography (OCT) are new non-invasive technique. They enable visualization of burrows, mite, larvae, eggs and fecal material (15, 16). The limitation of RCM and OCT is non-availability and expensive equipment. Histopathological examination can also allow visualization of burrows, female mite, eggs containing larvae, eggshells and fecal deposits (scyballa) (17). Nevertheless, skin biopsy is both time consuming and expensive.

Dermoscopy can be used to confirm the diagnosis of scabies in both adults and children, according to the IACS criteria (10). Nowadays, the "jet with contrail" was considered pathognomonic for scabies, regardless of the patient's age, the location of the lesion, type and duration of the infect ion (18). Even if only one skin lesion on the whole body presented this typical dermoscopic manifestation, it was sufficient to confirm the diagnosis of scabies.

In this study, 56 patients received dermoscopy examination and 50 patients were confirmed the diagnosis of scabies by the characteristic "jet with contrail." The sensitivity of dermatoscopic diagnosis of scabies was 89.3%, which was similar to what the literature has reported (19). There were six patients without characteristic dermoscopic features of the lesions throughout the body. The reason may be that erosion, scratches and blood callus covered and obscured primary lesions. Those six patients can be diagnosed with clinical scabies on account of the positive response to empiric treatment.

Because pruritus is so constant and violent in scabies, the scratching may catch viable mites, which can survive under the

nails and then colonize the skin starting from around the nail going proximally (20). Scabies mites are more readily to crawling in areas where the epidermis is thin and tender. This may be the reason why skin lesions tend to occur between the finger seams, the wrists, armpits, groins, buttocks, and genitals.

This study found that the positive detection rate of microscopic structures under the dermoscopy ordered by the external genitals, the finger seams and the trunk, which were statistically different (P-value < 0.05). Its high detection rate may stem from the fact that the epidermis thickness of finger seams and external genitals was thinner and the transmission of light was better. Therefore, skin can easily expose the scabies mite. In addition, genital area was more private with less scratching, resulting in less damagement of the primary skin lesions, so the burrows were more unbroken.

It suggests that when we use dermoscopy in clinical examination of patients suspected of scabies, we should focus on observing the skin lesions of external genitalia and finger seams, which increased the credibility of dermoscopy and avoid missed diagnosis. Of note, this is the first study to explore the regional distribution of the characteristic dermoscopic manifestations of scabies. We are the first to propose to focus on examining the external genitalia and finger seams with dermoscopy in the diagnosis of scabies, which has great guiding value for clinical practice.

This study revealed the characteristic manifestations of scabies under dermoscopy. It clearly showed the parasitic state of scabies, and had a more intuitive understanding of scabies. Dermoscopy can effectively decrease the misdiagnosis rate of clinical physicians. Besides, this study showed the non-characteristic manifestations under dermoscopy, which was neglected in the past studies. The significance of non-specific structures was to indicate the complicated infection and allergic status of different patients, and to indicate the skin barrier damage of different degrees in scabies patients (21).

This study has limitations due to its retrospective design. And the relatively small size of sample is another limitation of our study. We look forward to multi-center, large sample prospective studies to enhance the confidence of the results. Furthermore, the limitations of dermoscopy are that eggs or fecal material are not visible (8). It can be challenging in hair-bearing areas and awkward to perform in genital or other sensitive areas. Besides, the device needs to be carefully disinfected because mites can survive in the environment up to 72 h (22).

Data availability statement

The raw data supporting the conclusions of this article will be made available by the authors, without undue reservation.

Author contributions

Y-LN and HY: design, analysis, and interpretation of data, and drafting of the manuscript. X-YX: acquisition of data and statistical analysis. G-LF and Y-QZ: critical revision of the manuscript for important intellectual content, obtaining funding, and supervision. All authors read and approved the final manuscript.

Funding

This study was supported by the Scientific Research Project of Wuhan Municipal Health Commission (No. WX20C09).

Conflict of interest

The authors declare that the research was conducted in the absence of any commercial or financial relationships that could be construed as a potential conflict of interest.

Publisher's note

References

1. Heukelbach J, Wilcke T, Winter B, Feldmeier H. Epidemiology and morbidity of scabies and pediculosis capitis in resource-poor communities in Brazil. *Br J Dermatol.* (2005) 153:150–6. doi: 10.1111/j.1365-2133.2005.06591.x

2. Johnston G, Sladden M. Scabies: diagnosis and treatment. *BMJ.* (2005) 331:619–22. doi: 10.1136/bmj.331.7517.619

3. Arora P, Rudnicka L, Sar-Pomian M, Wollina U, Jafferany M, Lotti T, et al. Scabies: a comprehensive review and current perspectives. *Dermatol Ther.* (2020) 33:e13746. doi: 10.1111/dth.13746

4. Cox V, Fuller LC, Engelman D, Steer A, Hay RJ. Estimating the global burden of scabies: what else do we need? *Br J Dermatol.* (2021) 184:237–42.

5. Arlian LG, Morgan MS, Rider SD Jr. Sarcoptes scabiei: genomics to proteomics to biology. *Parasit Vectors.* (2016) 9:380. doi: 10.1186/s13071-016-1663-6

6. Karthikeyan K. Scabies in children. *Arch Dis Child Educ Pract Ed.* (2007) 92:e65–9. doi: 10.1136/adc.2005.073825

7. Sunderkötter C, Wohlrab J, Hamm H. Scabies: epidemiology, diagnosis, and treatment. *Dtsch Arztebl Int.* (2021) 118:695–704. doi: :10.3238/arztebl.m2021.0296

8. Engelman D, Yoshizumi J, Hay RJ, Osti M, Micali G, Norton S, et al. The 2020 International alliance for the control of scabies consensus criteria for the diagnosis of scabies. *Br J Dermatol.* (2020) 183:808–20. doi: 10.1111/bjd.18943

9. Danielsen, H. Scabies burrow under a dermatoscope. *Tidsskr Nor Laegeforen.* (2020) 15:140. doi: 10.4045/tidsskr.20.0792

10. Engelman D, Fuller LC, Steer AC. Consensus criteria for the diagnosis of scabies: a Delphi study of international experts. *PLoS Negl Trop Dis.* (2018) 12:e0006549. doi: 10.1371/journal.pntd.0006549

11. Fox G. Diagnosis of scabies by dermoscopy. *BMJ Case Rep.* (2009) 2009. doi: 10.1136/bcr.06.2008.0279

12. Micali G, Lacarrubba F, Verzì AE, Chosidow O, Schwartz RA. Scabies: advances in noninvasive diagnosis. *PLoS Negl Trop Dis.* (2016) 10:e0004691. doi: 10.1371/journal.pntd.0004691

13. Abdel-Latif AA, Elshahed AR, Salama OA, Elsaie ML. Comparing the diagnostic properties of skin scraping, adhesive tape, and dermoscopy in diagnosing scabies. *Acta Dermatovenerol Alp Pannonica Adriat.* (2018) 27:75–8.

14. Leung V, Miller M. Detection of scabies: a systematic review of diagnostic methods. *Can J Infect Dis Med Microbiol.* (2011) 22:143–6. doi: 10.1155/2011/698494

15. Lacarrubba F, Verzì AE, Micali G. Detailed analysis of in vivo reflectance confocal microscopy for *Sarcoptes scabiei* hominis. *Am J Med Sci.* (2015) 350:414. doi: 10.1097/maj.0000000000000336

16. Ruini C, Schuh S, Pellacani G, French L, Welzel J, Sattler E. In vivo imaging of *Sarcoptes scabiei* infestation using line-field confocal optical coherence tomography. *J Eur Acad Dermatol Venereol.* (2020) 34:e808–9. doi: 10.1111/jdv.16671

17. Head ES, Macdonald EM, Ewert A, Apisarnthanarax P. *Sarcoptes scabiei* in histopathologic sections of skin in human scabies. *Arch Dermatol.* (1990) 126:1475–7.

18. Piccolo V. Update on dermoscopy and infectious skin diseases. *Dermatol Pract Concept.* (2020) 10:e2020003. doi: 10.5826/dpc.1001a03

19. Dupuy A, Dehen L, Bourrat E, Lacroix C, Benderdouche M, Dubertret L, et al. Accuracy of standard dermoscopy for diagnosing scabies. *J Am Acad Dermatol.* (2007) 56:53–62. doi: 10.1016/j.jaad.2006.07.025

20. Scher RK. Subungual scabies. *J Am Acad Dermatol.* (1985) 12:577–8. doi: 10.1016/s0190-9622(85)80092-x

21. Mila-Kierzenkowska C, Woźniak A, Krzyżyńska-Malinowska E, Kałużna L, Wesołowski R, Poćwiardowski W, et al. Comparative efficacy of topical pertmehrin, crotamiton and sulfur ointment in treatment of scabies. *J Arthropod Borne Dis.* (2017) 11:1–9.

22. Hicks MI, Elston DM. Scabies. *Dermatol Ther.* (2009) 22:279–92. doi: 10.1111/j.1529-8019.2009.01243.x

frontiers | Frontiers in Medicine

TYPE Original Research
PUBLISHED 02 March 2023
DOI 10.3389/fmed.2023.1072160

OPEN ACCESS

EDITED BY
Federica Veronese,
Azienda Ospedaliero Universitaria Maggiore della Carità, Italy

REVIEWED BY
Irene Calzavara-Pinton,
University of Brescia,
Italy
Xing-Hua Gao,
The First Affiliated Hospital of China Medical University,
China

*CORRESPONDENCE
Kadri Orro
✉ kadrikene@gmail.com

†These authors have contributed equally to this work

SPECIALTY SECTION
This article was submitted to Dermatology, a section of the journal Frontiers in Medicine

RECEIVED 17 October 2022
ACCEPTED 06 February 2023
PUBLISHED 02 March 2023

CITATION
Orro K, Salk K, Abram K, Arshavskaja J, Meikas A, Karelson M, Neuman T, Kingo K and Spee P (2023) Assessment of soluble skin surface protein levels for monitoring *psoriasis vulgaris* in adult psoriasis patients using non-invasive transdermal analysis patch: A pilot study.
Front. Med. 10:1072160.
doi: 10.3389/fmed.2023.1072160

Assessment of soluble skin surface protein levels for monitoring *psoriasis vulgaris* in adult psoriasis patients using non-invasive transdermal analysis patch: A pilot study

Kadri Orro[1,2]*, Kristiina Salk[2], Kristi Abram[3,4], Jelena Arshavskaja[2], Anne Meikas[2], Maire Karelson[3,4], Toomas Neuman[2], Külli Kingo[3,4†] and Pieter Spee[2,5†]

[1]Department of Chemistry and Biotechnology, Tallinn University of Technology, Tallinn, Estonia, [2]FibroTx LLC, Tallinn, Estonia, [3]Clinic of Dermatology, Tartu University Hospital, Tartu, Estonia, [4]Clinic of Dermatology, Institute of Clinical Medicine, Tartu University, Tartu, Estonia, [5]PS! Pharmaconsult, Alleroed, Denmark

To improve the care of patients with chronic inflammatory skin conditions, such as psoriasis, there is a need for diagnostic methods that can facilitate personalized medicine. This exploratory pilot study aimed to determine whether non-invasive measurements of inflammation-related proteins from psoriatic skin can be sampled using the FibroTx Transdermal Analysis Patch (TAP) to assess disease severity and monitor pharmacodynamic changes. Ten healthy volunteers and 44 psoriasis vulgaris patients were enrolled in the exploratory pilot study. Skin surface protein measurements for healthy and lesional skin were performed using TAP. Patients' scores of psoriasis activity and severity (PASI) were documented, and differences in the thickness of skin layers were determined using sonography. The study assessed the skin surface protein levels of psoriasis patients undergoing whole-body treatment with narrow-band UVB to evaluate whether the levels of the skin surface proteins IL-1α, IL-1RA CXCL-1/2, and hBD-1 were associated with the disease activity and severity measurements. Using TAP technology, it was observed that there were clear differences in levels of IL-1α, IL-1RA, CXCL-1/2, and hBD-1 between psoriasis lesional and non-lesional skin. In addition, a positive correlation between CXCL-1/2 and desquamation, and between CXCL-1/2 and SLEB thickness was observed. During UVB treatment, the TAP measurements revealed a clear reduction of IL-1RA, CXCL 1/2, and hBD-1 on lesional skin. Further, skin surface measurements of IL-1RA and CXCL-1/2 displayed a different profile than those achieved by visual scoring of local inflammation, thus indicating that measuring the 'molecular root' of inflammation appears to have value as an objective, non-invasive biomarker measurement for scoring disease severity.

KEYWORDS

biomarker, transdermal analysis patch, psoriasis, inflammation, dermatology, skin care diagnostics, treatment monitoring

Introduction

Psoriasis is a chronic relapsing immune inflammatory dermatosis with different clinical manifestations that affects 1–3% of the world population (1, 2). Psoriasis vulgaris (PV) is the most common variant of psoriasis and is characterized by erythematous scaly plaques of the skin. It is caused by the interplay between immune cells, keratinocytes, and other skin-resident cells, mediated by adaptive and innate immune system components causing a hyperproliferation of keratinocytes and chronic inflammation in affected skin (2–6). Psoriasis patients often develop additional systemic comorbidities, such as arthritis, metabolic syndrome, diabetes, cardiovascular risk, and depression (7–9). Clinical evaluation of psoriasis is mainly performed visually using the Psoriasis Area Severity Index (PASI), a clinical score based on the assessment of the percentage of skin affected and severity of the skin erythema, induration, and desquamation (10). The PASI score allows monitoring of changes in affected skin areas over time, which may either reflect the progression, relapse, or improvement of the disease. However, several limitations of PASI have been addressed, such as not correlating the clinical extent of the disease with quality of life (11, 12) and that the PASI lacks sensitivity, as erythema, desquamation, and induration are scored with equal weight within each of the four body regions (13).

Treatment of PV depends on the severity and areas affected in patients - treatment options range from local ointments for mild psoriasis, to more harsh therapies for moderate and severe psoriasis, such as phototherapy [e.g., ultraviolet B (UVB)], photochemotherapy [e.g., psoralen ultraviolet A (PUVA)], systemic treatment with conventional agents [e.g., methotrexate, cyclosporine, and acitretin] or biological treatment [e.g., anti-tumor necrosis factor (anti–TNF-α) and interleukin inhibitors (anti-IL17, anti-IL-12/23, and anti-IL23)], where there are risks for developing side effects, such as infections (biologic therapies), or an increased risk for skin cancer (PUVA, phototherapy) (14–18). Therapeutic efficacy, defined as a diminishment in psoriasis clinical scores, does not occur instantly, and patients may not respond to therapy at all.

To improve psoriasis care, diagnostic and monitoring methods are needed that can facilitate personalized medicine. Proteins, such as interleukins, chemokines, cell surface receptors, growth factors, and anti-microbial peptides drive the biological processes underlying clinical hallmarks of psoriatic skin. We hypothesize that this psoriasis 'molecular footprint' may be very suitable for developing methods of detection and diagnosis of the disease, monitoring psoriasis progression, as well as measuring response to treatment.

Although skin biopsy remains one of the widely reported approaches for skin protein analyses from diseased skin (19, 20), less invasive alternatives have emerged in dermatological practice. Repetitive tape stripping has been considered a benchmark for minimally invasive methods of skin protein sampling (20–22). Further, other non-invasive methods for biomarker detection and profiling from the skin involve skin lavage (23), reverse iontophoresis (24), optical imaging (25), and a micro disk-library array patch method has also been described (26).

We have previously introduced a non-invasive method to measure soluble biomarkers directly from the skin (27). The FibroTx Transdermal Application Patch (TAP) consists of an adhesive bandage that contains a nitrocellulose insert on which specific antibodies have been printed for capturing proteins directly from the skin surface. TAP has shown the potential of detecting soluble skin surface biomarkers on healthy and irritated skin (27, 28). Further, using TAP, biomarkers on psoriatic lesions of pediatric patients receiving topical- and systemic treatment were determined without discomfort (29, 30).

The objectives of the present pilot study were to assess whether expression patterns of inflammatory proteins, IL-1α, IL-1RA, CXCL-1/2, and hBD-1, known to be involved in psoriasis, could be measured from the skin surface of adult psoriasis patients using the FibroTx TAP technology, whether the measurements correlated with the disease severity and further, to explore whether these skin surface proteins could be used to measure pharmacodynamic effects of psoriasis treatment.

Materials and methods

Study participants

The study was an explorative observational non-invasive study performed at the Dermatology Clinic of Tartu University Hospital in Estonia between 2015–2016, under the approval of Tallinn Medical Research Ethical (Decision No. 2551). Patients with moderate to severe PV visiting a dermatologist at Tartu University Hospital Dermatology clinic were included in the study. Patients included in the study had not received any systemic form of medical treatment and any kind of phototherapies for at least 4 weeks prior to the study and had not received any topical form of medical treatment for at least 2 weeks prior to the study. Pregnant or breastfeeding women and volunteers with a history of other skin diseases were excluded from participation. Healthy volunteers with no positive family history of psoriasis and other chronic dermatoses were serving as a control group. All participants signed informed consent prior to the study. Detailed information regarding participants is shown in Supplementary Tables S1–S3.

Measurements of transdermal analysis patch, skin disease severity scores, and sonography

At first, 10 healthy adult volunteers and 30 adult patients with PV were enrolled in the study to determine the differences in skin surface biomarkers. TAP-captured antibody micro-arrays coated with anti-interleukin one alpha (IL-1α), anti-interleukin one receptor antagonist (IL-1RA), −anti-chemokine (C-X-C motif) ligand 1 and 2 (CXCL-1/2), and anti-human beta-defensin 1 (hBD-1) were applied onto the skin of healthy volunteers and on the non-lesional and lesional skin of psoriasis patients. TAP-captured antibody micro-arrays were incubated on the skin for 20 min. Captured IL-1α and IL-1RA, CXCL-1/2, and hBD-1 were visualized using spot-enzyme linked immunosorbent assay (ELISA), as previously described (27). In addition, PASI (the range of PASI scores is 0–72) and assessment for local scores for erythema, induration, and desquamation (0–4 scale) of lesional skin were performed for patients at the exact location of the TAP measurements. Determination of differences in the thickness of skin layers [epidermis, sub-epidermal low-echogenic band (SLEB), and dermis] between non-lesional and lesional skin of patients was carried out using DermaLab Combo from Cortex Technology

according to the manufacturer's instructions. Ultrasound imaging was conducted from the same skin area as the FibroTx TAP measurements, after TAP removal from non-lesional and lesional skin.

Narrow-band ultraviolet B treatment

Further, 14 adult PV patients were included for monitoring skin surface biomarkers and PASI index and local scores for erythema, inflammation, and scaling response to narrow-band UVB treatment in combination with calcipotriol/betamethasone dipropionate ointment (Dovobet®) daily. Narrow-band UVB treatment was performed all together during the 10 weeks, three times a week. For the current pilot study, biomarker measurements with FibroTx TAP were performed before the first treatment (served as baseline), after 2 weeks of treatment, and after 4 weeks of treatment. Measurements with FibroTx TAP were performed on the same position on the skin at each time-points. The PASI score was determined before and after 4 weeks of treatment. In parallel to TAP measurements, visual assessment for erythema, induration, and desquamation were performed at the exact location of TAP measurements.

Statistical analyses

All statistical tests were performed using the statistics program JASP (version 0.9.2 for macOS). For statistical analysis, the normality of the data was tested with the Shapiro–Wilk test. Statistical significance for related groups analysis was determined using matched paired Wilcoxon signed-rank test, and the Mann–Whitney non-parametrical test was applied for two unrelated groups. For correlation analysis, non-parametrical Spearman's Rank correlation analysis was performed, and statistical significances were verified with probability value (p-value). Correlation coefficients were interpreted based on Cohen (31) to indicate weak (0.1), moderate (0.3), and strong (0.5) correlations. The level of statistical significance was set at 5% ($p < 0.05$).

Results

FibroTx transdermal analysis patch measurements revealed distinctive skin surface protein patterns between healthy and diseased skin

Skin surface levels of IL-1α, IL-1RA, CXCL-1/2, and hBD-1 detected on the skin of healthy volunteers appeared similar to the levels captured on the non-lesional skin of psoriasis patients (Figures 1A–D). However, notable differences were noticed in the amounts of IL-1α (3.14 vs. 0.98 ng/mL) and CXCL-1/2 (not detected vs. 0.06 ng/mL) when compared between healthy volunteers and lesional skin of psoriasis patients ($p < 0.001$ and $p < 0.01$, respectively). The trend of increase of anti-inflammatory IL-1RA and antimicrobial hBD-1 was detected on lesional skin when compared to the levels of these proteins captured on the skin surface of healthy volunteers, however, no statistical significance was observed. Comparing the levels of skin surface IL-1α, IL-1RA, CXCL-1/2, and hBD-1 captured from psoriasis patients' lesional and non-lesional skin revealed statistically higher levels of IL-1RA ($p < 0.001$), CXCL-1/2 ($p < 0.01$), and hBD-1 ($p < 0.05$) on lesional skin (Figures 1A–D; Supplementary Figures S1A–D). However, notable lower levels of IL-1α were detected on psoriatic lesions when compared to the non-lesional skin of the same patients ($p < 0.001$).

The inverse expression patterns of IL-1α and IL-1IL-1RA on lesional and non-lesional skin of psoriasis patients, as well as the biological link between IL-1α and IL-1RA (32), prompted us to analyze the molar ratio between IL-1α and IL-1RA on lesional and non-lesional skin of psoriasis patients. IL-1α and IL-1RA bind to the same receptor, the IL-1 receptor (IL-1R), as a pro-inflammatory agonist and an anti-inflammatory antagonist, respectively. Two forms of IL-1α exist, the immature form with an MW of 31 kDa, and the mature form of 18 kDa, which are both biologically active (33). Both isoforms were recognized by antibodies used for FibroTx TAP. IL-1RA was predominantly expressed as a 17.1 kDa protein (34). The analyses revealed that there was a clear molecular excess of IL-1α over IL-1RA on non-lesional skin of psoriasis patients and the skin of healthy volunteers, regardless of whether IL-1α was present in immature or in mature form or a combination thereof. Similarly, there was a clear excess of IL-1RA over IL-1α on the lesional skin of psoriasis patients regardless of the form of IL-1α (Supplementary Table S4).

Skin surface IL-1RA and CXCL-1/2 presented an association with edema-related sub-epidermal low-echogenic band

To determine whether differences in the molecular expression patterns of IL-1α, IL-1RA, CXCL-1/2, and hBD-1, between non-lesional and lesional skin sites of psoriasis patients associated with alterations in physical properties of skin layers, FibroTx TAP measurements of these four proteins were correlated with ultrasound measurements. First, a clear and statistically significant thickening of the epidermis ($p < 0.001$), SLEB ($p < 0.001$), and dermis ($p < 0.001$) was measured in lesional skin of psoriasis patients in comparison with non-lesional skin from the same patients (Figures 2A–D).

Correlating FibroTx TAP measurements of IL-1α, IL-1RA, CXCL-1/2, and hBD-1 and ultrasound measurements of non-lesional skin and lesional skin from the same patients revealed a positive correlation between IL-1RA and SLEB thickness ($r = 0.45$, $p = 0.013$, Supplementary Table S5A) for non-lesional skin, and strong positive correlation between CXCL-1/2 and SLEB thickness on lesional skin ($r = 0.512$, $p = 0.004$, Supplementary Table S5B).

Combining ultrasound measurements of the epidermis, dermis, or SLEB with the local scores for erythema, inflammation, and scaling of the patients did not reveal any significant correlations except for a significant positive correlation between SLEB thickness and induration ($r = 0.402$, $p = 0.028$, Supplementary Table S5C).

Skin surface proteins were normalizing over narrow-band ultraviolet B therapy

During the 4 weeks course of UVB treatment, levels of IL-1α Did Not change on the lesional skin of psoriasis patients, but there

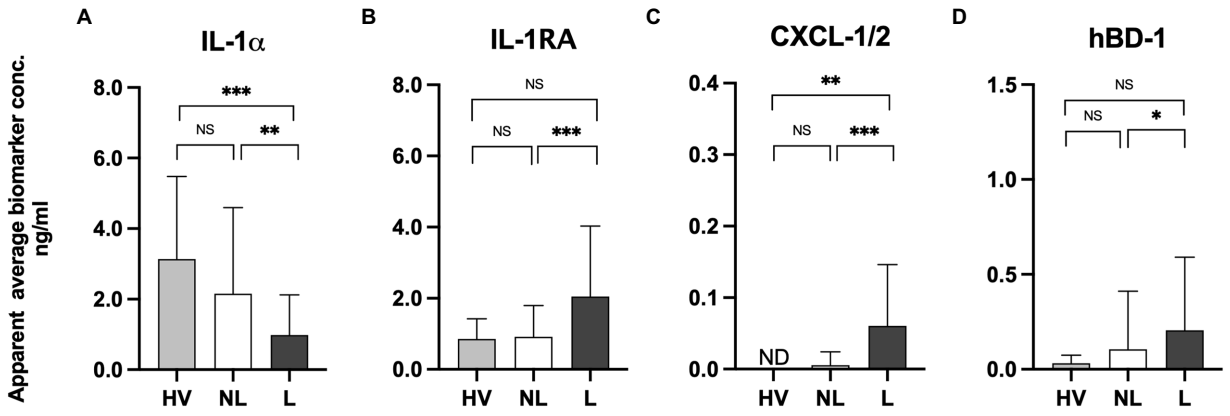

FIGURE 1
(A) Measurements of IL-1α, IL-1RA, CXCL-1/2, and hBD-1 on lesional and non-lesional skin of psoriasis patients and normal skin of healthy volunteers using the FibroTx TAP. The apparent average biomarker concentrations of IL-1α IL-1RA, CXCL-1/2, and hBD-1 detected from the skin surface of 10 healthy volunteers (grey bars), on non-lesional skin (NL; white bars) and lesional skin (L; black bars) of 30 psoriasis patients have been plotted. *Y*-axis: Apparent concentration of analyzed biomarker on the skin in ng/mL. *X*-axis: sampling site. Error bars on graphs present the standard deviations from the average of combined measurements of the participants. Statistical significance is indicated on panels **(A–D)**: *p<0.05, **p<0.01, *** p<0.001; NS-not significant.

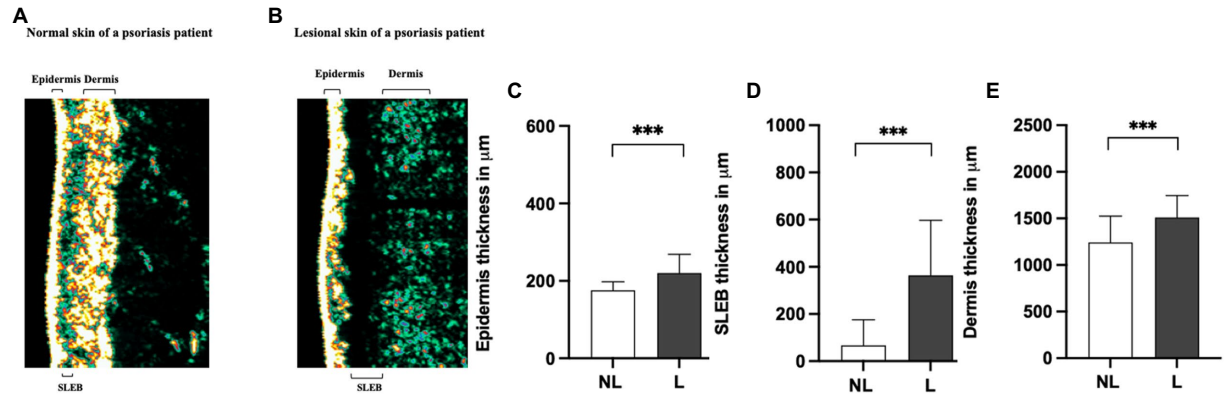

FIGURE 2
Comparison of sonography data of non-lesional and lesional skin of psoriasis patients. A representative image of the thickness of the epidermis, SLEB, and dermis in non-lesional (panel **A**) and lesional skin (panel **B**) of a psoriasis patient measured by ultrasound. 20-MHz ultrasound image of the non-lesional (panel **A**) and lesional skin area (panel **B**) of the same psoriasis patient is presented. The positions of the epidermis, SLEB, and dermis are indicated in the image. The apparent average epidermal thickness (panel **C**), SLEB thickness (panel **D**), and dermis thickness (panel **E**) analyzed from non-lesional skin (NL; white bars) and lesional skin (L; black bars) have been blotted. The ultrasound measurements are performed at the exact lesion and healthy apparent skin of the psoriasis patient where the FibroTx TAP measurements were performed and local clinical scores by the physician were stated. *Y*-axis: Average thickness of the epidermis, SLEB, and dermis, respectively, in µm. *X*-axis: sampling site. Error bars on graphs present the standard deviations from the average of combined measurements of the patients (N=30). Statistical significance was determined with paired sample Wilcoxon signed-rank test (*p < 0.05, **p < 0.01, ***p < 0.001).

was a modest decline In IL-1α on non-lesional skin (Figure 3). In contrast, levels of Pro-inflammatory IL-1RA ($p < 0.01$) and CXCL-1/2 ($p < 0.05$) showed a significant reduction in lesional skin in response to therapy. Over the four weeks of treatment, levels of IL-1RA on lesional skin reduced to a level similar to the amount of IL-1RA on non-lesional skin. No alterations were measured for IL-1RA on non-lesional skin during the course of treatment and CXCL-1/2 remained undetectable (Figure 3). The levels of antimicrobial peptide hBD-1 detected at baseline on non-lesional skin were nearly twofold lower compared to the levels captured on lesional skin. However, after four weeks of narrow-band UVB treatment, the levels of hBD-1 detected on non-lesional skin increased compared to the baseline with an approximately twofold increase, contrary to the levels of hBD-1 captured on lesional skin, which showed a nearly fourfold decrease compared to the amounts of baseline hBD-1 (Figure 3.). Kinetics of the downregulation of analyzed skin surface proteins showed a notable difference between the individual markers. Levels of IL-1α displayed a slower response reaching just 40% of reduction whereas IL-1RA and CXCL-1/2 were reduced by 75% and hBD-1 by 80% of their baseline levels on lesional skin after four weeks of treatment (Figure 3B).

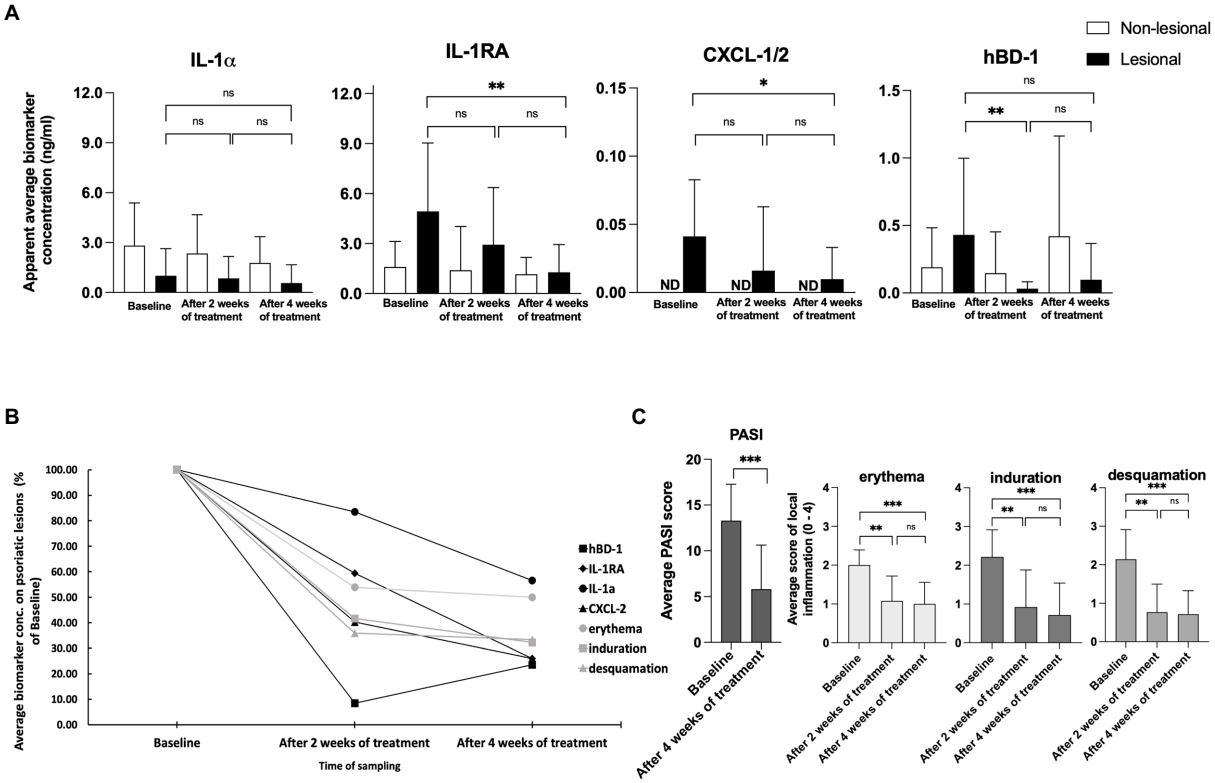

FIGURE 3
(A) Measurements of IL-1α, IL-1RA, CXCL-1/2, and hBD-1 on non-lesional and lesional skin of psoriasis patients during narrow band UVB treatment. Biomarker measurements were performed on healthy apparent and lesional skin before treatment, and after two and four weeks of treatment at the same skin site using FibroTx TAP. The apparent average biomarker concentration of non-lesional skin is plotted with white bars (panels A–D), and average biomarker measurements of lesional skin sites are presented with back bars (panels A–D). *Y*-axis: apparent concentration of IL-1α, IL-1RA, CXCL-1/2, and hBD-1 on the skin in ng/mL. *X*-axis: time point of biomarker sampling. Error bars in graphs A–D represent the standard deviations from the average of combined measurements of the patients (*N*=14); ND, not detected. Statistical significance was determined with paired sample Wilcoxon signed-rank test (*$p < 0.05$, **$p < 0.01$, ***$p < 0.001$). **(B)** Measurements of IL-1α, IL-1RA, CXCL-1/2, and hBD-1 on lesional skin of psoriasis patients during narrow band UVB treatment. Combined average levels of biomarkers IL-1α, IL-1RA, CXCL-1/2, and hBD-1 sampled with TAP on lesional skin of psoriasis patient (*N*=14) and scores of local erythema, induration, and desquamation of the same lesional site before and during treatment with narrow-band UVB combined with calcipotriol/betamethasone dipropionate ointment. Data presented as % of baseline values. **(C)** Changes in the psoriasis area severity index (PASI) and local scores for erythema, induration, and desquamation induced by narrow-band UVB treatment. The PASI score was documented before the treatment initiation and after 4weeks of treatment. Local scores for erythema, induration, and desquamation were documented before the treatment initiation, and after two and four weeks of treatment at the same lesion sites. Each bar plotted in Figure 3A represents an average measurement of an analyzed clinical score of psoriasis patients (*N*=14). Error bars on graphs present the standard deviations from the average of combined measurements of the patients (*N*=14). Statistical significance was determined with paired sample Wilcoxon signed-rank test (*$p<0.05$, **$p<0.01$, ***$p<0.001$).

Skin surface biomarkers associated with disease activity scores over narrow-band ultraviolet B therapy

As a result of the narrow-band UVB treatment, the PASI score dropped an average of 57.71 percent during treatment, a highly significant difference ($p<0.001$; Figure 3C). Local scores for erythema, induration, and desquamation showed high significant improvements of the lesions measured by FibroTx TAP ($p<0.01$, $p<0.01$, $p<0.01$, respectively, Figure 3C).

IL-1α, IL-1RA, and CXCL-1/2 are cytokines directly involved in psoriasis skin inflammation (32, 35). Therefore we decided to assess whether these skin surface proteins measured by TAP correlated with disease severity over time. We analyzed the correlation between the values of IL-1α, IL-1RA, CXCL-1/2, and hBD-1 measurements from psoriatic skin against the PASI and the values of erythema, induration, and desquamation, at the area of the FibroTx TAP measurements. Data collected on the baseline and after 4 weeks of treatment were combined for Spearman rank correlation analysis positive association between skin surface proteins, PASI ($r>0.4$), and the values of erythema, induration, and desquamation was observed over time for CXCL-1/2 and IL-1RA ($r>0.3$) indicating higher levels of skin surface CXCL-1/2, IL-1RA for higher disease severity (Supplementary Table S6). Moderate correlation for skin surface antimicrobial hBD-1 and erythema ($r=0.4$, $p=0.02$), and induration ($r=0.39$, $p=0.04$) was observed. No correlation between IL-1α and disease severity scores over UVB therapy was noted.

Analyses of the IL-1RA over IL-1α ratio also confirmed the clinically observed pattern of normalization of skin in lesions measured. The ratio between IL-1RA and IL-1α, measured on lesions (ng/mL), declined from 4.89 to 2.25. In contrast, the ratio between IL-1RA and IL-1α, measured on non-lesional skin, remained stable, changing from 0.57 to 0.65 during treatment (Supplementary Table S7).

No adverse events were reported in the FibroTx TAP measurements, neither on non-lesional skin nor on lesional skin, and neither in patients nor in healthy individuals either by visual assessment (e.g., signs of redness) or upon inquiry (e.g., irritation, itching, and pain).

Discussion and conclusion

This exploratory pilot study aimed to assess whether expression patterns of inflammatory proteins known to be involved in psoriasis measured non-invasively from the skin surface of adult psoriasis patients associated with the clinical scores for psoriasis severity and whether the changes in skin surface biomarker levels followed the clinical features in response to therapy. The choice for measuring skin surface proteins using the FibroTx TAP was because TAP is a non-invasive sampling technology that does not affect the skin, i.e., protein measurements are not biased by skin responding to the measurement method, and do not interfere with biological processes in and on the skin (28). Moreover, the method collects the analytes directly from the skin surface within one step and no additional extraction procedures after sampling are needed like in the case of the tape strip method (22).

The panel of IL-1α, IL-1RA, CXCL-1/2, and hBD-1 was chosen for the pilot study because these proteins have shown reliable quantitative and qualitative measurements from the skin surface using TAP (27, 29), and based on their role in inflammation of psoriasis reported in the literature. IL-1α and IL-1RA are examples of pro- and anti-inflammatory interleukins, respectively, that are known to play important roles in skin homeostasis and skin inflammation, including psoriasis (28, 32–35). The combination of chemokines CXCL-1 and -2 was chosen because of their role in attracting neutrophils to psoriatic skin lesions, which leads to T-cell activation (34, 36). Hence CXCL-1/2 is a valuable biomarker for monitoring inflammatory-related processes in the skin. Epithelial-produced antimicrobial peptide hBD-1 is detected also in immune cells, such as macrophages and monocytes (37), linking these signaling molecules with immune system regulation. Further, Uzuncakmak et al. monitored by invasive methods the alteration of tissue expression of human beta defensin-1 in PV following phototherapy (38), therefore presenting hBD-1 as an interesting candidate for non-invasive monitoring of its pattern in response to therapy.

Non-invasive skin surface measurements with TAP confirm that proteins such as IL-1RA, CXCL-1/2, and hBD-1 are present in higher amounts on lesional skin, whereas others, such as IL-α, are found in reduced amounts on lesional skin in comparison with non-lesional and healthy skin. This was supported by reports in the literature, which assessed these patterns through more invasive technologies, such as mRNA and immune histochemistry (IHC) analysis using skin biopsies and protein analysis (28, 34, 38–41). Therefore, it appears that non-invasive measurements of soluble proteins found on the skin, e.g., as measured by TAP, both qualitatively and quantitatively correlate with proteins found in the skin, as measured by invasive methods.

In the literature, there is ample evidence that IL-1α is found in decreased levels, and IL-1RA in increased levels in psoriatic lesional skin in comparison with non-lesional skin (32, 39, 40). TAP measurements of IL-1α and IL-1RA on the skin of adult psoriasis patients thus fit the bulk of evidence in the literature. One of the possible reasons for these levels of assessed IL-1α and IL-1RA on lesional versus non-lesional skin could be through skin barrier disruption, which is a distinguishing parameter for lesions. Preformed IL-1α is described to be stored in epidermis (42) and is released and depleted due to the skin barrier damage compared to the healthy tissue where the skin barrier is intact.

PV manifests itself in physical changes of the skin layers, such as thickening of the epidermis and the presence of a characteristic low-density layer between the epidermis and dermis, the so-called sub-epidermal low-echogenic band (SLEB) that can be measured *via* ultrasound (43, 44). Our measurements clearly showed a statistically significant thickening of the epidermis, SLEB, and dermis in lesional skin in comparison with non-lesional skin. A moderate positive correlation between CXCL-1/2 and SLEB thickness of lesional skin was observed. SLEB presents dermis-reduced echogenicity that is caused by edema and inflammatory cell infiltration at the inflamed lesions, which in turn can be explained by elevated levels of CXCL-1/2 produced by T-cells and keratinocytes in inflamed lesions. This connection between skin surface CXCL-1/2 and dermal SLEB suggests that local skin surface proteins can reflect the condition of the skin from deeper layers. Interestingly, neither ultrasound measurements nor visual assessments of lesional skin correlated in a highly statistically significant sense; only a mild correlation between skin induration and SLEB thickness was observed, and thus it appears that visual-, ultrasound- and protein measurements can quantify disease intensity.

We followed patients during short-wave UVB treatment to determine whether measurements of skin-surface IL-1α, IL-1RA, CXCL-1/2, and hBD-1 reflect disease intensity merely in a qualitative state, i.e., inflamed or not inflamed, or whether skin surface measurements of these biomarkers can reflect disease intensity quantitatively. Four weeks of narrow-band UVB treatment resulted in notable changes in skin surface protein levels (Figure 3) in addition to an improvement in disease severity scores (Figure 3C). Interestingly, the analyzed biomarkers displayed different treatment response kinetics – whereas IL-1RA, CXCL-1/2, and hBD-1 presented close to 80% reduction compared to baseline levels assessed on lesional skin, levels of IL-1α displayed slower and low response, reaching just 40% of reduction (Figure 3B) when compared to baseline levels. This distinction of IL-1α lower response kinetics could be explained by the importance of this cytokine in the regulation of innate immune defense mechanisms (45) and by the constant production of local keratinocytes. Therefore, pre-produced IL-1α could emerge from the depths of the epidermal layer whereas anti-inflammatory IL-1RA, synthesized previously in counter to inflammation, reduced in response to therapy. This hypothesis seems to be supported by the measurement of IL-1α and IL-1RA levels of the same psoriasis patients' non-lesional skin. Response kinetics and the detected alteration in levels of IL-1α on lesional skin resembled the kinetics and the detected reduction rate of skin surface IL-1α on healthy apparent skin, whereas kinetics and decreased levels of IL-RA were more robust on psoriatic lesion when compared with measurements of non-lesional skin.

Interestingly, although skin surface hBD-1 stated higher levels on psoriatic lesions than non-lesional skin, followed by local scores for erythema, induration, and desquamation during UVB therapy, reverse levels of hBD-1 were detected on psoriasis lesions compared to patients' non-lesional skin after 4 weeks of treatment. We hypothesized it could be related, on the one hand, to the integrity of the skin barrier host

defense mechanism of healthy skin and, on the other hand, due to the apoptosis caused by narrow-band UVB of local keratinocytes producing hBD-1 in psoriasis lesions.

Although correlations between skin surface protein levels and disease severity were observed, it was interesting that analysis of skin surface biomarker levels assessed with FibroTx TAP revealed that skin surface measurements of IL-1RA and CXCL-1/2 displayed a different pattern than achieved by visual evaluation of local inflammation (Figure 3C). Visual assessment for erythema, induration, and desquamation decreased after 2 weeks of treatment and displayed similar levels after 4 weeks of treatment, whereas IL-1RA and CXCL-1/2 normalized more gradually through therapy (Figure 3). This confirmed that measuring the 'molecular root' of inflammation appears to have value as an objective, non-invasive biomarker measurement for scoring disease intensity. The difference in kinetics of analyzed biomarkers suggested that changes in skin surface proteins are not a uniform reflection of skin healing, but rather reflect individual changes of expression in the skin. Nevertheless, the patient cohort of the current study was limited, and a study with a larger cohort of patients is needed for firm conclusions.

In conclusion, we could measure IL-1α, IL-1RA, CXCL-1/2, and hBD-1 on the skin of psoriasis patients, with clear differences between lesional and non-lesional skin, which supports the hypothesis that TAP is an applicable tool for non-invasive skin surface protein measurement on skin. Further, correlating skin surface measurements of analyzed proteins on the skin from psoriasis patients with clinical assessments of psoriasis severity suggests that these protein measurements may have potential as biomarkers. Nonetheless, a substantially larger study will be necessary to further validate measurements of IL-1α, IL-1RA, CXCL-1/2, and hBD-1 on the skin of psoriasis patients for diagnostic, prognostic, and therapeutic biomarker applications. Whether the conclusions about the applicability of the FibroTx TAP method and analyzed biomarkers can be applied to other skin diseases, skin surface biomarkers, and/or treatment methods is not known and will require additional research.

Data availability statement

The raw data supporting the conclusions of this article will be made available by the authors, without undue reservation.

Ethics statement

This research was conducted in accordance with the World Medical Association Declaration of Helsinki. Ethical approval for the studies is covered by Decision No. 2551 from the Tallinn Medical Research Ethical Committee. The Declaration of Helsinki protocols were followed. The patients/participants provided their written informed consent to participate in this study.

Author contributions

KO analyzed the data. KO, KK, and PS wrote the manuscript. KK, KA, MK, KO, and KS conducted TAP biomarker measurements from the skin of psoriasis patients. KO and KS designed, and KO, KS, and JA performed experiments related to TAP biomarker measurement performed on of skin of healthy volunteers. KA and AM performed ultrasound measurements. TN, KK, and PS were responsible for the overall study design. All authors have read and approved the final manuscript.

Funding

This study received funding from FibroTx LLC. The study was supported by the Estonian Research Council as personal research Grant PUT1465 and Estonian Research Council Team grant PRG1189 to KK, and the publication fee will be covered by the Estonian Research Council Team grant PRG1189 to KK.

Conflict of interest

KO, KS, JA, AM, and TN are all employed by the company FibroTx. TN is a founder and shareholder of FibroTx. PS is a consultant at FibroTx and employed by PS! Pharmaconsult.

The remaining authors declare that the research was conducted in the absence of any commercial or financial relationships that could be construed as a potential conflict of interest.

This study received funding from FibroTx LLC. FibroTx LLC had the following involvement with the study: overseeing the study design and providing the FibroTx Transdermal analysis Patches.

Publisher's note

Supplementary material

The Supplementary material for this article can be found online at: https://www.frontiersin.org/articles/10.3389/fmed.2023.1072160/full#supplementary-material

References

1. Boehncke, W-H. Etiology and pathogenesis of psoriasis. *Rheum Dis Clin*. (2015) 41:665–75. doi: 10.1016/j.rdc.2015.07.013

2. Rendon, A, and Schäkel, K. Psoriasis pathogenesis and treatment. *Int J Mol Sci*. (2019) 20:1475. doi: 10.3390/ijms20061475

3. Schön, MP, Boehncke, WH, and Brocker, EB. Psoriasis: clinical manifestations, pathogenesis and therapeutic perspectives. *Discov Med*. (2005) 27:253–8.

4. Langley, R, Kreuger, G, and Griffiths, C. Psoriasis: epidemiology, clinical features, and quality of life. *Ann Rheum Dis*. (2005) 64:18–23. doi: 10.1136/ard.2004.033217

5. Bata-Csörgö, Z, and Szell, M. The psoriatic keratinocytes. *Expert Rev Dermatol*. (2012) 7:473–81. doi: 10.1586/edm.12.48

6. Ortiz-Lopez, LI, Choudhary, V, and Bollag, WB. Updated perspectives on keratinocytes and psoriasis: keratinocytes are more than innocent bystanders. *Psoriasis*. (2022) 12:73–87. doi: 10.2147/PTT.S327310

7. Prey, S, Paul, C, Bronsard, V, Puzenat, E, Gourraud, PA, Aractingi, S, et al. Assessment of risk of psoriatic arthritis in patients with plaque psoriasis: a systematic review of the literature. *J Eur Acad Dermatol Venereol*. (2010) 24:31–5. doi: 10.1111/j.1468-3083.2009.03565.x

8. Tinggaard, AB, Hjuler, KF, Andersen, IT, Winther, S, Iversen, L, and Bøttcher, M. Prevalence and severity of coronary artery disease linked to prognosis in psoriasis and psoriatic arthritis patients: a multi-Centre cohort study. *J Intern Med*. (2021) 290:693–703. doi: 10.1111/joim.13311

9. Daugaard, C, Iversen, L, and Hjuler, KF. Comorbidity in adult psoriasis: considerations for the clinician. *Psoriasis*. (2022) 12:139–50. doi: 10.2147/PTT.S328572

10. Carlin, CS, Feldman, SR, Krueger, JG, Menter, A, and Krueger, GG. A 50% reduction in the psoriasis area and severity index (PASI 50) is a clinically significant endpoint in the assessment of psoriasis. *J Am Acad Dermatol*. (2004) 50:859–66. doi: 10.1016/j.jaad.2003.09.014

11. Choi, J, and Koo, JY. Quality of life issues in psoriasis. *J Am Acad Dermatol*. (2003) 49:S57–61. doi: 10.1016/S0190-9622(03)01136-8

12. Sarkar, R, Chugh, S, and Bansal, S. General measures and quality of life issues in psoriasis. *Indian Dermatol Online J*. (2016) 7:481–8. doi: 10.4103/2229-5178.193908

13. Clinical Review Report. (2017). Clinical Review Report: Ixekizumab (Taltz) [internet]. Ottawa (ON): Canadian Agency for Drugs and Technologies in health; APPENDIX 6, Validity of Outcome Measures. Available at: https://www.ncbi.nlm.nih.gov/books/NBK533695/ [Accessed February 14, 2023].

14. Kim, IH, West, CE, Kwatra, SG, Feldman, SR, and O'Neill, JL. Comparative efficacy of biologics in psoriasis: a review. *Am J Clin Dermatol*. (2012) 13:365–74. doi: 10.2165/11633110-000000000-00000

15. Laws, PM, and Young, HS. Current and emerging systemic treatment strategies for psoriasis. *Drugs*. (2012) 72:1867–80. doi: 10.2165/11634980-000000000-00000

16. Rustin, MH. Long-term safety of biologics in the treatment of moderate-to-severe plaque psoriasis: review of current data. *Br J Dermatol*. (2012) 167:3–11. doi: 10.1111/j.1365-2133.2012.11208.x

17. Patel, RV, Clark, LN, Lebwohl, M, and Weinberg, JM. Treatments for psoriasis and the risk of malignancy. *J Am Acad Dermatol*. (2009) 60:1001–17. doi: 10.1016/j.jaad.2008.12.031

18. Kamata, M, and Tada, Y. Efficacy and safety of biologics for psoriasis and psoriatic arthritis and their impact on comorbidities: a literature review. *Int J Mol Sci*. (2020) 21:1690. doi: 10.3390/ijms21051690

19. Félix Garza, ZC, Lenz, M, Liebmann, J, Ertaylan, G, Born, M, Arts, ICW, et al. Characterization of disease-specific cellular abundance profiles of chronic inflammatory skin conditions from deconvolution of biopsy samples. *BMC Med Genet*. (2019) 12:1–14. doi: 10.1186/s12920-019-0567-7

20. Tsoi, LC, Xing, X, Xing, E, Wasikowski, R, Shao, S, Zeng, C, et al. Noninvasive tape-stripping with high-resolution RNA profiling effectively captures a Preinflammatory state in Nonlesional psoriatic skin. *J Investig Dermatol*. (2022) 142:1587–1596.e2. doi: 10.1016/j.jid.2021.09.038

21. Guttman-Yassky, E, Diaz, A, Pavel, AB, Fernandes, M, Lefferdink, R, Erickson, T, et al. Use of tape strips to detect immune and barrier abnormalities in the skin of children with early-onset atopic dermatitis. *JAMA Dermatol*. (2019) 155:1358–70. doi: 10.1001/jamadermatol.2019.2983

22. He, H, Bissonnette, R, Wu, J, Diaz, A, Saint-Cyr Proulx, E, Maari, C, et al. Tape strips detect distinct immune and barrier profiles in atopic dermatitis and psoriasis. *J Allergy Clin Immunol*. (2021) 147:199–212. doi: 10.1016/j.jaci.2020.05.048

23. Portugal-Cohen, M, and Kohen, R. Non-invasive evaluation of skin cytokines secretion: an innovative complementary method for monitoring skin disorders. *Methods*. (2013) 61:63–8. doi: 10.1016/j.ymeth.2012.10.002

24. Morin, M, Björklund, S, Jankovskaja, S, Moore, K, Delgado-Charro, MB, Ruzgas, T, et al. Reverse Iontophoretic extraction of skin cancer-related biomarkers. *Pharmaceutics*. (2022) 14:79. doi: 10.3390/pharmaceutics14010079

25. Žurauskas, M, Barkalifa, R, Alex, A, Marjanovic, M, Spillman, D, Mukherjee, P, et al. Assessing the severity of psoriasis through multivariate analysis of optical images from non-lesional skin. *Sci Rep*. (2020) 10:1–9. doi: 10.1038/s41598-020-65689-4

26. Oh, DY, Na, H, Song, SW, Kim, J, In, H, Lee, AC, et al. ELIPatch, a thumbnail-size patch with immunospot array for multiplexed protein detection from human skin surface. *Biomicrofluidics*. (2018) 12:031101. doi: 10.1063/1.5032170

27. Orro, K, Smirnova, O, Arshavskaja, J, Salk, K, Meikas, A, Pihelgas, S, et al. Development of TAP, a non-invasive test for qualitative and quantitative measurements of biomarkers from the skin surface. *Biomark Res*. (2014) 2:20. doi: 10.1186/2050-7771-2-20

28. Falcone, D, Spee, P, Salk, K, Peppelman, M, van de Kerkhof, PCM, and van Erp, PEJ. Measurement of skin surface biomakers by transdermal analyses patch following different in vivo models of irritation: a pilot study. *Skin Res Technol*. (2017) 23:336–45. doi: 10.1111/srt.12340

29. Schaap, MJ, Bruins, FM, He, X, Orro, K, Peppelman, M, van Erp, PEJ, et al. Skin surface protein detection by transdermal analysis patches in pediatric psoriasis. *Skin Pharmacol Physiol*. (2021) 34:271–80. doi: 10.1159/000516110

30. Schaap, MJ, Bruins, FM, van den Brink, NJM, Orro, K, Groenewoud, HMM, de Jong, EMGJ, et al. Challenges in noninvasive skin biomarker measurements in daily practice: a longitudinal study on skin surface protein detection by the transdermal analysis patch in pediatric psoriasis. *Skin Pharmacol Physiol*. (2022) 35:319–27. doi: 10.1159/000527258

31. Cohen, J. *Statistical Power Analysis for the Behavioral Sciences. 2nd* ed. Hillsdale, NJ: L. Erlbaum Associates (1988).

32. Terui, T, Hirao, T, Sato, Y, Uesugi, T, Honda, M, Iguchi, M, et al. An increased ratio of interleukin-1 receptor antagonist to interleukin-1α in inflammatory skin diseases. *Exp Dermatol*. (1998) 7:327–34. doi: 10.1111/j.1600-0625.1998.tb00332.x

33. Kim, B, Lee, Y, Kim, E, Kwak, A, Ryoo, S, Bae, SH, et al. The interleukin-1α precursor is biologically active and is likely a key alarmin in the IL-1 family of cytokines. *Front Immunol*. (2014) 4:391. doi: 10.3389/fimmu.2013.00391

34. Malyak, M, Guthridge, JM, Hance, KR, Dower, SK, Freed, JH, and Arend, WP. Characterization of a low molecular weight isoform of IL-1 receptor antagonist. *J Immunol*. (1998) 161:1997–2003. doi: 10.4049/jimmunol.161.4.1997

35. Šahmatova, L, Sügis, E, Šunina, M, Hermann, H, Prans, E, Pihlap, M, et al. Signs of innate immune activation and premature immunosenescence in psoriasis patients. *Sci Rep*. (2017) 7:7553–13. doi: 10.1038/s41598-017-07975-2

36. Chiricozzi, A, Guttman-Yassky, E, Suárez-Fariñas, M, Nograles, KE, Tian, S, Cardinale, I, et al. Integrative responses to IL-17 and TNF-α in human keratinocytes account for key inflammatory pathogenic circuits in psoriasis. *J Investig Dermatol*. (2011) 131:677–87. doi: 10.1038/jid.2010.340

37. Ryan, LK, Dai, J, Yin, Z, Megjugorac, N, Uhlhorn, V, Yim, S, et al. Modulation of human β-defensin-1 (hBD-1) in plasmacytoid dendritic cells (PDC), monocytes, and epithelial cells by influenza virus, herpes simplex virus, and Sendai virus and its possible role in innate immunity. *J Leukoc Biol*. (2011) 90:343–56. doi: 10.1189/jlb.0209079

38. Uzuncakmak, TK, Karadag, AS, Ozkanli, S, Akbulak, O, Ozlu, E, Akdeniz, N, et al. Alteration of tissue expression of human beta defensin-1 and human beta defensin-2 in psoriasis vulgaris following phototherapy. *Biotech Histochem*. (2019) 95:243–8. doi: 10.1080/10520295.2019.1673901

39. Janssens, AS, Pavel, S, Tensenn, CP, Teunissen, MBM, Out-Luiting, JJ, Willemze, R, et al. Reduced IL-1Ra/IL-1 ratio in ultraviolet B-exposed skin of patients with polymorphic light eruption. *Exp Dermatol*. (2009) 18:212–7. doi: 10.1111/j.1600-0625.2008.00785.x

40. Tamilselvi, E, Haripriya, D, Hemamalini, M, Pushpa, G, and Swapna, S. Association of Disease Severity with IL-1 levels in methotrexate-treated psoriasis patients. *Scand J Immunol*. (2013) 78:545–53. doi: 10.1111/sji.12117

41. Ozlu, E, Karadag, AS, Ozkanli, S, Oguztuzun, S, Akbulak, O, Uzuncakmak, TK, et al. The investigation of antimicrobial peptides expression and its related interaction with methotrexate treatment in patients with psoriasis vulgaris. *Cutan Ocul Toxicol*. (2017) 36:321–6. doi: 10.1080/15569527.2016.1277430

42. Hulshof, L, Hack, DP, Hasnoe, Q, Dontje, B, Jakasa, I, Riethmüller, C, et al. A minimally invasive tool to study immune response and skin barrier in children with atopic der- matitis. *Br J Dermatol*. (2019) 180:621–30. doi: 10.1111/bjd.16994

43. Cucoș, M., Crișan, M., Lenghel, M., Dudea, M., and Croitoru, R., Dudea SM. Conventional ultrasonography and sonoelastography in the assessment of plaque psoriasis under topical corticosteroid treatment - work in progress. *Med Ultrason* 16, 107–113. (2014), doi: 10.11152/mu.2013.2066.162.mc1mc2

44. Șomlea, MC, Boca, AN, Pop, AD, Ilieș, RF, Vesa, SC, Buzoianu, AD, et al. High-frequency ultrasonography of psoriatic skin: a non-invasive technique in the evaluation of the entire skin of patients with psoriasis: a pilot study. *Exp Ther Med*. (2019) 18:4981–6. doi: 10.3892/etm.2019.8140

45. Boraschi, D, and Tagliabue, A. The interleukin-1 receptor family. *Semin Immunol*. (2013) 25:394–407. doi: 10.1016/j.smim.2013.10.023

frontiers | Frontiers in Medicine

TYPE Systematic Review
PUBLISHED 27 July 2023
DOI 10.3389/fmed.2023.1200963

OPEN ACCESS

EDITED BY
Elisa Zavattaro,
University of Eastern Piedmont, Italy

REVIEWED BY
Feroze Kaliyadan,
Sree Narayana Institute of Medical Sciences, India
Angelo Ruggiero,
University of Naples Federico II, Italy
Reinhart Speeckaert,
Ghent University Hospital, Belgium

*CORRESPONDENCE
Parsa Abdi
pabedinzadeg@mun.ca

RECEIVED 05 April 2023
ACCEPTED 13 July 2023
PUBLISHED 27 July 2023

CITATION
Abdi P, Anthony MR, Farkouh C, Chan AR, Kooner A, Qureshi S and Maibach H (2023) Non-invasive skin measurement methods and diagnostics for vitiligo: a systematic review. *Front. Med.* 10:1200963. doi: 10.3389/fmed.2023.1200963

Non-invasive skin measurement methods and diagnostics for vitiligo: a systematic review

Parsa Abdi [1]*, Michelle R. Anthony[2], Christopher Farkouh[3], Airiss R. Chan[4], Amritpal Kooner[5], Simal Qureshi[1] and Howard Maibach[6]

[1]Memorial University of Newfoundland, Faculty of Medicine, St. Johns, NL, Canada, [2]College of Medicine, University of Arizona, Tucson, AZ, United States, [3]Rush Medical College, Faculty of Medicine, Chicago, IL, United States, [4]Division of Dermatology, Faculty of Medicine, University of Alberta, Edmonton, AB, Canada, [5]Chicago College of Osteopathic Medicine, Midwestern University, Downers Grove, IL, United States, [6]Division of Dermatology, Faculty of Medicine, University of California, San Francisco, San Francisco, CA, United States

Vitiligo is a multifaceted autoimmune depigmenting disorder affecting around 0.5 to 2.0% of individuals globally. Standardizing diagnosis and therapy tracking can be arduous, as numerous clinical evaluation methods are subject to interobserver variability and may not be validated. Therefore, there is a need for diagnostic tools that are objective, dependable, and preferably non-invasive.

Aims: This systematic review provides a comprehensive overview of the non-invasive objective skin measurement methods that are currently used to evaluate the diagnosis, severity, and progression of vitiligo, as well as the advantages and limitations of each technique.

Methods: The Preferred Reporting Items for Systematic Reviews and Meta-Analyses (PRISMA) checklist was used for the systematic review. Scopus, Embase, Cochrane Library, and Web of Science databases were comprehensively searched for non-invasive imaging and biophysical skin measuring methods to diagnose, evaluate the severity of, or monitor the effects of vitiligo treatment. The risk of bias in included articles was assessed using the QUADAS-2 quality assessment scale.

Results: An extensive literature search resulted in 64 studies for analysis, describing eight imaging techniques (reflectance confocal microscopy, computer-aided imaging analysis, optical coherence tomography, infrared photography, third-harmonic generation microscopy, multiphoton microscopy, ultraviolet light photography, and visible light/digital photograph), and three biophysical approaches (dermoscopy, colorimetry, spectrometry) used in diagnosing and assessing vitiligo. Pertinent information about functionality, mechanisms of action, sensitivity, and specificity was obtained for all studies, and insights into the strengths and limitations of each diagnostic technique were addressed. Methodological study quality was adequate; however, statistical analysis was not achievable because of the variety of methods evaluated and the non-standardized reporting of diagnostic accuracy results.

Conclusions: The results of this systematic review can enhance clinical practice and research by providing a comprehensive overview of the spectrum of non-invasive imaging and biophysical techniques in vitiligo assessment. Studies with larger sample sizes and sound methodology are required to develop verified methods for use in future practice and research.

Systematic review registration: (PROSPERO) database, (CRD42023395996).

KEYWORDS

vitiligo, non-invasive techniques, diagnosis, imaging techniques, dermoscopy, reflectance confocal microscopy, ultraviolet light photography, wood's lamp

1. Introduction

Vitiligo is a common autoimmune depigmenting disorder associated with the loss of functional melanocytes and melanin in the epidermis, typically presenting as circumscribed depigmented macules to patches (1). Currently, around 0.5 to 2.0% of individuals are affected with vitiligo worldwide, but appropriate medical care and research are limited compared to other dermatological pathologies (1, 2). Vitiligo does not exhibit a gender predilection, but it does appear to prefer specific anatomical locations, including the face and extensor surfaces (1, 3). The disease tends to manifest around 10 to 30 years, with a mean age of diagnosis around 15.6 years, and 70–80% of vitiligo diagnoses occur before age 30 (1). Although, vitiligo is typically asymptomatic and benign, the psychological and cosmetic consequences to patients may be overwhelming.

The current gold standard for diagnosing vitiligo relies on clinical examination, yet certain presentations, particularly early or evolving lesions, may be missed, necessitating additional diagnostic tools for confirmation. Various numerical scales also exist to assess outcome measurements for vitiligo, including the including the well-validated Vitiligo Extent Score (VES), the Self-Assessment Vitiligo Extent Score (SA-VES), and Vitiligo Area Scoring Index (VASI) (4–6). Commonly used diagnostic techniques for vitiligo include dermoscopy, Wood's lamp, digital photography with computerized image analysis, and invasive methods such as skin biopsies, however, several emerging, non-invasive techniques are currently being investigated.

Non-invasive methods offer distinct advantages over invasive approaches as they enable the longitudinal tracking of the same skin area without causing inflammation, irritation, damage, or other adverse reactions that could hinder accurate assessment. Despite the widespread use of several non-invasive and objective diagnostic techniques in vitiligo assessment, a comprehensive review of these methods is lacking. Therefore, the purpose of this systematic review is to provide a comprehensive overview of these non-invasive techniques, their strengths, limitations, and potential implications in the diagnosis and assessment of vitiligo. In the context of non-invasive techniques, our systematic review focuses on eight imaging techniques (reflectance confocal microscopy, computer-aided imaging analysis, optical coherence tomography, infrared photography, third-harmonic generation microscopy, multiphoton microscopy, ultraviolet light photography, and visible light/digital photograph), and three biophysical approaches (dermoscopy, colorimetry, spectrometry) used in diagnosing and assessing vitiligo.

2. Materials and methods

2.1. Study design

A systematic review was carried out using the Preferred Reporting Items for Systematic Reviews and Meta-Analyses (PRISMA) checklist and is registered in the International Prospective Register of Systematic Reviews (PROSPERO) database (CRD42023395996) (7).

2.2. Search strategy

Four electronic databases—Scopus, Embase, Cochrane Library, and Web of Science—were used for a comprehensive literature search. The search was based on studies that used objective, non-invasive imaging and biophysical skin measuring methods to diagnose, evaluate the severity of, or monitor the effects of vitiligo treatment. A literature search and examination of PubMed MeSH terms were used to obtain skin measurement diagnostic techniques. The following criteria included the principal search words: "vitiligo, diagnosis, and assessment." An exhaustive list of all search terms used can be found in Supplementary material 1. If more data from the study was required, the authors were contacted. Additionally, a manual search was performed through the related articles' references list for relevant sources.

2.3. Eligibility criteria

Inclusion criteria included: (1) randomized controlled trials, non-randomized controlled trials, cohort studies, case series, and case reports; (2) studies that involved the assessment of cutaneous vitiligo (including segmental, nonsegmental, universal, generalized, mucosal, follicular, guttate, and hypopigmented vitiligo); (3) non-invasive objective imaging/biophysical tools for vitiligo diagnostic and measurement; (4) the investigation offered reliable data that could be studied, including the total number of participants and the insightful outcomes of each metric.

Exclusion criteria included: (1) invasive objective imaging/biophysical tools for vitiligo diagnostic and measurement; (2) research that did not offer adequate information on results in experimental or control groups; (3) *in vitro* and animal studies; (4) research reported in languages other than English; (5) meta-analysis, systematic reviews, and other reviews (not including primary source); (6) studies lacking full-text or only presenting abstracts.

The term "non-invasive" was defined as any procedure that theoretically cannot cause skin irritation, bleeding, or scarring. This criterion excluded biopsies, the epilation of eyelashes or hairs, the application of tape or glue to the skin, and the collection of excretions from sebaceous follicles or scrapings. Figure 1 depicts the PRISMA selection process flowchart used for this systematic review.

2.4. Data extraction

All four databases were searched to include published studies from inception until July 2, 2023. 8601 identified articles were independently reviewed for eligibility using the Covidence systematic review software by two authors (P. A. and M.A.) after duplicate removal from the list of publications. After an initial title and abstract screening, 192 articles underwent a full-text examination to determine their eligibility. A total of 64 studies remained after a full-text review for qualitative synthesis. Conflicts were settled through discussion or consulting a third, unbiased investigator (C.F). The study design, participant count, vitiligo

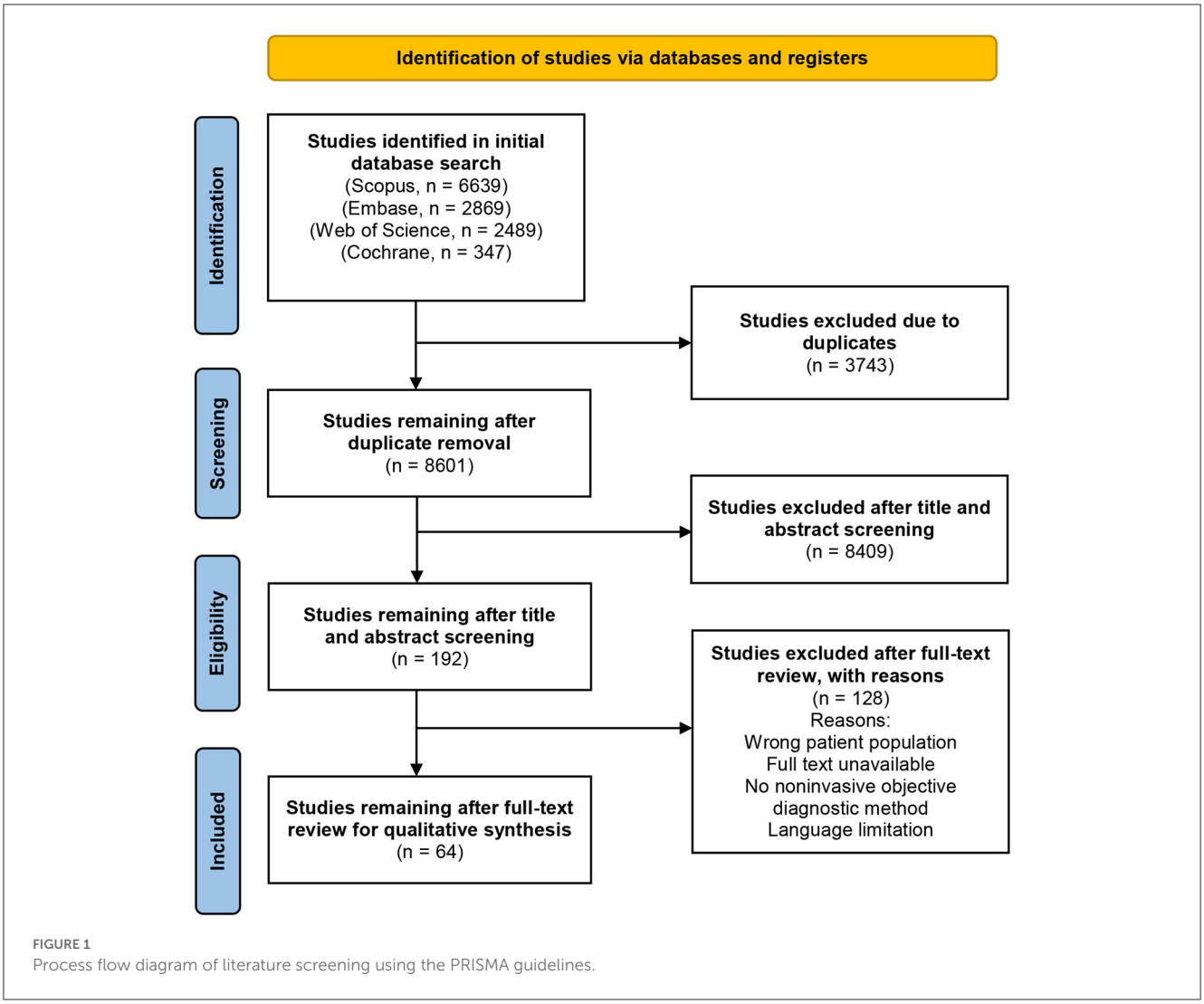

FIGURE 1
Process flow diagram of literature screening using the PRISMA guidelines.

classification, measurement sites, evaluated skin parameters, and study findings were extracted. Imaging techniques, and biophysical approaches were each given a narrative synthesis. Information about each method's advantages, limitations, and measurement principles was tabulated. Statistical analysis was not feasible due to the wide variety of tests evaluated and the non-standardized presentation of diagnostic accuracy outcomes.

2.5. Quality assessment

In this systematic review, the authors employed the Quality Assessment of Diagnostic Accuracy Studies (QUADAS-2) tool to assess the quality of the studies included (8). Two independent reviewers (P. A. and M.A.) evaluated the risk of bias, and any discrepancies were worked out through discussion or by consulting a third, unbiased investigator (C.F). The QUADAS-2 tool has four domains: patient selection, index test, reference standard, and flow and timing. Each domain has questions that assess the risk of bias and applicability of the study and addresses issues related to patient selection, index tests, reference standard validity, and potential bias in patient flow. The QUADAS-2 tool does not incorporate a quality score.

3. Results

3.1. Study characteristics

In total, 64 articles describing eight imaging modalities and three biophysical approaches utilized in diagnosing and evaluating vitiligo were included in this systematic review for analysis. Due to the employment of multiple diagnostics methods, several studies were included in numerous categories to ensure a holistic overview. Table 1 lists all imaging methods and biophysical skin measuring modalities considered for this review, along with the advantages and limitations of each technique.

TABLE 1 Summary table of imaging, biophysical and manual non-invasive techniques used in vitiligo diagnostics and therapy monitoring.

Classification of method	Technique	Study design(s)	Measurement principle	Advantages	Limitations
Imaging	Reflectance confocal microscopy (9–19)	10 cross-sectional; 1 case series	High-resolution cellular imaging of the epidermis and superficial dermis, based on the confocal principle	High-resolution; real-time imaging; surface imaging; multiplexing; fast procedure (10 minutes); portable system; cost-effective compared to another microscopy	Limited depth sensitivity; Lower signal-to-nose-ratio; requires smooth sample preparation; extensive training requirements for diagnostic interpretation; no z-axis imaging; sample specificity
	Computer-aided imaging analysis (20–37)	16 cross-sectional; 2 methodological; 1 prospective open label; 1 multiple-reader multiple-case diagnostic	Image processing using various methods including, ANN, CNN, DNN, PCA, ICA, fuzzy clustering, K-mean, GLCM, linear clustering	Comprehensive quantification; portable; mapping of facial distributions; machine learning capabilities; non-skin contact	Lack of imaging in z-axis; lacking real-time imaging; very expensive; extensive training requirements for diagnostic interpretation; novel techniques, without standard method
	Optical coherence tomography (38–41)	4 cross-sectional	Low-coherence interferometry to detect reflections of an infrared light source, which are used to create an image of the scanned tissue until the reticular dermis	Real-time imaging; rapid (2–10 min); cross-sectional imaging comparable to histology; deep surface penetration depth (1.5 mm); wide field of view; high spatial resolution (3–10 μm^2)	Extensive training requirements for diagnostic interpretation; expensive; lower axial resolution than RCM; lower resolution at reticular dermis; lowered image quality in uneven skin; only architectural changes; limited subcellular details
	Infrared photography (42)	1 cross-sectional	Utilizes the infrared domain of the electromagnetic spectrum for tissue assessment.	Painless; easy to use; rapid; cost-effective; real-time results; objective diagnostics	Equipment sensitivity; limited information on deep structures; operator dependence; no differentiation between arterial and venous structures; training needed for image interpretation
	Multiphoton microscopy (43, 44)	2 cross-sectional	Pulsed lasers to excite multiple low-energy photons, allowing high-resolution visualization of melanocyte density and distribution	High-resolution; label-free; real-time imaging; deep tissue penetration; multiparametric imaging; preservation of tissue integrity	Restricted field of view; lack of standardization; small sample size
	Third-harmonic generation microscopy (45)	1 cross-sectional	Nonlinear optical response of biological tissues, with melanin providing strong THG contrast in human epidermis	High-resolution; real-time imaging; non-toxic; cost-effective compared to another microscopy	Lack of standardization; limited availability; lack of specificity; small sample size; limited information on deep structures
	Ultraviolet light photography (46–52)	4 cross-sectional; 3 case series	Ultraviolet light emitted at wavelengths of 320–450 nm (peak 365 nm) to improve visual contrast. Melanin in the epidermis absorbs UV rays more selectively than visible light.	Improved accuracy compared to visible light; cost-effective; painless; easy to use; real-time results; portable; non-radiative	False negative results, particularly in darker skin tones; operator dependence; may be limited by lighting conditions; uneven skin color may make it difficult to assess the extent and distribution of depigmented skin
	Visible light and digital photography (53, 54)	2 cross-sectional	Capture and storage of digital photograph	Visual database; potential use in telemedicine	Limited color accuracy; interobserver variability; image quality affected by lighting conditions, technical ability; need for further validation
Biophysical	Dermoscopy (46, 49, 55–63)	8 cross-sectional; 2 case series; 1 cohort	Transillumination of a lesion to investigate with high magnification (usually 10-fold) to visualize subtle colors, features, and microstructures in epidermis and papillary dermis	Cost-effective; real-time; reduced surface shining; easily applicable; improved diagnostic accuracy; early detection; increased patient satisfaction; Improved inter-observer agreement; better patient education; avoidance of pressure artifacts (no fluid immersions needed)	Operator dependence; limited specificity; limited information on deep structures; difficulty with dark skin; training needed for image interpretation; no quantitative analysis; interobserver variability;
	Colorimetry (64, 65)	1 cross-sectional; 1 case series	Quantifies skin color and evaluates pigmentation response to treatment, based on the principle of Beer-Lambert's Law	Standardization; quantification of color; suitable for all skin types; portable; safe	Limited sensitivity and specificity; potential observer bias; interference from adjacent pigmented areas; regular calibration needed
	Spectrometry (66–71)	5 cross-sectional; 1 cohort	Assess disease activity in vitiligo with optical signals with high spectral resolution	Safe; portable; cost effective; objective measure; easy to use; quantifiable; ultrafast (<10 seconds analysis time)	Limited sensitivity and specificity; potential observer bias; sensitivity to environmental factors; complexity

3.2. Imaging techniques

3.2.1. Ultraviolet light photography

Ultraviolet (UV) light serves as a standard and extensively employed diagnostic tool for evaluating vitiligo. Among the reviewed studies, UV light was utilized as a diagnostic technique in seven studies, with Wood's lamp being the preferred choice in six of them (46–51, 55). The theory behind UV light photography suggests that UV rays are selectively absorbed by melanin in the epidermis compared to visible light. This theory is primarily discussed in the context of using UV cameras. However, when it comes to diagnosing vitiligo specifically, most studies relied on standard cameras that capture images within the visible spectrum only. Therefore, the prominent visualization of vitiligo in photography mainly results from enhanced skin fluorescence due to the absence of superimposed pigment, rather than direct UV absorption. The most frequently used device to diagnose vitiligo using UV light is Wood's light, also called a Wood's lamp. It is a handheld device that emits long-wave UV light (wavelengths of 320–450 nm, peak 365 nm) and is equipped with a magnifying lens to enable close examination of the skin (47). Other devices for UV assessment have also been reported, including softboxes, camera flash, and high output flash. Uitentuis et al. discovered that varied UV set-ups produced significantly different quality images, with the high output flash technique producing the best characteristics for vitiligo assessment (47).

Furthermore, one study conducted by Kaliyadan et al. utilized a simple hand-held black-light source, specifically a rudimentary flashlight. This study revealed that the hand-held source was equally effective in detecting fluorescence or enhancing skin lesions, when compared to a standard Wood's lamp (55). Anbar et al. compared the accuracy of vitiligo lesion identification by dermatologists and patients with and without Wood's lamp (50). They observed that lesions outlined using Wood's lamp were significantly more prominent, leading to the detection of new clinically unseen lesions or the identification of expansions of clinically apparent lesions that were otherwise invisible under regular lighting conditions (50). Furthermore, the effectiveness of UV photography in monitoring disease stability has been demonstrated in multiple studies. For instance, Wang et al. conducted a study where Wood's lamp was utilized to assess vitiligo activity and disease stability, both crucial components for successful epidermal grafting surgery. The researchers observed that by examining amelanotic lesions with well-defined borders under Wood's lamp, which serves as an indicator of stability, dermatologists can identify suitable candidates for grafting. Moreover, the use of Wood's lamp facilitates the early detection of re-pigmentation, enabling accurate surveillance and evaluation of treatment outcomes (48).

3.2.2. Reflectance confocal microscopy

Reflectance confocal microscopy (RCM) was used in eleven studies for vitiligo diagnosis and treatment monitoring (9–19). RCM performed *in vivo* is a non-invasive and repetitive imaging technique that generates real-time images with a resolution like histological images. The components of a reflectance confocal microscope include objective and condenser lenses, a detector, and a light source in the form of a near-infrared laser beam. The laser beam is directed to a particular spot on the skin. The microscope produces images from the stratum corneum to the upper dermis, with a maximum imaging depth of 250 μm and may be used as a non-invasive optical biopsy. RCM analysis facilitates recognizing typical characteristics of affected vitiligo skin and may be beneficial in distinguishing vitiligo in contrast to other hypopigmentary conditions such as post-inflammatory hypopigmentation, nevus depigmentosus, or nevus anemicus. The main RCM characteristics of vitiligo lesions observed throughout the studies included an apparent loss of melanin in the lesioned skin, an indistinct boundary separating the affected from the surrounding normal skin, loss of integrity of the bright dermal papillary rings generally seen at the dermo-epidermal junction level, and highly refractile inflammatory cell infiltration at the edge of the lesions. RCM has been shown useful to differentiate between active or stable vitiligo, proving to be useful in predicting stability in vitiligo. Pertaining to stable vitiligo, there is complete loss of melanin in affected skin, with no changes in the content of melanin nor the dermal papillary rings. In active vitiligo, there is also a loss of melanin alongside a disappearance of the dermal papillary rings (9).

3.2.3. Computer-assisted imaging analysis

Currently, multiple approaches have been investigated for computer-assisted imaging analysis of vitiligo. The literature search found twenty studies which used variations of computer-assisted imaging analysis for vitiligo diagnostics.

Convolutional Neural Networks (CNNs) have shown promising results in vitiligo diagnosis and were utilized in eight studies (20–25). CNNs analyze skin images and classify them as either vitiligo or non-vitiligo lesions using a model involving multiple convolutional layers that identify patterns and a fully connected layer that performs the classification. A large dataset of labeled images is utilized to optimize the network performance and to minimize the difference between its predictions and the true labels.

Compared to human raters, including practicing dermatologists, dermatology residents, and general practitioners, CNNs outperformed all groups consistently. This suggests the efficacy of machine learning in classifying vitiligo by case probability and the possible advantages of CNN techniques as a remote diagnosis tool for vitiligo in situations involving telemedicine or where a Wood's lamp is not accessible (21, 26).

Principal component analysis (PCA) and independent component analysis (ICA) were proposed as mechanisms for analyzing vitiligo lesion segmentation and progression in five different studies (20, 27–30). While CNN, PCA, and ICA all use machine learning for image analysis, CNNs are non-linear supervised learning techniques, while PCA and ICA are linear unsupervised learning techniques. Generally, PCA is used to segment RGB images into melanin and hemoglobin only images, followed by ICA-powered alignment of the two principal component axes. In a study by Nugroho et al., a set of 41 RGB images of vitiligo lesions from 18 patients used a combinational

PCA and ICA. They concluded that at a 95% confidence interval, there was a high sensitivity (0.9105 ± 0.0161), specificity (0.9973 ± 0.0009), and accuracy values (0.9901 ± 0.0028) (29). This diagnostic accuracy was comparable to other studies using PCA and ICA (20, 27–30, 72).

Two studies used Fuzzy C-Means (FCM), a cluster-based algorithm, to segment vitiligo lesions (31, 32). The algorithm follows a two-step mechanism, whereby skin segmentation is followed by vitiligo-specific segmentation. Both studies demonstrated considerably fast processing, illustrating the algorithm's promise for use in clinical settings and applicability for teledermatology applications. As the algorithm accepts low-resolution images as input, picture acquisition can be readily carried out using smartphone cameras. Furthermore, Nugraha et al. implemented the FCM software to develop a mobile application called Vi-DA (Vitiligo Diagnostic Assistance), allowing vitiligo patients to self-assess at home (32).

One study used artificial neural networks (ANN) of multilayer perceptron (MLP) type to quantifiable measure skin depigmentation based on the pattern of light refraction (33). Based on the light refraction pattern, the MLP was taught to analyze each pixel in an image and classify it as either having healthy or affected skin. The MLP then produces a binary picture from the original image, where cells with 0 and 1 represent healthy and vitiligo-affected skin, respectively. Compared to ICA/PCA and FCM, the proposed method outperformed both methods in specificity and sensitivity over an 8-test span (33).

Several studies demonstrated that computer-assisted imaging analysis provided quantitative data on vitiligo lesion stability, namely, consistent coloration over time, with little variation in pigmentation intensity, relatively constant lesions sizes, showing minimal or no expansion or contraction, and well-defined, regular borders, suggesting a lack of active disease progression.

3.2.4. Optical coherence tomography

Four studies utilized Optical Coherence Tomography (OCT) for vitiligo assessment (38–41). OCT measures differences in optical path light, where one light path is directed to a tissue sample while the other is to a reference mirror (73). Through lateral scanning, OCT effectively constructs high-resolution two or three-dimensional cross-sectional images of microstructural morphology in biological tissue *in situ* (74, 75). A study by Su et al. demonstrated that OCT could effectively diagnose vitiligo in its early stages (40). This was accomplished by utilizing OCT for *in vivo* imaging to reconstruct a three-dimensional skin microstructure. This successfully identified any loss of pigment in the early stages of vitiligo, despite white patches of skin becoming prominent only in the later stages of the disease (40). Xie et al. came to a similar conclusion, supporting the efficacy of OCT in the early diagnosis of vitiligo (39).

Furthermore, detecting the stratum basale and dermal papillae is vital to diagnosing skin pigmentation disorders. To effectively identify such epidermal structures, OCT analyzes the low scattering property of the dermal papillae, contrasting it with the high scattering property of the pigmented basal layer (39). OCT's ability to autodetect such papillae structures are accomplished by scanning large areas of skin and assessing the decrease or absence of the scattering contrasting between the epidermal structures. Gao et al. studied OCT's ability to accurately quantify the optical path length, measuring *in vivo* tissue's refractive index (41). Their research demonstrated the ability of OCT to evaluate a lower refractive index in skin tissue with vitiligo, showcasing the contrast in scattering coefficients of skin with vitiligo versus without. This change in scattering coefficients was associated with a decrease in melanin content, thus confirming OCT's effectiveness in diagnosing vitiligo. Furthermore, OCT has shown promise in evaluating vitiligo stability. By analyzing the epidermal microstructure, OCT can identify well-defined lesion borders, preserved structural integrity, and relatively constant scattering coefficients in stable vitiligo cases. In contrast, unstable vitiligo was shown to exhibit irregular borders, disrupted epidermal architecture, and changes in scattering coefficients (41).

3.2.5. Visible light and digital photography

Two studies investigated the use of visible light and digital photography for assessing vitiligo (53, 54). As vitiligo is primarily a clinical diagnosis, visible light and digital photography are essential tools for clinicians to use for educational, clinical or telemedicine applications. To better aid physicians in their assessments, digital photography's capture and storage help create a visual database of clinical presentations. The construction of robust visual databases is the foundation for advanced computational analysis to improve early diagnosis, monitor high-risk patients, and diagnose atypical lesions (53). For telemedicine, when imagining quality is consistent and adequate, it can substitute for inpatient physical examinations in up to 83% of cases (53). A recent article from Geel et al. highlights the importance of standardization in photographing vitiligo to improve documentation and comparison among different sites to produce a more efficient and reliable interpretation of results (54). Under visible light, distinguishing between hypomelanosis and amelanosis in vitiligo patients, particularly those with very fair skin (Type I or II) or children, has been shown to be challenging (76).

3.2.6. Other techniques

Three more imaging techniques employed in vitiligo diagnosis include infrared photography, multiphoton microscopy and third-harmonic generation microscopy. Table 1 provides a summary of the detailed characteristics.

3.3. Biophysical techniques

3.3.1. Dermoscopy

Dermoscopy, also known as epiluminescence microscopy, is a real-time, dynamic, nondiagnostic tool that enables *in vivo* examination of skin lesions. Clinically, dermoscopy is widely used in vitiligo diagnostics due to its ability to enhance visualization and detect subtle changes in pigmentation and skin lesions that may be difficult to discern with the naked eye. The technique involves using a handheld instrument equipped with a polarized light source and magnifying lens to visualize the epidermal layer's microstructures and the skin's superficial dermis. Dermoscopy can provide valuable

information about the structure and appearance of affected vitiligo skin lesions, allowing for improved diagnostic accuracy.

Dermoscopy was utilized in eleven different studies (46, 49, 55–63), of which two studies used ultraviolet light (46, 49), and one used high dynamic range conversion of images for diagnostic and monitoring purposes (55). Perifollicular changes and interfollicular pigmentation constituted the most common dermoscopic observations seen by Al-Refu et al. and Jha et al. (56, 57). Two studies showed that employing UV-dermoscopy can identify various distinctive microscopic characteristics of vitiligo not seen in polarized dermoscopy, namely, an enhanced perifollicular border and a more distinguishable depigmented junctional zone (46, 49). Kaliyadan et al. observed that prominent pigmentary features were perceived to show significant enrichments after HDR conversion (55). Furthermore, a novel study by Scarfi et al. proposed utilizing fluorescence-advanced videodermatoscopy which enables dynamic examination of superficial skin structures with a cellular resolution and holds potential for improved disease monitoring, prognosis, and treatment outcomes in vitiligo patients (58). Dermoscopy also offers valuable insights into assessing disease stability in vitiligo by identifying key features such as indistinct boundaries, perifollicular depigmentation, satellite lesions, and the micro-Koebner phenomenon. These characteristics are significantly associated with active vitiligo. Conversely, the presence of perifollicular repigmentation serves as a promising indicator of vitiligo stabilization. These insights can assist in evaluating the activity of vitiligo lesions and provide useful guidance for patient counseling regarding disease prognosis.

3.3.2. Colorimetry

The colorimeter is a non-invasive instrument used to quantify skin color and has also been utilized to determine the capacity for pigmentation. Colorimetry allows for objective quantification of epidermal changes associated with vitiligo and offers a standardized approach to evaluating disease stability. By precisely measuring parameters such as luminance value and melanin index, colorimetry provides valuable insights into the progression and response to treatment in vitiligo. Two articles illustrate the potential role and efficacy of the colorimeter as a non-invasive diagnostic tool for diagnosing vitiligo and its severity (64, 65). Brazzelli et al. used a portable colorimeter to evaluate the progressive development of vitiligo patches in a Caucasian male. The colorimeter evaluated an area of 8 mm^2 in diameter of skin over four months, and they found the luminance value significantly increased, indicating increased relative lightness and depigmentation.

Tawfik et al. utilized colorimetry to evaluate the treatment response of vitiligo to narrow-band UVB phototherapy over the course of six months. The results were significant for regimentation in 90% of patients, as shown by an increase in melanin index, indicating improved stability of vitiligo lesions. An important finding was that the colorimeter could assess regimentation a month before it was apparent clinically, implicating its potential use as a prognostic tool (27). Compared to other measurement assessment techniques, such as the point counting method, colorimetry was found to be less time intensive and more standardized across all anatomic regions (27).

3.3.3. Spectrometry

Six studies investigated the use of spectrometry in vitiligo assessment (66–71). These non-invasive tools can be used to assess disease activity in vitiligo patients. Spectrometers are portable tools used to investigate the physiological and morphological properties of skin tissue by utilizing optical signals with a high spectral resolution (72). The spectrometry mechanism of action involves exposing the epidermal surface to white light produced by an incandescent source. Melanin, one of the skin's chromophores, absorbs the majority of incoming light but exhibits a monotonic rise in intensity as wavelengths get shorter (absorption is almost wholly attenuated for wavelengths longer than 700 nm) (68). Spectrometers then detect backscattered photons emerging from various layers of skin tissue, resulting in a tissue surface emission profile. De Bruyne et al. used spectrometry on the perilesional skin of 70 vitiligo patients in different anatomic regions and noted a classification model generating a correct prediction in 82.9% of the cases (66). Poojary et al. analyzed using a portable fluorescence spectrometer for diagnosing vitiligo in 260 patients and recorded a similar sensitivity and specificity of 74.6% and 73%, respectively (67). They also observed a critical point (cut-off) of 975.995 nm to differentiate vitiligo from other hypopigmented with an increased sensitivity of 93.1% and specificity of 86.4%. Hegyi et al. utilized diffuse reflectance spectroscopy with an experimental spectrophotometer to measure skin pigmentation in patients with vitiligo undergoing PUVA therapy. They saw an increase in pigmentation compared to pre-treatment as demonstrated by a statistically significant difference in pre- and post-treatment melanin quantification (70). Park et al. utilized a narrow-band reflectance spectrophotometer to measure melanin indexes (Mis), relative melanin indexes (RMIs), and erythema to differentiate between two similar hypopigmented disorders, vitiligo and nevus depigmentosus (ND) (71). The study found that the mean Mis and RMIs are statistically different between patients with vitiligo and ND, with mean RMI scores of 50% and 74% for vitiligo and ND patients, respectively. Spectrometry techniques also offer a non-invasive means to assess vitiligo disease activity. Unlike invasive blood markers, spectrometry offers immediate and real-time information about the specific conditions of the skin and its biochemical alterations. Stability evaluation relies on monitoring the absence of significant changes in biochemical parameters and presents with distinctive benefits, including rapid analysis (<10 s), portability, and compactness, making it suitable for use in a dermatologist's office during consultations (66).

3.4. Quality assessment

Supplementary material 2 displays a visual representation of the methodological risk of bias assessment measured using the QUADAS-2 tool. The quality assessment of the included studies revealed a generally satisfactory level, as most studies demonstrated a low or unclear risk of bias. Notably, Domain 1 (Risk of Bias:

Patient Selection) exhibited the highest risk, while Domain 2 (Risk of Bias: Index Test) demonstrated the lowest level of bias (Supplementary material 3).

4. Discussion

There is a significant need for non-invasive objective skin measurement methods that can accurately diagnose and monitor the progression of vitiligo. This systematic review analyzed 64 studies on various non-invasive diagnostic modalities, including eight imaging techniques, and three biophysical methods. This is especially useful for clinical practice but may also contribute to further research advancements.

Imaging techniques offer valuable insights into the structural changes in the epidermis that occur with vitiligo, which may contribute to a deeper understanding of the underlying pathogenesis. Another advantage of these techniques is their ability to provide highly detailed images and provide more accurate and objective information about the distribution and extent of depigmentation, aiding in earlier-stage diagnoses, which can be particularly important in detecting the progression of vitiligo and monitoring the efficacy of treatments (68). Using computer-assisted imaging analysis, particularly machine learning, is a relatively new and emerging field. Machine learning algorithms can be trained to analyze images of the skin and provide highly accurate assessments of the extent and progression of the condition. Unlike traditional imaging techniques, which rely on human interpretation, machine learning algorithms can provide consistent and unbiased assessments of the skin (26). This can be especially useful for large-scale studies and for tracking skin changes over time. Machine learning algorithms can be trained to identify specific patterns and features in images of the skin, which can be used to distinguish between different types of pigmentary disorders, which can be particularly important for the accurate diagnosis of vitiligo, as it is often misdiagnosed (77). However, there are also some limitations to the use of imaging techniques for the diagnosis of vitiligo. For reliable and repeatable results, imaging equipment can be expensive to acquire and requires stringent procedures to be followed by experienced professionals. Resolution and penetration depth are also restricted for imaging techniques, including RCM and infrared photography (12). Due to the lack of a capillary form standard, it may be challenging to quantify vessel abnormalities using these imaging techniques (14). Some imaging techniques, such as RCM and OCT, are not portable and are more expensive than other diagnostic modalities, straining accessibility for clinicians (39). Similarly, computer-assisted imaging analyses have shown promise in vitiligo diagnosis; however, they are limited in their dependence on training data and ability to identify rare or unusual cases (24).

One key advantage of biophysical methods such as spectrometry and colorimetry over imaging techniques is the ability to measure color and reflectance properties of the skin quantitatively, providing healthcare professionals with a more precise understanding of the extent and severity of pigmentation loss (66). Furthermore, all these techniques are portable, rapid, and objective measurement techniques. While biophysical techniques offer several advantages in diagnosing and assessing vitiligo, they also have some limitations that should be considered. One limitation is the sensitivity and specificity of these techniques, particularly colorimetry, and spectroscopy, which can be affected by factors such as skin hydration, skin oiliness, and skin temperature (78). To ensure accurate and reliable results, it is essential to standardize the conditions under which these measurements are performed and to use validated protocols and devices.

It is also pertinent to mention the available scales for assessing the extent and severity of vitiligo, each with its own strengths and limitations. These techniques combine visual assessment and quantitative measurements to evaluate the size, location, and progression of depigmented patches on the skin. The scores generated by these assessments play a crucial role in tracking the condition's progression and evaluating the effectiveness of treatment interventions. One commonly used technique is the Vitiligo Area Scoring Index (VASI), which divides the affected skin into four body regions and assigns a score based on the percentage of affected skin. However, it may not provide a comprehensive evaluation in cases of irregularly shaped patches or those located in hard-to-see areas (4). Another widely used metric is the Vitiligo Extent Score (VES). The VES assesses vitiligo in 19 body regions using template photographs, however, does not account for the back of the scalp, the soles of the feet, or the palms of the hands. and has shown higher dependability and usability compared to VASI. A simplified version of the VES, known as the Self-Assessment Vitiligo Extent Score (SA-VES), was developed as a patient-reported outcome measure. The SA-VES demonstrated excellent reliability and correlation with physicians' assessments, offering a user-friendly and practical approach for assessing vitiligo extent in clinical practice and research. In most validation studies included in this review, the VES showed higher dependability and usability compared to the Vitiligo Area Scoring Index (4–6, 79). The Vitiligo Disease Activity Score (VIDA) evaluates disease activity on a six-point scale based on patient self-reported assessments (80). While initially promising, a recent study by Coias et al. found the VIDA to be an unreliable assessment of disease activity, as VIDA scores did not correlate with changes in VASI scores over time, indicating patients' inaccurate prediction of disease activity (81). The Vitiligo European Task Force (VETF) assessment combines the evaluation of vitiligo extent, disease stage (staging), and disease progression (spreading). To assess the extent of vitiligo, the rule of nines, which is already utilized in atopic dermatitis assessment, is employed (82). In addition to these metrics, the Potential Repigmentation Index (PRI) is used to evaluate the extent of pigment loss, while the Patient-administered Vitiligo Screening Tool (VISTO) tracks symptoms and signs associated with vitiligo (83, 84). Recently, a novel metric called the Vitiligo Extent Tensity Index (VETI) has been proposed. The VETI score combines elements of VASI, VETF, and parts of PRI to create a more comprehensive system that offers reproducible numerical ratings and reduced interobserver variability (85). The point counting is a simple, precise, and useful technique that is frequently used to estimate irregularly shaped skin surface areas and was adapted for vitiligo by Aydin et al. (86).

The results of this systematic study should be evaluated considering various limitations and potential biases. Several

studies in this systematic review had limited sample sizes, which impacted the generalizability of the results, hindering follow-up data from assessing the long-term effects of the different diagnostic methods. For practical linguistic reasons, English was the only language permitted for published studies, which has the potential to introduce language bias. Another limitation is that many of the studies provided an inadequate description of measurement sites, and there was often a lack of standardization and validation in the methods used. Moreover, due to the complexity of vitiligo symptoms, most methods could only measure a limited number of parameters. Subsequently, the information obtained may not be conclusive with a single diagnostic modality. Despite the abovementioned limitations, several methods exhibit encouraging potential for improved diagnosis and assessment, particularly in clinical and research contexts. Outside the widely used methods such as dermoscopy and Wood's lamp, RCT may be used as a non-invasive optical biopsy, computer-assisted imaging techniques can provide an effective remote diagnosis and allow patients to perform self-assessment at home, and spectroscopy and colorimetry are portable, rapid, and objective measurement techniques that may be particularly beneficial as an adjuvant to other diagnostic tools.

5. Conclusions

In conclusion, this systematic review summarizes the non-invasive imaging, biophysical, and manual methods now available for vitiligo diagnosis, severity evaluation, and therapeutic monitoring. While several of these techniques show promise and offer valuable insights regarding the structure and characteristics of vitiligo skin that cannot be obtained from the naked eye alone, suitable and verified protocols are required for further use of these tools in clinical and research settings. The systematic review provides valuable information for healthcare providers by offering a comprehensive summary of the available diagnostic techniques for vitiligo. The review results provide insight into each method's strengths and limitations and can inform clinical practice by guiding future research.

Data availability statement

The original contributions presented in the study are included in the article/Supplementary material, further inquiries can be directed to the corresponding author.

Author contributions

PA and MA contributed to the study design, including search strategy preparation, article screening, and data extraction and interpretation. PA, MA, CF, AC, AK, SQ, and HM were involved in drafting, revising, preparing the manuscript, and agreed to be accountable for all parts of the work and authorized the final version for submission. All authors contributed to the article and approved the submitted version.

Conflict of interest

The authors declare that the research was conducted in the absence of any commercial or financial relationships that could be construed as a potential conflict of interest.

Publisher's note

Supplementary material

The Supplementary Material for this article can be found online at: https://www.frontiersin.org/articles/10.3389/fmed.2023.1200963/full#supplementary-material

SUPPLEMENTARY MATERIAL 1
Keywords and search strategy (Ti, title; Ab, abstract; Kw, keywords; TS, topic (encompasses title, abstract, author keywords, keywords plus).

SUPPLEMENTARY MATERIAL 2
QUADAS-2 risk-of-bias quality assessment presented for 64 studies.

SUPPLEMENTARY MATERIAL 3
Weighted bar plots of the distribution of risk-of-bias judgements within each bias domain for included studies.

References

1. Bergqvist C, Ezzedine K. Vitiligo: a review. *Dermatology*. (2020) 236:571–92. doi: 10.1159/000506103

2. K Alghamdi KM, Kumar A, Taïeb A, Ezzedine K. Assessment methods for the evaluation of vitiligo. *J Eur Acad Dermatol Venereol*. (2012) 26:1463–71. doi: 10.1111/j.1468-3083.2012.04505.x

3. Abdi P, Maibach HI, Farkouh C, Law RM, Awad C. Lessons learned from anatomic susceptibility in vitiligo patients: a systematic review. *Curr Dermatol Rep*. (2023) 4:e384. doi: 10.1007/s13671-023-00384-x

4. Merhi R, Canu D, Barnetche T, Duchez E, Gey A, Andreu N,, et al. Assessment of vitiligo area scoring index (VASI), facial-VASI and vitiligo extent score using standardized photography of patients with vitiligo. *Br J Dermatol*. (2022) 187:422–4. doi: 10.1111/bjd.21246

5. van Geel N, Lommerts JE, Bekkenk MW, Prinsen CA, Eleftheriadou V, Taieb A, et al. Development and validation of a patient-reported outcome measure in vitiligo: The self assessment vitiligo extent score (SA-VES). *J Am Acad Dermatol*. (2017) 76:464–71. doi: 10.1016/j.jaad.2016.09.034

6. van Geel N, Lommerts JE, Bekkenk MW, Prinsen CA, Eleftheriadou V, Taieb A. Reliability, validity and feasibility of the vitiligo extent score (VES) and self-assessment vitiligo extent score (SA-VES) among vitiligo patients: a cross-cultural validation. *Clin Cosmet Investig Dermatol*. (2021) 14:949–57. doi: 10.2147/CCID.S324073

7. Moher D, Liberati A, Tetzlaff J, Altman DG, PRISMA Group. Preferred reporting items for systematic reviews and meta-analyses: the PRISMA statement. *BMJ*. (2009) 339:b2535. doi: 10.1136/bmj.b2535

8. Whiting PF, Rutjes AW, Westwood ME, Mallett S, Deeks JJ, Reitsma JB, et al. QUADAS-2: a revised tool for the quality assessment of diagnostic accuracy studies. *Ann Intern Med*. (2011) 155:529–36. doi: 10.7326/0003-4819-155-8-201110180-00009

9. Lai LG, Xu AE. *In vivo* reflectance confocal microscopy imaging of vitiligo, nevus depigmentosus and nevus anemicus. *Skin Res Technol Off J Int Soc Bioeng Skin ISBS Int Soc Digit Imaging Skin ISDIS Int Soc Skin Imaging ISSI*. (2011) 17:404–10. doi: 10.1111/j.1600-0846.2011.00521.x

10. Liu H, Wang L, Lin Y, Shan X, Gao M. The differential diagnosis of hypopigmented mycosis fungoides and vitiligo with reflectance confocal microscopy: a preliminary study. *Front. Med*. (2020) 7:609404 doi: 10.3389/fmed.2020.609404

11. Wei LI, Wang S, Xu AE. Role of *in vivo* reflectance confocal microscopy in determining stability in vitiligo: a preliminary study. *Indian J Dermatol*. (2013) 58:429–32. doi: 10.4103/0019-5154.119948

12. Kang HY, Bahadoran P, Ortonne JP. Reflectance confocal microscopy for pigmentary disorders. *Exp Dermatol*. (2010) 19, 233–9. doi: 10.1111/j.1600-0625.2009.00983.x

13. Xiang WZ, Xu AE, Xu J, Bi ZG, Shang YB, Ren QS. The application of dermal papillary rings in dermatology by in vivo confocal laser scanning microscopy. *Laser Phys*. (2010) 20:1767–73. doi: 10.1134/S1054660X10150016

14. Xiang W, Xu A, Xu J, Bi Z, Shang Y, Ren Q. *In vivo* confocal laser scanning microscopy of hypopigmented macules: a preliminary comparison of confocal images in vitiligo, nevus depigmentosus and postinflammatory hypopigmentation. *Lasers Med Sci*. (2010) 25:551–8. doi: 10.1007/s10103-010-0764-2

15. Xiang W, Song X, Peng J, Xu A, Bi Z. Real-time in vivo confocal laser scanning microscopy of melanin-containing cells: a promising diagnostic intervention. *Microsc Res Tech*. (2015) 78:1121–7. doi: 10.1002/jemt.22594

16. Pan ZY, Yan F, Zhang ZH, Zhang QA, Xiang LH. *In vivo* reflectance confocal microscopy for the differential diagnosis between vitiligo and nevus depigmentosus. *Int J Dermatol*. (2011) 50:740–5. doi: 10.1111/j.1365-4632.2010.04841.x

17. Ardigo M, Malizewsky I, Dell'Anna ML, Berardesca E, Picardo M. Preliminary evaluation of vitiligo using in vivo reflectance confocal microscopy. *J Eur Acad Dermatol Venereol*. (2007) 21:1344–50. doi: 10.1111/j.1468-3083.2007.02275.x

18. Gu J, Xia R, Zou Y. Reflectance confocal microscopy for identification of vulvar lichen sclerosus et atrophicus and vitiligo. *Am J Dermatopathol*. (2022) 44:867–73. doi: 10.1097/DAD.0000000000002269

19. Rajadhyaksha M, Grossman M, Esterowitz D, Webb RH, Anderson RR. *In vivo* confocal scanning laser microscopy of human skin: melanin provides strong contrast. *J Invest Dermatol*. (1995) 104:946–52. doi: 10.1111/1523-1747.ep12606215

20. van Geel N, Vandendriessche D, Vandersichel E, De Schepper S, Grine L, Mertens L, et al. Reference method for digital surface measurement of target lesions in vitiligo: a comparative analysis. *Br J Dermatol*. (2019) 180:1198–205. doi: 10.1111/bjd.17190

21. Zhang L, Mishra S, Zhang T, Zhang Y, Zhang D, Lv Y, et al. Design and assessment of convolutional neural network based methods for vitiligo diagnosis. *Front Med*. (2021) 8:754202. doi: 10.3389/fmed.2021.754202

22. Pangti R, Mathur J, Chouhan V, Kumar S, Rajput L, Shah S, et al. A machine learning-based, decision support, mobile phone application for diagnosis of common dermatological diseases. *J Eur Acad Dermatol Venereol JEADV*. (2021) 35:336–545. doi: 10.1111/jdv.16967

23. Luo W, Liu J, Huang Y, Zhao N. An effective vitiligo intelligent classification system. *J Ambient Intell Humaniz Comput*. (2020) 3:5. doi: 10.1007/s12652-020-02357-5

24. Guo L, Yang Y, Ding H, Zheng H, Yang H, Xie J, et al. A deep learning-based hybrid artificial intelligence model for the detection and severity assessment of vitiligo lesions. *Ann Transl Med*. (2022) 10:590. doi: 10.21037/atm-22-1738

25. Jain A, Way D, Gupta V, Gao Y, de Oliveira Marinho G, Hartford J, et al. Development and assessment of an artificial intelligence-based tool for skin condition diagnosis by primary care physicians and nurse practitioners in teledermatology practices. *JAMA Netw Open*. (2021) 4:e217249. doi: 10.1001/jamanetworkopen.2021.7249

26. Yanling LI, Kong AW, Thng S. Segmenting vitiligo on clinical face images using CNN trained on synthetic and internet images. *IEEE J Biomed Health Inform*. (2021) 25:3082–93. doi: 10.1109/JBHI.2021.3055213

27. Nugroho H, Fadzil MA, Yap VV, Norashikin S, Suraiya HH. Determination of skin repigmentation progression. *Annu Int Conf IEEE Eng Med Biol Soc IEEE Eng Med Biol Soc Annu Int Conf*. (2007) 54:3442–5. doi: 10.1109/IEMBS.2007.4353071

28. Shamsudin N, Hussein SH, Nugroho H, Ahmad Fadzil MH. Objective assessment of vitiligo with a computerised digital imaging analysis system. *Australas J Dermatol*. (2015) 56:285–9. doi: 10.1111/ajd.12247

29. Nugroho H, Ahmad Fadzil MH, Shamsudin N, Hussein SH. Computerised image analysis of vitiligo lesion: evaluation using manually defined lesion areas. *Skin Res Technol Off J Int Soc Bioeng Skin ISBS Int Soc Digit Imaging Skin ISDIS Int Soc Skin Imaging ISSI*. (2013) 19:e72–7. doi: 10.1111/j.1600-0846.2011.00610.x

30. Fadzil MA, Norashikin S, Suraiya HH, Nugroho H. Independent component analysis for assessing therapeutic response in vitiligo skin disorder. *J Med Eng Technol*. (2009) 33:101–9. doi: 10.1080/03091900802454459

31. Nurhudatiana. A computer-aided diagnosis system for vitiligo assessment: a segmentation algorithm. In *Intelligence in the Era of Big Data*, R. Intan, C. H. Chi, H. N. Palit, and L. W. Santoso, Eds., in Communications in Computer and Information Science. Berlin, Heidelberg: Springer. (2015) 4:323–31. doi: 10.1007/978-3-662-46742-8_30

32. Nugraha GA, Nurhudatiana A, Bahana R. Vi-da: vitiligo diagnostic assistance mobile application. *J Phys Conf Ser*. (2018) 978:012003. doi: 10.1088/1742-6596/978/1/012003

33. Chica JF, Zaputt S, Encalada J, Salamea C, Montalvo M. Objective assessment of skin repigmentation using a multilayer perceptron. *J Med Signals Sens*. (2019) 9:88–99. doi: 10.4103/jmss.JMSS_52_18

34. Nanny VA, Vander Haeghen Y, Ongenae K, NAEYAERT JM. A new digital image analysis system useful for surface assessment of vitiligo lesions in transplantation studies. *Eur J Dermatol EJD*. (2004) 14:150–5.

35. Neri P, Fiaschi M, Menchini G. Semi-automatic tool for vitiligo detection and analysis. *J Imaging*. (2020) 6:14. doi: 10.3390/jimaging6030014

36. Saini K, Singh S. Vitiligo disease prediction using K-mean, GLCM and voting classification. *AIP Conf Proc*. (2022) 25:020013. doi: 10.1063/5.0109172

37. Toh JJ, Bhoi S, Tan VW, Chuah SY, Jhingan A, Kong AW, et al. Automated scoring of vitiligo using superpixel-generated computerized digital image analysis of clinical photographs: a novel and consistent way to score vitiligo. *Br J Dermatol*. (2018) 179:220–1. doi: 10.1111/bjd.16563

38. Fouad YA, Salman AG, Mohamed TH, Abdelgawad RH, Hassen SI. Assessment of the Effect of vitiligo on subfoveal choroidal thickness using spectral-domain optical coherence tomography. *Clin Ophthalmol*. (2020) 14:2265–70. doi: 10.2147/OPTH.S255554

39. Xie J, Hao T, Li C, Wang X, Yu X, Liu L. Automatic evaluation of stratum basale and dermal papillae using ultrahigh resolution optical coherence tomography. *Biomed Signal Proc Control*. (2019) 53:101527. doi: 10.1016/j.bspc.2019.04.004

40. Su PH, Huang BH, Ng CY, Chang FY, Tsai MT. Characterization of vitiligo with optical coherence tomography. In *Biomedical Imaging and Sensing Conference 2021*, SPIE. (2021) 2:186–7. doi: 10.1117/12.2615970

41. Gao W, Lee P, Zhang X. Characterization of vitiligo by in vivo scattering coefficient of human skin. *J Innov Opt Health Sci*. (2011) 04:67–72. doi: 10.1142/S1793545811001216

42. Huang Z, Zeng H, Hamzavi I, Alajlan A, Tan E, McLean DI, et al. Cutaneous melanin exhibiting fluorescence emission under near-infrared light excitation. *J Biomed Opt*. (2006) 11:34010. doi: 10.1117/1.2204007

43. Shiu J, Zhang L, Lentsch G, Flesher JL, Jin S, Polleys C, et al. Multimodal analyses of vitiligo skin idenitfy tissue characteristics of stable disease. *JCI Insight*. (2023) 713:e154585. doi: 10.1172/jci.insight.154585

44. Lentsch G. Advances in multiphoton microscopy for non-invasive assessment of human skin biology and disease. UC Irvine. (2021). Available online at: https://escholarship.org/uc/item/6ts3s5p9 (accessed July 03, 2023).

45. Liao YH, Su YH, Shih YT, Chen WS, Jee SH, Sun CK, et al. *In vivo* third-harmonic generation microscopy study on vitiligo patients. *J Biomed Opt*. (2020) 25:014504. doi: 10.1117/1.JBO.25.1.014504

46. Lu QS, Chen X, Wang S, Xu SS, Wu T, Jiang G. Dermoscopy combined with Wood lamp, a diagnostic alternative for five pigmented lesions on the face: an observational study. *Chin Med J*. (2020) 133:2771–2. doi: 10.1097/CM9.0000000000001009

47. Uitentuis SE, Bekkenk MW, van Geel N, de Rie MA, Wolkerstorfer A. UV light set-ups for vitiligo photography, a comparative study on image quality and ease of use. *J Eur Acad Dermatol Venereol. JEADV*. (2019) 33:1971–5. doi: 10.1111/jdv.15666

48. Wang YJ, Chang CC, Cheng KL. Wood's lamp for vitiligo disease stability and early recognition of initiative pigmentation after epidermal grafting. *Int Wound J*. (2017) 14:1391–4. doi: 10.1111/iwj.12800

49. Yuan M, Xie Y, Zheng Y, Zhang Z, Yang C, Li J. Novel ultraviolet-dermoscopy: early diagnosis and activity evaluation of vitiligo. *Skin Res Technol*. (2023) 29:e13249. doi: 10.1111/srt.13249

50. Anbar TS, Atwa MA, Abdel-Aziz RT, Hegazy RA, Ibrahim SI, El Genedy RM, et al. Subjective versus objective recognition of facial vitiligo lesions: detection of subclinical lesions by Wood's light. *J Egypt Women's Dermatol Soc*. (2022) 19:7. doi: 10.4103/jewd.jewd_42_21

51. Bae JM, Lee RW. 365-nm narrowband Wood's lamp for vitiligo and hypopigmentation disorders. *J Am Acad Dermatol*. (2020) 83:e283–e284. doi: 10.1016/j.jaad.2019.08.064

52. Kaliyadan F, Kuruvilla J. Using a hand-held black-light source instead of a Wood's lamp. *J Am Acad Dermatol.* (2015) 72:e153–4. doi: 10.1016/j.jaad.2015.02.1096

53. Ratner D, Thomas CO, Bickers D. The uses of digital photography in dermatology. *J Am Acad Dermatol.* (1999) 41:749–56. doi: 10.1016/s0190-9622(99)70012-5

54. van Geel N, Hamzavi I, Kohli I, Wolkerstorfer A, Lim HW, Bae JM, et al. Standardizing serial photography for assessing and monitoring vitiligo: a core set of international recommendations for essential clinical and technical specifications. *J Am Acad Dermatol.* (2020) 83:1639–46. doi: 10.1016/j.jaad.2019.10.055

55. Kaliyadan F. High dynamic range conversion of dermoscopy images in general dermatology conditions—A pilot study. *Skin Res Technol Off J Int Soc Bioeng Skin ISBS Int Soc Digit Imaging Skin ISDIS Int Soc Skin Imaging ISSI.* (2019) 25:867–70. doi: 10.1111/srt.12748

56. Kumar Jha S, Sonthalia A, Lallas, Chaudhary KR. Dermoscopy in vitiligo: diagnosis and beyond. *Int J Dermatol.* 57:50–4. (2018). doi: 10.1111/ijd.13795

57. K. Al-Refu. Dermoscopy is a new diagnostic tool in diagnosis of common hypopigmented macular disease: a descriptive study. *Dermatol Rep.* (2019) 11:7916. doi: 10.4081/dr.2018.7916

58. Scarfì F, Gori A, Silvestri F, Trane L, Portelli F, Maida P, et al. Fluorescence-advanced videodermatoscopy: a promising and potential technique for the *in vivo* evaluation of vitiligo. *Dermatol Ther.* (2019) 32:e12863. doi: 10.1111/dth.12863

59. Ibrahim S, Hegazy RA, Gawdat HI, Esmat S, Mahmoud E, Rashed L, et al. Differentiating active from stable vitiligo: the role of dermoscopic findings and their relation to CXCL10. *J Cosmet Dermatol.* (2022) 21:4651–8. doi: 10.1111/jocd.14922

60. Nirmal B, Antonisamy B, Peter CD, George L, George AA, Dinesh GM. Cross-sectional study of dermatoscopic findings in relation to activity in Vitiligo: BPLeFoSK criteria for stability. *J Cutan Aesthetic Surg.* (2019) 12:36–41. doi: 10.4103/JCAS.JCAS_75_18

61. Gupta P, Vinay K, Bishnoi A, Kumaran MS, Parsad DA prospective observational study to sequentially determine the dermoscopic features of vitiligo and its association with disease activity in patients on medical treatment: dermoscopy and disease activity in vitiligo. *Pigment Cell Melanoma Res.* (2023) 36:33–41. doi: 10.1111/pcmr.13069

62. Khaled. Role of dermoscopy in the diagnosis of vitiligo and evaluating its clinical stability." Available online at: https://www.mmj.eg.net/article.asp?issn=1110-2098;year$=$2022;volume$=$35;issue$=$3;spage$=$1088;epage$=$1094;aulast$=$Khaled (accessed July 03, 2023).

63. Thatte SS, Khopkar US. The utility of dermoscopy in the diagnosis of evolving lesions of vitiligo. *Indian J Dermatol Venereol Leprol.* (2014) 80:505–8. doi: 10.4103/0378-6323.144144

64. Tawfik NZ, Anbar MT, Atwa MA. Assessment of changes in color and size of vitiligo lesions during treatment with narrow band ultraviolet B. *J Cosmet Dermatol.* (2022) 21:3522–9. doi: 10.1111/jocd.14625

65. Brazzelli V, Roveda E, Prestinari F, Barbagallo T, Bellani E, Trevisan V, et al. Vitiligo-like lesions and diffuse lightening of the skin in a pediatric patient treated with imatinib mesylate: a noninvasive colorimetric assessment. *Pediatr Dermatol.* (2006) 23:175–8. doi: 10.1111/j.1525-1470.2006.00208.x

66. De Bruyne S, Speeckaert R, Himpe J, Delanghe JR. Near-infrared spectroscopy as a potential non-invasive tool in the assessment of disease activity in vitiligo patients. *Exp Dermatol.* (2020) 29:570–4. doi: 10.1111/exd.14097

67. Poojary S, Jaiswal S, Wahi A, Sahoo A. A portable fluorescence spectrometer as a noninvasive diagnostic tool in dermatology: a cross-sectional observational study. *Indian J Dermatol Venereol Leprol.* (2019) 856:641–7. doi: 10.4103/ijdvl.IJDVL_440_18

68. Prince S, Malarvizhi S. Multi-Wavelength Diffuse Reflectance Plots for Mapping Various Chromophores in Human Skin for Non-Invasive Diagnosis. In *13th International Conference on Biomedical Engineering*, C. T. Lim and J. C. H. Goh, Eds., in IFMBE Proceedings. Berlin, Heidelberg: Springer. (2009) 3:323–6. doi: 10.1007/978-3-540-92841-6_79

69. Choi KW, Kim KH, Kim YH. Comparative study of the gross interpretation of phototesting and objective measurement with using a spectrophotometer for patients with psoriasis and vitiligo treated with narrow-band UVB. *Ann Dermatol.* (2009) 21:136–41. doi: 10.5021/ad.2009.21.2.136

70. Hegyi V, Petrovajová M, Novotný M. An objective assessment of melanin in vitiligo skin treated with Balneo PUVA therapy. *Skin Res Technol.* (2014) 20:108–15. doi: 10.1111/srt.12092

71. Park ES, Na JI, Kim SO, Huh CH, Youn SW, Park KC. Application of a pigment measuring device–Mexameter–for the differential diagnosis of vitiligo and nevus depigmentosus. *Skin Res Technol Int Soc Bioeng Skin ISBS.* (2006) 12:298–302. doi: 10.1111/j.0909-752X.2006.00187.x

72. Fawzy Y, Zeng H. Spectral imaging technology—A review on skin and endoscopy applications. *Recent Pat Med Imaging Discontin.* (2023) 4:101–9. doi: 10.2174/2210684704666140227233822

73. Olsen EA, Dunlap FE, Funicella T, Koperski JA, Swinehart JM, Tschen EH, et al. A randomized clinical trial of 5% topical minoxidil versus 2% topical minoxidil and placebo in the treatment of androgenetic alopecia in men. *J Am Acad Dermatol.* (2002) 47:377–85. doi: 10.1067/mjd.2002.124088

74. Welzel J. Optical coherence tomography in dermatology: a review. *Skin Re. Technol J Int Soc Bioeng Skin ISBS.* (2001) 7:1–9 doi: 10.1034/j.1600-0846.2001.007001001.x

75. Gambichler T, Moussa G, Sand M, Sand D, Altmeyer P, Hoffmann K. Applications of optical coherence tomography in dermatology. *J Dermatol Sci.* (2005) 40:85–94. doi: 10.1016/j.jdermsci.2005.07.006

76. Hajizadeh-Saffar M, Feather JW, Dawson JB. An investigation of factors affecting the accuracy of in vivo measurements of skin pigments by reflectance spectrophotometry. *Phys Med Biol.* (1990) 35:1301–15. doi: 10.1088/0031-9155/35/9/009

77. Chu H, Lee JW, Lee YI. Delayed treatment of generalized morphea due to misdiagnosis as vitiligo at an oriental medical clinic. *Ann Dermatol.* (2017) 29:649–50. doi: 10.5021/ad.2017.29.5.649

78. Kim S, Byun KM, Lee SY Influence of water content on Raman spectroscopy characterization of skin sample. *Biomed Opt Express.* (2017) 8:1130–8. doi: 10.1364/BOE.8.001130

79. van Geel N, Lommerts J, Bekkenk M, Wolkerstorfer A, Prinsen CA, Eleftheriadou V, et al. Development and validation of the vitiligo extent score (VES): an international collaborative initiative. *J Invest Dermatol.* (2016) 136:978–84. doi: 10.1016/j.jid.2015.12.040

80. Njoo MD, Das PK, Bos JD, Westerhof W. Association of the Köbner phenomenon with disease activity and therapeutic responsiveness in vitiligo vulgaris. *Arch Dermatol.* (1999) 135:407–13. doi: 10.1001/archderm.135.4.407

81. Coias J, Hynan LS, Pandya AG. Lack of correlation of the patient-derived vitiligo disease activity index with the clinician-derived vitiligo area scoring index. *J Am Acad.Dermatol.* (2018) 78:1016. doi: 10.1016/j.jaad.2017.11.034

82. Taieb A, Picardo M, other VETF members. The definition and assessment of vitiligo: a consensus report of the Vitiligo European task force. *Pigment Cell Res.* (2007) 20:27–35. doi: 10.1111/j.1600-0749.2006.00355.x

83. Benzekri L, Ezzedine K, Gauthier Y. Vitiligo Potential Repigmentation Index: a simple clinical score that might predict the ability of vitiligo lesions to repigment under therapy. *Br J Dermatol.* (2013) 168:1143–6. doi: 10.1111/bjd.12147

84. Sheth VM, Gunasekera NS, Silwal S, Qureshi AA. Qureshi. Development and pilot testing of a vitiligo screening tool. *Arch Dermatol Res.* (2015) 307:31–8. doi: 10.1007/s00403-014-1515-1

85. Feily. Vitiligo Extent Tensity Index (VETI) score: a new definition, assessment and treatment evaluation criteria in vitiligo. *Dermatol Pract Concept.* (2014) 4:81–4. doi: 10.5826/dpc.0404a18

86. Aydin F, Senturk N, Sahin B, Bek Y, Yuksel EP, Turanli AY. A practical method for the estimation of vitiligo surface area: a comparison between the point counting and digital planimetry techniques. *Eur J Dermatol EJD.* (2007) 17:30–2. doi: 10.1684/ejd.2007.0186

Frontiers in Medicine

Translating medical research and innovation into improved patient care

A multidisciplinary journal which advances our medical knowledge. It supports the translation of scientific advances into new therapies and diagnostic tools that will improve patient care.

Discover the latest Research Topics

See more →

Frontiers

Avenue du Tribunal-Fédéral 34
1005 Lausanne, Switzerland
frontiersin.org

Contact us

+41 (0)21 510 17 00
frontiersin.org/about/contact